

Studies on the Iron-Sulfur clusters of hydrogenase, sulfite reductase, nitrogenase and the prismane protein



40951

Promotor: Dr. C. Veeger
hoogleraar in de Biochemie

Co-promotor: Dr. W.R. Hagen
Universitair hoofddocent, vakgroep Biochemie

A.J. Pierik

**Studies on the Iron-Sulfur clusters of
hydrogenase, sulfite reductase, nitrogenase
and the prismane protein**

Proefschrift

ter verkrijging van de graad van doctor
in de landbouw- en milieuwetenschappen
op gezag van de rector magnificus,
Dr. C.M. Karszen,
in het openbaar te verdedigen
op maandag 18 oktober 1993
des namiddags te vier uur in de Aula
van de Landbouwniversiteit te Wageningen

BIBLIOTHEEK
LANDBOUWUNIVERSITEIT
WAGENINGEN

Aan mijn ouders en grootouders

STELLINGEN

1. Superclusters en Superspins bestaan.

Hoofdstuk 5, 7 en 8 van dit proefschrift.

Chan, M.K., Kim, J. & Rees, D.C. (1993) *Science* 260, 792-794.

Bolin, J.T., Ronco, A.E., Morgan, T.V., Mortenson, L.E. & Xuong, N.-H. (1993) *Proc. Natl. Acad. Sci. (USA)* 90, 1078-1082.

2. Interpretatie van spectroscopische resultaten van eiwitten met meerdere redox toestanden is alleen zinvol na bepaling van de redox halfwaarde potentialen.

Hoofdstuk 2, 5, 8 en 9 van dit proefschrift.

3. Het rhombische EPR signaal met $g=2.07$, 1.96 en 1.89 is een artefakt veroorzaakt door de aktivering van het zuurstof-stabiele ijzer-hydrogenase uit *Desulfovibrio vulgaris* (Hildenborough).

Hoofdstuk 2 van dit proefschrift.

Patil, D.S., Moura, J.J.G., He, S.H., Teixeira, M., Prickril, B.C., DerVartanian, D.V., Peck, H.D., LeGall, J. & Huynh, B.-H. (1988) *J. Biol. Chem.* 263, 18732-18738.

4. Het koper-bevattend nitriet reductase is net als aconitase een kannibalistisch enzym.

Masuko, M., Iwasaki, H., Sakurai, T., Suzuki, S. & Nakahara, A. (1984) *J. Biochem.* 96, 447-454.

Kennedy, M.C., Emptage, M.H., Dreyer, J.-L. & Beinert, H. (1983) *J. Biol. Chem.* 258, 11098-11105.

Libby, E. & Averill, B.A. (1992) *Biochem. Biophys. Res. Commun.* 187, 5129-1535.

5. Het door Fu *et al.* beschreven stereo- en regioselectieve karakter van de halohydrin-vorming uit 2,3-dehydroasialzuur wordt niet veroorzaakt door chloorperoxidase.

Fu, H., Kondo, H., Ichikawa, Y., Look, G.C. & Wong, C.-H. (1992) *J. Org. Chem.* 57, 7265-7270.

6. Het humane glutathion reductase is geen goed model voor de voorspelling van de structuur van de actieve plaats van het humane lipoamide dehydrogenase.

Jentoft, J.E., Shoham, M., Hurst, D. & Patel, M.S. (1992) *Proteins: Struct. Funct. Genet.* 14, 88-101.

7. De zuivering en karakterisering van het produkt van de nifN en nifE genen had moeten worden uitgevoerd met een wild-type stam en niet met *Azotobacter vinelandii* UW45.

Paustian, T.D., Shah, V.K. & Roberts, G.P. (1989) *Proc. Nat. Acad. Sci. USA* 86, 6082-6086.

8. Serine en threonine kunnen in tegenstelling tot wat Fraústo da Silva en Williams vermelden als liganden optreden in Mg^{2+} -eiwit-nucleotide complexen.

The Biological Chemistry of the Elements.

Fraústo da Silva, J.J.R. & Williams, R.J.P. (1991) Clarendon Press, Oxford.

Pai, E.F., Krengel, U., Petsko, G.A., Goody, R.S., Kabsch, W. & Wittinghofer, A. (1990) *EMBO J.* 9, 2351-2359.

9. Met de éénwording van de landen van de EEG moet de sluiting van de Engelse pubs verlaat worden tot één uur.

10. Onbeschermd in 't veld is men snel het haasje.

Stellingen behorende bij het proefschrift

'Studies on the Iron-Sulfur clusters of hydrogenase, sulfite reductase, nitrogenase and the prismatic protein'

Wageningen, 18 oktober 1993

A.J. Pierik

Voorwoord

Voor het tot stand komen van dit proefschrift is in tegenstelling tot wat de titelpagina en omslag suggereert meer dan één persoon betrokken geweest. Ik zal in dit voorwoord proberen de directe en indirecte bijdrage van al deze personen te specificeren, hoewel ik hiermee het risico loop (ongewenst) iemand te vergeten.

Allereerst wil ik mijn promotor professor C. Veeger en mijn co-promotor Fred Hagen bedanken. Door de zeer open houding ten aanzien van het onderzoek en het stimuleren van het bezoek aan (internationale) congressen en cursussen kon ik me verdiepen in allerlei facetten van de bio-anorganische chemie. Ik ben daarom in hoge mate dankbaar voor de supervisie. Fred wil ik bovendien bedanken voor de aangename alledaagse begeleiding en de praktische, theoretische en tekstuele bijdragen die een onmisbare rol hebben gespeeld.

Chronologisch vervolgend, wil ik mijn dank richten tot Marelle Boersma en Anita van Berkel. De eerste prille maanden in 1987/1988 op lab 5 heb ik veel steun gehad op praktisch gebied. Een voor jullie misschien onverwacht dank-je-wel voor de secure administratie van de experimenten in het verleden. Dagenlang heb ik doorgebracht met het lezen en vergelijken van resultaten. De vruchten van de secure boekhouding zijn op indirecte wijze terug te vinden in hoofdstuk 3 tot en met 5: de door Marelle als 'hydrogenase' gelabelde ingevroren monsters hebben geleid tot de ontdekking van het marelase (momenteel prismaan eiwit geheten).

Met de verhuizing naar lab 1/2 en de start van Ronnie Wolbert begon de oogst fase van het promotie onderzoek. Jouw punctuele aanvang van experimenten in de ochtend combineerde uitstekend met mijn meer naar de tweede helft van de dag verschoven ritme. Ondanks het onaangename parfum van *Desulfovibrio*, ontsnappingen van 300 liter water en het grote aantal gels en blots was jij altijd in een goede stemming. Samen met Fred Hagen, Marc Verhagen, Dirk Heering en de afstudeervakstudenten vormde lab 1/2 een hecht team. Deze verbondenheid uitte zich door de gemeenschappelijke hoge affiniteit voor ons koffiezet apparaatje, de assay-koelkast, Granucci en Sa Lolla. Marc Verhagen wil ik bedanken voor zijn hulp bij de afhandeling van allerlei zaken gedurende de laatste maanden.

Door hulp met het opwekken van antilichamen en N-terminale aminozuur volgorde bepaling hebben Anita Kaan en Walter van Dongen het onderzoek naar het prismaan eiwit versneld. Willy van den Berg en Jack Stokkermans hebben door de zeer prettige samenwerking en de opheldering van de primaire structuur van de prismaan eiwitten uit *Desulfovibrio vulgaris* (Hildenborough) en *D. desulfuricans* (ATCC 27774) ervoor gezorgd dat het prismaan eiwit onderzoek in een stroomversnelling is geraakt.

De samenwerking met Hans Wassink en Huub Haaker resulteerde in een hoofdstuk over het molybdeen-ijzer eiwit. Bedankt Hans voor de isolatie van het enzym en het leren van een aantal technieken. Huub, de vele discussies over nitrogenase en gerelateerde onderwerpen heb ik zeer op prijs gesteld.

Rafaël Israëls, Martina Duyvis, Joop van Helvoort, Carine Stevens, Wim Hilbrandts, Leonard Mallée, Sander Arendsen en Gerrit Portier hebben door hun afstudeervak te doen in ons lab in belangrijke mate bijgedragen tot de sfeer, gezelligheid en wetenschappelijke productie. Bedankt voor de energie die jullie hebben gestoken in het onderzoek.

Door de inspirerende samenwerking met Mike Jetten en Christof Holliger van de vakgroep Microbiologie kon ik kennismaken met koolmonoxide dehydrogenase en F-430. Peter Mutsaers, Leo de Folter, Auke van Heuzen, Dhr. Walinga, Tom Bongers, Jo Haas, Marja Snoek, Willem van Berkel, Adri Westphal en Simon Albracht hebben mij vertrouwd

gemaakt met diverse technieken. Martin Bouwmans, Bery Sachteleben en Laura Ausma zorgden voor allerlei administratieve zaken. Thomas Link has contributed by involving me in the study of the soluble domain of the Rieske protein. The efforts of Dick Dunham and Dick Sands have strenghtened the importance of Chapter 5. Many thanks for your valuable contributions. I am grateful to Barry Smith and Bob Eady who allowed me to spend a part of my postdoctoral time on the dutch graduation.

De praktische en/of morele steun van alle reeds met naam genoemde personen, Axel Berg, René Wientjens, Chris Oldfield, Jacques Benen, Phil Bastiaens, Ewart Pap en alle overige (ex)leden van de vakgroep Biochemie heb ik als zeer prettig ervaren. Naast de aangename uren op het Lab zorgden huisgenoten, de leden van de twee 'eetclubs', de werkgroep fossielen Wageningen en andere vrienden ervoor dat de terugkeer naar de geboortestad Wageningen aangenamer was dan ik ooit had kunnen vermoeden. Tenslotte wil ik mijn ouders en broer Leo bedanken, die door het fijne familieleven in de weekenden/vakanties en door hun gezonde nieuwsgierigheid naar mijn werk een zeer motiverende invloed hebben gehad. Er resteert één persoon die ik vanuit deze positie niet kan bedanken: door zijn vroegtijdige overlijden is Jan Redeker niet meer in ons midden. Jan, ik ben je erkentelijk voor jouw bijdrage tot hoofdstuk 2, jouw herinnering leeft voort in mijn gedachte.

The research was carried out at the Department of Biochemistry, Agricultural University, Wageningen, The Netherlands. The investigations were supported by the Netherlands Foundation for Chemical Research (SON) with financial aid from the Netherlands Organization for Scientific Research (NWO).

CONTENTS

	Page
Chapter 1: Introduction	1
Chapter 2: Redox properties of the iron-sulfur clusters in activated Fe-hydrogenase from <i>Desulfovibrio vulgaris</i> (Hildenborough)	33
Chapter 3: Novel Electron Paramagnetic Resonance Signals from an Fe/S Protein containing Six Iron Atoms	45
Chapter 4: Purification and biochemical characterization of a putative [6Fe-6S] prismane-cluster-containing protein from <i>Desulfovibrio vulgaris</i> (Hildenborough)	55
Chapter 5: Multi-frequency EPR and high-resolution Mössbauer spectroscopy of a putative [6Fe-6S] prismane-cluster-containing protein from <i>Desulfovibrio vulgaris</i> (Hildenborough): characterization of a supercluster and superspin model protein	65
Chapter 6: The third subunit of desulfoviridin-type dissimilatory sulfite reductases	83
Chapter 7: S=9/2 EPR signals are evidence against coupling between the siroheme and the Fe/S cluster prosthetic groups in <i>Desulfovibrio vulgaris</i> (Hildenborough) dissimilatory sulfite reductase	91
Chapter 8: Redox properties and EPR spectroscopy of the P clusters of the <i>Azotobacter vinelandii</i> MoFe protein	105
Chapter 9: Nigerythrin and rubrerythrin from <i>Desulfovibrio vulgaris</i> each contain two mononuclear iron centers and two dinuclear iron clusters	119
Chapter 10: The occurrence of high-spin states in iron-sulfur proteins	131
Chapter 11: Summary	145
Samenvatting	151
Curriculum Vitae	163

Abbreviations

A	hyperfine constant
A_x	absorbance at x nm
AAS	atomic absorption spectrometry
AMP	adenosine 5'-monophosphate
APS	adenosine 5'-phosphosulfate
ATCC	american type culture collection
β	Bohr magneton
B	magnetic field
CoA	coenzymeA
D	axial zero-field splitting parameter
DEAE	diethylaminoethyl
DSM	Deutsche Sammlung für Mikroorganismen
E	redox potential or rhombic zero-field splitting parameter
E_m	redox midpoint potential
E/D	rhombicity
EDTA	ethylenediaminetetraacetate
EPR	electron paramagnetic resonance
f	purity index
F	Faraday constant
FAD	flavin adenine dinucleotide
FeMoco	iron-molybdenum cofactor
FMN	flavin mononucleotide (riboflavin 5'-phosphate)
FPLC	fast protein liquid chromatography
H	Hamiltonian operator
Hepes	4-(2-hydroxyethyl)-1-piperazineethane sulfonic acid
I	nuclear spin quantum number
ICP-MS	inductively coupled plasma mass spectroscopy
IEF	isoelectric focussing
IgG	immunoglobulin G
INAA	instrumental neutron activation analysis
kDa	kilodalton
MCD	magnetic circular dichroism
m_s	projected angular momentum
mT	millitesla (unit of magnetic field)
n	number of electrons involved in a redox reaction
NAD(P)H	reduced nicotinamide-adenine dinucleotide
NCIB	national collection of industrial and marine bacteria
NHE	normal hydrogen electrode
pa	pro analysis
P	the (protein-bound) [8Fe-8S] clusters of nitrogenase component 1
PAGE	polyacrylamide gel electrophoresis
pI	isoelectric point
PIXE	particle-induced X-ray emission
R	gas constant or purity index
$S_{20,w}$	sedimentation coefficient in water at 20 °C
S	spin (operator) or Svedberg (10^{-13} s)

SD	standard deviation
SDS	sodium dodecylsulfate
T	absolute temperature
Tris	tris(hydroxymethyl)aminoethane
U	unit of enzymatic activity (1 μmol product per minute)
UV	ultraviolet
V_{zz}	total effective electric field gradient in principal axis
W	linewidth
Z	atomic number
ϵ_x	extinction coefficient at x nm
η	asymmetry parameter
σ	total resonance cross section

CIP-DATA KONINKLIJKE BIBLIOTHEEK, DEN HAAG

Pierik, A.J.

Studies on the iron-sulfur clusters of hydrogenase,
sulfite reductase, nitrogenase and the prismane protein /
A.J. Pierik. - [S.l. : s.n.]

Thesis Wageningen. - With ref. - With summary in Dutch.

ISBN 90-5485-174-0

Subject headings: iron-sulfur clusters / *Desulfovibrio*
vulgaris / enzymes.

Chapter 1

Introduction.

1. Introduction

1.1. Iron-sulfur clusters

Thirty years ago the research on metalloproteins entered a new era when iron-sulfur clusters were identified as constituents of proteins. The milestone marking the discovery by Beinert [1-2] of iron-clusters was the recognition of the association of electron paramagnetic resonance (EPR) signals with iron containing constituents of the respiratory chain. The detection of EPR signals in several non-heme iron proteins [3-7] and the discovery of the presence of acid-labile sulfur (S^2) [8-10] subsequently led to the full recognition of iron-sulfur clusters in proteins. At the moment, 33 years after Beinert's start, the several hundreds of iron-sulfur proteins [11] form the largest and most complex group of metalloproteins. High resolution three dimensional structures for a number of basic types of iron-sulfur clusters in proteins [12-18] and numerous model compounds have been established. Schematic structures of the well-known basic iron-sulfur clusters of these proteins are shown in Figure 1.

The joint efforts of physicists, chemists, (molecular) biologists and microbiologists have led to a library of an enormous amount of data on iron-sulfur clusters and proteins. Extensive reviews [19-23], the most important of which are the five so-called 'Iron-Sulfur books' [24-27], have summarized the rapidly expanding number of publications on the strongly interdisciplinary field. It should be appreciated that a review or description of all iron-sulfur proteins and possible spectroscopic techniques is certainly beyond the scope of this chapter. The aim of this Chapter is, therefore, to introduce the reader to the general historic background and introduce the concept of superclusters and superspins, which led to the discovery of new properties of iron-sulfur clusters.

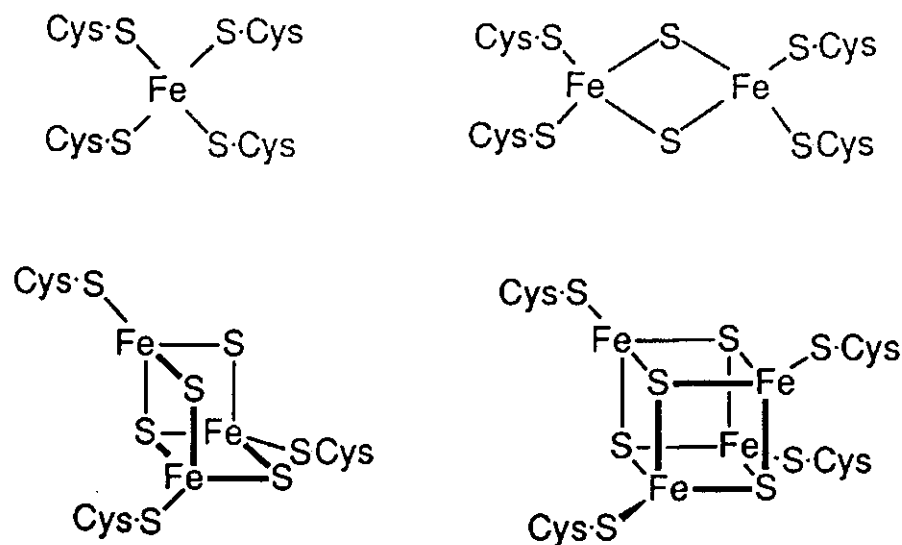


Fig. 1: Structures of the basic iron-sulfur clusters of well-characterized iron-sulfur proteins.

1.2. The complexity of iron-sulfur proteins: from rubredoxin to nitrogenase

1.2.1 Mononuclear 'iron-sulfur' proteins: the rubredoxin-type centre

The rubredoxin-type centre is the simplest structure present in iron-sulfur proteins. The bacterial protein rubredoxin (ruber, red (L), redox protein), which was discovered in 1965 [28] contains a single iron ion, tetrahedrally coordinated by four cysteine residues. Formally the absence of both (acid-labile) sulfur and clustering of iron ions excludes the use of the term iron-sulfur cluster for this centre. However since similar spectroscopic techniques and bacterial sources are used as for the iron-sulfur proteins *sensu stricto*, the proteins with rubredoxin-like centers nevertheless are conveniently designated as iron-sulfur proteins. Mononuclear iron centers with rubredoxin-like properties have been identified in four other types of proteins, differing in molecular mass, redox and spectroscopic properties (Table 1). Unlike rubredoxin, these proteins contain either more than one rubredoxin-type center and/or additional non-sulfur coordinated mono or dinuclear iron centers. Sulfate-reducing bacteria of the genus *Desulfovibrio* have proven not only to be a rich, but also a unique source for the varieties of the rubredoxin-type center in the so-called desulforedoxin, rubrerythrin, nigerythrin and desulfoferrodoxin proteins.

Table 1: Proteins with rubredoxin-type centers

Name	Metal-centers	Midpoint potential (mV)	Molecular mass (kDa)	Refs.
Rubredoxin	1 Fe ^{2+/3+} (Cys) ₄	-60 to +20	6.0	[12,28-36]
Desulforedoxin	2 Fe ^{2+/3+} (Cys) ₄	- 35	2*3.80	[37-41]
Rubrerythrin	2 Fe ^{2+/3+} (Cys) ₄	+281	2*21.544	[42-47] Chapter 9
	2 (Fe ^{2+/3+} -μO-Fe ^{2+/3+})	+246/+339		
Nigerythrin	2 Fe ^{2+/3+} (Cys) ₄	+213	2*27	Chapter 9
	2 (Fe ^{2+/3+} -μO-Fe ^{2+/3+})	+209/+300		
Desulfoferrodoxin	1 Fe ^{2+/3+} (Cys) ₄	unknown	14.0	[48,49]
	1 Fe ^{2+/3+} (N ₂ O) ₆	unknown		

Rubredoxin has been studied extensively since the discovery in the sixties. High resolution X-ray crystallographical structures of down to 1.0 Å resolution [12] are available for rubredoxins from four bacterial sources [32,50-52]. The simple nature of rubredoxin has allowed to evaluate its spectroscopic properties in considerably more detail than for any other iron-sulfur protein. However, information on the exact coordination of the iron ion in the other four rubredoxin-type centers is lacking. Though crystallisation of rubrerythrin has been reported in 1988 [43], no X-ray crystallographic structures are available at the moment for any of the four proteins with rubredoxin-type centers. In absence of actual structural data, thus a roughly tetrahedral, presumably all-cysteine coordination has been assumed. In desulforedoxin and desulfoferrodoxin a distortion from the tetrahedral geometrical arrangement was suggested by the presence of vicinal cysteine residues [39,41,48] and EPR

and Mössbauer spectroscopy [40,49].

Structural models derived from X-ray crystallography of the dinuclear iron centers of hemerythrin and ribonucleotide reductase (Figure 2) give an impression of the possible ligation of the non-rubredoxin-type dinuclear centers in rubrerythrin and nigerythrin.

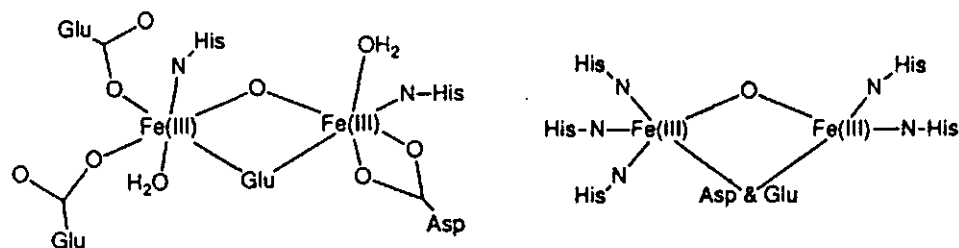


Fig. 2: The structure of the μ -oxo-bridged dinuclear iron center in ribonucleotide reductase (left) and hemerythrin (right) as revealed by X-ray crystallography (from [53], X-ray structures in [54,55])

Since the spectroscopic and protein sequence data on the coordination of the dinuclear centers in rubrerythrin and nigerythrin are not conclusive ([42-47], Chapter 9), the representation of the structures in Figure 2 should be regarded as informative. An actual assignment of the ligands will have to wait for X-ray crystallographic studies.

The function of all *Desulfovibrio* proteins with rubredoxin-type centers is enigmatic. The low-molecular mass rubredoxin and desulfuredoxin most probably act as electroncarriers in electron-transfer chains. Experiments with NADH:rubredoxin oxidoreductase from *Desulfovibrio gigas* and *Clostridium acetobutylicum* [56,57] did not reveal a physiological role, since the function of this flavoprotein itself is unknown. Only in *Pseudomonas oleovorans* a participation of rubredoxin is known in the electron transfer associated with alkane oxidation [58,59]. Recently, Friedrich and coworkers identified that in *Alcaligenes eutrophus* a rubredoxin-like protein is encoded by the *hoxR* gene in the hydrogenase operon [60]. This could imply that in sulfate-reducing bacteria rubredoxin is somehow involved in a cytoplasmic redox-chain linked to hydrogenase or in the biosynthesis/maturation of enzymes related to hydrogenase.

Table 2: Biological functions of proteins with dinuclear iron centers

Protein	Typical source	Function	Refs.
Ribonucleotide reductase	<i>Escherichia coli</i>	reduction of -OH to -H	[55,61]
Purple acid phosphatase	(bovine) spleen	cleavage PO_4^{3-} esters	[62]
Uteroferrin	pig uterus	?iron transport	[53,62]
Hydroxylase component of methane monooxygenase	<i>Methylococcus capsulatus</i>	activation of O_2 for insertion in CH_4	[63,64]
Hemerythrin	<i>Phascolopsis gouldii</i>	oxygen storage/transport	[59]
Rubrerythrin	<i>Desulfovibrio vulgaris</i>	unknown	[42-47]
Nigerythrin	<i>Desulfovibrio vulgaris</i>	unknown	Ch. 9

The heterogeneous functions of dinuclear iron centers make a conclusive assignment of the function of rubrerythrin and nigerythrin even more difficult since dinuclear iron clusters are known to perform a wide range of biological functions (Table 2). As will be discussed in Chapter 9 a catalytic or binding function seems to be likely.

1.2.2. The iron-sulfur clusters of simple iron-sulfur proteins

In 1962 a brown low-molecular mass protein with 'non-heme' iron was identified from the bacterium *Clostridium pasteurianum* by Mortenson and coworkers on the basis of its iron content, visible absorbance and function in electron-transfer to hydrogenase [65]. They called this protein ferredoxin (ferrum, iron (L), redox protein). The discovery of similar proteins isolated from other sources like the bacteria *Azotobacter*, *Pseudomonas*, photosynthetic bacteria and spinach [66-69] made it clear that a new class of chemical structures was present in a number of proteins. Subsequently the clustered nature of the iron ions, acid-labile sulfur and cysteine was revealed by the application of EPR spectroscopy [3-7] on proteins enriched or reconstituted with ^{57}Fe , ^{33}S and ^{80}Se [3,7,70-72]. This corroborated the earlier chemical analysis of Fry and San Pietro [8] and others [9,10] who discovered that sulfur in an acid-labile form was present in their non-heme iron protein preparations. It also became clear that the visible spectra, EPR characteristics and iron and acid-labile sulfur content allowed a ready discrimination of various iron-sulfur proteins and rubredoxin. An identification based on source, redox potential and iron content led to the classification into plant ferredoxin, adrenodoxin and putidaredoxin (containing 2 Fe and 2 S^{2-} ions, abbreviated as [2Fe-2S]), bacterial ferredoxins ([4Fe-4S] with low redox potential) and High Potential Iron Proteins (or HiPIPs, [4Fe-4S] with high redox potential).

The absence of 3-dimensional structures however still obstructed a clear appreciation of the various iron-sulfur clusters around 1970. After the decade of chemical and spectroscopic studies successive breakthroughs came in the early seventies with the X-ray crystallographic structures of the *Clostridium pasteurianum* rubredoxin [73], the HiPip from *Chromatium vinosum* [74], the *Peptococcus aerogenes* ferredoxin [75] and an inorganic model compound mimicking the spectroscopic features of plant ferredoxins [76]. The most intriguing finding was that both bacterial ferredoxin and HiPIP had cubane structures ([4Fe-4S]). Whereas the [4Fe-4S] centre can change from [4Fe-4S] $^{1+}$ to [4Fe-4S] $^{2+}$ and backwards in bacterial ferredoxins, HiPIPs shuttle between [4Fe-4S] $^{2+}$ to [4Fe-4S] $^{3+}$ (the cluster valence refers to the sum of ferric/ferrous and sulfide charges) [77,78]. In the [2Fe-2S] centers only [2Fe-2S] $^{1+}$ and [2Fe-2S] $^{2+}$ occurred [79]. An important landmark for the versatility of a spectroscopic approach was the elucidation of the crystal structure of the [2Fe-2S] ferredoxin from *Spirulina platensis* [80]. This pointed out that spectroscopic measurements had correctly shown that the [2Fe-2S] cluster in the crystallized model compound [76] and the protein were identical.

In 1980 a new iron-sulfur cluster was discovered by the observation of a 2 to 1 ratio of iron ions in the Mössbauer spectrum of *Desulfovibrio gigas* and *Azotobacter vinelandii* ferredoxin [81-82]. Because such a ratio could not be explained by the known structures a [3Fe-xS] cluster was proposed. Corroboration seemed to be found by the X-ray crystallographic structure of ferredoxin from *Azotobacter vinelandii*, interpreted with a [4Fe-4S] and a [3Fe-3S] structure [83]. Very soon the three iron center was recognised in other iron-sulfur proteins by Mössbauer and EPR spectroscopy [84-87]. In contrast with the cyclic [3Fe-3S] structure proposed by Stout et al. [83], the Mössbauer studies [86], elemental analysis [88] and Extended X-ray Absorption Fine Structure spectroscopy [89] indicated a cubane structure devoid of one iron-corner, i.e. a [3Fe-4S] cluster. This discrepancy was finally solved by redetermination of the structure in 1988 [90,91], confirming the results of

the chemical and spectroscopic measurements.

In the course of the investigations on the conversion of [4Fe-4S] and [3Fe-4S] in aconitase a new aspect of iron-sulfur clusters was discovered. The EPR spectrum of reduced aconitase was shown to be perturbed by addition of substrate (analogues) [92]. This was confirmed by electron-nuclear double resonance spectroscopy (ENDOR), which conclusively demonstrated that the perturbation was due to actual binding of the substrate [93]. The [4Fe-4S] center in aconitase in fact functioned as a Lewis acid. Electron transfer and redox catalysis thus were not the only function of iron-sulfur clusters. Very soon a number of other hydrolyases were found to contain [4Fe-4S] centers as their catalytic site (reviewed in [94]). Surprisingly the hydrolyase dihydroxy acid dehydratase was shown to bind substrates with a [2Fe-2S] cluster, suggesting that the Lewis acid catalysis was not restricted to the cubane structure [95]. Some evidence has been found that the function of some iron-sulfur clusters might be regulatory, rather than redox action or (Lewis acid) catalysis [94,96-98].

At the present time we can understand the basic properties of low-molecular mass iron-sulfur proteins and the majority of iron-sulfur enzymes. Some subjects will certainly benefit from additional studies. For instance the appraisal of histidine ligation in the [2Fe-2S] centers of the Rieske center in the mitochondrial bc₁ complex and various dioxygenases [99-102] should still culminate in a determination of the structure with X-ray crystallography. Structures for complexes of the respiratory chain and the photosynthetic system (see [103]) should confirm whether the spectroscopic predictions for their constituent iron-sulfur clusters are correct. The main research on the low-molecular mass 'simple' iron-sulfur clusters is expected to focus on very detailed structural, kinetic and electronic aspects. Application of molecular genetic techniques has already facilitated spectroscopic and structural studies by (over)expression of iron-sulfur proteins [36,102,104-107] and site-directed mutagenesis of the amino-acid environment [108-112]. The increased interest in Multi-dimensional Nuclear Magnetic Resonance spectroscopy of iron-sulfur proteins will provide more insight in dynamical aspects and the three-dimensional structure in aqueous solution [34,113-117]. Finally, the dynamics of electron transfer of iron-sulfur redox carriers, cluster interconversion, metal ion incorporation and ligand exchange are currently investigated in detail with electrochemical methods [118,119]. Though these further studies will lead to an even better understanding, the main challenge currently lies in the elucidation of the structures and properties of complex iron-sulfur proteins.

1.2.3. The iron-sulfur clusters of multiple electron transferring iron-sulfur proteins

The first indication for an iron-sulfur cluster with more than 4 iron ions was provided by Shah and Brill, who discovered that ≈ 7 iron and 1 molybdenum ion could be extracted from the nitrogenase molybdenum-iron (MoFe) protein [120]. Following the discovery of this so-called iron molybdenum cofactor (FeMoco) the interpretation of the Mössbauer spectral components was reassessed [121-124]. The spectroscopic properties, especially the unusual $S=3/2$ spin state, firmly established that the extracted and protein-bound FeMoco had to have a very similar structure. Although the fact that the FeMo cofactor was a larger iron-sulfur cluster was generally accepted at that time, it was not recognised that other iron-sulfur proteins might have larger clusters. For example, the residual 16 protein-bound iron ions of the nitrogenase MoFe protein (the so-called P-centres) were thought to be present in 'unusual' cubanes [122-124]. The practice of explaining peculiar spectroscopic data by the assumption that unusual cubanes instead of unidentified iron-sulfur clusters were present persisted up to about seven years ago.

The first strong tendency towards a non-cubane oriented description was displayed by Hagen and coworkers in 1986 [125]. By elemental analysis of the iron and acid-labile sulfur

content and subtraction of the contribution of the two cubane centers of the *Desulfovibrio vulgaris* (Hildenborough) Fe-hydrogenase they suggested that the active site of this hydrogenase is not a [4Fe-4S] cluster, but rather is a novel cluster comprised of approx. 6 Fe and S²⁻ [124]. The presence of an highly unusual g=5 EPR signal was interpreted as corroborating evidence for the unusual non-cubane nature of the cluster [126,127]. The suggestion that a 6-Fe containing cluster could be present did not come out of the blue, since

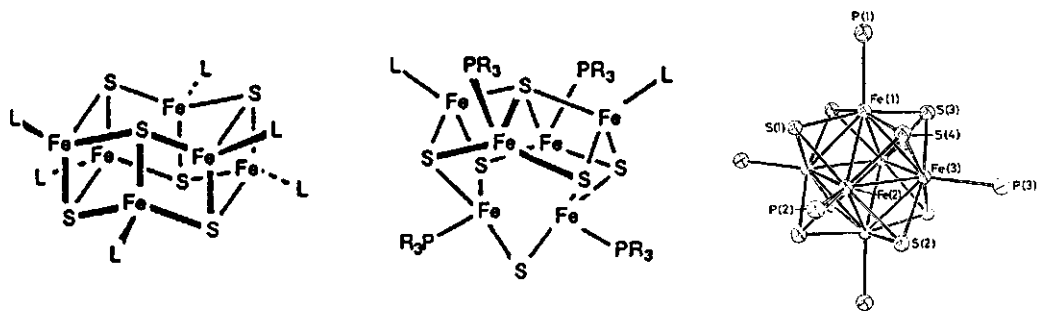


Fig. 3: Structures of [6Fe-6S]³⁺ prismane, [6Fe-9S]²⁻ basket and [6Fe-8S]²⁺ dice structures (from [128,129,132])

at that time prismane, basket and dice-shaped [6Fe-xS] model compounds were well-documented [128-132] (Figure 3). The second important notion was made in 1987 when the spin quantitation of EPR signals from a paramagnet with spin $S=7/2$ in solid-thionine oxidized nitrogenase MoFe protein was interpreted as evidence for 2 P clusters with 8 Fe ions each [133]. The proposed models of Hagen and coworkers were strongly criticized by other groups (for instance [134]).

Two remarkable discoveries suddenly paved the way to a more non-cubane oriented attitude of the scientific forum. First, the Fe-hydrogenases from *Clostridium pasteurianum* were subjected to a redetermination of its metal and acid-labile sulfur content in 1989 [135,136]. After this correction the doubts on the proposed concept of a 6-Fe containing hydrogen-activating iron-sulfur cluster were eliminated (see for instance [137,138]). Secondly, the low-resolution X-ray crystallographic structure of the *Clostridium pasteurianum* MoFe protein indicated that instead of four cubane-like structures two large 8 iron containing clusters were present [139]. This has been substantiated even more by the recent 2.7 Å resolution X-ray crystallographic studies on the MoFe proteins from *Azotobacter vinelandii* [140,141] and *Clostridium pasteurianum* [142], which have resolved the structures of the FeMoco and P-clusters almost at atomic level (Figure 4).

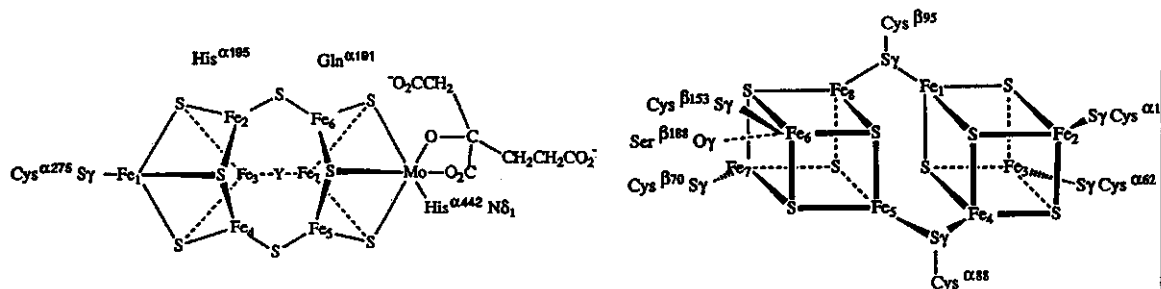
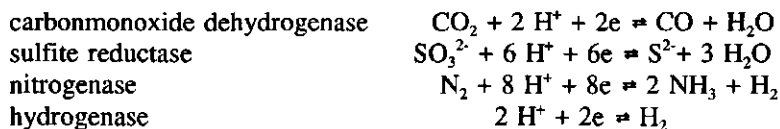


Fig. 4: Proposed structures for the FeMo cofactor (left) and P-cluster iron-sulfur centers of *Azotobacter vinelandii* molybdenum-iron protein as revealed by 2.7 Å resolution electron density maps (from [140,141])

The nitrogenase MoFe protein and Fe-hydrogenases are not expected to be the only iron-sulfur proteins with larger iron-sulfur clusters. Enzymes like dissimilatory sulfite reductase and carbonmonoxide dehydrogenase share the fact that they have iron-sulfur clusters enigmatic spectroscopic properties [143-146], a very high iron and acid-labile sulfur content [146-148] and the ability to catalyze exceptional redox reactions of simple substrates:



A reasonable assumption is therefore that these proteins all might have larger non-cubane iron-sulfur 'superclusters', which unlike the hitherto known iron-sulfur clusters are able to donate or accept more than one electron. Based on the earlier observations of high-spin EPR signals in hydrogenase [126,127] and the P and FeMoco clusters of the nitrogenase MoFe protein [121,133,149], superclusters are expected to have more complicated paramagnetic 'superspin' ground states. A striking similarity between the MCD spectroscopic characteristics of the H-cluster of the Fe-hydrogenase [136,150,151] and the oxidized P clusters of nitrogenase [151] has also been noted. The unusual Mössbauer spectroscopic properties [123,124,134,143-146,153,154] and the 'absence' of EPR signals in samples which had paramagnetic Mössbauer or MCD [123,124,143-146,148,150-154] would agree with the existence of the superspin nature. Since a larger number of clustered iron ions reduces the relative change of charge density on administration of electrons to the cluster, more than one redox state would be stabilized in these superclusters. This on its turn is in perfect harmony with multiple electron redox reactions. The well-documented metastability of larger iron-sulfur cluster, like the [6Fe-6S] prismane core [132], would account for the observation of the extrusion of [4Fe-4S] structures [155,156]. This supercluster-superspin concept, as outlined above, should be considered as the working model for the (re)investigation of the iron-sulfur clusters of multiple electron transferring enzymes described in this thesis.

1.3. The paramagnetism of iron-sulfur proteins

1.3.1. General

With the sulfur dominated tetrahedral coordination the stable 3+ and 2+ valencies of the iron ions in iron-sulfur clusters are thought to be exclusively in the high spin configuration [157]. Since, with the obvious exception of rubredoxin-like centers, the distance of every iron ion to neighbouring iron ions in iron-sulfur clusters is less than 0.3 nm [12-18,128-132,140,141] the individual spins of the iron ions are sensing each other. The magnetic interaction is sufficiently strong to result in a system which can be described as a single paramagnet with a total effective spin obtained by the vectorial addition of the individual spins of the constituent iron ions. This leaves us on one hand with the attractive perspective that we can treat the iron-sulfur cluster as a single paramagnet but on the other hand imposes the problem to decompose the resulting paramagnetism of the iron-sulfur cluster into contributions from its interacting $d^5 \text{Fe}^{3+}$ spin $S=5/2$ ions and $d^6 \text{Fe}^{2+}$ $S=2$ ions.

An instructive example for spin-coupling is the [2Fe-2S] cluster [157-159]. In the reduced form [2Fe-2S]¹⁺ is composed of one $S=5/2$ ferric and one $S=2$ ferrous ion. The theoretical total spin for the cluster can be between $S=1/2$ (ferromagnetic coupling) and $S=9/2$ (fully antiferromagnetic coupling). One should realize that a quantum mechanical treatment allows vectorial coupling not only to the classic 'antiparallel' $S=1/2$ and 'parallel' $S=9/2$ case, but

also to the intermediate $S=3/2$, $S=5/2$ and $S=7/2$ spin ground states. Fortunately the energetically favoured spin ground state of this cluster is $S=1/2$, giving rise to simple magnetic properties. In the oxidized form $([2\text{Fe}-2\text{S}]^{2+})$ with two $S=5/2$ ferric ions the cluster can be diamagnetic ($S=0$) or have a net spin of $S=1$, $S=2$, $S=3$, $S=4$ or $S=5$. In this case again simplicity rules and $S=0$ is the ground state. The predominance of anti-ferromagnetically coupled configurations results in a remarkably low total resultant spin for most iron-sulfur clusters. In iron-sulfur clusters the spin ground state is well separated from the usually more ferromagnetically coupled excited states [157-159]. The $[2\text{Fe}-2\text{S}]^{2+}$ cluster for instance has an $S=1$ excited state which is $\approx 400 \text{ cm}^{-1}$ above the $S=0$ ground state [161].

The actual description of the spin-coupling in the 3 and 4 Fe-ion containing clusters is more complex. High field Mössbauer studies and theoretical calculations have shown that the magnetic substructures of ferromagnetically coupled dimers are present in these clusters [157-159]. In $[4\text{Fe}-4\text{S}]^{1+}$ antiferromagnetic coupling of a $S=9/2 \text{ Fe}^{2+}\text{-Fe}^{3+}$ mixed valence dimer and a $S=4 \text{ Fe}^{2+}\text{-Fe}^{2+}$ dimer explains the $S=1/2$ ground state. The $[4\text{Fe}-4\text{S}]^{2+}$ cluster is diamagnetic ($S=0$) as a result of antiferromagnetic coupling of two $S=9/2 \text{ Fe}^{2+}\text{-Fe}^{3+}$ mixed valence dimers. In $[4\text{Fe}-4\text{S}]^{3+}$ one of the mixed-valence dimers is oxidized to $\text{Fe}^{3+}\text{-Fe}^{3+}$ which appears to be $S=4$ [160]. Antiferromagnetic coupling of $S=9/2$ and $S=4$ then leads to the observed $S=1/2$ spin ground state. In $[3\text{Fe}-4\text{S}]^{1+}$ two Fe^{3+} ions are coupled to $S=2$ or 3 , which antiferromagnetically couples with $S=5/2$ of the third Fe^{3+} to $S=1/2$.

With the exception of the $S=3/2 \text{ FeMoco}$ [149] and $S \geq 5/2 \text{ P-cluster centers}$ [122-124] of the nitrogenase MoFe protein spin ground states with $S > 1/2$ had not been observed in any iron-sulfur protein until the eighties. In 1980 however the discovery of the $S=2$ ground state in $[3\text{Fe}-4\text{S}]^0$ [81,82,84,86] made it clear that even simple iron-sulfur clusters could have a high-spin ground state. The $S=2$ state arose from the antiferromagnetic coupling of a $S=9/2$ mixed-valence dimer with $S=5/2$ of the third iron. The subsequent discovery of $S \geq 3/2$ spin states in $[4\text{Fe}-4\text{S}(\text{e})]^{1+}$ of glutamine amidotransferase [162], selenium substituted ferredoxin [163] and nitrogenase Fe-protein [164-166] made it clear that the high spin states were not very exceptional but occurred in various iron-sulfur clusters.

A very curious finding was the observation that some $[4\text{Fe}-4\text{S}(\text{e})]^{1+}$ cores not only could exhibit $S=3/2$, $S=5/2$ or $S=7/2$ ground states but that mixtures of species with $S=1/2$ and these $S \geq 3/2$ spins were present [163-166]. Although the occurrence of mixtures of spin states in proteins with paramagnetic centers was well-documented [40,167], this was new for iron-sulfur clusters. By thorough studies on crystallized $[4\text{Fe}-4\text{S}]^{1+}$ model compounds [168-170] it was shown that three main situations could occur:

- 1) Clusters had a 'pure' spin ground state of either $S=1/2$ or $S=3/2$.
- 2) A 'physical spin mixture' of clusters with a pure spin ground state of $S=1/2$ and $S \geq 3/2$ was present.
- 3) The clusters were 'spin-admixed', i.e. the magnetic properties were unlike those of isolated spin ground states and appeared quantummechanically mixed.

Situation 3 has not been encountered yet in protein-bound cubanes. The studies on solvent and nucleotide dependence of the composition of the spin mixture in the nitrogenase iron-protein [164-166] show that very subtle (? steric) changes influence the spin state. This has been corroborated by study of cubane model compounds with different ligands [168-170].

In this thesis (Chapter 5,7 and 8) and in collaborative EPR spectroscopic studies [171,172] the discovery of new examples of high spin systems ($S=3$ and $S=9/2$) and of spin mixtures in iron-sulfur clusters are described. Although the impression might be given that the magnetic properties of iron-sulfur clusters are very complex, one should realize that the vast majority of protein-bound iron-sulfur clusters still exhibits the simple $S=1/2$ or $S=0$ spin ground states. Even though the existence of spin mixtures and/or high spin ground states

complicate matters, the strong magnetic coupling and thermal isolation of the spin ground states makes spectroscopic studies easy compared to weakly coupled systems or spin-admixed systems. Currently no evidence has been obtained for weak coupling, admixtures or cross-over of energy levels of spin states in iron-sulfur clusters.

1.3.2. EPR spectroscopy of iron-sulfur proteins

Although magnetic susceptibility measurements, Mössbauer and (magnetic) circular dichroism spectroscopies all have made vital contributions to the characterization of the paramagnetism of iron-sulfur clusters, EPR spectroscopy seems to be most versatile method. Nearly all iron-sulfur proteins subjected to EPR spectroscopic characterization exhibit signals in at least one redox state. A description of the application of EPR spectroscopy will therefore be given. The reader is referred to reviews [24-27] and specific literature for detailed treatments on EPR [157,159,173-177], Mössbauer [178,179] and MCD spectroscopy [180].

On exposure to an externally applied magnetic field B two energetically different alignments of a paramagnet are possible (the Zeeman effect). In the classic description these energy levels correspond to the parallel and anti-parallel alignment of applied field and the spin of the paramagnet. By administration of electromagnetic radiation the paramagnet can be excited from the lowest to the highest energy level. This is the basis of Electron Paramagnetic Resonance spectroscopy, where in a tunable magnetic field of 0-1 Tesla the interaction with electromagnetic radiation of a constant microwave frequency is used. By this particular set-up (i.e. fixed frequency of radiation) and modulation of the applied magnetic field combined with phase-sensitive detection a high sensitivity is obtained, which allows measurements on picomol to micromol quantities of paramagnets. The price we have to pay for this sensitivity is the unusual appearance of EPR spectra: on the x-axis a magnetic field rather than a frequency or energy is displayed, whereas the y-axis scale is not absorbance but its derivative. The vertical scale can of course easily be transformed into the absorption spectrum by integration (Figure 5). An additional integration (with appropriate correction for transition probability [181,182]) will give the absolute measurement for the number of spins in the sample if the spectrometer has been calibrated with a known standard.

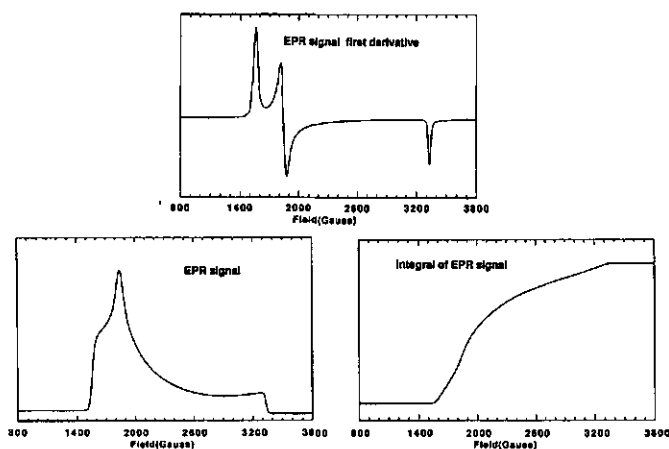


Figure 5: Conversion of the recorded EPR spectrum of the FeMo cofactor of nitrogenase (top trace) into its single and double-integrated form.

To see how information can be extracted from the EPR spectrum we have to inspect the resonance equation (1):

$$\Delta E = h\nu = g\mu_B B \quad (1)$$

in which ΔE is the energy separation of the two Zeeman level, $h\nu$ is the energy of the incident microwave quant, μ_B is the Bohr magneton, B is the applied magnetic field and g is a spectroscopic parameter describing the paramagnet. This so-called g -value characterizes a paramagnet. A free electron in vacuo exhibits an EPR resonance with a g -value of 2.0023, whereas ions, molecules or clusters have different g -values due to spin orbit interaction. These g -values allow identification of compounds by comparison and theoretical calculation.

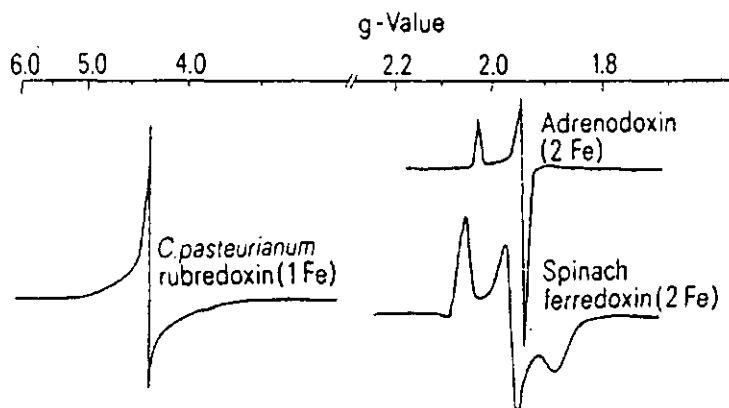


Figure 6: Isotropic (rubredoxin), axial (adrenodoxin) and rhombic (spinach ferredoxin) EPR spectra of iron-sulfur proteins.

However one complicating factor arises because most paramagnetic substances are not spherically symmetric. If a paramagnetic structure like an iron-sulfur cluster is placed in an external field the orientation of the molecule will influence the energy of the transition. This means that each orientation will exhibit a different g -value. If paramagnetic structures in random orientation (a frozen solution for instance) are measured we therefore expect to see an EPR spectrum composed of peaks corresponding to all possible orientations. In the normally recorded derivative of the EPR spectrum three main features (g_x , g_y and g_z), corresponding to the principal axes of the three dimensions are seen (Figure 5 top traces). The EPR spectrum of a system exhibiting different g -values for all three axes is called rhombic. Systems with two equivalent main axes will show two turning points in the EPR spectrum and are called axial (with $g_x = g_y = g_z$ and $g_{||} = g_{\perp}$), systems with a single g -value for the three orientations are denoted as isotropic ($g_x = g_y = g_z$) (see Figure 6). The orientation dependence of the g -values (g -anisotropy) is influenced by the chemical environment and the symmetry of a paramagnet. For iron-sulfur clusters a simple relation between g -anisotropy and the cluster symmetry cannot be made. Rubredoxin, adrenodoxin and spinach ferredoxin exhibit isotropic, axial and rhombic EPR spectra without an obvious direct link with the symmetry of the iron-sulfur centres.

EPR spectra can be simulated by summation of the contributions from the individual spatial orientations. By simulation more accurate information on the g -values and their linewidths can be extracted from a spectrum. It appears that the linewidth, like the g -values, depends on

the orientation. Theoretical models are available to simulate EPR spectra accounting for the combined anisotropy in linewidth and g-value. The observed linewidth of iron-sulfur clusters has three different origins [173,175]:

- 1) The interaction with magnetic metal nuclei, normally only ^{57}Fe , except for mixed metal clusters (V, $^{95/97}\text{Mo}$) (central hyperfine interaction)
- 2) The interaction with ligands (^{33}S , ^{77}Se , ^{17}O , N), solvent and protein (^1H , ^2H , ^{13}C , N, ^{17}O , ^{33}S) (superhyperfine interaction).
- 3) g-strain, which describes the existence of a distribution of the g-values.

By measurements at various microwave frequencies, isotope enrichment and simulation of EPR spectra the combined effect of these three factors affecting line-width can be deconvoluted. The effect of magnetic nuclei on the line-width can be used to probe the presence of the nuclei in and around an iron-sulfur cluster [3,7,70-72,93,171,Chapter 5]. The magnetic (super)hyperfine interaction can also be studied with specialized pulsed EPR techniques like Electron Spin Echo Envelope Modulation (ESEEM) [183] and Electron Nuclear Double Resonance spectroscopy [184].

For an explanation of the extremely important effect of temperature in EPR spectroscopy we have to realize that after absorption of the microwave quantum the paramagnet has to relax back to the Boltzmann equilibrated population of its two energy levels. If this relaxation is very fast (at high temperature) the lifetime is short. By the Heisenberg uncertainty principle this will lead to broadening of the lines of the EPR spectrum. For the typical relaxational properties of iron-sulfur clusters temperatures usually well below 50 K are required. If the incident microwave radiation is sufficiently low (i.e. the system does not saturate), the absorption of the microwave radiation will be proportional to the difference between the relative (Boltzmann) population of the lowest and highest energy level (at temperature T):

$$(1/(1+e^{-\Delta E/kT})) - (e^{-\Delta E/kT}/(1+e^{-\Delta E/kT}))) \approx \Delta E/2kT \quad (2)$$

(for the typical $\Delta=0.3 \text{ cm}^{-1}$ and $T < 100 \text{ K}$). Equation (2) shows that the EPR intensity for a fixed microwave energy is inversely related to temperature (the so-called Curie-Law).

1.3.3 EPR spectroscopy of $S \geq 3/2$ Kramers systems

In the previous treatment it was assumed that a paramagnet exhibited two energy levels on exposure to an external field. A quantummechanical treatment shows that $S > 1/2$ paramagnets even in the absence of a magnetic field have non-degenerate energy levels [173]. The behaviour of spin half-integer or Kramers systems ($S=3/2$, $S=5/2$,...) and spin integer or non-Kramers systems ($S=1$, $S=2$,...) is quite different. Half-integer spin systems have $(S+1/2)$ twofold degenerate levels (the so-called Kramers doublets). An external field splits these doublets linearly leading to a situation bearing a high resemblance to an $S=1/2$ system. Spin integer systems have level pairs of (quasi-)degenerate and a single non-degenerate level (Figure 7). Because in zero-field the doublets are already split and diverge increasingly as a function of the external field, the energy difference is in most cases too large to match the microwave quantum. Only in exceptional cases EPR transitions are observed.

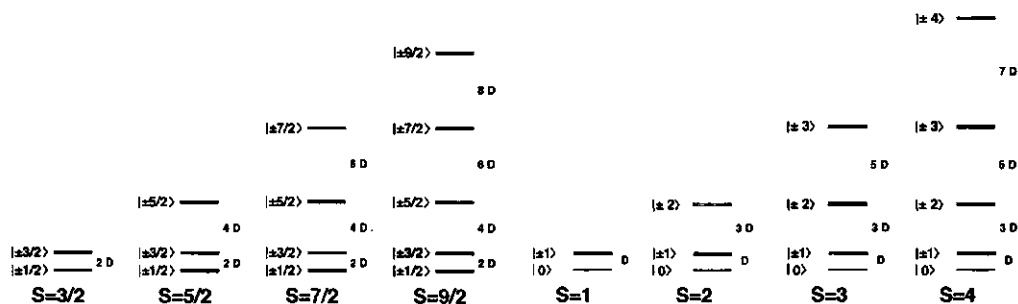


Figure 7: The splitting of energy levels in half-integer and integer spin systems.

The organization of the levels is for axial symmetry without an applied field. The splitting of the Kramers doublets is commonly quantummechanically described by the following Spin Hamiltonian:

$$H = \mathbf{S} \cdot \mathbf{D}' \cdot \mathbf{S} + \beta \mathbf{B} \cdot \mathbf{g} \cdot \mathbf{S} \quad (3)$$

in which the first term presents the zero-field interaction with tensor \mathbf{D}' and the spin vector \mathbf{S} , and the second term is the Zeeman interaction with the \mathbf{g} tensor in applied field \mathbf{B} and spin vector \mathbf{S} (β is the Bohr magneton). The eigenvalues of the Schrödinger equation using this spin Hamiltonian, spin S and its respective spin eigenfunctions $| -S \rangle, | -S+1 \rangle, \dots$ to $| +S \rangle$, corresponding to the allowed spin projections m_s , define the energies of the levels for a given magnetic field, orientation, and \mathbf{D}' and \mathbf{g} tensor. The degenerate pairs of $| -m_s \rangle$ and $| +m_s \rangle$ spin eigenfunctions form the Kramers doublets, also denoted as $| \pm m_s \rangle$. Equation (3) can be rearranged into its well-known representation equation (4) by the substitution of the axial and rhombic zero-field parameters D and E for the diagonal elements of the traceless \mathbf{D}' tensor:

$$H = D[S_z^2 - S(S+1)/3] + E(S_x^2 - S_y^2) + \beta \mathbf{B} \cdot \mathbf{g} \cdot \mathbf{S} \quad (4)$$

With the assumption that the Zeeman term is a perturbation to the zero-field interaction ($\mathbf{S} \cdot \mathbf{D}' \cdot \mathbf{S} \geq \beta \mathbf{B} \cdot \mathbf{g} \cdot \mathbf{S}$, the so-called weak field limit) the energies of the originally degenerate $| -m_s \rangle$ and $| +m_s \rangle$ spin functions split linearly with the magnetic field. An EPR transition can occur if the magnetic field induced splitting matches the microwave quantum (0.3 cm^{-1}). Because the doublets, though split, are energetically well-separated from each other compared to the microwave quantum, the EPR spectrum will be composed of a sum of subspectra from intradoublet transitions. In the weak field limit the search for the magnetic fields B that produce energy-splittings $h\nu$ between the levels of the doublet for a given D , E and \mathbf{g} tensor turns out to be relatively simple. As it happens the effective g -values calculated from the matching magnetic field B and the microwave frequency are independent of the D parameter and the microwave frequency for a given \mathbf{g} tensor and ratio E/D . Mathematically this means that instead of diagonalization with iterations in the magnetic field, we could in reverse also choose a magnetic field and use the resulting eigenvalue of the energy matrix to calculate the effective g -values. If the \mathbf{g} tensor is isotropic and spin-orbit coupling is negligible ($g=2$ along x , y and z axes) the only parameter left for a given total spin S and doublet $| \pm m_s \rangle$ is the ratio E/D . The absolute value of this dimensionless ratio E/D , the so-called rhombicity, can vary between 0 and $1/3$. Effective g -values as a function of the rhombicity have been calculated for the doublets of $S=3/2$ to $S=9/2$ (Chapter 7, [157,176]). Easily applicable representations of these calculations are the so-called rhombograms, in which effective g -

values are plotted as a function of the rhombicity (Figure 8). Each 'stack' forms the set of rhombograms of the individual doublets for a single spin system. Identification of the spin state and rhombicity can be achieved by finding a single vertical line in one of the stacks which matches the observed g -values. Some typical examples for Kramers spin systems in iron-containing proteins, which one can easily identify in Figure 8 are:

$S=3/2$ with $E/D=0.05$ in FeMoco of the MoFe protein $g=4.3$, $g=3.7$ and $g=2.0$ ($|\pm 1/2\rangle$)

$S=5/2$ with $E/D=0.00$ in myoglobin $g_{\perp}=6.0$ and $g_{\parallel}=2.0$ ($|\pm 1/2\rangle$)

$S=5/2$ with $E/D=0.33$ in rubredoxin $g_{\text{isotropic}}=4.3$ ($|\pm 3/2\rangle$), $g=9.7$ ($|\pm 1/2\rangle$ and $|\pm 5/2\rangle$)

$S=7/2$ with $E/D=0.04$ in P^{OX_2} of the MoFe protein $g=10.4$, $g=5.5$ ($|\pm 1/2\rangle$), $g=5.5$ ($|\pm 3/2\rangle$)

$S=9/2$ with $E/D=0.13$ in desulfoviridine $g=17.1$ ($|\pm 1/2\rangle$), $g=9.0$ ($|\pm 3/2\rangle$), $g=9.3$ ($|\pm 5/2\rangle$)

Comparison of the number of possible effective g -values read from the rhombograms with the above listed observable features in the EPR spectra shows that not all of the expected g -values can be detected. Some of the theoretically expected g -values correspond to very high fields which can not be obtained with the normal EPR instrumentation. Even if the g -values are in the detectable range, the amplitude of the EPR features might be too low due to the usual high anisotropy of the g -values. Since it is empirically observed that the spectral linewidth is inversely related to the square of the g -values, generally only the low-field g -values are observed.

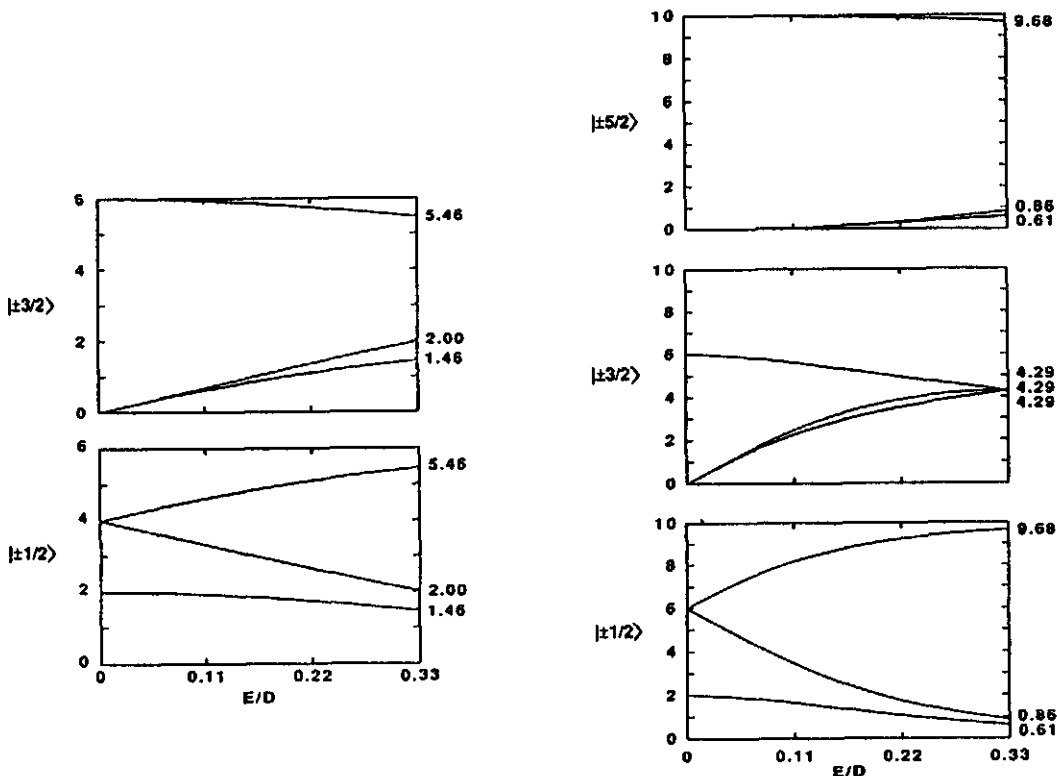
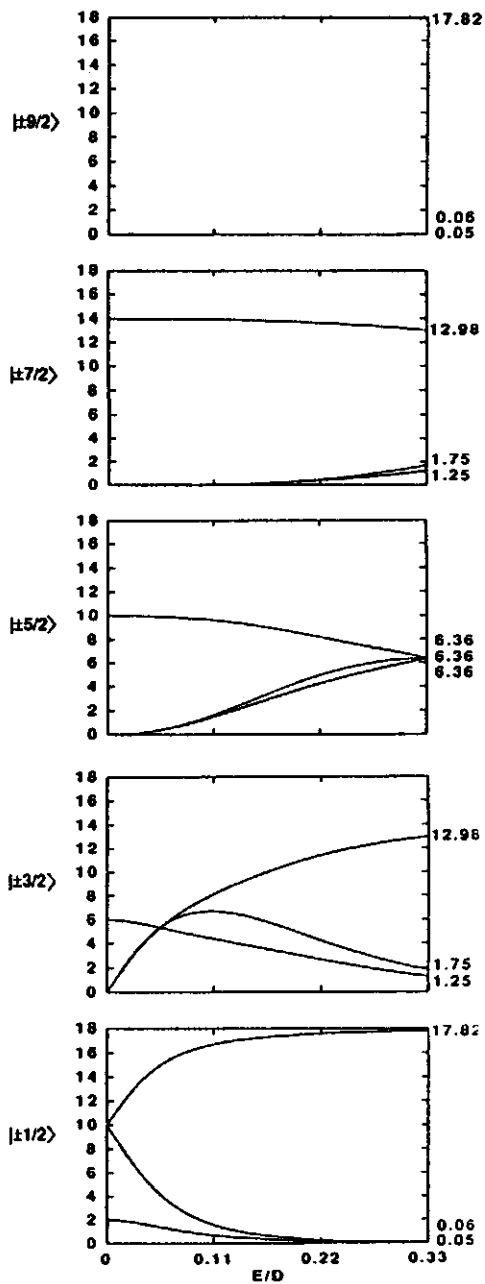
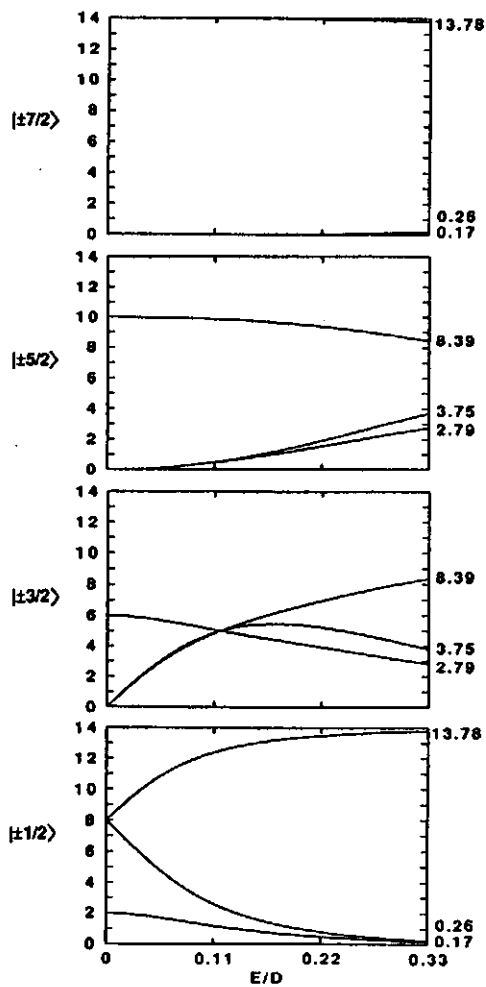


Figure 8a: Rhombograms for $S=3/2$ and $S=5/2$.

Figure 8b: Rhombograms for $S=7/2$ and $S=9/2$.

A fact that has not been considered yet is the relative contribution of the subspectra of the doublets to the resulting EPR spectrum. Although the energies of the doublets are well-separated compared to the 0.3 cm^{-1} energy of the microwave quantum, the thermal energy at the temperatures used for EPR spectroscopy is sufficient to populate doublets other than the ground-state doublet. For a given rhombicity the spacing of the doublets is linear with the axial zero-field splitting parameter D . Thus large D -values mean that only the ground state doublet will be populated significantly. This situation is exhibited by myoglobin ($D=+10 \text{ cm}^{-1}$) in which the $|\pm 3/2\rangle$ doublet lies too high to be sufficiently populated to be detected and only the subspectrum of the $|\pm 1/2\rangle$ ground state is observed. In this particular case the high fractional population of the $|\pm 1/2\rangle$ doublet is an advantage because it raises the contribution of the doublet with the least anisotropic g -values, i.e. the most intense subspectrum. If D values are small thermal energy can populate the other doublets and EPR resonances from other doublets can be observed. This occurs for instance in rubredoxin ($D=+1 \text{ cm}^{-1}$) where even at 4.2 K the $|\pm 3/2\rangle$ and $|\pm 5/2\rangle$ doublets are populated to a significant extent.

There appears to be no theoretical restriction for the sign of the D -value: high spin systems with negative D value have been observed in numerous cases. The negative D -value physically means that the order of the energies of the doublets is reversed. A well-known example is the $S=7/2$ system in the second oxidized form of the P-clusters of the MoFe protein [133]. The EPR non-detectable $|\pm 7/2\rangle$ doublet is lowest in energy. By raising the temperature the $|\pm 5/2\rangle$, $|\pm 3/2\rangle$ and $|\pm 1/2\rangle$ doublets are sequentially populated. Although the $|\pm 7/2\rangle$ and $|\pm 5/2\rangle$ doublets have high populations the anisotropies of their g -values do not allow detection. The $|\pm 3/2\rangle$ and $|\pm 1/2\rangle$ doublets however can be detected at elevated temperatures. The counteracting effect of the Curie-Law and the thermally induced population results in optimal intensity at intermediate temperatures.

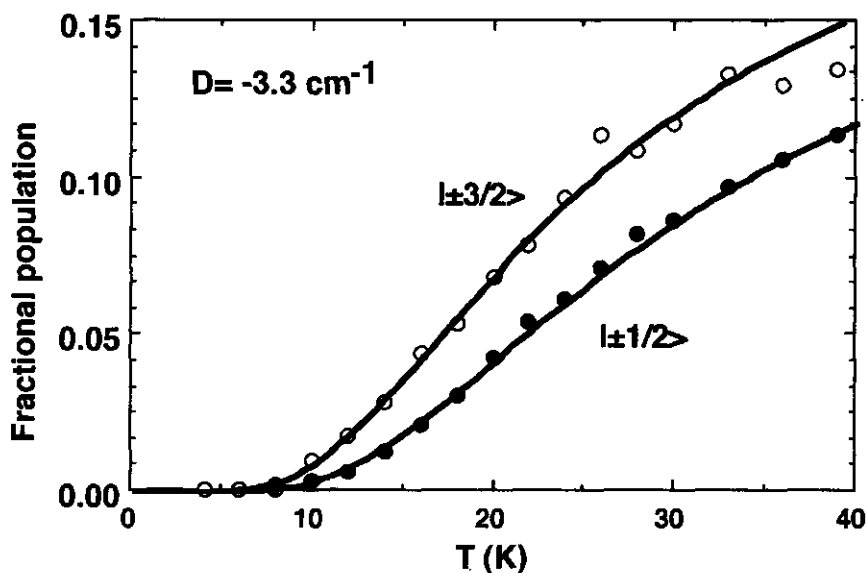


Figure 9: Determination of the D -value for the $S=7/2$ spin system of the oxidized P clusters *Klebsiella pneumoniae* MoFe protein by fitting the temperature dependence of the populations of the $|\pm 1/2\rangle$ and $|\pm 3/2\rangle$ doublets.

The areas enclosed by the $g=10.5$ ($|\pm 1/2\rangle$) and $g=5.68$ peaks ($|\pm 3/2\rangle$) were corrected for the Curie-Law dependence (see also Chapter 8 and [133]).

The study of the temperature dependence does not only confirm the assignment of the spin state, doublet and sign of the D value, but also allows a quantitative determination of the D value. Since the energy spacing of the doublets in multiples of D can be calculated from the eigenvalues of the Spin Hamiltonian for a given E/D , the Curie-Law corrected EPR intensities can be fit to the appropriate Boltzmann equation to determine the magnitude of D . Figure 9 shows the temperature dependence of the $|\pm 3/2\rangle$ and $|\pm 1/2\rangle$ doublets of the $S=7/2$ spin system of the P-clusters in the molybdenum-iron protein of nitrogenase. In this particular case the fit to the Boltzmann equation determined the D value within 10% accuracy. More frequently the loss intensity at higher temperatures due to Curie-Law behaviour and lifetime broadening limits the accuracy of the D value. In nearly all cases an estimation of the magnitude of the D value can be made. This is a useful check of the validity of the weak-field assumption. If the absolute value of D is smaller than 1 cm^{-1} the rhombogram-method can no longer be used. Particularly the EPR resonances at high field will be effected since the Zeeman term for these fields ($\beta B g S$) will be sizeable compared to the zero-field interaction $S \cdot D' \cdot S$ with a small D . The calculation becomes more complicated but can still be performed by solving the Schrödinger equation with iterative steps in the magnetic field for a given g tensor, D and E value until the observed g -value and the input of the field match (Chapter 7, [133,157]).

The accurate determination of D and E/D parameters not only serves a theoretical purpose, but is essential for spin quantitation. This arises first of all from the fact that an EPR observable doublet rarely accounts for the total spin concentration. In some cases the fractional population of an EPR active doublet is much lower than unity, leading to an underestimation of the actual spin concentration. The fact that other doublets can not be detected does not present a major problem as long as the fractional population of the EPR-active doublet is known. The fractional population can easily be evaluated from the energy spacings of the doublets, determined by the D and E/D values. The second important use of the D and E/D parameters originates from the extreme anisotropy of the EPR spectra of some high-spin systems. Since double integration is not possible in numerous cases quantitation has to rely on single integration of the peak-shaped low-field g -values. With the Aasa and Vänngård method [181] the double integral can be calculated if the two high-field g -values are known by theoretical calculation with the E/D and D parameters. Unfortunately the resulting spin quantitation will be less accurate since the errors in D and E/D will propagate not only in the fractional population but also in the single to double integral conversion factor. It has to be kept in mind that spin quantitation both with double and single integration methods assumes that the probability of the microwave induced transitions is 1. Formally only transitions within an $S=1/2$ system and the $|\pm 1/2\rangle$ doublets of high spin Kramers systems with high D values are fully allowed. These transitions obey the selection rule for the normal EPR spectrometer $|\Delta m_s|=1$, since the spin functions of the two levels have a pure $m_s=+1/2$ and $m_s=-1/2$ character. However the assumption that transitions within the $|\pm 3/2\rangle$, $|\pm 5/2\rangle$ or higher doublets are fully allowed is usually made on a pragmatic base rather than theoretically founded. Also, the transition within the $|\pm 1/2\rangle$ doublet of spin systems with a small D -value (Chapter 7) is supposed to be fully allowed, although the levels are not composed of pure $m_s=+1/2$ and $m_s=-1/2$ spin functions but are mixtures with other spin functions. Future theoretical studies are needed to shed light on this neglected aspect of the EPR spectroscopy of high-spin Kramers systems.

1.3.4 EPR spectroscopy of Non-Kramers systems

The study of Non-Kramers systems by EPR spectroscopy is severely complicated by the fact that the separation between the energy levels is too large to match the energy of the micro-wave quantum. In addition the transitions within the 'doublet' levels are not allowed in normal EPR spectroscopy, because $|\Delta_m|=0$. If the Zeeman interaction or the rhombic zero-field splitting mixes in the $m_s=0$ spin function the transitions can become partially allowed, and can in principle be detected by normal EPR spectroscopy [185,186]. In this situation the original notation of $|\pm n\rangle$ doublets does not apply and doublet levels composed of a linear combination of spin functions are denoted as $|n^\pm\rangle$.

By the application of parallel-mode EPR spectroscopy in which the microwave magnetic field and the magnetic field have a parallel orientation the selection rule for EPR transitions can be changed to $|\Delta_m|=0$ [157,167,186]. This enhances transitions of integer spin systems and completely abolishes the EPR signals of Kramers systems (Fig. 10). In practice a dual-mode cavity is used, which can operate both in the normal as well as in the parallel-mode. Still the observation of signals, even in the parallel-mode depends on the splitting of the levels of the non-Kramers doublets. For most integer spin systems the separation Δ between the levels is large. Because the levels are already split in zero-field and the splitting is not linear with the applied field the resonance condition for Kramers systems does not apply.

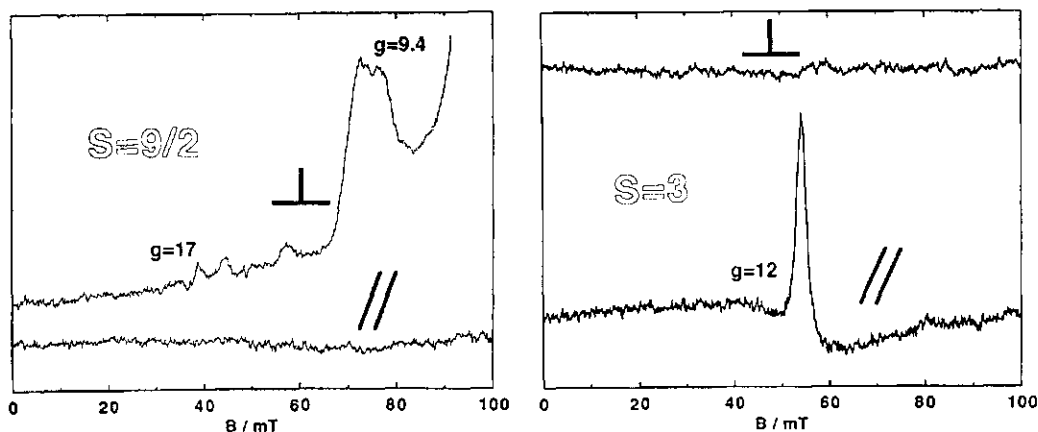


Fig. 10: The use of dual-mode EPR spectroscopy.

Signals from the $S=9/2$ non-integer spin system of dissimulatory sulfite reductase (Chapter 7) are lost in the parallel-mode (left), while signals from the $S=3$ integer spin system of the P-clusters (Chapter 8) show increased intensity (right).

Theoretical treatment [157,167,173,186] shows that for spin integer systems the relevant resonance condition is as following:

$$(h\nu)^2 = (g_{\text{eff}}\beta B)^2 + \Delta^2 \quad (5)$$

For a particular integer spin system the value of Δ is not only a function of spin Hamiltonian parameters but also depends on the orientation. It can be appreciated from equation (5) that

if Δ is comparable to the microwave quantum $h\nu$ the EPR resonance appears to be shifted towards zero-field, regardless of the effective g -value. The orientation dependence of the value of Δ , combined with the angle-dependence of the transition probability and distribution of the value of Δ generally lead to broad resonance signals at low field. Since by approximation the splitting Δ of a non-Kramers doublet $|n^{\pm}\rangle$ is a function of $|D|^*(E/D)^n$ [187,188] the likelihood to observe EPR signals of the $|3^{\pm}\rangle$ or $|4^{\pm}\rangle$ doublets increases (Chapter 5 and 8). However, determination of spin Hamiltonian parameters, spin quantitation and spin state remain difficult compared to Kramers systems.

1.4. Redox-potentiometry

Since all iron-sulfur clusters are stable in two or more redox states it is possible to study the interconversion between the individual redox states. Ideally this interconversion could be studied by classical electrochemistry. For iron-sulfur model compounds the use of cyclic voltammetry is a standard procedure (see [189-191]). With chemically modified working electrodes low-molecular mass iron-sulfur proteins, like rubredoxin, ferredoxin or the soluble domain of the Rieske protein can be studied (Figure 11) [118,119,192,193]. Unfortunately the direct interaction of > 20 kDa iron-sulfur proteins even with modified surfaces is more difficult. Some promising results have been obtained with cyclic or square-wave voltammetry of larger redox-proteins such as lipoamide dehydrogenase [194], succinate dehydrogenase [195], hydrogenase [194,196] and carbon monoxide dehydrogenase [196]. The responses were usually weak compared to low-molecular mass redox-proteins. It is thought that irreversible binding to electrode surfaces or the buried nature of redox centers prevents facile interactions with the electrode [118,119,194].

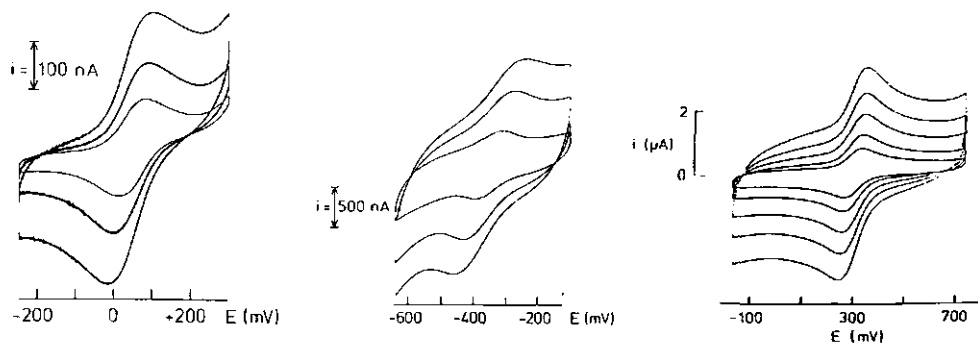


Fig. 11: Direct electrochemistry of low-molecular mass iron-sulfur proteins.

Cyclic voltammograms of *Megasphaera elsdenii* rubredoxin and ferredoxin (left and middle) and the soluble fragment of the bovine mitochondrial Rieske protein (right) allow a direct room temperature measurement of the redox-midpoint potential. The individual traces are recorded with scan rates from 1-100 mV s^{-1} .

(from [118] and [193]).

The general procedure to overcome this electrochemical inertness of redox-proteins uses so-called redox-mediators [197-199]. Redox-mediators are water-soluble organic dyes with well-known electrochemical properties [200], which can act as reporter molecules of redox

potential of the solution in absence of protein-electrode interaction. The redox-potential of the solution can be adjusted coulometrically [192,197,201] or as is more frequently done, with sodium dithionite or borohydride, titanium(III)citrate, potassium ferricyanide, or xanthine/xanthine oxidase (this thesis, [197-200,202,203]). The inherent problem is that the electrochemical response in cyclic voltammetry is not a function of the protein but of the mediators. Clearly other methods should be used to measure the redox state of the protein, while measuring the redox potential with the help of the mediators. A crucial assumption is that the mediators interact reversibly with the protein, resulting in a redox-equilibrium between oxidized and reduced mediators and the redox centers of the protein [197,198]. Usually the spectroscopic and biochemical properties (for instance enzymatic activity) are not influenced by the presence of mediators (this thesis).

In principle measurement of the redox state of an (iron-sulfur) protein can be done with UV-visible (UV-vis) and Circular Dichroism (CD) spectrophotometry [197,199] or even NMR spectroscopy [204] or room temperature EPR spectroscopy [205,206], since changes in spectra accompany a redox transition. For proteins like cytochromes, with very intense and sharp UV-vis and CD absorption bands the redox state is easily monitored ([198] and refs. therein). Unfortunately most mediating dyes and reductants/oxidants have relatively high contributions notably to the UV-vis spectra, while the spectral changes associated with the redox transition of iron-sulfur proteins are of low intensity. With exception of some low molecular mass iron-sulfur proteins [199] UV-vis or CD spectroscopy can not be used (note that these low-molecular mass [Fe-S] proteins are more conveniently studied by cyclic voltammetry!). The redox state thus has to be monitored with other, low temperature techniques, like EPR, Magnetic Circular Dichroism or Mössbauer spectroscopies. Although the necessary freezing of the mediator-protein mixture could induce changes of the redox equilibrium, redox (midpoint) potential ($dE_m/dT = \Delta S/(nF)$) and pH, it is known from simple iron-sulfur proteins, which can be studied both at room temperature and after freezing, that only minor changes occur [118,193,198]. Presumably the freezing process is faster than the temperature-induced redox-changes, so that the room temperature equilibrium population of oxidized and reduced iron-sulfur centers is maintained. Once frozen, no changes of the redox states of mediators and iron-sulfur centers can occur, as diffusional processes followed by electron transfer are stopped.

EPR spectroscopy is the method of choice for the measurement of the redox state in mediated titrations. The benefits of easy accessibility, low sample volume, (high) sensitivity and financial aspects (^{57}Fe , instrument, liquid He consumption) made and still makes the EPR technique superior over Mössbauer and MCD spectroscopies. However the parallel use of MCD and Mössbauer spectroscopy should be considered: particularly for very complex iron-sulfur proteins like nitrogenase [122,207,208]. Since almost any iron-sulfur center exhibit an EPR signal either in the oxidized or in the reduced state EPR spectroscopy is applicable for most iron-sulfur proteins. With a proper choice of temperature and microwave power sufficient resolution can be obtained if an iron-sulfur protein contains more than one cluster or other prosthetic groups (Chapter 2, 5, 7, 8 and 9).

The mediated redox-titration technique has been applied for a number of iron-sulfur proteins. Characteristic examples of the appearance of the redox titration curves are schematically shown in Figure 12. The three relevant equations, derived from the Nernst equation, describing the reversible part of the titration curves are as following:

$$\begin{aligned} \text{intensity of signal in reduced form} &= k/(1+\exp((E-E_1)*nF/RT)) & (6) \\ \text{intensity of signal in oxidized form} &= k/(1+\exp((E_1-E)*nF/RT)) & (7) \\ \text{intensity of signal in intermediate form} &= k/(1+\exp((E_2-E)*nF/RT)+\exp((E-E_3)*nF/RT)) & (8) \end{aligned}$$

in which k is a conversion factor to fit the measured EPR amplitude. E is the solution

potential as measured in the presence of mediators or alternatively set by equilibration with the H_2/H^+ (Chapter 2) or NADH/NAD^+ couple [199]. E1 is the redox midpoint potentials of an iron-sulfur site with only two redox states, whereas in (8) E2 and E3 refer to the low and high redox-potential redox transition of an iron-sulfur cluster with three redox states. R is the gas constant, T the absolute temperature, n is the number of electrons involved in the redox

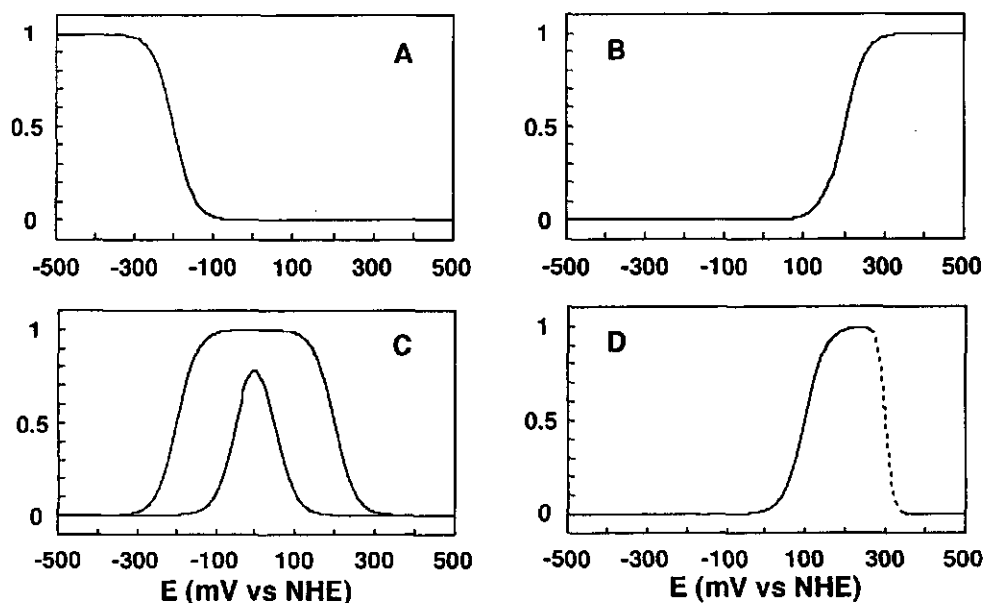


Fig. 12: Titration curves for some typical cases encountered with iron-sulfur proteins.

The vertical axis represents the relative intensity of EPR signals.

(A) The reduced cluster exhibits an EPR signal ($E_m = -200$ mV, $n=1$).

(B) The oxidized cluster exhibits an EPR signal ($E_m = +200$ mV, $n=1$).

(C) A cluster exhibits an EPR signal in an intermediate redox state, which attains full intensity (upper curve $E_m = -200$ mV & $+200$ mV, both $n=1$) or disproportionates (lower curve $E_m = -50$ mV & 50 mV, $n=1$).

(D) The oxidized cluster exhibits an EPR signal ($E_m = +100$ mV, $n=1$), but breakdown is observed at high potentials (dashed curve).

reaction and F is the Faraday constant. By a least-squared fit of the EPR amplitudes to the respective equations, the number of electrons involved and the redox midpoint potential(s) can be determined. Usually the accuracy of midpoint potentials is $\pm(5-50)$ mV, whereas the determination of the number of electrons involved is more cumbersome, due to slow equilibration or a limited number of data points close to the redox transition.

The information content of redox midpoint potentials per se is not the most informative issue. Equally important results are obtained by combination of EPR integration of the titration maxima and by the change of spin state (Chapter 2, 5 and 7-9). With titration experiments the redox state of the iron-sulfur clusters could be controlled more accurately and better-characterized redox states other than dithionite or ascorbate-reduced, as-isolated and thionine or potassium ferricyanide oxidized could be obtained. In fact the titration techniques has revealed new redox states, which have escaped attention in previous studies [122-124].

1.5. Outline of this thesis

Although three-dimensional structures or predicted structures heretofore based on spectroscopic evidence are available for most iron-sulfur proteins a number of multiple-electron transferring enzymes, like hydrogenase, sulfite reductase and nitrogenase MoFe protein have enigmatic iron-sulfur clusters. Their spectroscopic properties are not known in sufficient detail to identify or compare their constituent iron-sulfur clusters. Therefore the goal of this thesis is to unravel the redox and paramagnetic properties of these clusters by combined biochemical and spectroscopic studies on these unusual iron-sulfur proteins.

Initially the research started with the Fe-only hydrogenase isolated from the sulfate-reducing bacterium *Desulfovibrio vulgaris* (Hildenborough). Although the efforts to obtain the $g=5$ EPR signal [126,127] by dye-mediated redox titrations were not successful it was discovered that the titration experiments described by Patil and coworkers [209] were severely hampered by hysteresis, mal-equilibration due to activation of the oxygen-stable form and catalytic activity in the reduced form. Chapter 2 describes the reinvestigation of the redox properties and summarizes the results of extensive metal analyses and the resolution of the hydrogenase into fractions with low and high catalytic activity.

In the course of FPLC purification of the hydrogenase it was observed that a novel iron-sulfur protein with highly unusual EPR spectroscopic properties occasionally contaminated hydrogenase preparations. The dithionite reduced protein exhibited EPR signals reminiscent of prismane model compounds (Chapter 3). Since, based on chemical analysis a 6Fe-containing iron-sulfur cluster had been proposed for the H-cluster of the Fe-hydrogenase, this obviously prompted a more extensive investigation of the putative prismane-containing protein (Chapter 4 and 5). The iron-sulfur cluster of the as isolated protein appeared to occur as a spin mixture of $S=1/2$ and $S=9/2$ species. Multifrequency EPR and Mössbauer spectroscopy combined with redox titrations have been performed to characterize the iron-sulfur cluster in more detail. Subsequently Stokkermans and coworkers have identified and sequenced the gene coding for this protein and the corresponding protein from *Desulfovibrio desulfuricans* (ATCC 27774) [210-212].

The discovery of the unusual redox and EPR spectroscopic properties of this 'prismane protein' led to the investigation of three other complicated multi-electron transferring iron-sulfur enzymes: dissimilatory sulfite reductase, carbonmonoxide dehydrogenase and nitrogenase MoFe protein. Dissimilatory sulfite reductase was a readily available iron-sulfur enzyme obtained during the isolation of Fe-hydrogenase from *Desulfovibrio vulgaris* (Hildenborough). The scrutiny for pure and electrophoretic homogeneous preparations of the dissimilatory sulfite reductase for EPR spectroscopic studies unexpectedly led to the discovery of a third hitherto unrecognised 11 kDa subunit in this enzyme (Chapter 6). Recently the gene coding for the 11 kDa polypeptide has been sequenced [213].

Chapter 7 delineates the redox and spectroscopic results on the siroheme and $S=9/2$ superspin EPR signals of the dissimilatory sulfite reductase. The $S=9/2$ EPR signals are interpreted as evidence for the presence of a larger iron-sulfur supercluster. $S=9/2$ EPR signals from an iron-sulfur cluster with similar redox properties were also observed in carbonmonoxide dehydrogenase from *Methanothrix soehngenii*. The collaborative results on the cluster with $S=9/2$ and the other paramagnetic centers of the carbonmonoxide dehydrogenase have been described in the thesis of Jetten [148,171,214].

In Chapter 8 the redox and EPR spectroscopic properties of the nitrogenase MoFe protein from *Azotobacter vinelandii* are described. A long lasting controversy on the spin and redox states of the P-cluster iron-sulfur centers [122-124,133,134,152] was solved by the discovery of non-Kramers $g=12$ (parallel-mode) EPR signals for the two electron-oxidized form and observation of a spin mixture of $S=1/2$ and $S=7/2$ species in the three electron-oxidized form. It will be shown that in case of the MoFe protein $S=9/2$ EPR signals are not

associated with active enzyme.

During the efforts to obtain highly-purified Fe-hydrogenase and prismane protein from *Desulfovibrio vulgaris* (Hildenborough) a black protein was discovered. The biochemical and EPR spectroscopic properties were similar but not identical to the protein rubrerythrin isolated by LeGall and coworkers [42]. The protein was called nigerythrin due to its black color and dinuclear iron centers which exhibited an hemerythrin-like EPR signal.

Review tables are presented in Chapter 10 to give an update of the position of high spin systems in iron-sulfur proteins. In Chapter 11 the findings of this thesis are summarized.

References

1. Beinert, H. & Sands, R.H. (1959) Biochem. Biophys. Res. Comm. **1**, 171-174.
2. Beinert, H. & Lee, W. (1961) Biochem. Biophys. Res. Comm. **5**, 40-45.
3. Shethna, Y.I., Wilson, P.W., Hansen, R.E. & Beinert, H. (1964) Proc. Nat. Acad. Sci. **52**, 1263-1271.
4. Rieske, J.S., MacLennan, D.H. & Coleman, R. (1964) Biochem. Biophys. Res. Commun. **15**, 338-344.
5. Palmer, G. & Sands, R.H. (1966) J. Biol. Chem. **241**, 253.
6. Shethna, Y.I., Wilson, P.W. & Beinert, H. (1966) Biochim. Biophys. Acta **113**, 225-234.
7. DerVartanian, D.V., Orme-Johnson, W.H., Hansen, R.E. & Beinert, H. (1967) Biochem. Biophys. Res. Comm. **26**, 569-576.
8. Fry, K.T. & San Pietro, A. (1962) Biochem. Biophys. Res. Comm. **9**, 218-221.
9. Lovenberg, W., Buchanan, B.B. & Rabinowitz, J.C. (1963) J. Biol. Chem. **238**, 3899-3913.
10. Brumby, P.E., Miller, R.W. & Massey, V. (1965) J. Biol. Chem. **240**, 2222-2228.
11. Cammack, R. (1992) In: Advances in Inorganic Chemistry 38: Iron-Sulfur Proteins (Cammack, R. & Sykes, A.G., eds), pp. 281-322, Academic Press, San Diego.
12. Dauter, Z., Sieker, L.C. & Wilson, K.S. (1992) Acta Crystallogr. B **48**, 42-59.
13. Tsukihara, T., Fukuyama, K., Nakamura, M., Katsube, Y., Tanaka, N., Kakudo, M., Hase, T., Wada, K. & Matsubara, H. (1981) J. Biochem. **90**, 1763-1773.
14. Sheridan, R.P., Allen, L.C. & Carter, C.W. (1981) J. Biol. Chem. **256**, 5052-5057.
15. Backes, G., Mino, Y., Loehr, T.M., Meyer, T.E., Cusanovich, M.A., Sweeney, W.V., Adman, E.T., Sanders-Loehr, J. (1991) J. Am. Chem. Soc. **113**, 2055-2064.
16. Martin, A.E., Burgess, B.K., Stout, C.D., Cash, V.L., Dean, D.R., Jensen, G.M. & Stephens, P.J. (1990) Proc. Natl. Acad. Sci. USA **87**, 598-602.
17. Lauble, H., Kennedy, M.C., Beinert, H. & Stout, C.D. (1992) Biochemistry **31**, 2735-2748.
18. Georgiadis, M.M., Komiyama, H., Chakrabarti, P., Woo, D., Kornuc, J.J. & Rees, D.C. (1992) Science **257**, 1653-1659.
19. Orme-Johnson, W.H. & Orme-Johnson, N.R. (1978) Methods Enzymol. **53**, 259-274.
20. Xavier, A.V., Moura, J.J.G. & Moura, I. (1981) Structure Bonding **43**, 187-213.
21. Dreyer, J.-L. (1982) Experientia **38**, 521-529.
22. Thomson, A.J. (1985) Metalloproteins 1 (Harrison, P., ed.), pp 79-120, Verlag Chemie, Weinheim, Germany.
23. Beinert, H. & Kennedy, M.C. (1989) Eur. J. Biochem. **186**, 5-15.
24. Lovenberg, W. (ed.) (1973) Iron-Sulfur Proteins, Vol. I and II, Academic Press, New York.
25. Lovenberg, W. (ed.) (1977) Iron-Sulfur Proteins, Vol. III, Academic Press, New York.
26. Spiro, T.G. (ed.) (1982) Iron-Sulfur Proteins (Metal Ions in Biology volume 4), Wiley, New York.
27. Cammack, R. & Sykes, A.G. (eds.) (1992) Iron-Sulfur Proteins, (Advances in Inorganic

- Chemistry 38), Academic Press, San Diego.
28. Lovenberg, W. & Sobel, B.E. (1965) Proc. Natl. Acad. Sci. USA **54**, 193-199.
 29. Peisach, J., Blumberg, W.E., Lode, E.T. & Coon, M.J. (1971) J. Biol. Chem. **246**, 5877-5881.
 30. Lovenberg, W. & Walker, M.N. (1978) Methods Enzymol. **53**, 340-346.
 31. Moura, I., Moura, J.J.G., Santos, H.H., Xavier, A.V. and LeGall, J. (1979) FEBS Lett. **107**, 419-421.
 32. Watenpugh, K.D., Sieker, L.C. & Jensen, L.H. (1979) J. Mol. Biol. **131**, 509-522.
 33. Voordouw, G. (1988) Gene **69**, 75-83.
 34. Blake, P.R., Park, J.-B., Bryant, F.O., Aono, S., Magnuson, J.K., Eccleston, E., Howard, J.B., Summers, M.F. & Adams, M.W.W. (1991) Biochemistry **30**, 10885-10895.
 35. Blake, P.R., Park, J.-B., Adams, M.W.W. & Summers, M.F. (1992) J. Am. Chem. Soc. **114**, 4931-4933.
 36. Mathieu, I., Meyer, J. & Moulis, J.-M. (1992) Biochem. J. **285**, 255-262.
 37. Moura, I., Bruschi, M., LeGall, J., Moura, J.J.G. and Xavier, A.V. (1977) Biochem. Biophys. Res. Comm. **75**, 1037-1044.
 38. Moura, I., Xavier, A.V., Cammack, R., Bruschi, M. and LeGall, J. (1978) Biochim. Biophys. Acta **533**, 156-162.
 39. Bruschi, M., Moura, I., LeGall, J., Xavier, A.V., and Sieker, L.C. (1979) Biochem. Biophys. Res. Comm. **90**, 596-605.
 40. Moura, I., Huynh, B.H., Hausinger, R.P., LeGall, J., Xavier, A.V. & Münck, E. (1980) J. Biol. Chem. **255**, 2493-2498.
 41. Brumlik, M.J., Leroy, G., Bruschi, M. & Voordouw, G. (1990) J. Bact. **172**, 7289-7292.
 42. LeGall, J., Prickril, B.C., Moura, I., Xavier, A.V., Moura, J.J.G. & Huynh, B.-H. (1988) Biochemistry **27**, 1636-1642.
 43. Sieker, L.C., Turley, S., Prickril, B.C. & LeGall, J. (1988) Proteins: Struct., Funct., Genet. **3**, 184-186.
 44. Liu, M.-Y. & LeGall, J. (1990) Biochem. Biophys. Res. Comm. **171**, 313-318.
 45. Kurtz, D.M. & Prickril, B.C. (1991) Biochem. Biophys. Res. Comm. **181**, 337-341.
 46. Prickril, B.C., Kurtz, D.M., LeGall, J. & Voordouw, G. (1991) Biochemistry **30**, 11118-11123.
 47. Beeumen, J.J. Van, Driessche, G. Van, Liu, M.-Y. & LeGall, J. (1991) J. Biol. Chem. **266**, 20645-20653.
 48. Brumlik, M.J. & Voordouw, G. (1989) J. Bact. **171**, 4996-5004.
 49. Moura, I., Tavares, P., Moura, J.J.G., Ravi, N., Huynh, B.H., Liu, M.-Y. & LeGall, J. (1990) J. Biol. Chem. **265**, 21596-21602.
 50. Adman, E.T., Sieker, L.C. & Jensen, L.H. (1991) J. Mol. Biol. **217**, 337-352.
 51. Stenkamp, R.E., Sieker, L.C. & Jensen, L.H. (1990) Proteins, Struct. Funct. Genet. **8**, 352-364.
 52. Frey, M., Sieker, L.C., Payan, F., Haser, R., Bruschi, M., Pepe, G. & LeGall, J. (1987) J. Mol. Biol. **197**, 525-541.
 53. LeGall, J. (1968) Ann. Inst. Pasteur (Paris) **114**, 109-115.
 54. Petitdemange, H., Marczak, R., Blusson, H. & Gay, R. (1979) Biochem. Biophys. Res. Comm. **91**, 1258-1265.
 55. Peterson, J.A., Basu, D. & Coon, M.J. (1966) J. Biol. Chem. **241**, 5162-5164.
 56. Kok, M., Oldenhuis, R., Van der Linden, M.P.G., Meulenberg, C.H.C., Kingma, J. & Witholt, B. (1989) J. Biol. Chem. **264**, 5442-5451.
 57. Kortlüke, C., Horstmann, K., Schwartz, E., Rohde, M., Binsack, R. & Friedrich, B. (1992) J. Bact. **174**, 6277-6289.
 58. Wang, D.L., Holz, R.C., David, S.S., Que, L. & Stankovich, M.T. (1991) Biochemistry **30**, 8187-8194.

59. Holmes, M.A., Letrong, I., Turley, S., Sieker, L.C. & Stenkamp, R.E. (1991) J. Mol. Biol. **218**, 583-593.
60. Nordlund, P., Sjöberg, B.M. & Eklund, H. (1990) Nature **345**, 593-598.
61. Gerez, C., Atta, M., Fontecave, M., Gaillard, J., Scheer, C. & Latour, J.M. (1991) J. Inorg. Biochem. **43**, 536.
62. Doi, K., Antanaitis, B.C. & Aisen, P. (1988) Struct. Bonding **70**, 1-26.
63. Woodland, M.P., Patil, D.S., Cammack, R. & Dalton, H. (1986) Biochim. Biophys. Acta **873**, 237-242.
64. Liu, K.E. & Lippard, S.J. (1991) J. Biol. Chem. **266**, 12836-12839.
65. Mortenson, L.E., Valentine, R.C. & Carnahan, J.E. (1962) Biochem. Biophys. Res. Commun. **7**, 448-452.
66. Tagawa, K. & Arnon, D.I. (1962) Nature **195**, 537-543.
67. Dus, K., DeKlerk, H., Sletten, K. & Bartsch, R.G. (1967) Biochim. Biophys. Acta **140**, 291-311.
68. Suzuki, K. & Kimura, T. (1965) Biochem. Biophys. Res. Commun. **19**, 340-345.
69. Cushman, D.W., Tsai, R.L. & Gunsalus, I.C. (1967) Biochem. Biophys. Res. Commun. **26**, 577-583.
70. Tsibris, J.C.M., Namtvedt, M.J. & Gunsalus, I.C. (1968) Biochem. Biophys. Res. Commun. **30**, 323-327.
71. Tsibris, J.C.M., Tsai, R.L., Gunsalus, I.C., Orme-Johnson, W.H., Hansen, R.E. & Beinert, H. (1968) Proc. Natl. Acad. Sci. USA **59**, 959-965.
72. Orme-Johnson, W.H., Hansen, R.E., Beinert, H., Tsibris, J.C.M., Bartholomaeus, R.C. & Gunsalus, I.C. (1968) Proc. Natl. Acad. Sci. USA **60**, 368-372.
73. Herriott, J.R., Sieker, L.C., Jensen, L.H. & Lovenberg, W. (1970) J. Mol. Biol. **50**, 391-406.
74. Carter, C.W., Freer, S.T., Xuong, N.H., Alden, R.A. & Kraut, J. (1971) Cold Spring Harbor Symp. Quant. Biol. **36**, 381-385.
75. Adman, E.T., Sieker, L.C. & Jensen, L.H. (1973) J. Biol. Chem. **248**, 3987-3996.
76. Mayerle, J.J., Frankel, R.B., Holm, R.H., Ibers, J.A., Phillips, W.D. & Weiher, J.F. (1973) Proc. Natl. Acad. Sci. USA **70**, 2429-2433.
77. Herskovitz, T., Averill, B.A., Holm, R.H., Ibers, J.A., Phillips, W.D. & Weiher, J.F. (1972) Proc. Natl. Acad. Sci. USA **69**, 2437-2441.
78. Carter, C.W., Kraut, J., Freer, S.T., Alden, R.A., Sieker, L.C., Adman, E. & Jensen, L.H. (1972) Proc. Nat. Acad. Sci. USA **69**, 3526-3529.
79. Dunham, W.R., Bearden, A.J., Salmeen, I.T., Palmer, G., Sands, R.H., Orme-Johnson, W.H. & Beinert, H. (1971) Biochim. Biophys. Acta **253**, 134-152.
80. Fukuyama, K., Hase, T., Matsumoto, S., Tsukihara, T., Katsube, Y., Tanaka, N., Kakudo, M., Wada, K. & Matsubara, H. (1980) Nature **286**, 522-524.
81. Emptage, M.H., Kent, T.A., Huynh, B.H., Rawlings, J., Orme-Johnson, W.H. & Münck, E. (1980) J. Biol. Chem. **255**, 1793-1796.
82. Huynh, B.H., Moura, J.J.G., Moura, I., Kent, T.A., LeGall, J., Xavier, A.V. & Münck, E. (1980) J. Biol. Chem. **255**, 3242-3244.
83. Stout, C.D., Ghosh, D., Pattabhi, V. & Robbins, A.H. (1980) J. Biol. Chem. **255**, 1797-1800.
84. Thomson, A.J., Robinson, A.E., Johnson, M.K., Cammack, R., Rao, K.K. & Hall, D.O. (1981) Biochim. Biophys. Acta **637**, 423-432.
85. Bell, S.H., Dickson, D.P.E., Johnson, C.E., Cammack, R., Hall, D.O. & TRao, K.K. (1982) FEBS Lett. **142**, 143-146.
86. Kent, T.A., Dreyer, J.-L., Kennedy, M.C., Huynh, B.H., Emptage, M.H., Beinert, H. & Münck, E. (1982) Proc. Natl Acad. Sci. USA **79**, 1096-1100.
87. Peisach, J., Beinert, H., Emptage, M.H., Mims, W.B., Fee, J.A., Orme-Johnson, W.H.,

- Rendina, A.R. & Orme-Johnson, N.R. (1983) J. Biol. Chem. **258**, 13014-13016.
88. Beinert, H., Emptage, M.H., Dreyer, J.-L., Scott, R.A., Hahn, J.E., Hodgson, K.O. & Thomson, A.J. (1983) Proc. Natl. Acad. Sci. USA **80**, 393-396.
89. Antonio, M.R., Averill, B.A., Moura, I., Moura, J.J.G., Orme-Johnson, W.H., Teo, B.-K. & Xavier, A.V. (1982) J. Biol. Chem. **257**, 6646-6649.
90. Stout, C.D. (1988) J. Biol. Chem. **263**, 9256-9260.
91. Stout, G.H., Turley, S., Sieker, L.C. & Jensen, L.H. (1988) Proc. Nat. Acad. Sci. USA **85**, 1020-1022.
92. Emptage, M.H., Dreyer, J.-L., Kennedy, M.C. & Beinert, H. (1983) J. Biol. Chem. **258**, 11106-11111.
93. Beinert, H. & Kennedy, M.C. (1989) Eur. J. Biochem **186**, 5-15.
94. Switzer, R.L. (1989) BioFactors **2**, 77-86.
95. Flint, D.H. & Emptage, M.H. (1988) J. Biol. Chem. **263**, 3558-3564.
96. Fu, W., O'Handley, S., Cunningham, R.P. & Johnson, M.K. (1992) J. Biol. Chem. **267**, 16135-16137.
97. Thomson, A.J. (1992) FEBS Letters **285**, 230-236.
98. Prodromou, C., Artymiuk, P.J. & Guest, J.R. (1992) Eur. J. Biochem. **204**, 599-609.
99. Fee, J.A., Findling, K.L., Yoshida, T., Hille, R., Tarr, G.E., Hearshen, D.O., Dunham, W.R., Day, E.P., Kent, T.A. & Münck, E. (1984) J. Biol. Chem. **259**, 124-133.
100. Batic, C.J., La Haie, E. & Ballou, D.P. (1987) J. Biol. Chem. **262**, 1510-1518.
101. Gurbiel, R.J., Batic, C.J., Sivaraja, M., True, A.E., Fee, J.A., Hoffmann, B.M. & Ballou, D.P. (1989) Biochemistry **28**, 4861-4871.
102. Gurbiel, R.J., Ohnishi, T., Robertson, D.E., Daldal, F. & Hoffman, B.M. (1991) Biochemistry **30**, 11579-11584.
103. Krauss, N., Hinrichs, W., Witt, I., Fromme, P., Pritzkow, W., Dauter, Z., Betzel, C., Wilson, K.S., Witt, H.T., Saenger, W. (1993) Nature **361**, 326-331.
104. Voordouw, G., Hagen, W.R., Krüse-Wolters, M., Van Berkel-Arts, A. & Veeger, C. (1987) Eur. J. Biochem. **162**, 31-36.
105. Ta, D.T. & Vickery, L.E. (1992) J. Biol. Chem. **267**, 11120-11125.
106. Uhlmann, H., Beckert, V., Schwarz, D. & Bernhardt, R. (1992) Biochem. Biophys. Res. Commun. **188**, 1131-1138.
107. Davasse, V. & Moulis, J.-M. (1992) Biochem. Biophys. Res. Commun. **185**, 341-349.
108. Kent, H.M., Ioannidis, I., Gormal, C., Smith, B.E. & Buck, M. (1989) Biochem. J. **264**, 257-264.
109. Lowery, R.G., Chang, C.L., Davis, L.C., McKenna, M.-C., Stephens, P.J. & Ludden, P.W. (1989) Biochemistry **28**, 1206-1212.
110. Manodori, A., Cecchini, G., Schröder, I., Gunsalus, R.P., Werth, M.T. & Johnson, M.K. (1992) Biochemistry **31**, 2703-2712.
111. Zhao, J., Li, N., Warren, P.V., Golbeck, J.H. & Bryant, D.A. (1992) Biochemistry **31**, 5093-5099.
112. Soman, J., Iismaa, S. & Stout, C.D. (1991) J. Biol. Chem. **266**, 21558-21562.
113. Gaillard, J., Albrand, J.-P., Moulis, J.-M. & Wemmer, D.E. (1992) Biochemistry **31**, 5632-5639.
114. Busse, S.C., La Mar, G.N. & Howard, J.B. (1991) J. Biol. Chem. **266**, 23714-23723.
115. Skjeldal, L., Markley, J.L., Coghlan, V.M. & Vickery, L.E. (1991) Biochemistry **30**, 9078-9083.
116. Ye, X.M., Pochapsky, T.C. & Pochapsky, S.S. (1992) Biochemistry **31**, 1961-1968.
117. Cheng, H., Grohmann, K. & Sweeney, W. (1992) J. Biol. Chem. **267**, 8073-8080.
118. Hagen, W.R. (1989) Eur. J. Biochem. **182**, 523-530.
119. Armstrong, F.A. (1992) In: Advances in Inorganic Chemistry 38: Iron-Sulfur Proteins (Cammack, R. & Sykes, A.G., eds), pp. 117-163, Academic Press, San Diego.

120. Shah, V.K. & Brill, W.J. (1977) Proc. Natl Acad. Sci. USA **74**, 3249-3253.
121. Rawlings, J., Shah, V.K., Chisnell, J.R., Brill, W.J., Zimmermann, R., Münck, E. & Orme-Johnson, W.H. (1978) J. Biol. Chem. **253**, 1001-1004.
122. Zimmermann, R., Münck, E., Brill, W.J., Shah, V.K., Henzl, M.T., Rawlings, J. & Orme-Johnson, W.H. (1978) Biochim. Biophys. Acta **537**, 185-207.
123. Huynh, B.H., Münck, E. & Orme-Johnson, W.H. (1979) Biochim. Biophys. Acta **527**, 192-203.
124. Huynh, B.H., Henzl, M.T., Christner, J.A., Zimmermann, R., Orme-Johnson, W.H. & Münck, E. (1980) Biochim. Biophys. Acta **623**, 124-138.
125. Hagen, W.R., Van Berkel-Arts, A., Krüse-Wolters, K.M., Voordouw, G. & Veeger, C. (1986) FEBS Letters **203**, 59-63.
126. Hagen, W.R., Van Berkel-Arts, A., Krüse-Wolters, K.M., Dunham, W.R. & Veeger, C. (1986) FEBS Letters **201**, 158-162.
127. Voordouw, G., Hagen, W.R., Krüse-Wolters, M., Van Berkel-Arts, A. & Veeger, C. (1987) Eur. J. Biochem. **162**, 31-36.
128. Ceconi, F., Ghilardi, C.A. & Midollini (1981) J. Chem. Soc. Chem. Commun. **1981**, 640-641.
129. Christou, G., Sabat, M., Ibers, J.A. & Holm, R.H. (1982) Inorg. Chem. **21**, 3518-3526.
130. Saak, W., Henkel, G. & Pohl, S. (1984) Angew. Chem. **96**, 153-154.
131. Kanatzidis, M.G., Dunham, W.R., Hagen, W.R. & Coucouvanis, D. (1984) J. Chem. Soc. Chem. Commun. **1984**, 356-358.
132. Kanatzidis, M.G., Hagen, W.R., Dunham, W.R., Lester, R.K. & Coucouvanis, D. (1985) J. Am. Chem. Soc. **107**, 953-961.
133. Hagen, W.R., Wassink, H., Eady, R.R., Smith, B.E. & Haaker, H. (1987) Eur. J. Biochem. **169**, 457-465.
134. Lindahl, P.A., Papaefthymiou, V., Orme-Johnson, W.H. & Münck, E. (1988) J. Biol. Chem. **263**, 19412-19418.
135. Adams, M.W.W., Eccleston, E. & Howard, J.B. (1989) Proc. Natl. Acad. Sci. USA **86**, 4932-4936.
136. Zambrano, I.C., Kowal, A.T., Mortenson, L.E., Adams, M.W.W. & Johnson, M.K. (1989) J. Biol. Chem. **264**, 20974-20983.
137. George, G.N., Prince, R.C., Stockley, K.E. & Adams, M.W.W. (1989) Biochem. J. **259**, 597-600.
138. Adams, M.W.W. (1990) Biochim. Biophys. Acta **1020**, 115-145.
139. Bolin, J.T., Ronco, A.E., Mortenson, L.E., Morgan, T.V., Williamson, M. & Xuong, N.-H. (1990) in Nitrogen Fixation: Achievements and Objectives (Gresshoff, P.M., Roth, L.E., Stacey, G. & Newton, W.E., eds), pp. 117-124, Chapman and Hall, New York.
140. Kim, J. & Rees, D.C. (1992) Science **257**, 1677-1682.
141. Kim, J. & Rees, D.C. (1992) Nature **360**, 553-560.
142. Bolin, J.T., Campobasso, N., Muchmore, S.W., Minor, W., Morgan, T.V. & Mortenson, L.E. (1993) In: New Horizons in Nitrogen Fixation (Palacios, R., Mora, J. & Newton, W.E., eds.), Nijhoff/Junk, Dordrecht (The Netherlands), 89-94.
143. Christner, J.A., Münck, E., Janick, P.A. & Siegel, L.M. (1981) J. Biol. Chem. **256**, 2098-2101.
144. Christner, J.A., Münck, E., Janick, P.A. & Siegel, L.M. (1983) J. Biol. Chem. **258**, 11147-11156.
145. Moura, I., LeGall, J., Lino, A.R., Peck, H.D., Fauque, G., Xavier, A.V., DerVartanian, D.V., Moura, J.J.G. & Huynh, B.H. (1988) J. Am. Chem. Soc. **110**, 1075-1082.
146. Lindahl, P.A., Ragsdale, S.W. & Münck, E. (1990) J. Biol. Chem. **265**, 3880-3888.
147. Ragsdale, S.W., Clark, J.E., Ljungdahl, L.G., Lundie, L.L. & Drake, H.L. (1983) J. Biol. Chem. **258**, 2364-2369.

148. Jetten, M.S.M., Hagen, W.R., Pierik, A.J., Stams, A.J.M. & Zehnder, A.J.B. (1991) Eur. J. Biochem. **195**, 385-391.
149. Münck, E., Rhodes, H., Orme-Johnson, W.H., Davis, L.C., Brill, W.J. & Shah, V.K. (1975) Biochim. Biophys. Acta **400**, 32-53.
150. Thomson, A.J., George, S.J., Richards, A.J.M., Robinson, A.E., Grande, H.J., Veeger, C. & Van Dijk, C. (1985) Biochem. J. **227**, 333-336.
151. Stephens, P.J., Devlin, F., McKenna, M.C., Morgan, T.V., Czechowski, M., DerVartanian, D.V., Peck, H.D. & LeGall, J. (1985) FEBS Lett. **180**, 24-28.
152. Johnson, M.K., Thomson, A.J., Robinson, A.E. & Smith, B.E. (1981) Biochim. Biophys. Acta **671**, 61-70.
153. Wang, G., Benecky, M.J., Huynh, B.H., Cline, J.F., Adams, M.W.W., Mortenson, L.E., Hoffman, B.M. & Münck, E. (1984) J. Biol. Chem. **259**, 14328-14331.
154. Rusnak, R.M., Adams, M.W.W., Mortenson, L.E. & Münck, E. (1987) J. Biol. Chem. **262**, 38-41.
155. Grande, H.J., Dunham, W.R., Averill, B., Van Dijk, C. & Sands, R.H. (1983) Eur. J. Biochem. **136**, 201-207.
156. Kurtz, D.M., McMillan, R.S., Burgess, B.K., Mortenson, L.E. & Holm, R.H. (1979) Proc. Natl Acad. Sci. USA **76**, 4986-4989.
157. Hagen, W.R. (1992) In: Advances in Inorganic Chemistry 38: Iron-Sulfur Proteins (Cammack, R. & Sykes, A.G., eds), pp. 165-222, Academic Press, San Diego.
158. Noodleman, L. & Case, D.A. (1992) In: Advances in Inorganic Chemistry 38: Iron-Sulfur Proteins (Cammack, R. & Sykes, A.G., eds), pp. 423-470, Academic Press, San Diego.
159. Trautwein, A.X., Bill, E., Bominaar, E.L. & Winkler, H. (1991) Structure and Bonding **78**, 1-95.
160. Noodleman, L. (1988) Inorg. Chem. **27**, 3677-3679.
161. Palmer, G., Dunham, W.R., Fee, J.A., Sands, R.H., Iizuka, T. & Yonetani, T. (1971) Biochim. Biophys. Acta **245**, 201-207.
162. Vollmer, S.J., Switzer, R.L. & Debrunner, P.G. (1983) J. Biol. Chem. **258**, 14284-14293.
163. Moulis, J.-M., Auric, P., Gaillard, J. & Meyer, J. (1984) J. Biol. Chem. **259**, 11396-11402.
164. Hagen, W.R., Eady, R.R., Dunham, W.R. & Haaker, H. (1985) FEBS Lett. **189**, 250-254.
165. Lindahl, P.A., Day, E.P., Kent, T.A., Orme-Johnson, W.H. & Münck, E. (1985) J. Biol. Chem. **260**, 11160-11173.
166. Watt, G.D. & McDonald, J.W. (1985) Biochemistry **24**, 7226-7231.
167. Hagen, W.R. (1982) Biochim. Biophys. Acta **708**, 82-98.
168. Laskowski, E.J., Reynolds, J.G., Frankel, R.B., Foner, S., Papaefthymiou, G.C. & Holm, R.H. (1979) J. Am. Chem. Soc. **101**, 6562-6570.
169. Carney, M.J., Holm, R.H., Papaefthymiou, G.C. & Frankel, R.B. (1986) J. Am. Chem. Soc. **108**, 3519-3521.
170. Carney, M.J., Papaefthymiou, G.C., Spartalian, K., Frankel, R.B. & Holm, R.H. (1988) J. Am. Chem. Soc. **110**, 6084-6095.
171. Jetten, M.S.M., Pierik, A.J. & Hagen, W.R. (1991) Eur. J. Biochem. **202**, 1291-1297.
172. Stokkermans, J.P.W.G., Houba, P.H.J., Pierik, A.J., Hagen, W.R., Van Dongen, W.M.A.M. & Veeger, C. (1992) Eur. J. Biochem. **210**, 983-988.
173. Abragam, A. & Bleaney, B. (1970) Electron Paramagnetic Resonance of Transition Ions, Clarendon Press, Oxford.
174. Orme-Johnson, W.H. & Sands, R.H. (1973) In: Iron-Sulfur Proteins, Vol. II (Lovenberg, W., ed.), pp. 195-238, Academic Press, New York.
175. Hagen, W.R. (1989) In: Advanced EPR Applications in Biology and Biochemistry (Hoff,

- A.J., ed.), pp. 785-811, Elsevier, Amsterdam.
176. Moura, I., Macedo, A. & Moura, J.J.G. (1989) In: Advanced EPR Applications in Biology and Biochemistry (Hoff, A.J., ed.), pp. 813-838, Elsevier, Amsterdam.
 177. Cammack, R. & Cooper, C.E. (1993) Methods Enzymol., in press.
 178. Oosterhuis, W.T. (1974) Structure Bonding 20, 59-99.
 179. Münck, E. (1978) Methods Enzymol. 54, 346-379.
 180. Johnson, M.K., Robinson, A.E. & Thomson, A.J. (1982) In: Iron-Sulfur Proteins (Metal Ions in Biology volume 4)(Spiro, T.G., ed.), pp. 368-406, Wiley, New York.
 181. Aasa, R. & Vänngård, T. (1975) J. Magn. Res. 19, 308-315.
 182. De Vries, S. & Albracht, S.P.J. (1979) Biochim. Biophys. Acta 546, 334-340.
 183. Mims, W.B. & Peisach, J. (1989) In: Advanced EPR Applications in Biology and Biochemistry (Hoff, A.J., ed.), pp. 1-57, Elsevier, Amsterdam.
 184. Hoffmann, B.M. (1989) In: Advanced EPR Applications in Biology and Biochemistry (Hoff, A.J., ed.), pp. 541-591, Elsevier, Amsterdam.
 185. Hendrich, M.P. & Debrunner, P.G. (1989) Biophys. J. 56, 489-506.
 186. Stevenson, R.C. (1984) J. Magn. Res. 57, 24-42.
 187. Hendrich, M.P., Pearce, L.L., Que, L., Chasteen, N.D. & Day, E.P. (1991) J. Am. Chem. Soc. 113, 3039-3044.
 188. Juarez-Garcia, C., Hendrich, M.P., Holman, T.R., Que, L. & Münck, E. (1991) J. Am. Chem. Soc. 113, 518-525.
 189. Mascharak, P.K., Papaefthymiou, G.C., Frankel, R.B. & Holm, R.H. (1981) J. Am. Chem. Soc. 103, 6110-6116.
 190. Ohno, R., Ueyama, N. & Nakamura, A. (1990) Inorg. Chim. Acta 169, 253-255.
 191. Kanatzidis, M.G., Salifoglou, A. & Coucouvanis, D. (1986) Inorg. Chem. 25, 2460-2468.
 192. Armstrong, F.A., George, S.J., Cammack, R., Hatchikian, E.C. & Thomson, A.J. (1989) Biochem. J. 264, 265-273.
 193. Link, T.A., Hagen, W.R., Pierik, A.J., Assmann, C. & Von Jagow, G. (1992) Eur. J. Biochem. 208, 685-691.
 194. Verhagen, M.F.J.M. & Hagen, W.R., unpublished results.
 195. Sucheta, A., Ackrell, B.A.C., Cochran, B. & Armstrong, F.A. (1992) Nature 356, 361-362.
 196. Smith, E.T., Ensign, S.A., Ludden, P.W. & Feinberg, B.A. (1992) Biochem. J. 285, 181-185.
 197. Wilson, G.S. (1978) Methods Enzymol. 54, 396-410.
 198. Dutton, P.L. (1978) Methods Enzymol. 54, 411-435.
 199. Ke, B., Bulen, W.A., Shaw, E.R. & Breeze, R.H. (1974) Arch. Biochem. Biophys. 162, 301-309.
 200. Clark, W.M. (1960) Oxidation-Reduction potentials of Organic systems, Williams & Wilkins Co., Baltimore.
 201. Watt, G.D., Burns, A., Lough, S. & Tennent, D.L. (1980) Biochemistry 21, 4926-4932.
 202. Holliger, C., Pierik, A.J., Reijerse, E.J. & Hagen, W.R. (1993) J. Am. Chem. Soc. 115, 5651-5656.
 203. Massey, V. (1991) In: Flavins and Flavoproteins (Curti, B., Ronchi, S. & Zanetti, G., eds.), pp. 59-66, De Gruyter, Berlin.
 204. Bertini, I., Briganti, F., Luchinat, C., Messori, L., Monnanni, R., Scozzafava, A. & Vallini, G. (1992) Eur. J. Biochem. 204, 831-839.
 205. Kay, C.J. & Barber, M.J. (1990) Anal. Biochem. 184, 11-15.
 206. Pierik, A.J. (1992) unpublished results. (Rubredoxin from *Megasphaera elsdenii* has a detectable $g=4.3$ EPR signal at 290 K)
 207. Smith, B.E., O'Donnell, M.J., Lang, G. & Spartalian, K. (1980) Biochem. J. 191, 449-455.

208. Marritt, S., Pierik, A.J., Thomson, A.J., Hagen, W.R., Lowe, D.J., Albracht, S.P.J. & Smith, B.E. (1993) In: New Horizons in Nitrogen Fixation (Palacios, R., Mora, J. & Newton, W.E., eds.), Nijhoff/Junk, Dordrecht (The Netherlands), 153.
209. Patil, D.S., Moura, J.J.G., He, S.H., Teixeira, M., Prickril, B.C., DerVartanian, D.V., Peck, H.D., LeGall, J. & Huynh, B.H. (1988) J. Biol. Chem. 263, 18732-18738.
210. Stokkermans, J.P.W.G. (1993) Thesis, Agricultural University Wageningen, The Netherlands.
211. Stokkermans, J.P.W.G., Pierik, A.J., Wolbert, R.B.G., Hagen, W.R., Van Dongen, W.M.A.M. & Veeger, C. (1992) Eur. J. Biochem. 208, 435-442.
212. Stokkermans, J.P.W.G., Van den Berg, W.A.M., Van Dongen, W.M.A.M. & Veeger, C. (1992) Biochim. Biophys. Acta 1132, 83-87.
213. Karkhoff-Schweizer, R.R., Bruschi, M. & Voordouw, G. (1993) Eur. J. Biochem. 211, 501-507.
214. Jetten, M.S.M. (1992) Thesis, Agricultural University Wageningen, The Netherlands.

Chapter 2

Redox properties of the iron-sulfur clusters in activated Fe-hydrogenase from *Desulfovibrio vulgaris* (Hildenborough).

Antonio J. Pierik, Wilfred R. Hagen, Jan S. Redeker, Ronnie B.G. Wolbert, Marelle Boersma, Marc F.J.M. Verhagen, Hans J. Grande, Cees Veeger, Peter Mutsaers, Dick H. Sands and W. Dick Dunham

(1992) Eur. J. Biochem. 209, 63-72.

Redox properties of the iron-sulfur clusters in activated Fe-hydrogenase from *Desulfovibrio vulgaris* (Hildenborough)

Antonio J. PIERIK¹, Wilfred R. HAGEN¹, Jan S. REDEKER¹, Ronnie B. G. WOLBERT¹, Marelle BOERSMA¹, Marc F. J. M. VERHAGEN¹, Hans J. GRANDE¹, Cees VEEGER¹, Peter H. A. MUTSAERS², Richard H. SANDS³ and W. Richard DUNHAM³

¹Department of Biochemistry, Agricultural University, Wageningen, The Netherlands
²Cyclotron Laboratory, Eindhoven University of Technology, The Netherlands
³Biophysics Research Division, Institute of Science and Technology, The University of Michigan, Ann Arbor, MI, USA

Received June 10, 1992) – EJB 92 0817

The periplasmic Fe-hydrogenase from *Desulfovibrio vulgaris* (Hildenborough) contains three iron-sulfur prosthetic groups: two putative electron transferring [4Fe-4S] ferredoxin-like cubanes (two F-clusters), and one putative Fe/S supercluster redox catalyst (one H-cluster). Combined elemental analysis by proton-induced X-ray emission, inductively coupled plasma mass spectrometry, instrumental neutron activation analysis, atomic absorption spectroscopy and colorimetry establishes that elements with $Z > 21$ (except for 12–15 Fe) are present in 0.001–0.1 mol/mol quantities, not correlating with activity. Isoelectric focussing reveals the existence of multiple charge conformers with pI in the range 5.7–6.4. Repeated re-chromatography results in small amounts of enzyme of very high H₂-production activity determined under standardized conditions (≈ 7000 U/mg). The enzyme exists in two different catalytic forms: as isolated the protein is 'resting' and O₂-insensitive; upon reduction the protein becomes active and O₂-sensitive. EPR-monitored redox titrations have been carried out of both the resting and the activated enzyme. In the course of a reductive titration, the resting protein becomes activated and begins to produce molecular hydrogen at the expense of reduced titrant. Therefore, equilibrium potentials are undefined, and previously reported apparent E_m and n values [Patil, D. S., Moura, J. J. G., He, S. H., Teixeira, M., Prickril, B. C., DerVartanian, D. V., Peck, H. D. Jr, LeGall, J. & Huynh, B.-H. (1988) *J. Biol. Chem.* 263, 18732–18738] are not thermodynamic quantities. In the activated enzyme an $S = 1/2$ signal ($g = 2.11, 2.05, 2.00; 0.4$ spin/protein molecule), attributed to the oxidized H cluster, exhibits a single reduction potential, $E_{m,7} = -307$ mV, just above the onset potential of H₂ production. The midpoint potential of the two F clusters (2.0 spins/protein molecule) has been determined either by titrating active enzyme with the H₂/H⁺ couple ($E_m = -330$ mV) or by dithionite-titrating a recombinant protein that lacks the H-cluster active site ($E_{m,7.5} = -340$ mV). There is no significant redox interaction between the two F clusters ($n \approx 1$).

The iron-sulfur protein hydrogenase catalyzes the reversible activation of molecular hydrogen, a process involving the transfer of two electrons. Most presently known hydrogenases are also nickel proteins. The nickel ion is generally assumed to be the redox-active catalytic center [1, 2]. A small subclass formed by the Fe-hydrogenases; these enzymes presumably contain no other potentially redox active transition metals than an iron [3]. By exclusion, this implies that the H₂ activation is located on an iron-sulfur cluster. Redox catalysis is not

an established property of iron-sulfur clusters, therefore, the study of Fe-hydrogenase has an added fundamental relevance. Furthermore, of all hydrogenases, the *Desulfovibrio vulgaris* (Hildenborough) Fe-hydrogenase exhibits the highest specific activity in the hydrogen-production assay (cf. reviews [1, 3]). Therefore, knowledge of its active-site structure and mechanism has a potential technological relevance.

Fe-hydrogenases have two types of Fe/S clusters: one H cluster and two or four F clusters [3]. The activation of molecular hydrogen (2e⁻ extraction) is thought to take place at the H cluster, an Fe/S cluster of unknown structure, which we have hypothesized to bear similarity to the [6Fe-6S] prismatic model compounds [4]. Sequence comparison indicates that the protein coordination to the H cluster includes five Cys residues [5].

Reduction equivalents are channeled through the F clusters. These are presumably of the ferredoxin [4Fe-4S]⁽²⁺¹⁺⁾ cubane type (1e⁻ transfer). At present only four

Correspondence to W. R. Hagen, Laboratorium voor Biochemie, Landbouwwageningen, Dreijenlaan 3, NL-6703 HA Wageningen, The Netherlands

Abbreviations. PIXE, particle-induced X-ray emission; INAA, instrumental neutron activation analysis; ICP-MS, inductively coupled plasma mass spectrometry; AAS, atomic absorption spectrometry; HE, normal hydrogen electrode.

Enzymes. Fe-hydrogenase or H₂: ferricytochrome-c₃ oxidoreductase (EC 1.12.2.1); Fe-hydrogenase or ferredoxin: H⁺ oxidoreductase (EC 1.18.99.1).

Fe-hydrogenases have been purified to homogeneity. There are two F clusters in *D. vulgaris* Fe-hydrogenase [6], in *Megasphaera elsdenii* Fe-hydrogenase [7], and in *Clostridium pasteurianum* Fe-hydrogenase II [8]. The latter enzyme has a very low H₂-production activity. *C. pasteurianum* Fe-hydrogenase I probably contains four F clusters [5, 8]. The *D. vulgaris* Fe-hydrogenase has been crystallized repeatedly but internal crystal disorder has thus far precluded analysis by X-ray crystallography [9, 10].

With EPR spectroscopy six different signals have been identified from *D. vulgaris* hydrogenase: (a) the 'F-signal' from the two weakly dipole-coupled, reduced F clusters [11]; (b) the 'H signal', a rhombic signal ($g = 2.11, 2.05, 2.00$) [12]; (c) a 'second rhombic signal' ($g = 2.07, 1.96, 1.89$) [9]; (d) the '3Fe signal', a signal reminiscent of the EPR from the oxidized [3Fe-4S] cluster ($g = 2.02$) [11]; (e) an 'axial signal' ($g = 2.06, 2.00$) [13]; (f) a 'high-spin signal' ($g = 5.0$) [12]. Only two of these, the H signal and the F signal, have also been identified in all three other Fe-hydrogenases [14–16].

The redox properties associated with the first four signals have been studied by Patil et al. using 'resting' (or 'as-isolated', 'O₂-insensitive', 'de-activated') hydrogenase in EPR-monitored reductive titrations with sodium dithionite [17]. We have repeated these experiments and although we find the data of Patil et al. to be reproducible, we also find that they are not interpretable in a pure thermodynamic framework because the hydrogenase activates during the reductive titration. We have, therefore, extended our studies to pre-activated enzyme and to recombinant protein that lacks the H cluster. We have also re-examined some basic properties of *D. vulgaris* hydrogenase, viz. metal content, surface charge, and standardized specific activity.

MATERIALS AND METHODS

Strain, growth and harvesting

The sulfate-reducing anaerobe *Desulfovibrio vulgaris*, subspecies Hildenborough (NCIB 8303) was grown on Saunders' medium N [18] as stirred 240-l batch cultures in a home-built glass rectangular fermentor at 35°C under nitrogen atmosphere. In the mid-to-late-log phase (absorbance at 600 nm ≈ 0.8) 200 g cells were harvested by continuous centrifugation (Sharples laboratory Super-centrifuge) at a flow rate of 0.4 l/min. After resuspension in 3 vol. water at 4°C, the periplasm was extracted essentially according to [19] by gentle disintegration of the cell wall with EDTA (1:1 dilution to a final concentration of 50 mM Na₂ EDTA plus 50 mM Tris/HCl pH 9, raising the temperature to 32°C and stirring until the onset of viscosity). The resulting suspension was immediately cooled and centrifuged (7000 g, 30 min, 4°C). The pH of the supernatant was adjusted to 8.0 by gentle addition of 1 M KH₂PO₄ and thoroughly dialyzed against standard buffer (10 mM Tris/HCl pH 8.0, 4°C). Minor precipitates formed during dialysis were removed by centrifugation (14000 g, 30 min, 4°C).

Enzyme purification

The first part of the purification scheme is a slight modification and an order-of-magnitude scaling-up of the original procedure described by van der Westen et al. [19]. All steps were carried out at 4°C except for the final purification with FPLC (ambient temperature). The dialyzed extract was applied to a column (5 cm \times 20 cm) of DEAE-Sephacel

Table 1. Purification of *D. vulgaris* (Hildenborough) periplasmic hydrogenase. The periplasmic extract was prepared from freshly harvested cells (178 g wet mass) according to Materials and Methods. Activity was measured with the Chen and Mortenson [28] manometric hydrogen-production assay.

Fraction	Volume	Protein	Activity	Specific activity
	ml	mg	kU	U/mg
Periplasmic extract	1130	5850	181.5	31
Extract after dialysis	1550	5810	136.5	23
DEAE-Sephacel	209	743	112.2	238
Sephadex G-150	74	134	83.3	622
Hydroxyapatite	91	26.0	57.0	2192
FPLC MonoQ	2.0	10.7	35.2	3290
MonoQ two-fold rerun	0.6	0.6	4.2	6900

(Pharmacia) pre-equilibrated with standard buffer. After application, the column was washed with 1000 ml standard buffer with 20 mM NaCl and eluted with a linear gradient (1600 ml) of 20–400 mM NaCl in standard buffer. Active fractions were pooled, dialyzed against standard buffer, and concentrated on a small (2.5 cm \times 8 cm) column of DEAE-Sephacel. The concentrate (≈ 15 ml) was applied to a column (3.5 cm \times 100 cm) of Sephadex G-150 equilibrated and eluted with 25 mM potassium phosphate pH 7.5. Fractions were pooled on the basis of activity and a limiting purity index $f = A_{400}/A_{280} > 0.25$. The pool was applied to a column (2.5 cm \times 9 cm) of hydroxyapatite (Bio-Gel HT, Bio-Rad) pre-equilibrated with 25 mM potassium phosphate pH 7.5. The column was eluted with a linear gradient (600 ml) of 25–300 mM potassium phosphate pH 7.5. Fractions with $f > 0.33$ were pooled, dialyzed against standard buffer, and concentrated on YM 30 filters in Diaflo Amicon concentrator (50 and 10 ml). The concentrate was split-up in portions of 1–2 mg and in subsequent runs applied to a preparative MonoQ HR 5/5 anion-exchange column attached to Pharmacia FPLC system. The column was eluted with a 40 ml gradient of 0–500 mM NaCl in standard buffer. The eluate was fractionated according to the peak pattern of on-line monitored absorbance at 280 and 436 nm and subsequently checked for their f factor and activity. Fractions with $f > 0.33$ were pooled and Na₂EDTA was added to a concentration of 0.5 mM. The final preparation was frozen in liquid nitrogen after dialysis against 5 mM Tris/HCl pH 8.0 and concentration on Centricon devices with YM-30 filter. The results of a typical purification are summarized in Table 1; the last step is discussed in Results.

Recombinant (H-cluster-lacking) protein

Recombinant *D. vulgaris* (Hildenborough) Fe-hydrogenase was isolated and purified from the TG1 derivative *Escherichia coli*, strain JM101, transformed with plasmid pHV150 (plasmid pUC9 with an insert consisting of a *lac* promoter plus the two structural genes for hydrogenase *hydA* and *hydB*). The construction of the clone, isolation from 10¹¹ cultures and purification of the recombinant protein has previously been described [20]. TG1 (pHV150) produces about ten times more hydrogenase subunits/cell protein than *D. vulgaris*; however, only some 10% is soluble and properly assembled into an $\alpha\beta$ dimer [21], from which the recombinant hydrogenase is purified. Its protein part is almost indistinguishable from the native enzyme.

istinguishable from wild-type hydrogenase, however, the F clusters are present substoichiometrically and the H cluster is completely absent [20]. The specific activity is lower than 0.1 U/mg in the hydrogen-production assay. The Fe/S clusters in the recombinant protein do not react with molecular hydrogen; they can be reduced with dithionite.

Megasphaera elsdenii Fe-hydrogenase

The fermentative rumen bacterium *Megasphaera elsdenii*, strain LC 1 [22], was grown as in [23]. The Fe-hydrogenase was isolated and purified anaerobically as previously described [7].

Hydrogen-production activity

No general agreement exists at this time on the standard conditions for assaying H_2 -production activity (1 unit $\equiv 1 \mu\text{mol } H_2/\text{min}$ at 30°C). Therefore, direct comparison of literature data is in general not possible. The reaction studied is usually the methyl-viologen semiquinone cation radical: H^+ oxidoreductase activity, with the radical produced by reduction of the viologen with excess sodium dithionite. The major problem is the choice of pH. It affects: (a) the substrate concentration, (b) the $2H^+ + 2e \rightleftharpoons H_2$ equilibrium, (c) the extent of reduction of the methyl viologen via the pH dependence of the midpoint potential of the $S_2O_3^{2-}/SO_3^{2-}$ couple, (d) the stability of the enzyme and of the methyl-viologen semiquinone and (e) the catalytic performance of the enzyme itself. In addition to the pH problem there are other problems related to the viologen concentration, the method of H_2 detection, the purity of sodium dithionite and the stimulating or inhibiting effects of certain salts and buffers.

The activity has no well-defined pH optimum. For all Fe-hydrogenases it increases continuously with decreasing pH down to the range in which enzyme inactivation sets in [24–26], probably by destabilization of [Fe-S] centres. In their initial description of the assay, Peck and Gest prescribed a buffer of appropriate pH and subsequently used 63 mM potassium phosphate pH 6.5 [27]. Also, they used 13 mM methyl viologen, a concentration at which dimerization of the semiquinone is considerable (the dissociation constant is typically 2 mM, depending on the ionic strength; see [23] and references quoted therein). The assay was considerably modified in the proposal of Chen and Mortenson: 50 mM Tris/HCl pH 8 and 1 mM methyl viologen [28]. Although the complication of significant semiquinone dimerization is avoided, these modified conditions result in significantly suboptimal activity numbers because the pH is high, the viologen concentration is low, and Tris buffer has an inhibitory effect in at least some Fe-hydrogenases, in particular the ones from *M. elsdenii* [15] and from *D. vulgaris* (our unpublished observations).

An additional complication is in the detection of the molecular hydrogen produced. This is conveniently done manometrically in a Warburg apparatus [27, 28] or by gas chromatography with catharometric detection [29]. The assay conditions of Chen and Mortenson combined with H_2 detection in the Warburg were specifically designed as a convenient method to determine activity on undiluted samples all the way through a purification procedure [28]. Suitable amounts of hydrogenase for this manometric hydrogen production assay are 0.01–2 U for the conventional 13–22 ml Warburg vessels. Gas chromatography has a larger dynamic range combined with a much lower H_2 -detection limit. With a Varian

3400 gas chromatograph (0.5-nm molecular sieve column 150 cm \times 0.6 cm, catharometric detection) progression curves can easily be recorded for 0.0001–10 U hydrogenase by injection of 10–250- μl volumes of the 6-ml headspace, sampling every 0.2–90 min. The gas chromatograph is calibrated with diluted and pure hydrogen gas (10–500 μl). The calibration of the head-space volume is checked by standard addition of hydrogen to the head-space of the vials.

Working with purified samples of *D. vulgaris* Fe-hydrogenase, we have compared the two methods in parallel experiments. In both methods we detected H_2 evolution from 3.25 g/l dithionite ($> 87\%$ purity obtained from Merck) with 1 mM methyl viologen as redox mediator, 0.5 mg/ml bovine serum albumin (Sigma) as stabilizer, in 50 mM Tris/HCl pH 8.0 at 30°C in 2-ml volume. The vessels were shaken at 150 strokes of ≈ 4 cm/min. For both assays, linearity of hydrogen production was observed during the production of 0–15 μmol hydrogen with 0.05–2 U (Warburg) and 0.0005–5 U (gas chromatograph) of hydrogenase. It is obvious that the buffering capacity of 100 μmol Tris buffer is insufficient to keep the pH at 8.0 during the generation of up to 15 μmol of the acidic HSO_3^- from dithionite. The pH of reaction mixtures just after the production of 1–15 μmol hydrogen was usually in the range of 7.9–7.2. As the Fe-hydrogenase exhibits a higher activity at lower pH [25], both assays must have an artificial linearity during the production of 1–15 μmol hydrogen. This could result from a balancing effect between the activity increase due to the lower pH and an activity decrease due to hydrogen inhibition [25] or to lowering of the methyl-viologen-semiquinone concentration by production of sulfite [25]. Our comparison between the results of the manometric and gas chromatographic procedure applies to a constant pH 8.0 during the assay. Although the assay conditions were exactly identical and linearity and calibration of the manometric and gas-chromatographic procedure were thoroughly checked, resulting activity numbers were not mutually consistent. The gas chromatographic method systematically gives 30–50% higher values. We have presently no explanation for this discrepancy.

We have elaborated, above, on the multiple complications that arise in attempts to compare Fe-hydrogenase activity data taken under non-identical conditions. We emphasize their importance for a meaningful comparison of our present work with other studies on hydrogenase. Specifically, we intend to contrast our previous and present work with that from Huynh and collaborators, who have been working on what appears to be the same enzyme from the same bacterial source [13, 17, 30]. The dispute concerns difference in specific activity (cf. the comparison of the two preparations in [1]), difference in iron stoichiometry [4, 13], and difference in redox properties (see below). All activity data reported in Results and Discussion and in all our previous work, refer to measurements with the, intentionally, suboptimal manometric assay of Chen and Mortenson [28]. Contrarily, activities of the preparations described in [13, 17, 30] refer to the Peck and Gest assay [27], or to a modification thereof using 100 mM potassium phosphate pH 7.6 [30], and subsequent gas chromatographic detection of H_2 . An apparent increase in (specific) activity, by at least 30%, ensues from each of the following substitutions: (a) Tris/HCl by potassium phosphate; (b) initial pH 8.0 by pH 7.6; (c) manometric by gas chromatographic detection. Furthermore, the use of 13 mM [27] instead of 1 mM methyl viologen [28] in our experiments results in a striking 2–2.5-fold increase of the apparent (specific) activity (cf. Fig. 5 in [25]) both with the Warburg and the gas chromatographic procedure.

Hydrogenase pre-activation

Resting, O₂-insensitive protein was converted to active, O₂-sensitive enzyme by means of a complete argon, hydrogen, argon redox cycle (cf. [12, 31]). For the hydrogen activation the protein was incubated under 120 kPa hydrogen pressure with continuous stirring for 30 min at ambient temperature. Subsequently the H₂ was replaced with argon (120 kPa pressure) in 6–8 vacuum/argon cycles under continuous stirring. For the reductive dye-mediated redox titrations the hydrogenase was activated by adding the anaerobic resting enzyme to a pre-reduced mediator mixture.

Redox titrations

Reductive titrations with buffered sodium dithionite and oxidative titrations with potassium ferricyanide or 2,6-dichloroindophenol were carried out at 25°C in an anaerobic cell under argon. The potential of the stirred solution was measured at a platinum electrode (Radiometer P-1312) with respect to the potential of a saturated calomel electrode (Radiometer K-401). All potentials have been recalculated with respect to the normal hydrogen electrode (NHE). Redox mediator dyes (40 µM each) were *N,N,N',N'*-tetramethyl-*p*-phenylenediamine, 2,6-dichloroindophenol, phenazine ethosulfate, methylene blue, resorufin, indigo disulfonate, 2-hydroxy-1,4-naphthoquinone, anthraquinone-2-sulfonate, phenosafranin, safranin o, neutral red, benzyl viologen, methyl viologen.

Titrations with the H₂/H⁺ couple were done by stirred incubation of the protein under H₂ pressures of 10–120 kPa for 30 min at ambient temperature. The H⁺ concentration was pre-set by passing the protein over a small Bio-Gel P-6DG molecular sieve column (2-ml bed volume) equilibrated with 100 mM buffer of variable pH, using piperazine (pH 4.5–5.1), Mes (pH 5.3–6.0), Hepes (pH 6.3–8.9), or Ches (pH 9.3–10.2). The resulting bulk potential was calculated (at 25°C) according to:

$$E = -0.05915[\text{pH} + 1/2 \log(p_{\text{H}_2}/p_0)], \quad (1)$$

with $p_0 \equiv 101.3$ kPa (i.e. atmospheric pressure).

Elemental analysis

Colorimetry

The procedures for determination of protein, iron and molybdenum/tungsten with the microbiuret, ferene and dithiol methods, respectively, were as outlined in [32] and the references therein.

PIXE

Multi-elemental analysis was performed with particle-induced X-ray emission (PIXE) at the Eindhoven University of Technology. Sample application to the Millipore MF SCWP 8-µm filters was according to [32, 33]. Energy-dispersive X-ray emission spectra were digitally recorded during the irradiation with a 3-MeV proton beam from a cyclotron and analyzed with the software as described in [34]. Iron as determined by the ferene method served as internal standard for the determination of other elements.

ICP-MS

Inductively coupled plasma mass spectroscopy (ICP-MS) [35] was carried out with a VG Instruments PlasmaQuad at

the Koninklijke/Shell-Laboratorium (Amsterdam). Data were analyzed with the software supplied by the manufacturer. Samples were mixed with 1% HNO₃ prior to analysis. Controls were included of buffer blanks and of samples with known concentrations of relevant elements. We note that the argon plasma, the aqueous nitric acid matrix, and the polypeptide backbone (or, more likely its decomposition products) produce some artificial peaks in the mass spectrum. For most elements interferences can easily be excluded or quantitated by checking the isotope composition of the elements. The element of interest that is most seriously affected by background interference is Fe. Contributions of the background (i.e. ⁴⁰Ar¹⁶O) were 2–16% for the nominal mass of 56 Da. With a careful correction for the usually slowly drifting background, reliable quantitative determination of Fe was possible.

INAA

Instrumental neutron activation analysis (INAA) [36] was performed at the Interuniversitair Reactor Centrum, Delft. Samples were desalted by gel-filtration on BioGel P-6DG equilibrated with demineralized water, and lyophilized by freeze-drying in the polyethylene INAA vials. INAA is not very sensitive for Fe and therefore has an inherently large relative error of 20–3% for our samples containing quantities of 1–27 µg Fe/vial. We have, nevertheless, used the Fe content as an internal standard to correct for possible losses during the gel-filtration and lyophilization pre-treatment.

AAS

Nickel was determined by atomic absorption spectroscopy (AAS) at 231.4 nm with a Perkin-Elmer atomic absorption spectrometer (ICP 5500) equipped with an HG-400A graphite furnace atomizer. Samples were successively mixed with HNO₃ and ethanol to final concentrations of 5% and 20% (by vol.), respectively. Prior to injection into the graphite furnace samples were spun (7000 g, 10 min) to remove denatured protein. The recovery of Ni added as NiCl₂ to the protein was > 95%.

Isoelectric focussing

Flat-bed isoelectric focussing on Serva Precotes (pI 5–7) was performed on a LKB Ultrophor electrophoresis unit at 4°C. Markers were parvalbumin (rabbit muscle), carbonic anhydrase (bovine erythrocytes) and alcohol dehydrogenase (horse liver), with isoelectric points at 4°C of 5.3, 5.8 and 6.8 respectively [37]. Activity staining was according to [38].

Spectroscopy

Ultraviolet/visible data were obtained with a DW-200 spectrophotometer. EPR spectroscopy was done with Bruker EPR 200 D spectrometer with peripheral equipment and data handling as described in [39]. The modulation frequency was always 100 kHz.

RESULTS

Metal content of *D. vulgaris* and *M. elsdenii* Fe-hydrogenase

The metal content of Fe-hydrogenases has been for several years a matter of debate and will continue to be so. There are

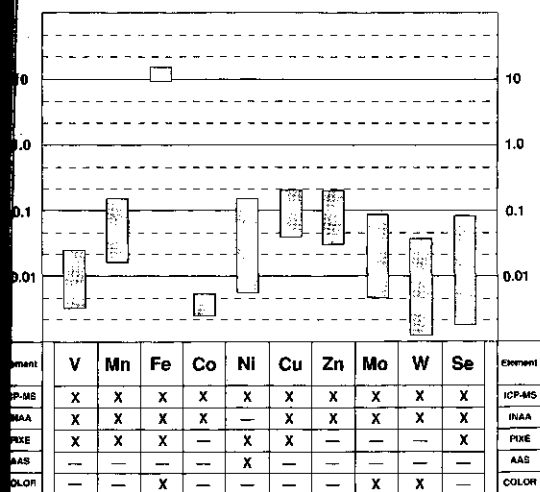


Fig. 1. Elemental analysis of *D. vulgaris* Fe-Hydrogenase. The bars indicate the range of observed amounts of the elements, analyzed with various tagged techniques. The diagram summarizes the results from determinations on preparations with specific activities of 2100–6900 U/mg. For elements other than Fe the lower end of the bars indicates the limit of detection for 0.1–1 mg amounts of Fe-hydrogenase per determination. Ferene (Fe) and dithiol (Mo and W) were analyzed by PIXE and AAS methods, and the ICP-MS, INAA, PIXE and AAS methods were according to Materials and Methods.

three aspects to this problem. The first question is whether or not the enzyme contains metal ions other than iron [11, 13]. The second question is how many iron ions are contained in the protein molecule and how are these distributed over the different Fe/S clusters (cf. [3] and references quoted therein). The third problem is what percentage of purified protein is non-protein with respect to each of the different Fe/S clusters [20].

A number of hydrogenase preparations was subjected to multi-elemental analysis with a range of suitable techniques. Fig. 1 summarizes the combined results on various Fe-hydrogenase preparations with specific activities ranging over 2100–6900 U/mg. Note that quantitative analysis of substoichiometric amounts consumes 10^2 – 10^5 more enzyme than quantitative analysis of the Fe content. Substoichiometric amounts of V, Mn, Co, Ni, Cu, Zn, Mo, W, and Se could be quantitated (Fig. 1). In a previous determination by PIXE significant (i.e. almost stoichiometric) amounts of Ni, Cu, and W were reported [11]. The present PIXE data were obtained with support filters thoroughly washed with EDTA (in order to remove Zn), with severalfold higher protein concentration, and with improved data analysis [36]. These three factors combined resulted in a substantially lower background and more reliable background correction. Even with proper precautions to exclude contamination and after an extensive EDTA dialysis, preparations of the Fe-hydrogenase are inevitably contaminated with 0.04–0.09 ion Cu and/or Zn/mol-enzyme. Nickel and selenium were usually present at much lower levels. At least five high-activity preparations contained 0.01 mol/mol amounts of Ni and Se. The content of these elements and the other elements presented in Fig. 1 had no correlation with the specific activity of the hydrogenase preparations used. This strongly suggests that these elements are not functional in *D. vulgaris* Fe-hydrogenase. We have also taken the oppor-

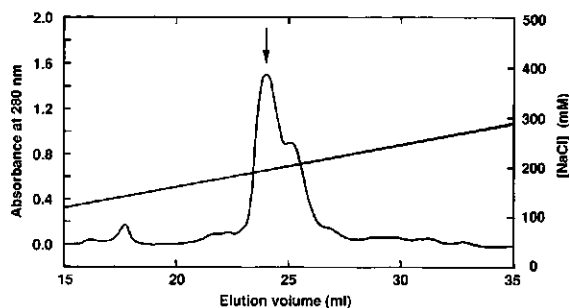


Fig. 2. Charge conformers of *D. vulgaris* Fe-hydrogenase partially resolved by shallow-gradient preparative anion-exchange FPLC. The hydrogenase preparation (3.2 mg) applied onto the HR 5/5 MonoQ column had a specific activity of 3300 U/mg. After two reruns of the fraction indicated by the arrow, 0.6 mg hydrogenase with a specific activity of 6900 U/mg was obtained.

tunity to establish that the selenium content of *M. elsdenii* Fe-hydrogenase is < 0.2 mol/mol, as this datum has not previously been reported.

Variations in pI, specific activity and Fe content

Higuchi et al. have reported that the solubilized nickel-hydrogenase from *D. vulgaris* (Miyazaki F), purified to homogeneity according to SDS/PAGE, resists crystallization unless it is separated with HPLC into three hydrogenase subfractions [40]. These components were not distinguishable in terms of activity or spectral properties (*ibidem*). It is possible that they represent species with minor differences in surface charge. A determination of the chemical modification involved was not reported. One could imagine oxidation of a non-cluster-bound cysteine to cysteinate or deamidation of glutamine or asparagine residues. Incited by the difficulties that we encountered in the crystallization of the *D. vulgaris* (Hildenborough) Fe-hydrogenase, we searched for inhomogeneity in this protein similar to that of the Miyazaki enzyme.

Fig. 2 gives the elution profile (280 nm) of a typical preparative FPLC anion-exchange chromatography run according to the one-to-last step in the purification scheme of Table 1. All peaks in the 20–33-ml elution range exhibited a normal two-band (45.8 + 10.1 kDa) pattern on SDS/PAGE. The hydrogenase main peak eluting at 200 mM NaCl (23–26 ml) appears to consist of two components. The top fraction (arrow) does not significantly differ in its purity factor, $f = 0.355 \pm 0.005$, from most of the other bands in the 20–33-ml range. However, it has a higher specific H_2 -production activity. By repeating this anion-exchange chromatography step, fractions are obtained with specific activities in the manometric H_2 -production assay ranging from very low to very high values: 50–6900 U/mg.

In isoelectric focussing the fractions are found to differ significantly (Fig. 3). The high-activity fraction mainly consists of a diffuse band at $pI \approx 6.2$. The other fractions exhibit a number of well-focussed, intense bands at pI 5.7–6.4. When duplicate gels were stained for H_2 -uptake activity with benzyl viologen and triphenyl tetrazolium chloride [38], initially only the diffuse band at $pI \approx 6.2$ would color. However, upon prolonged incubation eventually a second band with $pI \approx 5.8$ became colored (indicated in Fig. 3). Native electrophoresis of hydrogenase preparations (not shown) confirmed that the

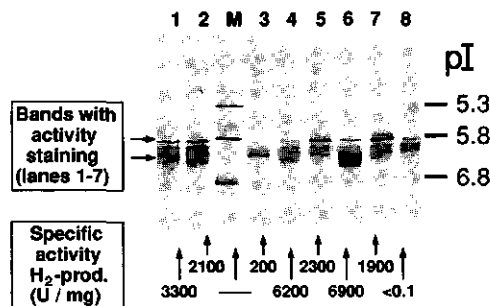


Fig. 3. Isoelectric focussing of multiple charge conformers of *D. vulgaris* Fe-hydrogenase. Fe-hydrogenase with indicated specific activity was separated on flat-bed isoelectric focussing. Lanes 1 and 2, Fe-hydrogenase obtained with the purification procedure described in Materials and Methods; lanes 3–5 and 6–7, Fe-hydrogenase fractions obtained by repeated shallow gradient anion-exchange chromatography of the preparations of lanes 1 and 2, respectively; lane 8, inactive (H-cluster-lacking) *D. vulgaris* Fe-hydrogenase expressed in *E. coli*; lane M, marker mixture of proteins with pI indicated on the right. The lanes contain 3–6 μ g protein. Activity staining with H_2 , triphenyltetrazolium chloride and benzyl viologen at pH 7 [38] was observed for the two bands indicated with horizontal arrows.

multiple bands are not an artifact of the isoelectric focussing technique. The nature and significance of the diffuseness of the pI \approx 6.2 band is at present not understood.

A logical step towards resolution of the different charge conformers was to try chromatofocussing. The hydrogenase emerged from the MonoP HR 10/30 FPLC chromatofocussing column at pH values below 5. This seriously affected the recovery of activity, probably due to the lability of the [Fe-S] centres at low pH. When the pH of the fractions eluting from the column was immediately adjusted to pH 8, the recovery of activity was about 70%. The resolution of charge conformers was, in the best runs, comparable to the separation on the MonoQ anion-exchange column. In one experiment we checked the performance of different charge conformers in both the H_2 -production and H_2 -consumption manometric assay. Within experimental error, the various species had the typical H_2 -consumption/ H_2 -production ratio of 10 (cf. [19]).

After incubation under H_2 of fractions enriched in the main peak and in the right shoulder (cf. Fig. 2), drastically different EPR spectra resulted. The main high-activity form showed a fully developed F signal. The lower activity shoulder showed a faint F signal. After reduction by dithionite, the EPR spectrum (F signal) of the fractions was identical (not shown). The behaviour of the 'shoulder' fraction is reminiscent of the inactive *D. vulgaris* hydrogenase expressed in *E. coli* (cf. Fig. 6 in [20]).

We interpret the combined results, above, as follows. Purified *D. vulgaris* Fe-hydrogenase occurs in a number of forms with different pI, probably reflecting heterogeneity of charge. The protein can be enriched in the individual charge conformers by anion-exchange chromatography, chromatofocussing, native electrophoresis and isoelectric focussing. The charge conformers also differ in their specific H_2 -production and H_2 -consumption activity and in their H_2 -reducibility (monitored on the EPR F signal). Thus, it appears that the charge heterogeneity reflects not just surface charge modification but also differences in a catalytically vital part of the protein.

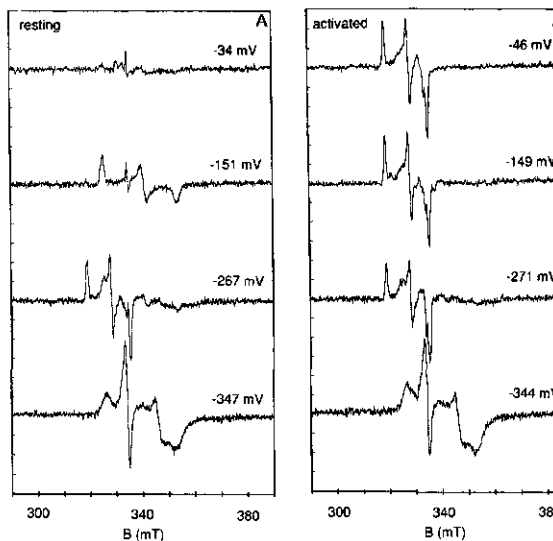


Fig. 4. A comparison of resting (A) and pre-activated (B) *D. vulgaris* Fe-hydrogenase by EPR-monitored, reductive titration. The enzyme 60 μ M protein, in the presence of 40 μ M each of redox mediators, 100 mM Tris/HCl pH 7.0, was titrated to the indicated potentials with sodium dithionite in the same buffer. The hydrogenase was pre-activated with a H_2/Ar cycle as described in Materials and Methods. EPR conditions: microwave frequency, 9.33 GHz; microwave power 13 μ W; modulation amplitude, 1.0 mT; temperature, 13 K.

We have previously reported on the presence of 13–15 Fe mol/mol in *D. vulgaris* hydrogenase [4]. If the last FPI step in the purification scheme (Fig. 2 and Table 1) is omitted the Fe number is lower (9–11 Fe ions/molecule). The colorimetrically determined iron content of highly active hydrogenase always was 12–15 mol/mol. Results of iron determination with colorimetry were within experimental error identical to those obtained with ICP-MS and INAA methods.

Reductive titration of resting and activated hydrogenase

We have repeated the mediated, reductive titration of resting Fe-hydrogenase with sodium dithionite, as previously reported by Patil et al. [17]. We have quantitatively confirmed their results in terms of apparent midpoint potentials, apparent n values, and EPR integrated intensities. Specifically, find (cf. Fig. 4A) the following sequence of events upon lowering the bulk potential with dithionite: (a) the second rhombic signal ($g = 2.07, 1.96, 1.89$) appears to a maximum $S = 1/2$ spin intensity of ≈ 0.45 ; (b) the second rhombic signal disappears with an apparent $E_{m,7} \approx -250$ mV, concomitant with the appearance of the H signal (a rhombic signal with $g = 2.11, 2.05, 2.00$) and the H signal increases to a maximum $S = 1/2$ spin intensity of ≈ 0.33 ; (c) around $E \approx -300$ mV the H signal collapses and the F signal from the two regucubanes appears with a steeply sloping titration curve suggesting strong redox interaction between the two cubanes (i.e. $n \approx 2$; cf. [17]).

Patil et al. have proposed an interpretation of these events in terms of redox transitions under thermodynamic equilibrium conditions [17]. We argue against this proposal on the basis of the following observations. The sequence of events is not reversible. During the first reducing cycle

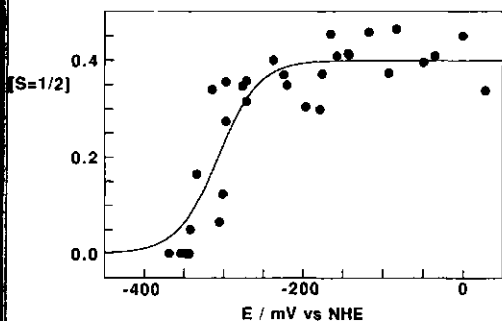


Fig. 5. Oxidoreductive titration of the H signal ($g = 2.10$) from hydro-*pre-activated D. vulgaris* Fe-hydrogenase. The protein and EPR conditions were as in Fig. 4. The data points were obtained from three independent titrations of two Fe-hydrogenase preparations. The solid line is a least-squares fit to all data points assuming a Nernstian $n = 1$ with $E_m = -307$ mV.

hydrogenase activates. Upon reoxidation the second rhombic signal does not reappear. The titration curve of the H cluster is no longer bell-shaped. In Fig. 4B the equivalent of the three-point titration is presented but for H_2/Ar -cycle-activated hydrogenase. The pattern is considerably simplified and, in fact, now very similar to that observed with *M. elsdenii* Fe-hydrogenase [7]. Only the H signal and the F signal are observed. The H signal now has a single transition potential. We conclude that the responses of the second rhombic signal following lowering of the bulk potential represent transients in the active activation process. Only the H signal and the F signal represent redox-active species in the active enzyme.

Oxidoreductive titration of the H signal from *hydro-activated hydrogenase*

The hydrogenase was activated with a H_2/Ar cycle, diluted with a mixture of redox mediators, and then titrated reductively with sodium dithionite and/or oxidatively with potassium ferricyanide. As only relatively small amounts of highly active enzyme can be obtained, the enzyme-consuming titration experiments reported in this paper were performed with samples with intermediate specific activities of 2400–3000 U/mg. The integrated intensity of the resulting $S = 1/2$ H cluster, EPR signal is plotted in Fig. 5 versus the bulk potential. The H signal shows a single, reversible reduction-oxidation step at $E_{m,7.0} \approx -307$ mV. The titration curve does not show the artifactual abrupt cut off that was observed in the reductive titration of resting enzyme [17]. Nevertheless, data points at low potentials are probably somewhat influenced by the H_2 production from solvent protons and dithionite electrons. This inherent uncertainty precludes an exact determination of the curvature of the Nernst plot; therefore, an n value can not be assigned to the H cluster. We have shown an $n = 1$ Nernst curve in Fig. 5 for convenience, not for interpretational purposes. The $S = 1/2$ intensity of the fully oxidized H signal does not exceed 0.4 spin.

Redox titration with molecular hydrogen

There is only one possible way to redox-titrate an active hydrogenase enzyme while at the same time circumventing the kinetic complication of H_2 production at the expense of added reducing equivalents. The use of molecular hydrogen as the

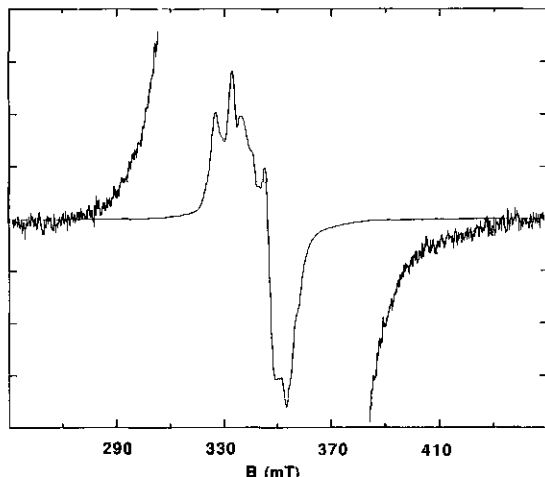


Fig. 6. Broad-wing EPR interaction spectrum from the two F clusters in very concentrated, hydrogen-reduced *D. vulgaris* Fe-hydrogenase. The enzyme, 2 mM protein in 200 mM Hepes pH 7.0, was reduced by stirred incubation under 120 kPa H_2 pressure at ambient temperature for 20 min. The extent of the wings from dipole-dipole broadening are emphasized by a 100-fold blow up. Limits for proper spin quantitation by double integration should, therefore, span almost the full 200-mT scan range. EPR conditions: microwave frequency, 9.325 GHz; microwave power, 2 mW; modulation amplitude, 0.8 mT; temperature, 15 K.

reductant (and solvent proton as the associated oxidant) ensures that bulk electron transfer is limited to within the Nernstian system: H_2/H^+ plus oxidized/reduced enzyme. We have titrated the Fe-hydrogenase with the H_2/H^+ couple by applying a hydrogen pressure of around 120 kPa to enzyme solutions of varying pH. At neutral pH this produces a potential of -416 mV (cf. Eqn 1). Therefore, the H signal ($E_m^7 \approx -300$ mV) is not observable in these experiments.

The F clusters are presumably two ferredoxin-type cubanes [6] and they are subject to mutual weak dipolar interaction [11]. The F signal is a complex interaction spectrum but its double integral should still be proportional to the cubane concentration. A practical problem is that the magnetic interaction creates broad wings of low amplitude to both sides of the spectrum so that the limits of integration are difficult to determine. We have prepared an Fe-hydrogenase sample of very high concentration (2 mM), reduced the enzyme with H_2 at pH 7, and taken the EPR spectrum in order to obtain a very low-noise F signal. This spectrum is given in Fig. 6. From a 100-fold blow up, it is evident that the integration limits should span a field scan more than twice the width of the main spectral feature.

The $S = 1/2$ spin intensity of the F signal as a function of the potential, poised with the H_2/H^+ couple, is presented in Fig. 7. At low potential the signal quantitatively accounts for two $[4Fe-4S]^{1+}$ clusters. The solid line in Fig. 7 is a Nernst curve for two independent $n = 1$ acceptors of identical reduction potentials, $E_m = -330$ mV. The slope in the data appears to be slightly less than that expected for $n = 1$, and this may reflect a slight difference between the reduction potentials of the two clusters (< 20 mV). In contrast to the suggestion brought forward by Patil et al. [17], there is no sign of positive redox interaction between the two clusters;

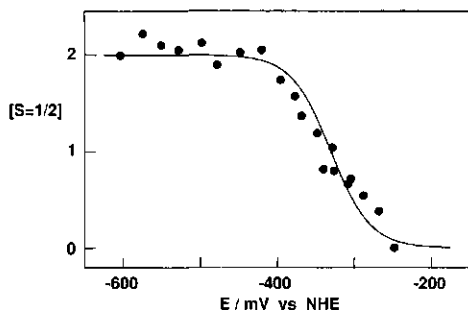


Fig. 7. Redox titration with the H_2/H^+ couple of the F signal from *D. vulgaris* Fe-hydrogenase by variation of the pH at constant H_2 pressure. The enzyme, 50–70 μM protein in 100 mM buffer of variable pH (detailed in Materials and Methods), was incubated under H_2 and then measured by EPR as in Fig. 4. On the ordinate axis the spin quantitation is plotted as determined by double integration. The abscissa axis gives the potential calculated for the H_2/H^+ couple according to Eqn (1). The solid line is a least-squares fit to all data points assuming two identical and independent $n = 1$ acceptors each with $E'_m = -330$ mV.

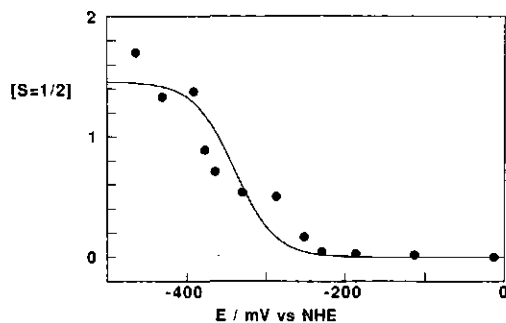


Fig. 8. Reductive titration of the F signal from inactive (H-cluster-lacking) *D. vulgaris* Fe-hydrogenase expressed in *E. coli*. The recombinant protein was 50 μM with 40 μM each of the redox mediators in 50 mM Hepes pH 7.5. The reductant was buffered sodium dithionite. EPR conditions were as in Fig. 4. The solid line is a least-squares fit to all data points assuming two identical and independent $n = 1$ acceptors each with $E'_m = -340$ mV. Addition of excess dithionite in buffer to the inactive hydrogenase in absence of mediators also gives a limiting 1.5 spin/protein.

specifically, the cluster pair does not at all behave as a single, two-electron acceptor.

Redox titration of the H-cluster-free recombinant protein

Cloning and expression of the two structural genes (the *hydA* + *hydB* operon) of *D. vulgaris* Fe-hydrogenase in *E. coli* allows for the isolation and purification of an inactive 'recombinant' protein that is almost indistinguishable from wild-type hydrogenase except that the F clusters are present for only ≈ 60 – 80% and the H cluster appears to be completely absent [20]. The EPR F signal does not show up upon incubation under H_2 but it does develop upon reduction with sodium dithionite. Because the recombinant protein does not interact with hydrogen, a dye-mediated equilibrium redox titration is not disturbed by enzyme activation and/or H_2 -production activity. Thus, the potential of the F clusters are

readily determined. From the data in Fig. 8 it can be estimated that the two clusters (73% incorporation) each titrate with $E_{m,7.5} \approx -340$ mV and $n \approx 1$.

DISCUSSION

The protein and the metal ions

The site of hydrogen activation in Fe-hydrogenases or encompasses, to all likelihood an iron-sulfur cluster. Its structure is not known; its elemental stoichiometry is not firmly established. A problem of normalization has clouded the field for several years. We have initiated the debate by comparing four different methods of protein determination for the *D. vulgaris* enzyme. This work led us to conclude that (a) the 'easy' determinations (in particular the Lowry and the Bradford methods) bore systematic errors of significance when applied to Fe-hydrogenase; and that (b) the total number of Fe ions/molecule of protein was greater than previously assumed, namely, approximately 14 [4, 7]. This revised stoichiometry was based on the Biuret protein determination, because this polypeptide-bond-oriented complexation method should be less prone to deviations from the average absorption coefficient for a particular protein.

Subsequently, Adams and his collaborators re-determined the protein concentration of *C. pasteurianum* Fe-hydrogenase I and II samples (hitherto determined with the Lowry method) by amino-acid analysis, and they found that Fe numbers for both these proteins had to be corrected upward by an astounding factor of two [8]. The same method was then applied by Patil et al. on the *D. vulgaris* Fe-hydrogenase and combined with elemental analysis by plasma emission spectroscopy, the result was some 10 Fe ions/protein molecule [1]. In the hands of these workers protein concentration determined with the biuret method versus the amino-acid analysis differed by 10% (*ibidem*). Since the molecular mass of the mature protein is exactly known [6, 41], and since the accuracy of the iron determination is not questioned, it is implied that the difference in Fe contents reported by us [4, 7] and Patil et al. [17] (i.e. ≈ 14 versus ≈ 10) is a real one. On the assumption that 8 Fe atoms are in the F clusters, the remaining difference (i.e. ≈ 6 versus ≈ 2) would apply to the H-cluster active site.

In view of this gross difference, we have again evaluated the metal content of a number of *D. vulgaris* Fe-hydrogenase preparations. We have not limited our analyses to iron, because in early investigations from this laboratory significant amounts of Ni, Cu, Zn were found with PIXE [11]. We have now combined a methodologically improved PIXE with ICP-MS, INAA, AAS, and colorimetry to arrive at the conclusion that the name 'Fe-hydrogenase' is appropriate as the highly active protein contains only small amounts of any metal other than iron.

The overall result of the new iron determinations is different from our previous work, i.e. there are some 11–15 Fe ions/highly purified protein molecule. Thus, the controversy over the Fe stoichiometry remains. However, our present work provides a new clue to the nature of varying Fe numbers. The protein appears to exist in some four slightly different forms as judged from isoelectric focussing, from native PAGE and from FPLC. This inhomogeneity is reflected in unsatisfactory crystallization results, in a varying lag time for activation to H_2 -uptake activity (not shown), in differential H_2 -reducibility (and related specific activity and EPR response).

have previously hypothesized that the purified Fe-hydrogenase from *M. elsdenii* exists as a mixture of fully active holoenzyme and inactive protein still carrying the two clusters but deficient in the H cluster [7]. We now propose a theory over this hypothesis to the *D. vulgaris* enzyme.

This may provide a framework for the interpretation of spectroscopic data, however, it does not fully resolve the difference in reported iron numbers. We propose that the relative content of apo-protein is directly related to the protein isolation procedures. In the original scheme of van der Westengen et al. (of which our procedure is an upscaling and extension) the hydrogenase is extracted from the periplasm of freshly harvested cells by partial digestion of the outer membrane with EDTA at 32°C [19]. When this is done in Tris/HCl buffer of pH 9.0 the hydrogenase de-activates to a resting, O₂-sensitive, form. The molecular mechanism of this process is not known but it works equally well on purified, H₂-activated enzyme [31]. Contrarily, in the procedure described by Huynh et al. harvested cells are suspended in Tris/HCl buffer of pH 7.6 and then stored for two days at -80°C. They are subsequently defrosted for 20 h and after centrifugation the hydrogenase is purified from the supernatant [13]. It is not clear to what extent this procedure results in de-activated enzyme; when applied to purified protein it does not work [31]. It is likely that the freezing/defreezing causes rupture of the periplasmic membrane. For the isolation of cytoplasmic proteins we have disrupted freshly harvested *D. vulgaris* cells with a chilled Manton-Gaulin press [32, 39]. When the Fe-hydrogenase is isolated from this starting material and purified to homogeneity by using an identical purification procedure as outlined in this paper, the specific activity is usually between 1000–2000 U/mg in the Chen and Mortenson H₂-production assay. One should compare this finding with the observation that purification starting with a periplasmic extract and a final HPLC MonoQ step yields hydrogenase with ≈ 7000 U/mg in addition to low-activity species. Apparently, the specific activity of Fe-hydrogenase can differ over some two or three orders of magnitude without changes in the usual purity index (0.36) or SDS/PAGE purity (> 99%).

Patil et al. reported a specific H₂-production activity of 7000 U/mg when measured in the gas chromatograph and apparently under the conditions according to the Peck and Mortenson procedure [13, 17, 30, 42]. We find 7000 U/mg in the standard manometric assay. A comparison of these determinations would require our number to be multiplied by a factor of 2–3. This suggests that the specific activity of preparations purified according to our current procedure is significantly higher.

In order to begin to work towards a resolution (or at least normalization) of the problems of the specific activity and homogeneity of Fe-hydrogenases and the derived problems of interpreting, e.g., spectroscopic data, we propose that future work should contain the following information: (a) protein determination according to the micro-biuret method and/or amino-acid analysis; (b) a H₂-production activity determination according to exactly defined conditions; (c) an iron stoichiometry number, e.g. according to the ferrous ferrioxalometric determination.

Redox properties of the clusters

Patil et al. EPR-monitored a dithionite titration of resting *D. vulgaris* hydrogenase and deduced a complicated scheme of redox events: two components titrated with bell-shaped response curves, a third component was subject to 'a strong

cooperative effect' [17]. We have shown here that all these responses reflect non-equilibrium transients in the reductive activation of the enzyme. When the protein is pre-activated with its substrate H₂, which is subsequently removed by substitution with argon, the results of an ensuing titration experiment point to a much simpler scheme. There are just two components each with a single redox transition.

From the H₂/H⁺ titration of activated enzyme and the dithionite/ferricyanide titration of inactive, recombinant protein it can be concluded that the F clusters are independent (i.e. non-interacting), indistinguishable, $n = 1$ electron-transferring groups with a reduction potential $E_m \approx -335$ mV. There is no indication that this potential is dependent on the pH. Double integration of the EPR from activated enzyme at high pH, therefore at high H₂/H⁺ ratios, gives two $S = 1/2$ systems/enzyme molecule. Thus, on the very reasonable assumption that the F clusters are cubanes [6], eight of the Fe ions have been accounted for.

The rhombic signal with $g = 2.11, 2.05, 2.00$ is ascribed to the H cluster [3]. At neutral pH the signal titrates with a reduction potential $E_m = -307$ mV. The maximally developed signal has a double integral corresponding to ≈ 0.4 spin $S = 1/2$ systems/enzyme molecule. This substoichiometric number can be interpreted in two ways: either the remaining spins are not EPR-detectable, or the samples are partially apoprotein with respect to the H cluster. Validity of the latter interpretation exclusively would imply that the H cluster encompasses a very large number of iron ions. It is possible that a small percentage of the preparations lack the H cluster and, therefore, that the observed total Fe content is slightly low. Stephens et al. have reported on indications from magnetic CD spectroscopy that the EPR H signal is accompanied by an EPR-silent high-spin component of unidentified spin [43]. We have previously reported on a very unusual high-spin signal (a single line with $g_{eff} = 5.0$) in H₂/Ar-cycled hydrogenase [4]. The relation, if any, between the magnetic CD high-spin signal and the EPR $g = 5$ signal is presently still obscure. In the experiments described in this paper (specifically that of Fig. 5) no $g = 5$ EPR signal was observed. In our view the crucial remaining problem is the low intensity of the H-cluster EPR signal. It is now abundantly clear that the signal can not be related to metals other than iron. It also appears that missing intensity is not in half-integer superspins ($S \geq 7/2$), because we have found none for hydrogenase where we have been successful with several other Fe/S proteins (nitrogenase [44], sulfite reductase [39], CO dehydrogenase [45], the prismane protein [46]). Clearly, the resolution of this problem requires further spectroscopic studies on normalized protein samples.

The two redox potentials that we have found are both significantly more positive than the potential of the hydrogen electrode. The half-maximal hydrogen production activity of Fe-hydrogenases as a function of the applied potential is approximately equal to the hydrogen electrode potential [24, 25]. This would seem to imply that in order for the *D. vulgaris* (Hildenborough) Fe-hydrogenase to operate in hydrogen production, a considerable reductive power must be continuously exerted by the enzyme's natural electron donor system. It would also seem to imply that the oxidized form of the H cluster, associated with the rhombic EPR H signal, is not necessarily a catalytically competent redox state.

Elemental analysis by ICP-MS was carried out by Dr A. A. van Heuzen at the Koninklijke/Shell-Laboratorium, Amsterdam. Elemental analysis by INAA was carried out by Th. G. van Meerten and A.

van der Meer at the Interuniversitair Reactor Centrum, Delft (The Netherlands). Mr I. Walinga helped us with the atomic absorption spectroscopy at the Department of Soil Science and Plant Nutrition, Wageningen. Mr L. C. de Folter helped us with the PIXE spectroscopy at the Cyclotron Laboratory in Eindhoven (The Netherlands). This investigation was supported by the Netherlands Foundation for Chemical Research (SON) with financial aid from the Netherlands Organization for Scientific Research (NWO) and by the National Institutes of Health (GM 12176 & 32785 to RHS).

REFERENCES

- Fauque, G., Peck, H. D. Jr, Moura, J. J. G., Huynh, B. H., Berlier, Y., DerVartanian, D. V., Teixeira, M., Przybyla, A. E., Lespinat, P. A., Moura, I. & LeGall, J. (1988) *FEMS Microbiol. Rev.* **54**, 299–344.
- Albracht, S. P. J. (1990) *Colloq. Ges. Biol. Chem. Mosbach* **41**, 40–51.
- Adams, M. W. W. (1990) *Biochim. Biophys. Acta* **1020**, 115–145.
- Hagen, W. R., van Berkel-Arts, A., Krüse-Wolters, K. M., Voordouw, G. & Veeger, C. (1986) *FEBS Lett.* **203**, 59–63.
- Meyer, J. & Gagnon, J. (1991) *Biochemistry* **30**, 9697–9704.
- Voordouw, G. & Brenner, S. (1985) *Eur. J. Biochem.* **148**, 515–520.
- Filipiak, M., Hagen, W. R. & Veeger, C. (1989) *Eur. J. Biochem.* **185**, 547–553.
- Adams, M. W. W., Eccleston, E. & Howard, J. B. (1989) *Proc. Natl Acad. Sci. USA* **86**, 4932–4936.
- Hagen, W. R. (1988) in *Photocatalytic production of energy-rich compounds* (Grassi, G. & Hall, D. O., eds) pp. 241–249, Elsevier, London.
- Hagen, W. R., Pierik, A. J., Wolbert, R. B. G., Verhagen, M. F. J. M. & Veeger, C. (1991) in the *Proceedings of the Third International Conference on Molecular biology of hydrogenases*, pp. 72–75.
- Grande, H. J., Dunham, W. R., Averill, B., van Dijk, C. & Sands, R. H. (1983) *Eur. J. Biochem.* **136**, 201–207.
- Hagen, W. R., van Berkel-Arts, A., Krüse-Wolters, K. M., Dunham, W. R. & Veeger, C. (1986) *FEBS Lett.* **201**, 158–162.
- Huynh, B. H., Czechowski, M. H., Krüger, H.-J., DerVartanian, D. V., Peck, H. D. Jr & LeGall, J. (1984) *Proc. Natl Acad. Sci. USA* **81**, 3728–3732.
- Erbes, D. L., Burrell, R. H. & Orme-Johnson, W. H. (1975) *Proc. Natl Acad. Sci. USA* **72**, 4795–4799.
- Van Dijk, C., Grande, H. J., Mayhew, S. G. & Veeger, C. (1980) *Eur. J. Biochem.* **107**, 251–261.
- Adams, M. W. W. & Mortenson, L. E. (1984) *J. Biol. Chem.* **259**, 7045–7055.
- Patil, D. S., Moura, J. J. G., He, S. H., Teixeira, M., Prickril, B. C., DerVartanian, D. V., Peck, H. D., Jr, LeGall, J. & Huynh, B.-H. (1988) *J. Biol. Chem.* **263**, 18732–18738.
- Saunders, G. F., Campbell, L. L. & Postgate, J. R. (1964) *J. Bacteriol.* **87**, 1073–1078.
- Van der Westen, H. M., Mayhew, S. G. & Veeger, C. (1978) *FEBS Lett.* **86**, 122–126.
- Voordouw, G., Hagen, W. R., Krüse-Wolters, K. M., van Berkel-Arts, A. & Veeger, C. (1987) *Eur. J. Biochem.* **162**, 31–36.
- Van Dongen, W., Hagen, W. R., van den Berg, W. & Veeger, C. (1988) *FEMS Microbiol. Lett.* **50**, 5–9.
- Elsden, S. R., Volcani, B. E., Gilchrist, F. M. C. & Lewis, J. H. (1956) *J. Bacteriol.* **72**, 681–689.
- Van Dijk, C., Mayhew, S. G., Grande, H. J. & Veeger, C. (1978) *Eur. J. Biochem.* **102**, 317–330.
- Van Dijk, C. & Veeger, C. (1981) *Eur. J. Biochem.* **114**, 209–214.
- Grande, H. J., van Berkel-Arts, A., Breghe, J., van Dijk, C., Veeger, C. (1983) *Eur. J. Biochem.* **131**, 81–88.
- Adams, M. W. W. (1987) *J. Biol. Chem.* **262**, 15054–15061.
- Peck, H. D. Jr & Gest, H. (1956) *J. Bacteriol.* **71**, 70–80.
- Chen, J.-S. & Mortenson, L. E. (1974) *Biochim. Biophys. Acta* **371**, 283–298.
- LeGall, J., Ljungdahl, P. O., Moura, I., Peck, H. D. Jr, Xavier, A. V., Moura, J. J. G., Teixeira, M., Huynh, B. H., DerVartanian, D. V. (1982) *Biochem. Biophys. Res. Commun.* **106**, 610–616.
- Patil, D. S., He, S. H., DerVartanian, D. V., LeGall, J., Huynh, B. H. & Peck, H. D. Jr (1988) *FEBS Lett.* **228**, 85–88.
- Van Dijk, C., van Berkel-Arts, A. & Veeger, C. (1983) *FEBS Lett.* **156**, 340–344.
- Pierik, A. J., Wolbert, R. B. G., Mutsaers, P. H. A., Hagen, W. R. & Veeger, C. (1992) *Eur. J. Biochem.* **206**, 697–704.
- Kivits, H. P. M., De Rooij, F. A. J. & Wijnhoven, G. P. J. (1990) *Nucl. Instrum. Methods* **164**, 225–229.
- Johansson, G. I. (1982) *X-ray Spectrometry* **11**, 194–200.
- Olivares, J. A. (1988) *Methods Enzymol.* **158**, 205–222.
- Versieck, J. (1988) *Methods Enzymol.* **158**, 267–286.
- Wolbert, R. B. G., Hilhorst, R., Voskuilen, G., Nachtegaal, J., Dekker, M., Van 't Riet, K. & Bijsterbosch, B. H. (1989) *Eur. J. Biochem.* **184**, 627–633.
- Ballantine, S. P. & Boxer, D. H. (1985) *J. Bacteriol.* **163**, 454–459.
- Pierik, A. J. & Hagen, W. R. (1991) *Eur. J. Biochem.* **195**, 503–516.
- Higuchi, Y., Yasuoka, N., Kakudo, M., Katsube, Y., Yagi, T. & Inokuchi, H. (1987) *J. Biol. Chem.* **262**, 2823–2825.
- Prickril, B. C., Czechowski, M. H., Przybyla, A. E., Peck, H. D., Jr & LeGall, J. (1986) *J. Bacteriol.* **167**, 722–725.
- Patil, D. S., Czechowski, M. H., Huynh, B. H., LeGall, J., Peck, H. D. Jr & DerVartanian, D. V. (1986) *Biochem. Biophys. Res. Commun.* **137**, 1086–1093.
- Stephens, P. J., Devlin, F., McKenna, M. C., Morgan, T., Czechowski, M., DerVartanian, D. V., Peck, H. D. Jr & LeGall, J. (1985) *FEBS Lett.* **180**, 24–28.
- Hagen, W. R., Wassink, H., Eady, R. R., Smith, B. E. & Haas, H. (1987) *Eur. J. Biochem.* **169**, 457–465.
- Jetten, M. S. M., Pierik, A. J. & Hagen, W. R. (1991) *Eur. J. Biochem.* **202**, 1291–1297.
- Pierik, A. J., Hagen, W. R., Dunham, W. R. & Sands, R. H. (1992) *Eur. J. Biochem.* **206**, 705–719.

Chapter 3

Novel Electron Paramagnetic Resonance Signals from an Fe/S Protein containing Six Iron Atoms.

Wilfred R. Hagen, Antonio J. Picrik and Cees Veeger

(1989) J. Chem. Soc., Faraday Trans. I 85, 4083-4090.

Novel Electron Paramagnetic Resonance Signals from an Fe/S Protein containing Six Iron Atoms

Wilfred R. Hagen,* Antonio J. Pierik and Cees Veeger

Department of Biochemistry, Agricultural University, Dreijenlaan 3,
NL-6703 HA Wageningen, The Netherlands

An EPR study is presented of an unusual iron-sulphur protein recently isolated from *Desulfovibrio vulgaris* (Hildenborough). The protein is a 50 kDa monomer and contains six iron atoms. The EPR spectrum of the dithionite-reduced protein is very similar to those found for model compounds which contain the [6Fe-6S]³⁺ prismane core. The spectrum is from a rapidly relaxing $S = 1/2$ ground state with $g = 2.004, 1.819, 1.32$. Spin quantification reveals the presence of nearly one spin system per protein molecule. In a higher, intermediate oxidation state the protein exhibits another $S = 1/2$ ground-state signal with $g = 1.968, 1.953, 1.903$. The fully oxidized protein shows no EPR spectrum. We believe we have found a single prismane-containing protein, that can exist in the redox states $3+ (S = 1/2)$, $4+ (S = 0 \text{ or integer})$, $5+ (S = 1/2)$ and $6+ (S = 0)$.

A biological iron-sulphur cluster is a structure of two or more Fe ions and a similar number of sulphide ions. The structure is ligated (to the Fe atoms) by side groups of amino acids in a polypeptide, predominantly by S from cysteines. The iron ions carry the formal valency III or II; they are probably always high-spin, *i.e.* $S = 5/2$ or $S = 2$. The Fe atoms are all mutually exchange-coupled, therefore the overall structure is also a magnetic cluster whose paramagnetism is described with a single resulting spin and associated effective g , A , D tensor.

Following the detection of the $g = 1.94$ signal in heart-muscle preparations in the late 1950s by Beinert and Sands,¹ the next decade provided the time span to relate this signal to a chemical and magnetic structure on the basis of a variety of magnetic-resonance spectroscopic data:^{2,3} the [2Fe-2S] cluster is biologically operative as a single-electron-transferring group in which one of the irons always is Fe^{III}, while the other shuttles between Fe^{III} and Fe^{II}. The fully reduced state with two iron(II) ions is never observed. The exchange coupling is several hundred wavenumbers and is antiferromagnetic, resulting in spin ladders with ground states characterized by $S = 0$ or $S = 1/2$, respectively.

The subsequently discovered [4Fe-4S] cubane clusters have long been considered to be straightforward extensions of the [2Fe-2S] clusters.⁴⁻⁶ Although the increase to six J -couplings between Fe pairs has thus far prohibited quantitative considerations of the coupling scheme, until recently the ground state for [4Fe-4S] clusters was always found to be $S = 0$ or $S = 1/2$. Although three out of the five theoretically possible valency states of the [4Fe-4S] cluster were actually detected, a cluster in any particular protein was always found to act as a single-electron-transferring group, *i.e.* to shuttle either between the one- and two-electron reduced state or between the two- and three-electron reduced state (where we define the all-Fe^{III} cluster as the fully oxidized state). A difference with [2Fe-2S] clusters was revealed by Mössbauer spectroscopy: reducing electrons in [4Fe-4S] clusters are not located on identifiable iron ions but are delocalized over the cluster.

The relatively simple picture just outlined no longer holds. Over the last decade we

Fe/S Protein containing Six Iron Atoms

have witnessed a dramatic increase in our knowledge of biological iron-sulphur clusters as regards their structures, magnetic properties and biological functions.

The [3Fe-4S] cluster was discovered.⁷⁻⁹ This cluster can exist as an incomplete cubane^{10,11} or as a structure with a linear array of irons.¹² The cubane-like [3Fe-4S] shuttles (at least by chemical reduction-oxidation) between the fully oxidized and the one-electron-reduced state. The magnetic ground states are $S = 1/2$ and $S = 2$, respectively. The linear cluster is only known in the fully oxidized state with $S = 5/2$.

The extension of the magnetism to high-spin ground states is not limited to reduced [3Fe-4S] clusters. The seleno derivatives of the [4Fe-4S] clusters in some ferredoxins exist as mixtures of spin states with $S = 1/2$, $S = 3/2$ and $S = 7/2$.¹³ The dimeric Fe-protein of nitrogenase is thought to carry a single [4Fe-4S] cluster. Its magnetism is a static (not thermally equilibrated) mixture of $S = 1/2$ and $S = 3/2$ ground states.¹⁴⁻¹⁶ The $\alpha_2\beta_2$ tetrameric MoFe-protein of nitrogenase possibly contains four [4Fe-4S] clusters (the so-called P-clusters) which are thought to be in the four-electron-reduced form, with $S = 0$, in dithionite-reduced enzyme.¹⁷ In thionine-oxidized enzyme half of these clusters exhibit EPR with an $S = 7/2$ ground state.^{18,19} In all these high-spin systems, including the $S = 2$ [3Fe-4S] cluster,²⁰ $|\Delta m_s| \neq 1$ transitions have been observed.

The biological functioning ascribed to iron-sulphur clusters is no longer limited to single-electron transfer. In aconitase the [4Fe-4S] cluster acts as a non-redox active, catalytic centre.²¹ A third function, two-electron transfer associated catalysis, has been implicated for an iron-sulphur cluster of unknown structure: the active site of iron-only (*i.e.* non-nickel-containing) hydrogenase probably is (or encompasses) a single iron-sulphur cluster.^{22,23} This enzyme catalyses the synthesis of molecular hydrogen from two protons and two electrons. The capacity to take up two electron equivalents implies the existence, if only transiently, of three different redox states. Only two redox states are found for biological [2Fe-2S] and [3Fe-4S] clusters. Although they are known thus far to use only two redox states in their biological action, [4Fe-4S] clusters can exist in at least three different states. This fact, combined with the delocalization of reducing electrons over cubanes, leads us to the following hypothesis: the more Fe ions an iron-sulphur cluster contains, the better it is suited to accommodating a pair of electrons. In other words, clusters such as that in the active site of hydrogenase are likely to contain at least four Fe ions.

We have previously proposed that the active site of hydrogenase contains six iron ions.²⁴ This number is an approximate one deduced from two sets of observations. First, the hydrogenase contains a total of some 14 Fe. Owing to experimental uncertainty associated with the determination of Fe in a protein matrix, and also with the determination of protein concentration, the error in the iron stoichiometry is probably of the order of 10%. Secondly, on the basis of the protein sequence data²⁵ and of EPR data,²⁶ exactly eight of the approximately 14 Fe can be assigned to two regular cubanes which are likely to function as entry sites for the reducing equivalents. This leaves very approximately six (*i.e.* with an uncertainty of one or two) irons to be accommodated by the active site.

Model compounds containing a [6Fe-6S] core, also called the prismane core, have been synthesized by Coucouvanis and co-workers.²⁷ These authors also suggested looking for prismanes in iron-sulphur proteins with unusual characteristics. The matter is by no means a trivial one as prismanes are metastable structures that are easily converted into cubanes. Also, the prismane optical spectrum is uninformative, and the EPR spectrum, although very characteristic, is difficult to detect because of extreme g anisotropy and fast spin-lattice relaxation.²⁷ The prismane EPR fingerprint has not been found in hydrogenase, although the enzyme does exhibit other EPR signals which are unique for iron-sulphur proteins.²²

We have now isolated another iron-sulphur protein from the same bacterial source as that from which the hydrogenase is isolated. The protein contains six iron atoms in total and it exhibits the characteristic prismane EPR signal.

W. R. Hagen, A. J. Pierik and C. Veeger

Experimental

Desulfovibrio vulgaris (strain Hildenborough NCIB 8303) was grown and its hydrogenase was isolated and purified according to the procedures of van der Westen *et al.*²⁰ The purification is essentially a three-step column chromatography involving anion exchange (DEAE Sephacel), molecular sieving (G-150) and adsorption (hydroxyapatite). With purity checks by means of Pharmacia-FPLC (Mono Q) the hydrogenase was found on occasion to be contaminated with another brownish protein, which was subsequently obtained on a small scale in pure form from the Mono Q eluate. Further chromatography revealed that the protein copurifies with hydrogenase on the first two columns, however, it does not readily bind to the hydroxyapatite, in contrast to the behaviour of hydrogenase. A detailed account of the purification and biochemical characterization will be presented elsewhere. Here, we summarize thus far obtained information which is relevant for the interpretation of the EPR data.

The protein exhibits a single band on SDS-PAGE (60 kDa) and on isoelectric focussing gels (pI 4.8). Sedimentation equilibrium experiments in the analytical ultracentrifuge indicate the molecular mass to be 50 kDa. On the basis of this number the protein contains 6 (± 0.5) Fe atoms (average of three different preparations; determined by colorimetry and by particle induced X-ray emission spectroscopy). Acid-labile sulphur is present. Molybdenum, tungsten and selenium were below the detection limit in PIXE spectroscopy. The UV-visible spectrum is typical for iron-sulphur proteins with a broad shoulder at 400 nm. The protein has no hydrogenase activity and there is no immunological cross-reactivity with the iron-hydrogenase.

EPR data were taken on a Bruker EPR 200 D spectrometer. Sample cooling was with a home-built helium-flow cryostat. The sample temperature was calibrated with a dummy sample containing two 5 k Ω Allen-Bradley carbon resistors just below and above the 1.5 cm measuring area of the TE₁₀₂ cavity. The spectrometer was interfaced to an Olivetti M24 PC with software written in Asyst for data acquisition, correction of background signals, double integration procedures and *g*-value determinations. Quantification of spin concentrations was according to Aasa and Vänngård.²⁰ The external standard for integration was 10 mmol dm⁻³ CuSO₄/10 mmol dm⁻³ HCl/2 mol dm⁻³ NaClO₄. Anaerobic reduction and oxidation of protein samples was carried out in the EPR tubes connected to a scrubbed argon/vacuum manifold as previously described.²²

Results and Discussion

EPR Spectra of the fully Reduced State

The spectra in fig. 1 are from a frozen solution of 0.3 mmol dm⁻³ of the iron-sulphur protein reduced under argon atmosphere with 10 mmol dm⁻³ of buffered sodium dithionite. An effective *g* tensor with principal values 2.004, 1.819, 1.32, is read from the most pronounced features of the spectrum, taken at a temperature of 16 K. Additionally, the spectrum exhibits a number of intermediate features, especially one that peaks at 1.933, and also broad shoulders on the low- and high-field extremes of the powder pattern.

Spin-lattice relaxation is rapid. No saturation is observable at 16 K with microwave powers up to 200 mW. Also, above 16 K the spectrum rapidly broadens, as can be seen from the trace obtained at *T* = 32 K. Lowering of the detection temperature below 16 K leaves the shape of the spectrum invariant; however, power saturation becomes observable. In fact, at *T* = 4.2 K (spectra not shown) the relaxation has slowed down to the extent that we have not been able to obtain truly unsaturated data, as this required attenuation of the 200 mW incident power by values in excess of 40 dB.

In table 1 data are summarized on the determination of spin concentration. These quantifications rely on the assumption that the observed resonance is from an isolated

Fe/S Protein containing Six Iron Atoms

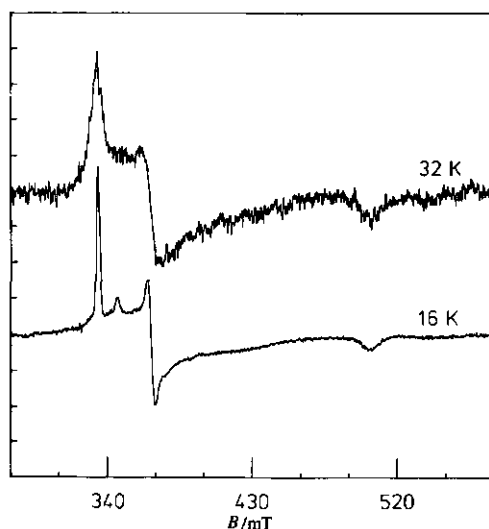


Fig. 1. Prismane-like EPR signal of the dithionite-reduced 6Fe iron-sulphur protein from *D. vulgaris* (H). The protein was $272 \mu\text{mol dm}^{-3}$ in 25 mmol dm^{-3} Hepes buffer, pH 7.5 and was reduced under argon with 10 mmol dm^{-3} sodium dithionite for 3 min at ambient temperature. EPR conditions: microwave frequency, $9331 \pm 3 \text{ MHz}$; modulation frequency, 100 kHz; modulation amplitude, 0.63 mT; microwave power, 200 mW; temperature (relative gain), 16 K ($1 \times$) and 32 K ($6.3 \times$).

Table 1. Spin quantification of the prismane-like spectrum from dithionite-reduced 6Fe iron-sulphur protein

method of integration	T/K	microwave power/mW	[spins]
1st integral at $g = 2.004$	4.2	0.02	0.76
		0.08	0.67
		0.2	0.53
		0.8	0.53
		8.0	0.2
1st integral at $g = 2.004$	16.0	20.0	0.92
		200.0	0.90
total second integral	16.0	200.0	0.57
1st integral at $g = 1.32$	32.0	200.0	0.69

Kramers doublet, *i.e.* that the ground multiplet is an effective $S = 1/2$ system. Double integration of these extremely wide spectra is not overly reliable because it is very sensitive to minor instabilities in the baseline. Indeed, we have experienced that for these spectra the well known (but unpublished) reliability rule of thumb, that the numerical end values of the first and second integral should differ by at least a factor of 1000, is usually not met. We have therefore made the quantifications on the basis of the first integral of isolated, absorption-shaped peaks, as described by Aasa and Vänngård.²⁹ At $T = 4.2 \text{ K}$ the stoichiometry of effective $S = 1/2$ systems per 50 kDa protein molecule,

W. R. Hagen, A. J. Pierik and C. Veeger

based on the area under the $g = 2.004$ peak, approaches unity when we move towards non-saturating power levels (*cf.* table 1). At $T = 16$ K we still find nearly one spin system. At $T = 32$ K the peak at $g = 2.004$ is no longer isolated from the derivative feature at $g = 1.819$, therefore, we must quantify on the weak peak at $g = 1.32$. The resulting spin concentration is only slightly less than that found at lower temperatures. We conclude that the integrated signal intensity follows Curie's law, possibly with a slight population of an excited state when $T = 32$ K. The observed spin system is an $S = 1/2$ ground state, and there is approximately one system per protein molecule.

Comparison with the EPR of Synthetic Prismanes

We have previously studied²⁷ frozen solutions of synthetic clusters of the type $[\text{Fe}_6\text{S}_6(\text{L})_6]^{3-}$ by EPR spectroscopy, in which $\text{L} = \text{Cl}^-$, Br^- , I^- , RS^- , RO^- . All these compounds exhibit very similar EPR spectra which, in turn, are similar to the iron-sulphur protein spectra reported here in the following characteristics: (1) the EPR is from an $S = 1/2$ ground state; (2) relaxation is relatively fast; (3) broadening sets in above a temperature of some 10 K; (4) there is a sharp peak with a g value just above the free-electron value and a derivative feature with a zero crossing at $g = 1.7-1.8$.

The third g value is usually not directly readable from the powder spectrum. This is probably due to the fact that the linewidth in the model-compound spectrum is an order of magnitude larger than in the protein spectra presented here. For two prismane models the complete set of principal g values was previously determined by spectral simulation,²⁷ and those results are compared in table 2 with the values for the protein. The correspondence is striking, especially between the protein and the model that has sulphur coordinating to the prismane iron atoms.

It thus appears that the spectrum of the 6Fe-protein is very much a reduced linewidth version of the prismane model spectra. We can now also understand a previously puzzling observation in the analysis, by spectral synthesis, of the prismane model spectra.²⁷ Although this analysis was based on a sophisticated model (the statistical theory of g strain)^{30,31} for the description of inhomogeneously broadened EPR powder patterns, the simulations would never fully fit the data unless an artificial 'residual broadening' would be included in the simulator in addition to the g strain broadening. If the prismane spectra would also contain, in addition to the features at the principal g values, intermediate features similar to (but broader) than those observed in the spectra from the protein, then their contribution to the EPR powder shape may well have been simulated by the artificial 'residual broadening'. In fact, in some of the prismane model spectra [*cf.* fig. 6 in ref. (27)] a clear low-field shoulder is discernible very similar to that visible in the 16 K spectrum in fig. 1.

The previous does of course not explain the physical origin of the intermediate features and the shoulders. Similar features have been observed in proteins that contain two cubanes,³² or one cubane and a [3Fe-4S] cluster,²⁰ as a result of inter-cluster dipolar interaction. Here, the extra features appear to be an intrinsic property of the 6Fe cluster itself. We feel that this property may be related to a structural property in which the prismane differs from hitherto encountered biological iron-sulphur clusters:²⁷ in addition to the commonly found 'short' Fe-Fe distances of 2.7-2.8 Å, there is also a set of 'long' Fe-Fe distances of some 3.8 Å. We realize that much theoretical and experimental work is still ahead of us to make and interpret this link on more than an intuitive basis.

Spectra of the untreated, 'as-isolated' Protein

The protein, as isolated, does not show the prismane EPR fingerprint. It exhibits yet another EPR signal with characteristics not previously found for iron-sulphur proteins.

Fe/S Protein containing Six Iron Atoms

Table 2. Comparison of principal g values for prismane model compounds²⁷ and the 6Fe iron-sulphur protein

compound	g_1	g_2	g_3
$(Et_4N)_3(Fe_6S_6Cl_6)$	2.038	1.71	1.2
$(Et_4N)_3[Fe_6S_6(SC_6H_4-p-Me)_6]$	2.029	1.79	1.3
6Fe iron-sulphur protein	2.004	1.819	1.32

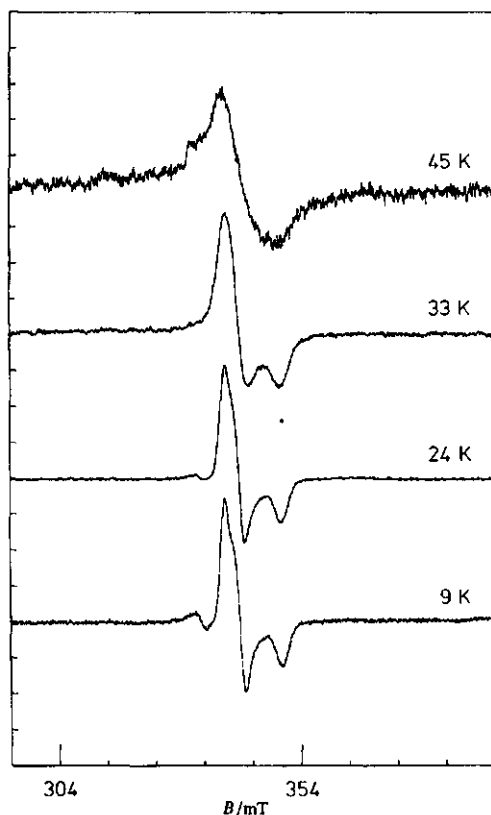


Fig. 2. Temperature dependence of the EPR signal in 6Fe iron-sulphur protein 'as isolated' (same preparation as for fig. 1). EPR conditions were as for fig. 1 except for (temperature, microwave power, relative gain), (45 K, 80 mW, 9.1 \times); (32.5 K, 80 mW, 2.3 \times); (23.5 K, 32 mW, 1 \times); (8.9 K, 0.32 mW, 3.6 \times).

The shape of this signal as a function of the detection temperature is presented in fig. 2. The spectrum taken at $T = 9$ K is not broadened by spin-lattice relaxation. A further lowering to $T = 4.2$ K does not affect the spectral shape (not shown). Raising the temperature above ca. 20 K results in a gradual broadening of the spectrum to non-detectability above ca. 50 K.

The microwave power saturation behaviour of this signal is not unusual. The power

W. R. Hagen, A. J. Pierik and C. Veeger

Table 3. Spin quantification of the signal from 6Fe iron-sulphur protein 'as isolated'

sample	T/K	[spins]
A (272 $\mu\text{mol dm}^{-3}$)	4.2	0.10
	5.7	0.09
	8.9	0.12
	11.2	0.12
	17.3	0.12
	23.5	0.11
	32.5	0.07
	38.0	0.06
	45.0	0.04
	B (60 $\mu\text{mol dm}^{-3}$)	11.0

levels given in the legend to fig. 2 are the values just above which saturation sets in at that particular temperature. At $T = 4.2$ K this value is 0.013 mW.

The spectrum has three main features from which we read the principal g values to be 1.968, 1.953, 1.903. On the low-field side there is an additional feature observable which crosses the baseline at an effective g value of 1.999. These g values are not reminiscent of any known Fe/S spectrum. They are rather more indicative of the d^1 configurations Mo^V or W^V , as, e.g. observed in sulphite oxidase.³³ However, we have been unable to detect any molybdenum or tungsten in our protein samples by colorimetry and by PIXE spectroscopy. We propose that the signal represents another redox state of the 6Fe cluster.

The spectrum is sufficiently sharp to give reliable results in the spin quantification by double integration. In table 3 the numbers are reported as a function of temperature, again assuming an effective $S = 1/2$. The spin concentration is approximately constant from 4 K up to 24 K and then decreases. Again we conclude that the spectrum is from an $S = 1/2$ ground state, possibly with some depopulation at higher temperatures.

Redox States of the Putative 6Fe Cluster

The spin concentration for the protein as isolated is substoichiometric and sample dependent (cf. table 3). This suggests that the protein as isolated is not purely in one redox state. When the protein is anaerobically oxidized with tenfold excess potassium ferricyanide, the d^1 -like spectrum of fig. 2 essentially disappears and no other signals are observed. This suggests that the protein has become diamagnetic. When the protein is reduced with dithionite the d^1 -like spectrum disappears and is replaced by the signal which is a fingerprint for three-electron-reduced prismatic. Replacing a half-integer spin by another half-integer spin by means of reduction implicates a two-electron transfer step. We summarize the previous in the following working hypothesis.

The iron-sulphur protein, of unknown biological function, that we have inadvertently isolated from the sulphate-reducing anaerobe *D. vulgaris* (H), contains a single [6Fe-6S] cluster. The cluster can exist in four different redox states (at least in the test tube), namely: the fully oxidized state of 6Fe^{III} , i.e. $[\text{6Fe-6S}]^{6+}$, $S = 0$; the one-electron-reduced state $[\text{6Fe-6S}]^{5+}$, $S = 1/2$; the two-electron-reduced state $[\text{6Fe-6S}]^{4+}$, $S = \text{integer or } 0$; and the three-electron-reduced state $[\text{6Fe-6S}]^{3+}$, $S = 1/2$.

We have not yet determined sulphide quantitatively, neither have we carried out a full redox titration. We are presently involved in scaling up the isolation of this protein in order to be able to put our hypothesis to a further test and to be able to find out what the biological function is of this intriguing novel iron-sulphur protein.

Fe/S Protein containing Six Iron Atoms

We thank M. Boersma for skilful technical assistance. We are indebted to P. Mutsaers for his PIXE determinations at Eindhoven Technical University. We thank C. Schillemans for the interfacing of the spectrometer and for writing the acquisition/analysis program. This work was supported by the Netherlands Foundation for Chemical Research (SON) with financial aid from the Netherlands Organization for Scientific Research (NWO).

References

- 1 H. Beinert and R. H. Sands, *Biochem. Biophys. Res. Commun.*, 1960, **3**, 41.
- 2 J. F. Gibson, D. O. Hall, J. H. M. Thornley and F. R. Whatley, *Proc. Natl Acad. Sci. U.S.A.*, 1966, **56**, 987.
- 3 R. H. Sands and W. R. Dunham, *Q. Rev. Biophys.*, 1975, **7**, 443.
- 4 Iron-Sulphur Proteins, ed. W. Lovenberg (Academic Press, New York, 1973), vol. 1.
- 5 Ref. (4), vol. 2.
- 6 Ref. (4), 1977, vol. 3.
- 7 M. H. Emptage, T. A. Kent, B. H. Huynh, J. Rawlings, W. H. Orme-Johnson and E. Münck, *J. Biol. Chem.*, 1980, **255**, 1793.
- 8 C. D. Stout, D. Ghosh, V. Patabhi and A. Robbins, *J. Biol. Chem.*, 1980, **255**, 1797.
- 9 Iron-Sulphur Proteins, ed. T. G. Spiro (John Wiley, New York, 1982).
- 10 G. H. Stout, S. Turley, L. C. Sieker and L. H. Jensen, *Proc. Natl Acad. Sci. U.S.A.*, 1988, **85**, 1020.
- 11 H. Beinert, M. H. Emptage, J.-L. Dreyer, R. A. Scott, J. E. Hahn, K. O. Hodgson and A. J. Thomson, *Proc. Natl Acad. Sci. U.S.A.*, 1983, **80**, 393.
- 12 M. C. Kennedy, T. A. Kent, M. Emptage, H. Merkle, H. Beinert and E. Münck, *J. Biol. Chem.*, 1984, **259**, 14463.
- 13 J. Gaillard, J.-M. Moulis, P. Auric and J. Meyer, *Biochemistry*, 1986, **25**, 464.
- 14 W. R. Hagen, R. R. Eady, W. R. Dunham and H. Haaker, *FEBS Lett.*, 1985, **189**, 250.
- 15 P. A. Lindahl, E. P. Day, T. A. Kent, W. H. Orme-Johnson and E. Münck, *J. Biol. Chem.*, 1985, **260**, 11160.
- 16 G. D. Watt and J. W. McDonald, *Biochemistry*, 1985, **24**, 7226.
- 17 B. E. Smith, D. J. Lowe, G.-X. Chen, M. J. O'Donnell and T. R. Hawkes, *Biochem. J.*, 1983, **209**, 207.
- 18 W. R. Hagen, H. Wassink, R. R. Eady, B. E. Smith and H. Haaker, *Eur. J. Biochem.*, 1987, **169**, 457.
- 19 P. A. Lindahl, V. Papaefthymiou, W. H. Orme-Johnson and E. Münck, *J. Biol. Chem.*, 1988, **263**, 19412.
- 20 W. R. Hagen, W. R. Dunham, M. K. Johnson and J. A. Fee, *Biochim. Biophys. Acta*, 1985, **828**, 369.
- 21 M. H. Emptage, T. A. Kent, M. C. Kennedy, H. Beinert and E. Münck, *Proc. Natl Acad. Sci. U.S.A.*, 1983, **80**, 4674.
- 22 W. R. Hagen, A. van Berkel-Arts, K. M. Krüse-Wolters, W. R. Dunham and C. Veeger, *FEBS Lett.*, 1986, **201**, 158.
- 23 G. Voordouw, W. R. Hagen, K. M. Krüse-Wolters, A. van Berkel-Arts and C. Veeger, *Eur. J. Biochem.*, 1987, **162**, 31.
- 24 W. R. Hagen, A. van Berkel-Arts, K. M. Krüse-Wolters, G. Voordouw and C. Veeger, *FEBS Lett.*, 1986, **203**, 59.
- 25 G. Voordouw and S. Brenner, *Eur. J. Biochem.*, 1985, **148**, 515.
- 26 M. Filipiak, W. R. Hagen, H. J. Grande, W. R. Dunham, A. van Berkel-Arts, M. Krüse-Wolters and C. Veeger, *Recl. Trav. Chim. Pays-Bas*, 1987, **106**, 230.
- 27 M. G. Kanatzidis, W. R. Hagen, W. R. Dunham, R. K. Lester and D. Coucouvanis, *J. Am. Chem. Soc.*, 1985, **107**, 953.
- 28 H. M. van der Westen, S. G. Mayhew and C. Veeger, *FEBS Lett.*, 1978, **86**, 122.
- 29 R. Aasa and T. Vänngård, *J. Magn. Reson.*, 1975, **19**, 308.
- 30 W. R. Hagen, D. O. Hearshen, R. H. Sands and W. R. Dunham, *J. Magn. Reson.*, 1985, **61**, 220.
- 31 W. R. Hagen, D. O. Hearshen, L. J. Harding and W. R. Dunham, *J. Magn. Reson.*, 1985, **61**, 233.
- 32 R. Mathews, S. Charlton, R. H. Sands and G. Palmer, *J. Biol. Chem.*, 1974, **249**, 4326.
- 33 J. L. Johnson and K. V. Rajagopalan, *J. Biol. Chem.*, 1976, **251**, 5505.

Chapter 4

Purification and biochemical characterization of a putative [6Fe-6S] prismane-cluster-containing protein from *Desulfovibrio vulgaris* (Hildenborough).

Antonio J. Pierik, Ronnie B.G. Wolbert, Peter H.A. Mutsaers,
Wilfred R. Hagen and Cees Veeger

(1992) Eur. J. Biochem. 206, 697-704.

Purification and biochemical characterization of a putative [6Fe-6S] prismane-cluster-containing protein from *Desulfovibrio vulgaris* (Hildenborough)

Antonio J. PIERIK¹, Ronnie B. G. WOLBERT¹, Peter H. A. MUTSAERS², Wilfred R. HAGEN¹ and Cees VEEGER¹

¹Department of Biochemistry, Agricultural University, Wageningen, The Netherlands
²Cyclotron Laboratory, Eindhoven University of Technology, The Netherlands

Received January 27, 1992) – EJB 92 0099

A novel iron-sulfur protein has been isolated from the sulfate-reducing bacterium *Desulfovibrio vulgaris* (Hildenborough). It is a stable monomeric protein, which has a molecular mass of 52 kDa, as determined by sedimentation-equilibrium centrifugation. Analysis of the metal and acid-labile sulfur content of the protein revealed the presence of 6.3 ± 0.4 Fe/polypeptide and 6.2 ± 0.7 S²⁻/polypeptide. Non-iron transition metals, heme, flavin and selenium were absent. Combining these data with the observation of a very anisotropic $S = 1/2$ [6Fe-6S]³⁺ prismane-like EPR signal in the dithionite-reduced protein, we believe that we have encountered the first example of a prismane-cluster-containing protein. The prismane protein has a slightly acidic amino acid composition and isoelectric point (pI = 4.9). The ultraviolet/visible spectrum is relatively featureless ($\epsilon_{280} = 81 \text{ mM}^{-1} \cdot \text{cm}^{-1}$, $\epsilon_{400} = 25 \text{ mM}^{-1} \cdot \text{cm}^{-1}$, $\epsilon_{400, \text{red}} = 14 \text{ mM}^{-1} \cdot \text{cm}^{-1}$). The shape of the protein is approximately globular ($s_{20, \text{w}} = 4.18$ S). The N-terminal amino acid sequence is MF^S/cFQ^S/cQETAKNTG. Polyclonal antibodies against the protein were raised. Cytoplasmic localization was inferred from subcellular fractionation studies. Cross-reactivity of antibodies against this protein indicated the occurrence of a similar protein in *D. vulgaris* (Monticello) and *Desulfovibrio desulfuricans* (ATCC 27774). We have not yet identified a physiological function for the prismane protein despite trials for some relevant enzyme activities.

Iron-sulfur clusters constitute the redox-active site of a large number of biological electron-transfer components. The ubiquity of these versatile redox centers is documented by their involvement in vital steps of biochemical pathways: the mitochondrial respiratory chain, photosynthesis, Krebs' cycle, methanogenesis, nitrogen fixation, sulfate and nitrate reduction [1]. The knowledge of iron-sulfur clusters in biological systems in general is based on spectroscopically and crystallographically scrutinized electron-transfer proteins. Our reference collection of X-ray crystallographical structures formed by the [2Fe-2S] dinuclear site in ferredoxin, the [4Fe-4S] cubane in high-phosphate iron protein, ferredoxin and soluble-cubane ferredoxin, the [3Fe-4S] cluster in ferredoxin and [3Fe-4S]/[4Fe-4S] ferredoxin [2]. A number of inorganic model compounds mimicking these polypeptide-ligated iron-sulfur cores have been synthesized and characterized (reviewed in [3]).

Not only electron transport and oxidoreduction, but also iron-based substrate coordination and catalysis of non-redox

reactions can be accomplished by iron-sulfur clusters [4]. The best-characterized example is aconitase, for which an X-ray crystallographical structure is available [5].

Unfortunately, the basic set of structures and their respective spectroscopic properties is not sufficient to explain the EPR characteristics of multielectron redox proteins [6]. Straightforward elucidation of the structure of the iron-sulfur sites is hampered by the lack of sufficient resolution of the crystallographical structures, the absence of amino acid sequence data, and/or the lability of many iron-sulfur centres in the aerobic environment [7, 8]. As a working hypothesis for the description of these structures and their magnetism, we have recently proposed the supercluster/superspin concept [9, 10]. This hypothesis explains the absence of classical iron-sulfur clusters and the presence of unusual EPR spectra in multielectron redox proteins with a high Fe/S content by proposing the existence of superclusters of more than four magnetically coupled Fe ions, giving rise to unprecedented superspin ($S \geq 7/2$) paramagnetism. This concept particularly addresses the high Fe/S content of complex enzymes such as hydrogenase [11], nitrogenase component 1 [12], dissimilatory sulfite reductase [13] and carbonmonoxide dehydrogenase [14]. The existence of larger iron-sulfur clusters, e.g. the [6Fe-6S] prismane core, is also documented by inorganic model compounds [15–17]. In a previous publication, we reported that an unusual iron-sulfur protein of the sulfate-reducing bacterium *Desulfovibrio vulgaris* (Hildenborough) exhibited

Correspondence to W. R. Hagen, Laboratorium voor Biochemie, Landbouwniversiteit, Dreijenlaan 3, NL-6703 HA Wageningen, The Netherlands

Abbreviation. APS, adenosine 5'-phosphosulfate.

Enzymes. Desulfovibridin or dissimilatory sulfite reductase (EC 1.99.1); carbonmonoxide dehydrogenase or acetyl-CoA synthase (EC 1.2.99.2); nitrogenase (EC 1.18.6.1); Fe-hydrogenase (EC 8.99.1).

an EPR signal reminiscent of the $[6\text{Fe-6S}]^{3+}$ prismane cluster, while EPR signals characteristic of classical iron-sulfur clusters were absent [18]. Preliminary results on the redox properties and the $S = 9/2$ superspin EPR signals of this protein have been communicated [9, 10]. We present a biochemical and biophysical characterization of this prismane protein in this and in a subsequent paper [19].

MATERIALS AND METHODS

Growth and isolation

Desulfovibrio vulgaris (Hildenborough) NCIB 8303 was maintained on Postgate's medium [20]. For localization experiments of *Desulfovibrio* strains, cells were grown in Saunders' N medium [21] to an absorbance of approximately 0.8 at 660 nm. Large-scale growth of *D. vulgaris* (Hildenborough) for isolation of the protein was in modified Saunders' medium [22]. A 1% inoculum was used to start 240-l batch cultures in a home-built fermentor. Anaerobiosis was obtained by vigorous bubbling with nitrogen gas (99.99%). A 60-h growth period at 35°C allowed the isolation of 150–200 g wet cells.

Cells were harvested with a Sharpless continuous-flow centrifuge. The cell paste was suspended in 3 vol. 10 mM Tris/Cl, pH 8.0, in a chilled 1-l Waring blender (10 strokes). Cells were disrupted by three passages through a chilled Manton-Gaulin press (84 MPa). A spatula of DNase and RNase (Sigma) was added. A supernatant containing soluble proteins was separated from a blackish precipitate and dark-red membranes by successive centrifugation steps at $10000 \times g$ (20 min) and $100000 \times g$ (60 min), respectively. The pH of the supernatant was adjusted to 8.0 with 1 M Tris/Cl, pH 9, and diluted with demineralized water to yield a solution with a conductivity of 2 mS/cm. The soluble protein fraction was applied onto a DEAE-Sephacel column (5 cm \times 20 cm), equilibrated with 10 mM Tris/Cl, pH 8.0. Cytochromes were eluted with starting buffer. After washing with 1 l 10 mM Tris/Cl, pH 8.0, plus 20 mM NaCl, a 20–400 mM NaCl gradient in 10 mM Tris/Cl, pH 8.0, (2 l) was applied to separate the bound proteins into two main fractions: a brownish fraction (60–110 mM NaCl) with the prismane protein (see below), (partially inactivated) periplasmic hydrogenase, adenosine-5'-phosphosulfate (APS) reductase, assimilatory sulfite reductase and a greenish-brown fraction containing desulfoviridin and ferredoxin. The brownish fraction (typically 400 ml) was concentrated using an Amicon device with YM-30 filter. This concentrate was applied in two 10-ml batches onto a 1.5 cm \times 100 cm Sephadex G-150 gel-filtration column equilibrated with 25 mM potassium phosphate, pH 7.5. A brown fraction containing the prismane protein eluted at approximately 330 ml and was resolved from a yellow/brown APS reductase fraction. The prismane-protein-containing fractions were passed through a 2 cm \times 10 cm Ultragel hydroxyapatite column equilibrated with 25 mM potassium phosphate, pH 7.5, to remove periplasmic hydrogenase and assimilatory sulfite reductase. The eluate was combined with a 50-ml 25 mM potassium phosphate, pH 7.5, wash of the column and was concentrated (Amicon/YM-30). After desalting on Sephadex G-25 (20 mM Tris/Cl, pH 8.0) and microfiltration, proteins were applied onto a MonoQ 5/5 anion-exchange chromatography column attached to a Pharmacia FPLC system. A 60-ml 0–1 M NaCl gradient in 20 mM Tris/Cl, pH 8.0, resolved the prismane protein eluting at approximately 130 mM NaCl from several other proteins which eluted at higher NaCl concentrations.

Purification, as described, was performed aerobically at 4°C, FPLC at ambient temperature (18–22°C). Minor precipitates formed during the successive stages of purification were removed by centrifugation at $20000 \times g$ (15 min). During preliminary studies, Western blots (see immunological techniques) were used for the identification of fractions eluting from the first two columns. Later purifications were followed by tracing coeluting enzymes: APS reductase (DEAE-Sephacel) and periplasmic hydrogenase (Sephadex G-150). The final part of the purification was routinely judged by SDS/PAGE with Coomassie-blue staining (see electrophoresis).

Molecular mass determination

A Pharmacia FPLC system equipped with a Superose (HR 10/30) was used for gel filtration. The column was equilibrated with 50 mM potassium phosphate/150 mM KCl (pH 7.2). Molecular mass markers were α -chymotrypsinogen (23.7 kDa), ovalbumin (43.5 kDa), *D. vulgaris* (Hildenborough) periplasmic hydrogenase (57 kDa including Fe and S^{2-} contents), bovine serum albumin (67 kDa), bovine liver catalase (248 kDa) and horse spleen apoferritin (\approx 467 kDa).

For gel filtration under denaturing conditions, 6 M guanidinium hydrochloride/0.1 M Tris/0.5 mM Na_2EDTA adjusted to pH 8.6 (HCl) was used. The prismane protein and markers (chymotrypsinogen, ovalbumin, bovine serum albumin and α/β subunits of *D. vulgaris* (Hildenborough) periplasmic hydrogenase) were iodoacetylated prior to gel filtration. Protein solution (2–4 mg/ml) in elution buffer was incubated with 2 mM dithiothreitol at 80°C for 5 min. Subsequently, sulfhydryl groups were blocked by treatment with iodoacetic acid (20 mM) at room temperature in the dark (60 min).

Sedimentation velocity and sedimentation equilibrium measurements were made with an MSE analytical ultracentrifuge with scanning optics. Prismane protein samples were equilibrated with 100 mM potassium phosphate, pH 7.5, 0.02% NaN_3 on a 1 cm \times 10 cm Sephadex G-25 column. Data were analyzed according to Filipiak et al. [23].

Electrophoresis

Tris/glycine based gels (cf. [24]) were cast and run either in a home-built electrophoresis system or with the use of LKB Midget gel-electrophoresis system. For native electrophoresis, SDS was omitted. The composition (molar vol.) of the stacking gel was 4% acrylamide and 0.1% bisacrylamide; running gels were 10–20% acrylamide and 0.4–0.07% bisacrylamide. Molecular masses were estimated with the Pharmacia 14.4–94-kDa marker kit. Gel scanning was performed on a LKB Ultroskan XL system equipped with a HeNe laser (633 nm). Flat-bed isoelectric focussing on Ser Precotes (pI 5–7) was performed on a LKB Ultraphor electrophoresis unit at 4°C. Markers were hen egg trypsin inhibitor, superoxide dismutase, carbonic anhydrase (bovine erythrocytes) and ribonuclease A (bovine pancreas), with isoelectric points at 4°C of 4.6, 5.3, 5.8 and 8.0 respectively [25].

Immunological techniques

The prismane protein (500 μg) was subjected to preparative SDS/PAGE (30 \times 14 \times 0.15 cm). Protein was detected by precipitation of the SDS by addition of 100 mM KCl [26].

er excision and electroelution (ISCO system), 100- μ g amounts were mixed with Freund's complete adjuvant and injected subcutaneously in male New Zealand white rabbits. 10 μ g BC mice were injected with the 10- μ g amounts. Boosts of antigen in Freund's incomplete adjuvant were administered bi-weekly. Serum obtained after bleeding was used without further purification.

For immunoblotting, SDS/PAGE-separated proteins were transferred onto nitrocellulose (Schleicher and Schüll, 0.45 μ m) [27]. Goat anti-(rabbit IgG) antibodies or goat anti-mouse IgG antibodies conjugated to alkaline phosphatase (Bio-Rad, Richmond, USA and Promega Biotec, Madison, WI, USA, respectively) were used as secondary antibodies for immunostaining.

Cellular localization

Cells were harvested by centrifugation at 5000 \times g (5 min). After suspension in demineralized water (0°C) 1 vol. 10 mM Na₂EDTA/100 mM Tris/Cl, pH 9, was added. Incubation at 32°C for 20–30 min and subsequent centrifugation at 5000 \times g (5 min) released an orange/red periplasmic fraction [22]. Spheroplasts were resuspended in 10 mM Tris/Cl, pH 8, and disrupted by two passages through a chilled 10-ml French pressure cell. The resulting spheroplast lysate was spun at 10000 \times g (5 min) to remove cell debris. Finally, centrifugation at 100000 \times g (60 min) yielded a greenish cytoplasmic supernatant. The reddish membrane pellet was suspended in 10 mM Tris/Cl, pH 8.0, and spun at 100000 \times g (60 min). The pellet was resuspended for further measurements. The following assays were performed to probe the quality of the fractionation: hydrogenase activity was measured by a manometric hydrogen-production assay [22], APS reductase by the AP/SO₃²⁻ ferricyanide-reduction assay [28], and desferrioxamine was estimated from the visible spectrum [$A_{630} - A_{650} \times 2$] [29].

Ultraviolet/visible spectroscopy

Spectra were recorded on a DW-2000 spectrophotometer interfaced with an IBM computer. Measurements of absorbances at single wavelengths for the determination of absorption coefficients and chemical analysis were made with a Beckman DU-40 spectrophotometer with a PI-2 logarithmic converter.

Amino acid and N-terminal analysis

Prior to amino acid analysis protein samples were desalted on Sephadex G-25. For the determination of cysteine and methionine, protein lyophilates were treated with performic acid and HBr [30] and evaporated to dryness. Hydrolysis was carried out for 24 h at 110°C (6 M HCl). Minor corrections were made for the degradation of labile amino acids as estimated from time-dependent recoveries of control protein samples. The content of tyrosine and tryptophan was determined by comparison of ultraviolet spectra of trichloroacetic acid-precipitated protein dissolved in 0.10 M NaOH with spectra of tyrosine/tryptophan mixtures [31]. Tryptophan was also estimated fluorimetrically [32]. Standard addition of free tryptophan was used to correct for minor quenching. Bovine serum albumin and periplasmic hydrogenase served as appropriate standards, containing two [33] and six [34] tryptophan residues, respectively.

N-terminal analysis of protein samples blotted onto an Immobilon-P (Millipore) support was carried out by gas-phase sequencing (Dr Amons, Leiden University, The Netherlands).

Chemical analysis

Protein was determined with the microBiuret method at 330 nm [35] after trichloroacetic acid/deoxycholate precipitation [36]. Fatty-acid-free bovine serum albumin (Sigma) served as standard using $A_{279}^{1\%} = 6.67$ at 279 nm [37]. Careful checks for both standard and sample were made, including centrifugation, omission of precipitation, recording of spectra and blank determinations without copper reagent.

Iron was determined colorimetrically after treatment with 1% (mass/vol.) HCl at 80°C for 20 min. The pH of the resulting reaction mixture (500 μ l) was adjusted to 5.0 ± 0.2 with 250 μ l 0.4 M NH₄Cl. Addition of 25 μ l 10% (mass/vol.) SDS was followed by reduction of Fe³⁺ with 50 μ l freshly prepared 0.1 M ascorbic acid solution. The mixture was vortexed and the color reaction was started by the addition of 25 μ l iron chelator (25 mM). Bathophenanthroline disulfonate [38] or ferene [39] was used. Mohr's salt [(NH₄)₂Fe(SO₄)₂ · 6 H₂O; Merck p.a.] was used as a standard.

Acid-labile sulfur was determined aerobically with the methylene-blue method [40]. Care was taken to prevent loss or oxidation of sulfide. Solutions were pipetted gently and a low surface/volume ratio was maintained, except after the FeCl₃ addition. As protein quenched the formation of methylene blue from iron-sulfur proteins in our experiments, we used standard addition of a freshly prepared anaerobic 1–2 mM Na₂S solution in 10 mM NaOH. Sodium sulfide crystals (Na₂S · 9 H₂O, Merck p.a.) were rinsed with demineralized water and thoroughly dried with Whatman paper. Titration of the sulfide standard with iodine/thiosulfate [41] confirmed the titre of the gravimetrically prepared solution.

Molybdenum was determined with a microadaptation of the dithiol method [42]. Ammonium heptamolybdate (Merck p.a.), *Azotobacter vinelandii* nitrogenase component 1 (kindly donated by Dr H. Haaker) and cow milk xanthine oxidase (Boehringer) were standards.

Elemental analysis was performed by particle-induced X-ray emission at the Eindhoven University of Technology, The Netherlands. Samples were diluted with ethanol to 20% (by vol.) ethanol, prior to application onto Millipore MF SCWP 8- μ m filters (cf. [43]). The filters were left to dry in air. Typical samples contained approximately 0.5 mg protein/5 cm². Standards contained 0.05–5 μ g element/5 cm². The filters, mounted in commercial slide frames, were irradiated with a 3-MeV proton beam from a cyclotron. Energy dispersive X-ray spectra were digitally recorded and analyzed with the software as described in [44].

Materials

DEAE-Sephacel and Sephadex G-150 were from Pharmacia, Bio-Gel HTP from Bio-Rad, SDS from BDH Biochemicals and iron chelators from Aldrich. Other chemicals were obtained from Merck.

RESULTS AND DISCUSSION

Purification

While assessing the purity of samples of *D. vulgaris* (Hildenborough) periplasmic hydrogenase, we noted a con-

Table 1. Purification of *D. vulgaris* (Hildenborough) prismatic protein. The cell-free extract was prepared from 213 g freshly harvested wet cells according to Materials and Methods.

Fraction	Volume	Protein
	ml	mg
Extract	655	11 500
DEAE-Sephacel	220	2130
YM-30 concentrate	24	1970
Sephadex G-150	60	397
Hydroxyapatite	110	201
FPLC MonoQ	1.0	5.2

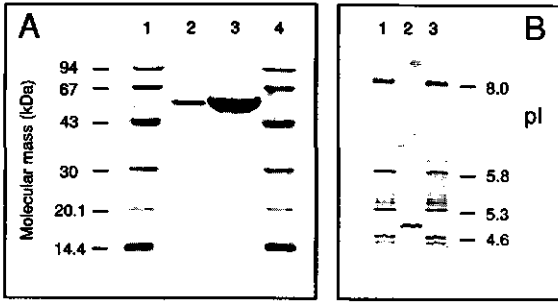


Fig. 1. Homogeneity of *D. vulgaris* (Hildenborough) prismatic protein as revealed by SDS/PAGE (A) and IEF (B). Electrophoresis of FPLC-purified prismatic protein (lanes 2 in A and B, 1 μ g; lane 3 in A, 10 μ g) and marker mixtures (other lanes) was carried out according to Materials and Methods.

taminant protein with a molecular mass of 59 kDa, as determined by SDS/PAGE. Subsequent purification of this protein by anion-exchange FPLC of side-fractions from a hydrogenase purification yielded 0.5 mg brownish protein. To obtain a useful tool for characterization and purification of this protein, antibodies were raised against the polypeptide. Pilot purifications of this protein from *D. vulgaris* cells, monitored by Western blotting with immunodetection, allowed us to purify a few milligrams of the protein. A preliminary EPR characterization [18] pointed towards the presence of a [6Fe-6S]³⁺ prismatic cluster in the dithionite-reduced protein. This assignment is corroborated by analytical and spectroscopic results presented below and in a subsequent paper [19].

The routine purification starting from about 200 g wet cells provides about 5 mg prismatic protein (Table 1). Assuming 50% recovery for the purification, about 0.1% soluble cellular protein of *D. vulgaris* (Hildenborough) is prismatic protein. This purification yields preparations of 80–90% purity, as estimated by densitometric scanning of Coomassie-blue-stained SDS/PAGE gels.

For experiments relying on the homogeneity of the protein the gel-filtration and FPLC anion-exchange steps were repeated at the expense of the yield. The purity of the prismatic protein after these additional purification steps was 95–99%. Throughout the experiments described in this paper, such preparations were used.

Homogeneity and molecular mass

The prismatic protein exhibited a single band on Coomassie-blue-stained SDS/PAGE gels (Fig. 1A). In gels with varying total monomer concentrations of 10–20%,

the apparent molecular mass of the polypeptide was 59.2 ± 1.8 kDa. We specifically checked, but found no evidence for, a small subunit, contrary to the cases of *D. vulgaris* periplasmic hydrogenase [11] and dissimilatory sulfite reductase [45]. Native electrophoresis of the prismatic protein at pH 9.5 showed a single brown band with a relative mobility of 0.44 with respect to the bromophenol-blue front on Coomassie-blue and iron staining [46] of the native gel demonstrated that the protein comigrated with the iron-sulfur chromophore (not shown). The protein displayed a brown band on flat-bed isoelectric focussing. Close examination of the Coomassie-blue-stained or *in situ* iron-stained [47] isoelectric-focussing gel revealed that the brown band coincided with two very closely spaced bands (Fig. 1B). The average isoelectric point was 4.9 ± 0.1 at 4°C, with $\Delta pI \approx 0.03$ space between the bands. SDS/PAGE in a second dimension (not shown) proved unequivocally that the polypeptide, iron and brown chromophore were contained in a single entity.

Gel filtration of the iodoacetylated denatured prismatic protein gives a molecular mass of 62 ± 6 kDa. The native molecular mass as estimated by gel filtration (50 mM potassium phosphate/150 mM KCl, pH 7.2) is 54 ± 4 kDa. The gel filtration elution profiles exhibited single symmetrical peaks at 280 nm.

To obtain a reliable molecular mass for chemical determinations, in the absence of the complete amino acid sequence the prismatic protein was subjected to short-column Yphantis [47] sedimentation-equilibrium centrifugation. Sedimentation-velocity experiments showed that the protein sedimented as a single boundary, observed by scanning at 280 nm at 400 nm. A $s_{20,w}$ of 4.18 ± 0.13 S ($n = 4$) was calculated from data obtained with solutions of 0.2–1 mg prismatic protein/ml 100 mM potassium phosphate, pH 7.5, spun at 45000 rpm (20°C). No significant protein concentration dependence was noted. This value compares with the sedimentation coefficient of the similarly sized *D. vulgaris* periplasmic hydrogenase, 4.1 S [23]. Sedimentation-equilibrium runs at rotor speeds in the range 11000–19000 rpm using identical conditions attained equilibrium after 40–80 h. Using a partial specific volume of 0.738 cm³/g, calculated [48] from the amino acid composition (Table 4), a molecular mass of 52.0 ± 0.9 kDa ($\lambda = 400$ nm, $n = 5$) and 48.9 ± 1.5 kDa ($\lambda = 280$ nm, $n = 4$) was found. SDS/PAGE of samples subjected to a 100% centrifugation showed no significant breakdown of the prismatic protein polypeptide. Background absorbance of the radial axis was negligible at 400 nm. At 280 nm, however, we had to correct for 2–10% background absorbance. All better fits of $\ln(A)$ vs. r^2 were obtained with the data taken at 400 nm. We therefore attach greater value to the 400-nm data and use a molecular mass of 52 kDa for quantitative chemical analysis. The sedimentation velocity coefficient and the native gel-filtration behaviour are in agreement with a 52-kDa monomeric structure.

Chemical analysis of cofactors

Table 2 summarizes the combined results of protein, iron and acid-labile sulfur determinations of several batches of prismatic protein. To assess possible interferences of microBiuret, iron-chelator and methylene-blue colorimetric determinations, we thoroughly checked blanks, calibration spectra of color complexes and standard additions. No significant interferences were found for the protein and iron determination. Bathophenanthroline disulfonate and ferene chelat-

Table 2. Iron-sulfur composition and optical absorption coefficients of *D. vulgaris* (Hildenborough) prismsane protein. The protein, iron, and acid-labile sulfur content were determined according to Materials and Methods. Stoichiometries and absorption coefficients were based on determination of the protein concentration with the microBiuret method and calculated using a molecular mass of 52 kDa. n.d., not determined. Preparation 11 was used for ultraviolet/visible spectroscopy in Fig. 2.

Preparation	Fe/protein	S ²⁻ /protein	ϵ at	
			280 nm	400 nm
atoms/molecule			mM ⁻¹ · cm ⁻¹	
	5.5	n.d.	n.d.	n.d.
	6.8	n.d.	n.d.	n.d.
	6.4	n.d.	80.7	26.0
	6.3	6.7	91.5	27.7
	6.6	5.2	80.5	26.8
	6.5	6.4	82.5	24.4
	6.2	n.d.	85.5	21.3
	n.d.	n.d.	84.3	25.5 ^a
	n.d.	6.4	82.9	25.8
	n.d.	n.d.	75.7	24.6
	6.9	n.d.	82.9	26.0 ^a
	5.9	n.d.	70.0	22.7 ^a
	n.d.	n.d.	79.0	23.7 ^a
mean	6.3 ± 0.4	6.2 ± 0.7	81.4 ± 5.5	25.0 ± 1.9
± SD (n)	(9)	(4)	(11)	(11)

^a Preparation used for the determination of $\epsilon_{\text{reduced}}$.

Table 3. Physical and chemical properties of *D. vulgaris* (Hildenborough) prismsane protein.

Parameter	Value
Molecular mass	52.0 ± 0.9 kDa
η_{inh}	4.18 ± 0.13 S
η_{sp}/c	4.9 ± 0.1
Fe/protein	6.3 ± 0.4 atoms/molecule
S ²⁻ /protein	6.2 ± 0.7 atoms/molecule
Fe ²⁺ /protein	< 0.03 atoms/6Fe
Other transition metals	< 0.05 atoms/6Fe
Mo/protein	< 0.03 atoms/6Fe
ϵ_{280} (isolated)	81 ± 5 mM ⁻¹ · cm ⁻¹
ϵ_{400} (isolated)	25.0 ± 1.9 mM ⁻¹ · cm ⁻¹
ϵ_{400} (dithionite reduced)	14.1 ± 1.0 mM ⁻¹ · cm ⁻¹

yielded identical iron contents within experimental limits (3%). We noted some problems with the methylene-blue method. Recovery of acid-labile sulfur added to protein was 90%. Thus, protein quenched the synthesis of methylene blue from sulfide or, alternatively, methylene blue is adsorbed by the protein [49]. Protein also affected the visible spectrum of the methylene-blue component formed. Methylene blue formed from acid-labile sulfur in the absence of protein exhibited a spectrum identical with authentic methylene blue. However, the A_{670}/A_{750} of the product formed in the presence of protein was lower (1.5 instead of 2.0). Beinert [50] briefly mentioned that this ratio is not entirely constant. A tentative explanation is that binding of methylene blue to the denatured typeptide occurs with a concomitant spectral change of the methylene blue. For quantitative determinations, standard conditions of sulfide and the 670-nm absorbance were used.

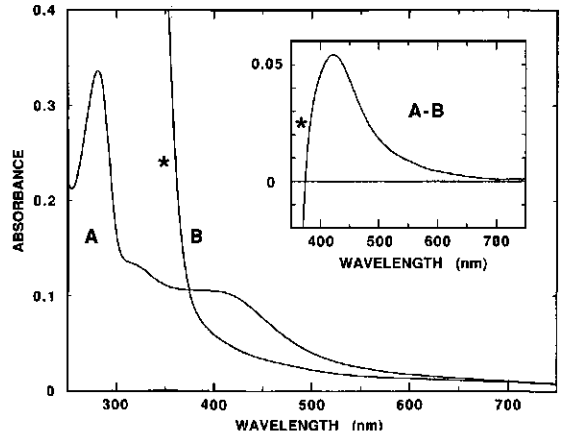


Fig. 2. Ultraviolet/visible spectroscopy of *D. vulgaris* (Hildenborough) isolated prismsane protein (0.21 mg/ml, 50 mM HEPES, pH 7.5) (A), dithionite reduced (B) and isolated minus dithionite-reduced (inset, A - B). Asterisks denote spectral contributions from excess dithionite and its decomposition products.

Elemental analysis with proton-induced X-ray emission accurately reproduced the Fe content as determined by the colorimetric technique (three batches). However, the standard deviation for duplicate determinations of the same sample was larger. This can be explained by a minor heterogeneity of the spreading of the samples over the filter (cf. [43]). We therefore used the iron present in the prismsane protein samples as an internal standard for the determination of other elements, and relied on the colorimetric method for the iron content. Proton-induced X-ray emission revealed that the prismsane protein as isolated (three batches) contained less than 0.05 atoms V, Cr, Mn, Co, Ni, Cu, Se, Mo or W/6 Fe atoms. The relatively high and variable Zn content of the filters (80–120 ng/cm²) complicated an accurate analysis of the Zn content of the prismsane protein. Two preparations contained less than 0.05 atoms Zn/6 Fe atoms and one preparation about 0.1 atom Zn/6 Fe atoms.

Since the prismsane protein isolated exhibited an EPR signal reminiscent of a Mo(V) center [18], the molybdenum content was cross-checked by a colorimetric procedure. Molybdenum released from xanthine oxidase and nitrogenase component 1 was readily detected, whereas less than 0.03 mol Mo/mol protein was found in the prismsane protein.

The heme content of the prismsane protein was less than 0.005 mol/mol, as estimated from the absence of potential α -band absorbances in the 500–600-nm region of the (difference) visible absorbance spectrum (Fig. 2). Non-covalently bound FMN and FAD were not detected by fluorescence spectroscopy of acid extracts of the protein. The presence of protein-bound flavin was excluded by ultraviolet/visible spectroscopy of alkaline solutions of trichloroacetic-acid-precipitated protein.

Ultraviolet/visible spectroscopy

The absorbance spectrum of the prismsane-containing protein exhibits a broad 400-nm band and a pronounced aromatic peak centered at 280 nm (Fig. 2). The A_{400}/A_{280} ratio of the isolated protein is 0.307 ± 0.031 ($n = 11$). Absorption coefficients at 280 nm and 400 nm are 81.4 ± 5.5 mM⁻¹ · cm⁻¹

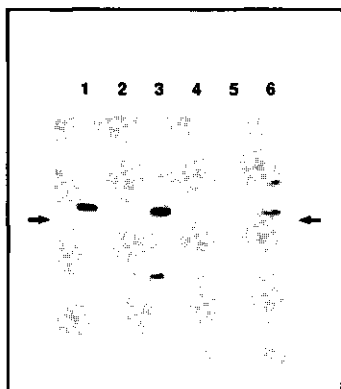


Fig. 3. Cellular localization of *D. vulgaris* (Hildenborough) prismsane protein by immunostaining. Western blots were immunostained after treatment with 500-fold-diluted rabbit antiserum against *D. vulgaris* (Hildenborough) prismsane protein. Lane 1, lysed cells; lane 2, periplasma; lane 3, cytoplasm; lane 4, membranes (each lane equivalent to 80 μg cells); lane 5, purified periplasmic Fe-hydrogenase (200 ng); lane 6, purified prismsane protein (10 ng). Arrows indicate the electrophoretic mobility of the prismsane protein, as revealed by Coomassie-blue staining after SDS/PAGE.

and $25.0 \pm 1.9 \text{ mM}^{-1} \cdot \text{cm}^{-1}$, respectively (Table 2). Titration with substoichiometric amounts of potassium ferricyanide resulted in an increase in absorption coefficient at 400 nm of $1.0 \text{ mM}^{-1} \cdot \text{cm}^{-1}$ in addition to the contribution by potassium ferricyanide.

The 400-nm absorption coefficient of the dithionite-reduced protein is $14.1 \pm 1.0 \text{ mM}^{-1} \cdot \text{cm}^{-1}$ ($n = 4$). Similar results were obtained with hydrogen reduction in the presence of 5 nM catalytic traces of methylviologen/hydrogenase (pH 8.0). The featureless shape of the visible spectrum, both of the isolated protein and the dithionite-reduced protein, compares to that of bacterial ferredoxins containing [4Fe-4S] or $2 \times [4\text{Fe-4S}]$ clusters. It clearly has no resemblance to the structured visible spectra of rubredoxin-like and [2Fe-2S] containing proteins.

Cellular localization

Freshly grown *D. vulgaris* (Hildenborough) cells were fractionated by EDTA extraction, disruption and centrifugation, as described in Materials and Methods. From the EDTA extractability [22] and membrane-translocation mechanism [51] it is known that in *D. vulgaris* (Hildenborough) a highly active Fe-hydrogenase resides in the periplasm, whereas APS reductase and dissimilatory sulfite reductase (desulfoviridin) are present in the cytoplasm [52]. These enzymes were used as convenient markers in our fractionation procedure. In typical localization experiments, about 90% of the respective enzymes in the correct fractions were recovered. The hydrogenase activity of the cytoplasmic fraction (5–10%) was due to incomplete extraction as was indicated by Western blotting with immunodetection using polyclonal antibodies against the α -subunit of the periplasmic hydrogenase. A minor contamination with the soluble marker enzymes was found in the membrane fraction. The localization of the prismsane protein was studied by immunostaining of Western blots containing fractions equivalent to 80 μg cells (Fig. 3). It is clear that the prismsane protein is cytoplasmic. Although it is possible that

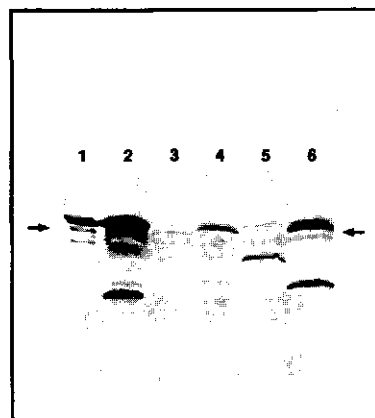


Fig. 4. Screening for a prismsane protein in *Desulfovibrio* strains by immunostaining. Western blots were immunostained after treatment with 1000-fold-diluted mouse antiserum against *D. vulgaris* (Hildenborough) prismsane protein. Lane 1, purified prismsane protein (20 ng); lane 2, cells from *D. vulgaris* (Hildenborough; NCIB 8303); lane 3, *D. gigas* (NCIB 9332); lane 4, *D. desulfuricans* (ATCC 27774); lane 5, *D. desulfuricans* Norway 4 (NCIB 8310); lane 6, *D. vulgaris* (Monticello) (NCIB 9442); (lanes 2–6, extracts of 500 μg cells/lane). Arrows indicate the electrophoretic mobility of the prismsane protein as revealed by Coomassie-blue staining after SDS/PAGE.

the protein was released from membranes during the process of cell disruption [52], the absence of a relevant immunoblot response of the membrane fraction strongly argues against this possibility. A fully soluble nature of the prismsane protein is also indicated by both amino acid composition (Table 1) and aqueous solubility ($> 40 \text{ mg/ml}$). No significant cross-reactivity of the antiserum was noted with *D. vulgaris* (Hildenborough) periplasmic hydrogenase (Fig. 3, lane 5) or the *lacZ-hydC* fusion product [53] (not shown), nor did antiserum against these proteins react with the prismsane protein on Western blots (not shown). Mouse sera were also used in immunoblot experiments. No differences were seen.

Occurrence in other *Desulfovibrio* strains

Immunoblots of cell-free extracts of *Desulfovibrio* strains treated with mouse antiserum exhibited a clear cross-reactive band with a similar mobility [*D. vulgaris* (Monticello)], a faint band with similar mobility (*Desulfovibrio desulfuricans* ATCC 27774) or faint bands with lower mobilities (*D. desulfuricans* Norway 4 and *Desulfovibrio gigas*; Fig. 4). If we assume the subunit structure and molecular mass of the prismsane protein in *Desulfovibrio* strains to be similar, the presence of prismsane protein in *D. vulgaris* (Monticello) and *D. desulfuricans* (ATCC 27774) is indicated by our data. The presence in the latter species is corroborated by a recent report confirming prismsane-protein EPR signals [9, 10, 18, 19] in protein isolated from *D. desulfuricans* (ATCC 27774) [54].

Amino acid composition and N-terminal sequence

The results of the amino acid analysis of the prismsane protein are shown in Table 4. Performic acid oxidation allowed an rough estimation of cysteine residues. Substances

Table 4. Amino acid composition of *D. vulgaris* (Hildenborough) prismatic protein. Addition of the atomic masses of 6Fe and 6S to the total molecular mass of the constituent amino acids (51.5 kDa) yields the observed native molecular mass (52.0 kDa).

Amino acid	Amino acid composition	
	relative	calculated
	mol/mol leucine	mol/mol protein
Asx	1.061	48
Six	0.952	43
Ter	0.487	23
Thr	0.585	27
Tro	0.690	31
Lis	0.190	9
Lys	0.713	32
Arg	0.296	14
Gly	0.995	45
Ala	1.111	50
Val	0.760	34
Ile	0.531	24
Leu	1	45
Tyr	0.290	13
Phe	0.385	18
Trp	0.092	4
Met	0.106	5
Cys	0.377	17 ^a
Total	—	481

^a This value probably is an overestimation (see text).

uting near the cysteic acid peak considerably complicated quantitation and might have caused an overestimation of the number of cysteine residues. The preponderance of acidic over basic amino acid residues is in agreement with the slightly acidic isoelectric point.

The N-terminal sequence of the prismatic protein was determined with gas-phase sequencing: MF^S/cFQ^S/QETAKNTG. Presumably the N-terminal methionine represents the deformed initiator methionine of the prismatic protein. Comparison of the N-terminal sequence with several protein sequence data banks did not result in significant matches.

Physiological function

A number of relevant activity measurements [28] were carried out in order to investigate the physiological function of the prismatic protein. The hydrogen-producing hydrogenase activity was 0.7 U/g. Fumarate, sulfite, nitrite, thiosulfate and PS reductase activity were less than 5 U/g. Lactate and formate dehydrogenase activity was less than 0.1 U/mg. The activity with NADH or NADPH was low; in diaphorase assays with 2,6-dichloroindophenol or horse heart cytochrome *c* as acceptor the activity was less than 1 U/g. Inactivation as an explanation for the absence of enzyme activity is unlikely. The stability of the protein (as judged by e.g. solubility, intactness of the polypeptide and visible chromophore) on exposure to trypsin or *Staphylococcus aureus* V8 protease, incubation at room temperature for more than 100 h and repeated dilution/concentration and freezing/thawing cycles is remarkable.

Conclusions

The results presented here delineate the biochemical properties of a new type of iron-sulfur protein and provide a

basic set of data necessary for a detailed biophysical study [19]. By an extensive evaluation of the homogeneity and by chemical analysis of protein preparations, the iron and acid-labile sulfur content was pinpointed at about 6.3 atoms/molecule (Tables 2 and 3). If we assume a reasonable relative inaccuracy of 10–20% for the combined results of iron/acid-labile-sulfur, protein determination and molecular mass, the Fe/S content is restricted to 5, 6 or 7 atoms/molecule. As above, EPR and Mössbauer spectroscopy [18, 19] prove that rubredoxin-like, [2Fe-2S], [3Fe-4S] and [4Fe-4S] centers are absent in the protein, the presence of a single, larger Fe/S (super)cluster is thus indicated. Furthermore, the striking similarity between the EPR *g* tensors of the [6Fe-6S]³⁺ model compound and the protein [18] lends additional support to an assignment as prismatic protein. However, one should recall that (bi)capped prismatic structures exist and might share spectroscopic properties with their prismatic parent [16, 17].

We anticipate that the 52-kDa prismatic protein is not an electron carrier but rather an iron-sulfur redox enzyme. A physiological function (i.e. enzyme activity), however, has not been detected yet. The presence of a [6Fe-6S] supercluster with superspin paramagnetism (see also [19]) points towards a multielectron redox enzyme (EC class 1). We will continue to put efforts in the elucidation of the physiological function of the prismatic protein. Determination of the DNA sequence of the prismatic-protein gene (presently in progress), sequence comparison and identification of potential flanking genes will stimulate future work. Knowledge of the primary structure would improve the reliability of the Fe/S stoichiometry by substitution of the sedimentation equilibrium molecular mass. We expect that the purity, remarkable stability and homogeneity with respect to charge allows crystallization of the prismatic protein.

We wish to thank Dr W. M. A. M. van Dongen and Mrs A. Kaan for their kind help with immunological techniques and N-terminal sequencing. We are indebted to Mr L. C. de Folter (Eindhoven University of Technology, The Netherlands) for help with the proton-induced X-ray emission measurements. Mr L. J. G. M. Bongers (Dept of Human and Animal Physiology, Agricultural University, Wageningen) kindly carried out the amino acid analysis. Mr J. Haas took care of the handling of animals. Mr A. H. Westphal skillfully participated in the ultracentrifugation data analysis. This investigation was supported by the Netherlands Foundation for Chemical Research (SON) with financial aid from the Netherlands Organization for Scientific Research (NWO).

REFERENCES

- Thomson, A. J. (1985) in *Metalloproteins* (Harrison, P. M., ed.) vol. 1, pp. 79–120, Verlag Chemie, Weinheim.
- Fujii, T., Moriyama, H., Takana, N., Wakagi, T. & Oshima, T. (1991) *J. Biochem. (Tokyo)* 110, 472–473.
- You, J.-F., Snyder, B. S., Papaefthymiou, G. C. & Holm, R. H. (1990) *J. Am. Chem. Soc.* 112, 1067–1076.
- Switzer, R. L. (1989) *Biofactors* 2, 77–86.
- Beinert, H. & Kennedy, M. C. (1989) *Eur. J. Biochem.* 186, 5–15.
- Hagen, W. R. (1987) in *Cytochrome systems* (Papa, S., Chance, B. & Ernster, L., eds) pp. 459–466, Plenum Press, New York.
- Bolin, J. T., Ronco, A. E., Mortenson, L. E., Morgan, T. V., Williamson, M. & Xuong, N. H. (1990) in *Nitrogen fixation: achievements and objectives* (Gresshoff, P. M., Roth, L. E., Stacey, G. & Newton, W. E., eds), pp. 117–122, Chapman and Hall, New York.
- McRee, D. E., Richardson, D. C., Richardson, J. S. & Siegel, L. M. (1986) *J. Biol. Chem.* 261, 10277–10281.

9. Hagen, W. R., Pierik, A. J. & Veeger, C. (1990) *Ital. Biochem. Soc. Trans.* 1, 85.
10. Hagen, W. R., Pierik, A. J., Wolbert, R. B. G., Wassink, H., Haaker, H., Veeger, C., Jetten, M. K., Stams, A. J. M. & Zehnder, A. J. B. (1991) *Biofactors* 3, 144.
11. Hagen, W. R., Van Berkel-Arts, A., Krüse-Wolters, K. M., Dunham, W. R. & Veeger, C. (1986) *FEBS Lett.* 201, 158–162.
12. Hagen, W. R., Wassink, H., Eady, R. R., Smith, B. E. & Haaker, H. (1987) *Eur. J. Biochem.* 169, 457–465.
13. Pierik, A. J. & Hagen, W. R. (1991) *Eur. J. Biochem.* 195, 505–516.
14. Jetten, M. S. M., Pierik, A. J. & Hagen, W. R. (1991) *Eur. J. Biochem.* 202, 1291–1297.
15. Kanatzidis, M. G., Hagen, W. R., Dunham, W. R., Lester, R. K. & Coucouvanis, D. (1985) *J. Am. Chem. Soc.* 107, 953–961.
16. Coucouvanis, D. (1991) *Acc. Chem. Res.* 24, 1–8.
17. Noda, I., Snyder, B. S. & Holm, R. H. (1986) *Inorg. Chem.* 25, 3851–3853.
18. Hagen, W. R., Pierik, A. J. & Veeger, C. (1989) *J. Chem. Soc. Faraday Trans. 1* 85, 4083–4090.
19. Pierik, A. J., Hagen, W. R., Dunham, W. R. & Sands, R. H. (1992) *Eur. J. Biochem.* 206, 705–719.
20. Postgate, J. R. (1951) *J. Gen. Microbiol.* 5, 714–724.
21. Saunders, G. F., Campbell, L. L. & Postgate, J. R. (1964) *J. Bacteriol.* 87, 1073–1078.
22. Van der Westen, H. M., Mayhew, S. G. & Veeger, C. (1978) *FEBS Lett.* 86, 122–126.
23. Filipiak, M., Hagen, W. R. & Veeger, C. (1989) *Eur. J. Biochem.* 185, 547–553.
24. Laemmli, U. K. (1970) *Nature* 227, 680–685.
25. Wolbert, R. B. G., Hilhorst, R., Voskuilen, G., Nachtegaal, H., Dekker, M., Van't Riet, K. & Bijsterbosch, B. H. (1989) *Eur. J. Biochem.* 184, 627–633.
26. Prussak, C. E., Almazan, M. T. & Tseng, B. Y. (1989) *Anal. Biochem.* 178, 233–238.
27. Towbin, H., Staehelin, T. & Gordon, J. (1979) *Proc. Natl Acad. Sci. USA* 76, 4350–4354.
28. Odom, J. M. & Peck, H. D. (1981) *J. Bacteriol.* 147, 161–169.
29. Aketagawa, J., Kojo, K. & Ishimoto, M. (1985) *Agric. Biol. Chem.* 49, 2359–2365.
30. Hirs, C. H. W. (1967) *Methods Enzymol.* 11, 59–62.
31. Bencze, W. L. & Schmid, K. (1957) *Anal. Chem.* 29, 1193–1196.
32. Pajot, P. (1976) *Eur. J. Biochem.* 63, 263–269.
33. King, T. P. & Spencer, M. (1970) *J. Biol. Chem.* 245, 6134–6148.
34. Voordouw, G. & Brenner, S. (1985) *Eur. J. Biochem.* 148, 515–520.
35. Goa, J. (1953) *Scand. J. Clin. Lab. Invest.* 5, 218–222.
36. Bensadoun, A. & Weinstein, D. (1976) *Anal. Biochem.* 70, 241–250.
37. Foster, J. F. & Sterman, M. D. (1956) *J. Am. Chem. Soc.* 78, 3656–3660.
38. Blair, D. & Diehl, H. (1961) *Talanta* 7, 163–174.
39. Hennessy, D. J., Reid, G. R., Smith, F. E. & Thompson, S. L. (1984) *Can. J. Chem.* 62, 721–724.
40. Lovenberg, W., Buchanan, B. B. & Rabinowitz, J. C. (1963) *J. Biol. Chem.* 238, 3899–3913.
41. Vogel, A. I. (1961) *A textbook of quantitative inorganic analysis*, 3rd edn, pp. 370–371, Longmans, London.
42. Hart, L. L., McGartoll, M. A., Chapman, H. R. & Bray, R. C. (1970) *Biochem. J.* 116, 851–864.
43. Kivits, H. P. M., De Rooij, F. A. J. & Wijnhoven, G. P. J. (1979) *Nuclear Instrum. Methods* 164, 225–229.
44. Johansson, G. I. (1982) *X-ray spectrom.* 11, 194–200.
45. Pierik, A. J., Duyvis, M. G., Van Helvoort, J. M. L. M., Wolbert, R. B. G. & Hagen, W. R. (1992) *Eur. J. Biochem.* 205, 111–115.
46. Ohmori, D., Tanaka, Y., Yamakura, F. & Suzuki, K. (1985) *Electrophoresis* 6, 351–352.
47. Yphantis, D. A. (1964) *Biochemistry* 3, 297–317.
48. Cohn, E. J. & Edsall, J. T. (1943) *Proteins, amino acids and peptides*, p. 372, Van Nostrand-Reinhold, Princeton, New York.
49. King, T. E. & Morris, R. O. (1967) *Methods Enzymol.* 10, 634–637.
50. Beinert, H. (1978) *Anal. Biochem.* 131, 373–378.
51. Van Dongen, W., Hagen, W. R., Van den Berg, W. & Veeger, C. (1988) *FEMS Microbiol. Lett.* 50, 5–9.
52. Kremer, D. R., Veenhuis, M., Fauque, G., Peck, H. D., LeGall, J., Lampreia, J., Moura, J. J. G. & Hansen, T. A. (1988) *Arch. Microbiol.* 150, 296–301.
53. Stokkermans, J., Van Dongen, W., Kaan, A., Van den Berg, W. & Veeger, C. (1989) *FEMS Microbiol. Lett.* 58, 217–222.
54. Ravi, N., Moura, I., Tavares, P., LeGall, J., Huynh, B. H. & Moura, J. J. G. (1991) *J. Inorg. Biochem.* 43, 252.

Chapter 5

Multi-frequency EPR and high-resolution Mössbauer spectroscopy of a putative [6Fe-6S] prismane-cluster-containing protein from *Desulfovibrio vulgaris* (Hildenborough): characterization of a supercluster and superspin model protein.

Antonio J. Pierik, Wilfred R. Hagen, W. Dick Dunham and
Dick H. Sands

(1992) Eur. J. Biochem. 206, 705-719.

Multi-frequency EPR and high-resolution Mössbauer spectroscopy of a putative [6Fe-6S] prismane-cluster-containing protein from *Desulfovibrio vulgaris* (Hildenborough)

Characterization of a supercluster and superspin model protein

Antonio J. PIERIK¹, Wilfred R. HAGEN¹, W. Richard DUNHAM² and Richard H. SANDS²

¹Department of Biochemistry, Agricultural University, Wageningen, The Netherlands

²Biophysics Research Division, Institute of Science and Technology, The University of Michigan, Ann Arbor, USA

Received January 27, 1992) – EJB 92 0100

The putative [6Fe-6S] prismane cluster in the 6-Fe/S-containing protein from *Desulfovibrio vulgaris*, strain Hildenborough, has been enriched to 80% in ⁵⁷Fe, and has been characterized in detail by S-, X-, P- and Q-band EPR spectroscopy, parallel-mode EPR spectroscopy and high-resolution ⁵⁷Fe Mössbauer spectroscopy. In EPR-monitored redox-equilibrium titrations, the cluster is found to be capable of three one-electron transitions with midpoint potentials at pH 7.5 of +285, +5 and –165 mV. As the fully reduced protein is assumed to carry the [6Fe-6S]³⁺ cluster, by spectroscopic analogy to prismane model compounds, four valency states are identified in the titration experiments: [6Fe-6S]³⁺, [6Fe-6S]⁴⁺, [6Fe-6S]⁵⁺, [6Fe-6S]⁶⁺. The fully oxidized 6+ state appears to be diamagnetic at low temperature. The prismane protein is aerobically isolated predominantly in the one-electron-reduced 5+ state. In this intermediate state, the cluster exists in two magnetic forms: 10% is low-spin *S* = 1/2; the remainder has an unusually high spin *S* = 9/2. The *S* = 1/2 EPR spectrum is significantly broadened by ligand (2.3 mT) and ⁵⁷Fe (3.0 mT) hyperfine interaction, consistent with a delocalization of the unpaired electron over 6Fe and indicative of at least some nitrogen ligation. At 35 GHz, the *g* tensor is determined as 1.971, 1.951 and 1.898. EPR signals from the *S* = 9/2 multiplet have their maximal amplitude at a temperature of 12 K due to the axial zero-field splitting being negative, *D* ≈ –0.86 cm^{–1}. Effective *g* = 15.3, 5.75, 5.65 and 5.23 are observed, consistent with a rhombicity of |*E/D*| = 0.061. A second component has *g* = 9.7, 8.1 and 6.65 and |*E/D*| = 0.108. When the protein is reduced to the 4+ intermediate state, the cluster is silent in normal-mode EPR. An asymmetric feature with effective *g* ≈ 16 is observed in parallel-mode EPR from an integer spin system with, presumably, *S* = 4. The fully reduced 3+ state consists of a mixture of two *S* = 1/2 ground state. The *g* tensor of the major component is 2.010, 1.825 and 1.32; the minor component has *g* = 1.941 and 1.79, with the third value undetermined. The sharp line at *g* = 2.010 exhibits significant convoluted hyperfine broadening from ligands (2.1 mT) and from ⁵⁷Fe (4.6 mT). Zero-field high-temperature Mössbauer spectra of the protein, isolated in the 5+ state, quantitatively account for the 0.8 fractional enrichment in ⁵⁷Fe, as determined with inductively coupled plasma mass spectrometry. The six irons are not equivalent; the six quadrupole pairs are in a 2:1 pattern. Upon reduction to the 3+ state, the spectra change shape dramatically with indication of localized valencies. Four of the six irons appear to be relatively unaffected, while the remaining two exhibit a considerable increase in quadrupole splitting and an increase in the isomer shift, each consistent with a full charge reduction. From temperature and field-dependent Mössbauer studies on the 5+ and 3+ states, it is concluded that all six irons are paramagnetic and part of the same spin system. A mixed-ligand prismane model is proposed in which four Fe form an electron-delocalized core, flanked on opposite sites by two Fe of distinctly more ionic character, as they are coordinated by nitrogen. In the corresponding vector-coupling model for the *S* = 9/2 state, the two ionic ferric ions couple ferromagnetically through the delocalized core structure. With the characterization of this model protein, a frame of reference is provided for the spectroscopic study of more complex Fe/S enzymes.

Correspondence to W. R. Hagen, Laboratorium voor Biochemie, Landbouwwetenschappelijke Universiteit, Dreijenlaan 3, NL-6703 HA Wageningen, The Netherlands

Abbreviation. ICP-MS, inductively coupled plasma mass spectrometry.

Enzymes. Desulfoviridin, dissimilatory sulfite reductase (EC 1.1.1.99.1); carbon-monoxide dehydrogenase, acetyl-CoA synthase (EC 1.1.1.99.2); nitrogenase (EC 1.18.6.1); Fe-hydrogenase (EC 1.18.99.1).

Over the past few years, we have tried to gain insight into the nature of the Fe/S cluster(s) of complex redox enzymes, namely, Fe-hydrogenase [1–3], MoFe-nitrogenase [4, 5], sulfite reductase [6] and carbon-monoxide dehydrogenase [7, 8]. These enzymes appear to have two general properties in common. They all exhibit unusual EPR spectra that have, in several instances, been identified as resulting from a very high

cluster spin $S = 7/2$ and $S = 9/2$. Also, the number of iron and acid-labile sulfur ions associated with the clusters appears to be significantly higher than the maximum of 4Fe/S encountered in other proteins. Hence, we use the terms superspin and supercluster as epithets for this type of cluster [9].

The enzymes just mentioned all contain a considerable number of Fe and acid-labile S^{2-} grouped into several clusters. This complexity, combined with the lack of structural information on these proteins, makes the study of their clusters presently difficult. In an attempt to tackle this problem from a different perspective a model protein, the prismatic protein from *Desulfovibrio vulgaris* has been studied. The purification and biochemical characterization of this 6Fe/S-containing protein is described in [10]. We have previously presented EPR spectroscopic evidence indicating that the 6Fe/S are arranged in a single [6Fe-6S] supercluster [11]. We describe below an EPR and Mössbauer spectroscopic analysis of the prismatic protein in different redox states. The combined results allow us to propose a structural model and a magnetic-coupling model for the biological 6Fe cluster.

MATERIALS AND METHODS

The purification and biochemical characterization of the prismatic protein from *D. vulgaris* (subspecies Hildenborough), NCIB 8303, is described in [10].

Metallic iron 95.2% enriched in ^{57}Fe was obtained from Russia via Intersales-Holland BV, Hengelo, NL. The growth of *D. vulgaris* on ^{57}Fe -enriched medium in a 240-l batch culture differed from the standard procedure only in that tap water was replaced with demineralized water, and the iron source in the growth medium was replaced with ^{57}Fe -EDTA (255 mg metallic iron). Precultures were also grown on enriched medium. Enrichment of the batch culture was estimated to be $\leq 87\%$ based on colorimetric Fe determinations of the concentrated growth medium before and after addition of ^{57}Fe -EDTA stock. A determination of the $^{57}\text{Fe}/^{56}\text{Fe}$ ratio in the total concentrated growth medium with inductively coupled plasma/mass spectrometry (ICP-MS, courtesy of Drs C. Hess-Riechmann and K. Schneider, Universität Bielefeld, FRG) gave an enrichment of $77 \pm 3\%$. The final enrichment after growth and purification was $78 \pm 3\%$, as determined with ICP-MS on a sample of purified [3] desulfoviridin. This corresponds with the value of 80% as determined by quantitative Mössbauer spectroscopy (see Results and Discussion).

Deuterium oxide, 99.8 ^2H atoms/100 H atoms, and 30% (by mass) sodium deuteriooxide in $^2\text{H}_2\text{O}$ (>99 ^2H atoms/100 H atoms), both from Janssen Chimica (Beerse, Belgium), were used to prepare deuterated Hepes buffer, $p^2\text{H}$ 7.5. Prismatic protein in $^2\text{H}_2\text{O}$ was prepared by diluting purified protein 1:40 in deuterated Hepes buffer and reconcentration on a Centricon YM30 device. This procedure was repeated once. The final global enrichment was checked with ^1H NMR to be 99 ^2H atoms/100 H atoms).

Reductive titrations were done at 25°C in a 1.5-ml anaerobic cell under purified argon. The bulk potential of the stirred solution was measured at a Radiometer P-1312 platinum microelectrode with respect to the potential of a Radiometer K-401 saturated calomel electrode. Reported potentials are all recalculated with reference to the normal hydrogen electrode. The freshly prepared reductant and oxidant were sodium dithionite and $\text{K}_3\text{Fe}(\text{CN})_6$ in 0.5 M anaerobic Hepes, pH 7.5. Redox equilibrium was obtained as judged by the

attainment of a stable solution potential within a few minutes after addition of the titrant to the reaction mixture. The enzyme solution in 50 mM Hepes, pH 7.5, was incubated with the following mixture of mediators (each at a final concentration of 40 μM): N,N,N',N' -tetramethyl-*p*-phenylene diamine; 2,6-dichloroindophenol; phenazine ethosulfate; methylene blue; resorufine; indigo disulfonate; 2-hydroxy-1,4-naphthoquinone, anthraquinone disulfonate, phenosafranin; safranin O; neutral red; benzyl viologen; methyl viologen. At equilibrium samples were drawn and transferred to EPR tubes under a slight overpressure of purified argon then directly frozen in liquid nitrogen.

Normal-mode X-band EPR data were taken in Wageningen on a Bruker 200 D EPR spectrometer with peripheral instrumentation and data acquisition/quantification as described before [6]. Effective g values for $S = 9/2$ spectra were calculated as previously outlined [4, 6]. Parallel-mode X-band EPR was measured in the laboratory of Dr. S. P. J. Albracht (The University of Amsterdam) on a Varian E-236 EPR spectrometer equipped with the Varian E-236 bimodal rectangular cavity, as previously described in [12]. The spectrometer in Amsterdam was also used for Q-band measurements using Albracht's helium-flow system for the 35-GHz cylindrical cavity [13]. Additional X-band data and all the S-band and P-band data were collected in Ann Arbor on Varian E-112 spectrometer and on the home-built S-band and P-band spectrometers described in [14]. The microwave source in the S-band spectrometer is a 70-mW solid-state oscillator; the P-band spectrometer has a 200-mW klystron. In all frequency bands, the modulation frequency was 100 kHz.

Mössbauer spectra were obtained with a home-built spectrometer and associated hardware as described elsewhere [15, 16]. Part of the spectra presented have been corrected for source line shape and converted from transmission to absorption spectra. Previous examples of this approach to Mössbauer spectroscopy of ^{57}Fe -proteins, including theoretical simulation of experimental spectra, can be found in [17, 18].

RESULTS AND DISCUSSION

EPR of the 3+ state in dithionite-reduced protein

Throughout the paper we will label redox states as 3+, 4+, 5+ and 6+. This labeling is based on the assumption that the fully reduced prismatic protein contains a [6Fe-6S] $^{3+}$ cluster. The reader is reminded that this is a working hypothesis based on three previous observations [11]: (a) the stoichiometry is approximately six; (b) there is a striking similarity in g values between model compounds containing the [6Fe-6S] $^{3+}$ core and dithionite-reduced prismatic protein; (c) the EPR signal of the dithionite-reduced protein integrates approximately one $S = 1/2$ system/protein molecule.

We have assumed that both the prismatic models and the dithionite-reduced prismatic protein have magnetically isolated $S = 1/2$ ground states. The assignment of $S = 1/2$ to the models is consistent with magnetic susceptibility data at with the temperature and frequency dependence of the EPR [19]. An EPR line-width study of one of the prismatic models indicated that magnetic isolation was only marginally achievable by trading off EPR signal/noise for chemical, therefore magnetic, dilution (cf. Fig. 7 in [19]). This problem of line broadening is typical of the EPR of small model compounds in frozen solution; however, it is generally absent from

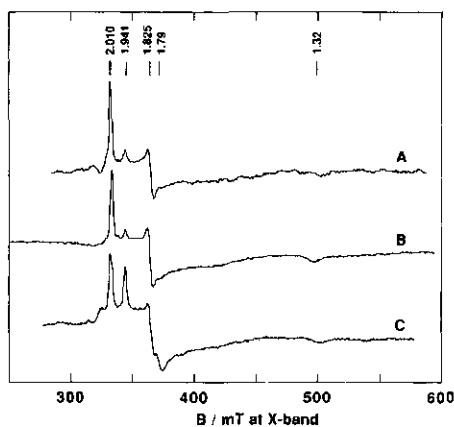


Fig. 1. Prismane-fingerprint EPR from the dithionite-reduced *D. vulgaris* (Hildenborough) prismane protein (the 3+ state). (A) P-band spectrum of 0.35 mM protein in 50 mM Hepes buffer, pH 7.5; (B) X-band spectrum of the same sample to show that the g values are frequency independent; (C) X-band spectrum of a different sample showing an increased ratio of the minor over the major component. EPR conditions: microwave frequency, 15484, 9224, 9337 MHz; microwave power, 40, 200, 200 mW; modulation amplitude, 0.4, 1, 1.8 mT; temperature, 15 K.

metalloprotein EPR, where the protein serves as a natural diamagnetic diluant [20].

We are thus in a better position with the prismane protein to look for signs of interaction in the EPR. In our initial analysis of the X-band spectrum, we already noted extra features in addition to the expected three g turning points [11]. With reference to Fig. 1 B, we note that the most striking of these features is the extra absorption peak at $g = 1.941$ between the highest two g values, 2.010 and 1.825; other features are found between the lowest two g values, 1.825 and 1.32, and as low-field and high-field shoulders. Note that the g values 2.010 and 1.825, reported here, are a slight correction (i.e. +0.005) to the previously reported values [11]. However, these values are also measured from the spectral turning points and not based on any rigorous mathematical analysis of the spectral shape.

For EPR studies, we have made 12 preparations of prismane protein each from a separate 240-l batch culture. Each sample exhibited the typical pattern of Fig. 1 B, although the relative intensities of the intermediate features compared to the main g peaks appeared to vary slightly. In only one out of the 12 preparations, the intermediate peak at $g = 1.941$ has considerably increased intensity compared to the $g = 2.010$ peak, although the purification procedure was standard. A spectrum from this single sample is given in Fig. 1 C, as it indicates that the $g = 1.941$ peak is a separate spectral entity with a second g at 1.79. The third g is undetermined.

Following the early work on prismane models [19], the prismane protein was also subjected to multi-frequency EPR (3–35 GHz). Just as with the models, it was found that samples of prismane protein gave detectable signals in X- and Q-bands and not in S- and P-bands. The P-band spectrometer is special in that it takes regular-sized X-band samples and with these reaches the sensitivity of the X-band machines. In Fig. 1 A and B, we compare the 15-GHz and 9-GHz spectrum. All features appear to be independent of frequency. Specifi-

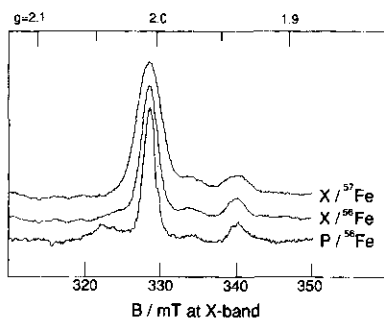


Fig. 2. Hyperfine (^{57}Fe), superhyperfine (^{14}N), and g -strain broadening of the $g = 2.010$ line from dithionite-reduced prismane protein. The data analysis is explained in the text. EPR conditions are as in Fig. 1.

cally, the two sets of g values 2.010, 1.825 and 1.32, and 1.941 and 1.79, are real g tensors. However, the low-field shoulder and the very broad feature around $g_{\text{eff}} \approx 1.6$ are also unaffected. Thus, the spectrum is not standard in that there are more frequency-invariant features than g tensor components. The shape of the spectrum from the 3+ state (specifically, the intensity ratio of the $g = 2.010$ and $g = 1.941$ species) is independent of the pH when measured in 0.2 M Mes, pH 5.5, or 0.2 M Ches, pH 9.5 (not shown).

Hyperfine broadening of the 3+ state EPR

Contributions from unresolved hyperfine components to the spectrum are presented in Fig. 2. As the frequency independence of peak positions implied electron spin-spin interactions to be insignificant, the line shape is taken to be a Gaussian from a convolution of g -strain and hyperfine broadening [20]. Since the different broadening mechanisms are physically independent, we have for the overall inhomogeneous line width:

$$W = \sqrt{(W_{g\text{-strain}}^2 + W_{\text{metal hyperfine}}^2 + W_{\text{ligand hyperfine}}^2)}, \quad (1)$$

where the last term is the sum broadening of all independent contributions from all nuclear magnetic ligands. The second term is only significantly non-zero for ^{57}Fe -enriched protein. When measured in magnetic-field units, the first term changes linearly with the microwave frequency; the other two terms are frequency independent. Thus, the three spectra in Fig. 2 form a sufficient data set to determine the individual three components of W along the g -tensor z -axis. The observed full width at half height for the three spectra at $g = 2.010$ (from top to bottom) are 3.95, 2.61 and 3.11 mT, which yields

$$W_{g\text{-strain}} = 1.2(5) \text{ mT at X-band (9225 MHz)},$$

$$W_{\text{metal hyperfine}} = 2.9(6) \text{ mT (frequency independent)},$$

$$W_{\text{ligand hyperfine}} = 2.2(9) \text{ mT (frequency independent)}.$$

Given a set of n equivalent nuclei, where the enrichment factor of an $I = 1/2$ nucleus has the average value f , we can write the probability of the combination where exactly i of the n nuclei have $I = 1/2$ as

$$f^i (1-f)^{n-i} \binom{n}{i}, \quad (2)$$

where $\binom{n}{i}$ is the binomial coefficient and represents the number of permutations of the combination. Referring to previous

work on hyperfine patterns [21], the Fourier transform of the entire pattern in the present case is

$$\sum_{i=0}^n f^i (1-f)^{n-i} (\pi) \cos^i(At/2), \quad (3)$$

where t is the argument of the Fourier space and A is the hyperfine constant. By back-transforming test spectra from the above equation, we were able to establish that

$$A_{\text{Fe}} = g W_{\text{metal hyperfine}}/5.0, \quad (4)$$

if $n=6$, W (mT) is the full width at half height, and f equals 0.8 (80% enrichment, as determined by ICP-MS and by Mössbauer quantitation). Therefore, A_z (^{57}Fe) ≈ 1.2 mT, where the quotation marks are to indicate that we measure along the z -axis of the g tensor. This number is similar to the A_z values for iron hyperfine splittings in the $[4\text{Fe-4S}]^{3+}$, $[2\text{Fe-2S}]^{1+}$ and $[4\text{Fe-4S}]^{1+}$ clusters in proteins as determined by EPR and electron nuclear double resonance [22–24].

The most striking contribution to the linewidth is the 2.29 mT from unresolved ligand hyperfine splittings. This number is much too high to be caused only by magnetic nuclei (H, N) in the second and/or higher coordination spheres. The corresponding number at g_z for $[2\text{Fe-2S}]^{1+}$ in spinach ferredoxin can be calculated from Fig. 4 in [25] to be approximately 1 mT. Thus, in the prismane protein there is some 2 mT additional broadening. We take this to indicate that the protein ligation to the prismane is not exclusively through cysteine sulfur, but also involves nitrogen.

The peak at $g = 2.010$ was also studied at X-band with a sample in deuterated buffer. No sharpening was detectable compared to the spectrum of Fig. 2 (not shown). Therefore, exchangeable protons do not contribute to the line width.

Multi-frequency $S = 1/2$ EPR of the 5+ state

We previously reported a signal from the prismane protein as it was isolated [11]. Temperature dependence indicated the signal to represent an $S = 1/2$ system; however, quantitation amounted to only 0.1 spin/protein molecule. The signal is unusual for an iron-sulfur protein in that all three g values are below the free-electron value. The g values and stoichiometric intensity are typical for d^1 ions such as Mo(V) or W(V); however, in preliminary analytical determinations, we were unable to detect these elements in the protein. We proposed that the signal is from $[6\text{Fe-6S}]^{5+}$ (*ibidem*; see also below). In more extensive elemental analyses, the content of Mo and W has now been determined to be <0.03 /protein molecule (cf. [10]). We have now further characterized the signal by multi-frequency EPR.

In Fig. 3, the $g < 2$ spectrum of the isolated protein is presented at four different microwave frequencies, 3–35 GHz. Evidently, the signal is from a single g tensor ($S = 1/2$) as three features are observed whose position on a g -value scale does not depend on the frequency. Unusual for iron-sulfur EPR, g anisotropy is virtually completely blurred in the inhomogeneous line shape at S-band. This broadening from unresolved ligand hyperfine splittings is considerable even at X-band. Only at the Q-band frequency hyperfine broadening has become insignificant compared to g -strain broadening, and we can rather accurately read out the g -tensor principal elements as 1.971, 1.951 and 1.898.

In Fig. 4, the X-band and P-band traces of Fig. 3 are replotted as dotted traces to compare them to the spectra from prismane protein enriched in ^{57}Fe . We decompose contribu-

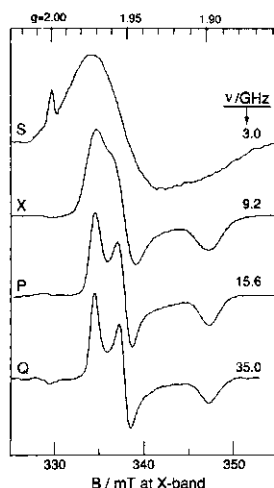


Fig. 3. Frequency dependent $S = 1/2$ EPR from the isolated prismane protein (the 5+ state). The data reveal a single g tensor plus an unusually large contribution of ligand hyperfine broadening. EPR conditions (S, X, P, Q): microwave frequency, 2966, 9225, 15557, 35018 MHz; microwave power, 0.44, 0.5, 5, 126 mW; modulation amplitude, 0.16, 1, 0.4, 1.25 mT; temperature, 19, 15, 15, 20 K.

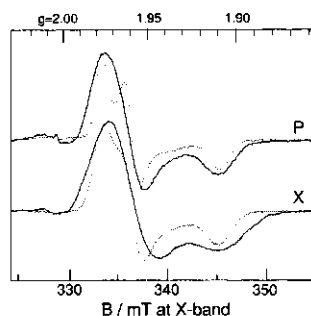


Fig. 4. Hyperfine (^{57}Fe), superhyperfine (^{14}N), and g -strain broadening of the $S = 1/2$ signal from the isolated prismane protein. Samples 80% enriched in ^{57}Fe . The data analysis is explained in the text. EPR conditions are as in Fig. 3.

tions to the line width along the same lines as for the 3-spectra in Fig. 2. However, here we look at the peak at the lowest g value, $g = 1.898$, as the low-field part of the spectrum has insufficient resolution. The observed line-width values are 3.75 mT and 5.86 mT (^{57}Fe) in P-band and 2.80 mT and 3.75 mT (^{57}Fe) in X-band. From these numbers we obtain:

$$W_{g\text{-strain}} = 1.8 \text{ mT at X-band (9227 MHz)},$$

$$W_{\text{metal hyperfine}} = 4.6 \text{ mT (frequency independent)},$$

$$W_{\text{ligand hyperfine}} = 2.1 \text{ mT (frequency independent)}.$$

The value for $W_{\text{metal hyperfine}}$ is the average of the numbers obtained from the P-band (4.50 mT) and X-band (4.83 mT) spectra.

Again using the Fourier transform of the hyperfine pattern, we now find that A_x (^{57}Fe) ≈ 1.7 mT. This is somewhat

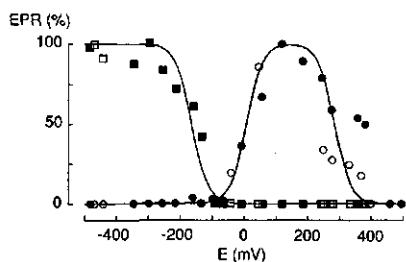


Fig. 5. Oxido-reductive titration at pH 7.5 of $S = 1/2$ components in *D. vulgaris* prismatic protein with dithionite and ferricyanide in the presence of appropriate mediators. (\square , \blacksquare) The prismatic-fingerprint signal (the 3+ state) monitored at $g = 1.825$; (\circ , \bullet) signal with all $g < 2$ (the 5+ state) monitored at $g = 1.898$. (\blacksquare , \bullet) Titration in two directions starting from the isolated protein, which corresponds approximately to the top of the bell-shaped curve. (\square , \circ) A titration starting from the fully oxidized state. EPR conditions: microwave frequency, 9.33 GHz; microwave power, 13 mW; modulation amplitude, 0.63 mT; temperature, 15 K.

rather than that found for the 3+ state and, thus, also somewhat higher than the value common for regular Fe/S clusters. Note that the $[6\text{Fe-6S}]^{3+}$ is isoelectronic with $3[2\text{Fe-2S}]^{1+}$ (average Fe valency of +2.5), however, the $[6\text{Fe-6S}]^{5+}$ structure has no analog in simple Fe/S (bio)chemistry. The increased Fe hyperfine interaction is not the result of the electron being less delocalized onto the protein ligand, because the magnitude of the ligand hyperfine broadening is comparable to that in the 3+ state. This latter observation is another indication of nitrogen coordination to the cluster.

Again, as with the 3+ spectrum, deuteration of the buffer does not result in a sharper X-band spectrum (not shown).

Redox titrations monitored with $S = 1/2$ EPR

The prismatic protein was anaerobically titrated with reductant and oxidant in the presence of a mixture of redox mediators covering a broad potential range (see Materials and Methods). The result of these titrations in 50 mM Hepes, pH 7.5, is presented in Fig. 5 as relative EPR intensities of the $S = 1/2$ signals assigned above to the 3+ and the 5+ state. The isolated protein is in an intermediate redox state, the 5+ state, and this still holds after mixing with the mediator cocktail. Thus, the starting point of the titration, before addition of titrant, has an equilibrium potential of some 100 mV vs the normal hydrogen electrode. From this point, the protein was reductively titrated with sodium dithionite and oxidatively titrated with potassium ferricyanide. In a second experiment (the open symbols in Fig. 5), reversibility was tested as follows: the protein was first completely oxidized with ferricyanide to the EPR silent 6+ state, then it was partially re-reduced with dithionite to the 5+ state, and finally was stepwise reduced with dithionite to full reduction or re-oxidized with ferricyanide to the 6+ state. The solid lines in Fig. 5 are $n = 1$ Nernst curves.

The titration clearly defines four separate redox states responding to the putative valencies 3+ to 6+ of the $[6\text{Fe-6S}]$ cluster. The $S = 1/2$ prismatic signal of the 3+ state, detected at $g_z = 1.825$, appears with a midpoint potential of 65 mV. We have previously shown that this signal represents approximately 0.6–0.9 spin/50-kDa protein molecule

[11]. With the corrected molecular mass of 52 kDa [10], and including the spin intensity of the minor component with $g_z = 1.941$ (single-integration method), the complete EPR spectrum of reduced protein essentially represents unit stoichiometry, therefore, the percentage reduction on the ordinate axis is an absolute value.

The titration of the $S = 1/2$ signal with all $g < g_z$ ascribed to the 5+ state has the typical bell shape of an intermediate redox state. We previously found a spin intensity of 0.10–0.12 in the isolated enzyme [11]. The plateau of the bell-shaped curve in Fig. 5 also corresponds to some 0.1 spin/protein molecule. The isolated protein is indeed predominantly in the 5+ state. This conclusion implies that we should account for the missing 90% intensity of this half-integer spin system (see below).

The 5+ signal disappears upon reduction with dithionite as an $n = 1$ acceptor with a midpoint potential of -5 mV. The cluster comes into the 4+ state which should be integer spin or $S = 0$. Consistent with this assignment, no signal is observed in regular-mode EPR.

When the 5+ state is oxidized with ferricyanide, we also expect to make an even-electron system. Indeed, we observe the 5+ signal to disappear with no new signals detected. Apparently, the 6+ state is diamagnetic, $S = 0$. In this capacity to reach reversibly the fully oxidized state, the putative $[6\text{Fe-6S}]$ cluster differs from the classical dinuclear and cubane clusters. We observe some hysteresis in the oxidation curve that is probably not intrinsic to the protein. In the potential range around $+0.3$ V, where appropriate mediators are not available, it is difficult to establish redox equilibrium. The $n = 1$ Nernst fit on all points gives a 6+/5+ potential of $+285$ mV; however, it should be obvious that this number is significantly less accurate than the other two reduction potentials.

Characterization of an $S = 9/2$ system from the 5+ state

In the 5+ state, only 10% of the protein is recovered in the $S = 1/2$ spectrum. If the concept of a cluster in a single valence state is valid then the remaining 90% should also be half-integer spin. We have, therefore, looked for high-spin EPR in concentrated samples of the prismatic protein.

The isolated protein has a number of weak resonances at low magnetic field values. The temperature dependence of these lines can be seen in Fig. 6. For the non-saturated spectrum of a ground-state Kramers doublet, the signal amplitude should decrease with increasing temperature. It is clear from Fig. 6 that the amplitudes of the high-spin resonances go through a maximum as a function of temperature. Therefore, these resonances are from one or more excited states. The spectrum has its maximal amplitude at a temperature of about 12 K. We use this spectrum (Fig. 7) for a g analysis.

The spectral feature with the lowest magnetic field value has an absorption shape peaking at an effective g of 15.3. This observation is the starting point for our analysis that develops along the same lines as our recent identification of $S = 9/2$ EPR in *D. vulgaris* dissimilatory sulfite reductase [6]. We take the system spin to be half-integer and the relevant spin Hamiltonian to be

$$H_s = D[S_z^2 - S(S+1)/3] + E(S_x^2 - S_y^2) + g\beta B \cdot S \quad (5)$$

We assume, as is very common for metalloprotein EPR, that the Zeeman interaction is considerably smaller than the zero-field interaction, i.e. we are in the weak-field limit. This assumption is tested later by estimating the magnitude of the

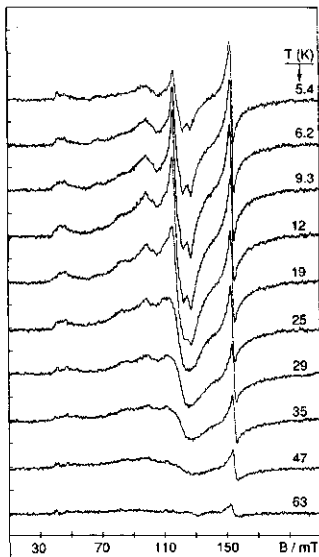


Fig. 6. Temperature dependence of low-field $S = 9/2$ resonances from *D. vulgaris* prismsane protein in the $5+$ state. For all spectra, spectrometer settings were the same except for temperature. The line at $g = 4.3$ (155 mT) is from adventitious ferric ion and is partially saturated at low temperatures. The other signals are not saturated. EPR conditions: microwave frequency, 9.33 GHz; microwave power, 80 mW; modulation amplitude, 0.8 mT.

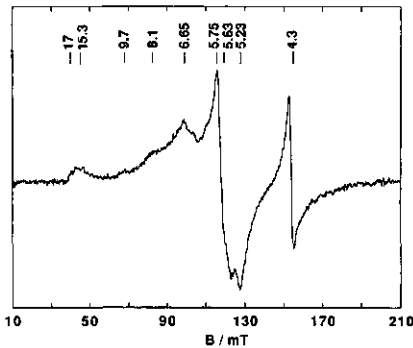


Fig. 7. Effective g assignment of the low-field $S = 9/2$ EPR. The spectrum was recorded at the optimal temperature of 12 K, i.e. at which the amplitude is maximal and lifetime broadening is not significant. EPR conditions were as in Fig. 6.

zero-field splitting parameter, D . Under these assumptions, and with the real value, $g \approx 2$, the system spin S and the highest effective g are related as $4S \geq g_{\text{max}}$. We observe that $g_{\text{max}} = 15.3$, therefore, the system spin is $S \geq 9/2$. As in [6], we assume $S = 9/2$ and we proceed to prove consistency with the observed (Fig. 7) effective g values.

In the weak-field limit, and with the real g fixed at 2.00, the five times three effective g of the EPR subspectra from within the Kramers doublets of the $S = 9/2$ system are a function of the rhombicity, $0 \leq |3E/D| \leq 1$, only. We have recently

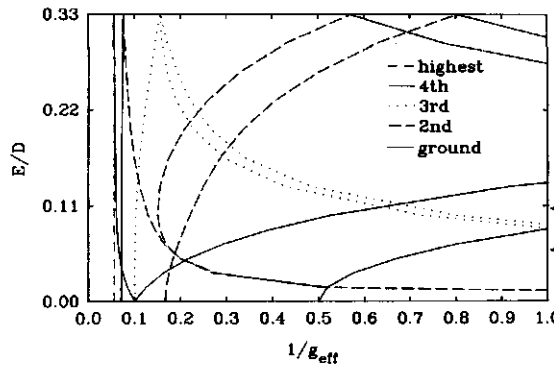


Fig. 8. Rhombogram (inverted representation) for $S = 9/2$ calculated in the weak-field limit (i.e. $D > g\beta B$) with real $g = 2.00$. The present form of the rhombogram is an alternative to the linear representation [6] and allows for a direct read-out of all peak positions for a given rhombicity, E/D , on a reciprocal effective g scale, i.e. on a linear magnetic-field scale. The two arrows indicate the two rhombicity values found for the prismsane protein $S = 9/2$ EPR (cf. Fig. 7 and Table 1).

given a graphic representation (the rhombogram) of the relations for $S = 9/2$ in [6]. An alternative, fully analogous representation (the inverted rhombogram) is obtained by plotting the rhombicity against the inverse of the effective g value, as in Fig. 8. Fitting of the experimental g values comes down to moving a horizontal line along the rhombicity axis (Fig. 8), where the intersections of this line with all curves define a stick spectrum of effective g values on an inverse g scale, i.e. on a linear magnetic-field scale.

The peak at $g = 15.3$ can only come from the $|\pm 1/2\rangle$ doublet. Since its amplitude goes through a maximum with increasing temperature, the zero-field splitting parameter, must be negative. The $|\pm 1/2\rangle$ doublet has the highest energy within the $S = 9/2$ multiplet. The $g = 15.3$ line defines a rhombicity of $E/D = 0.061$ and this value in turn defines all other 14 g values (Table 1). The second g of the $|\pm 1/2\rangle$ doublet is predicted at $g = 3.8$. However, with an inhomogeneous broadening from isotropic g strain (cf. [20]), the width should be $(15.3/3.8)^2$ approximately 16 times greater than that at $g = 15.3$. Evidently, this line is not observable. The main prediction for $E/D = 0.061$ is a near-isotropic, therefore easily observable, spectrum from within the $|\pm 3/2\rangle$ doublet at $g = 5.2-5.7$. This is indeed the major feature of the spectrum in Fig. 7.

The other features of Fig. 7 are not fit by the model. The line at $g = 4.3$ is of course the well-known isotropic resonance from contaminating ferric ion ($S = 5/2$, $|E/D| \approx 1/3$, $m_s = \pm 3/2$). The remaining resonances at $g = 9.7$, 8.1 and 6.65 are the $S = 9/2$ model for $E/D = 0.108$, and $m_s = \pm 3/2$, $\pm 1/2$. The $S = 9/2$ spin occurs in two forms of different rhombicity. This is a very common phenomenon in high-spin EPR metalloproteins. It was also observed for the $S = 9/2$ system in sulfite reductase [6]. The relative intensities of the two forms of lines varies slightly from preparation to preparation (not shown). The rhombicity $E/D = 0.108$ predicts a line at $g = 16.7$ for the $|\pm 1/2\rangle$ doublet. With equal probability for two rhombicities, the amplitude of this peak should be about 20% of that at $g = 15.3$ as a consequence of the increase in g anisotropy. We observe sufficient intensity at $g = 16.7$ to account for this prediction.

Table 1. Calculated and observed effective g -values for $S = 9/2$ in *D. variabilis* (Hildenborough) prisma protein in the $5+$ state. The theoretical g values were calculated in the weak-field limit as in [6]. The following abbreviations are used: wide, too wide to be detected; outside, resonance line falls outside range of magnetic field; obsc, obscured by adventitious iron signal; n.s., no significant transition probability.

D	Doublet	g_x	g_y	g_z
61	$ \pm 1/2\rangle$	1.32 wide	15.25 15.3	3.78 wide
	$ \pm 3/2\rangle$	5.23 5.2(3)	5.74 5.7(5)	5.68 5.6(5)
	$ \pm 5/2\rangle$	9.89 9.7	0.47 outside	0.55 outside
	$ \pm 7/2\rangle$	13.98 n.s.	≈ 0 outside	≈ 0 outside
	$ \pm 9/2\rangle$	18.00 n.s.	≈ 0 outside	≈ 0 outside
	08	$ \pm 1/2\rangle$	0.73 wide	16.66 17
$ \pm 3/2\rangle$		4.42 obsc	8.06 8.1	6.68 6.6(5)
$ \pm 5/2\rangle$		9.62 9.7	1.44 wide	1.61 wide
$ \pm 7/2\rangle$		13.92 n.s.	≈ 0 outside	≈ 0 outside
$ \pm 9/2\rangle$		17.98 n.s.	≈ 0 outside	≈ 0 outside

Temperature dependence and quantification of the $S = 9/2$ EPR

The magnitude of the zero-field splitting can be obtained from a fit of EPR intensity to a Boltzmann distribution over the $S = 9/2$ multiplet. The close-to-isotropic pattern around 5.5 from within the $|\pm 3/2\rangle$ doublet is the subspectrum with the largest amplitude. The feature with the next-to-highest intensity is the derivative line at $g = 6.65$. We have used both the area of the $g \approx 5.5$ feature and the amplitude of the positive lobe at $g \approx 6.7$ with respect to the base line zero-field as the $|\pm 3/2\rangle$ intensity to fit the Boltzmann distribution over the five doublets as a function of the temperature. The results are graphically presented in the Fig. 9B. Both fits are optimal for $D = -0.86 \text{ cm}^{-1}$. This result is not significantly sensitive to whether we calculate the energy levels for axial symmetry ($E = 0$) or for the intermediate rhombic case with $|E/D| = 0.1$. We have also taken the first integral of the feature peaking at $g = 15.3$ as the $|\pm 1/2\rangle$ intensity, and the corresponding fit gives essentially the same value of $D = -0.86 \text{ cm}^{-1}$ (Fig. 9A). Therefore, D is valid for the complete $S = 9/2$ spectrum, i.e. including both populations of ambicity.

Next, we quantify the $S = 9/2$ spin concentration by double integration [26] of the subspectra from the $|\pm 3/2\rangle$ doublets. We take the $T = 12 \text{ K}$ spectrum in which the multiplet is maximally developed. The quantification of $S = 9/2$ spins gives a value of 0.6–1.3 prisma protein $^{-1}$. The uncertainty in this number depends on the uncertainties in D determination ($\pm 15\%$) and, especially, in the integration of partially resolved subspectra.

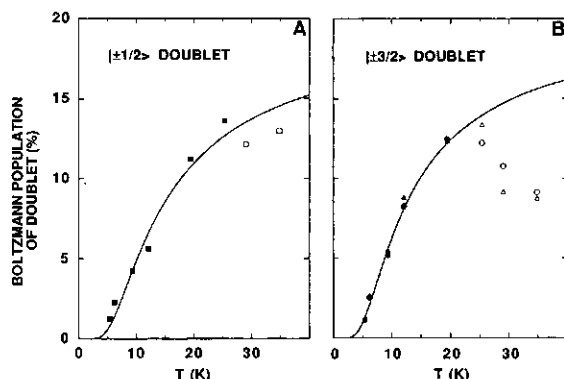


Fig. 9. Thermal (de)population of the highest doublet ($m_S = \pm 1/2$) and the one-to-highest doublet ($m_S = \pm 3/2$) of the inverted ($D < 0$) $S = 9/2$ multiplet in the prisma protein. The data points are the peak area at $g = 15.3$ (\blacksquare), the amplitude at $g = 6.65$ (\blacktriangle) and the area of the feature around $g \approx 5.5$ (\bullet) multiplied by the detection temperature (i.e. corrected for Curie-law temperature dependence). The line plotted and the scaling of the ordinate were obtained by fitting the data to a Boltzmann distribution over the sublevels of an $S = 9/2$ system with $D = -0.86 \text{ cm}^{-1}$. The deviation above $T \approx 25 \text{ K}$ (\circ , \square , \triangle) reflects lifetime broadening.

Table 2. Frequency dependence of the $S = 9/2$ EPR. The zero crossing of the $g_{\text{eff}} \approx 5.5$ subspectrum in S-, X-, P- and Q-bands.

Microwave frequency	Zero crossing
GHz	g_{eff}
2.97	5.58
9.23	5.57
15.56	5.56
35.11	5.50

Frequency dependence and reduction potential of the $S = 9/2$ system

Effective g values of high-spin systems are a function of the microwave frequency. This dependency can in principle be used to determine D . We have attempted to measure the $S = 9/2$ spectrum at other than X-band frequencies. Due to the diminished sensitivity in these frequency bands, only the zero crossing of the $g \approx 5.5$ subspectrum was detected. The results are given in Table 2. Only a slight reduction in the effective g is observed with increasing frequency. This slight curvature is insufficient to determine D , however the data are not inconsistent with the previously determined $D = -0.86 \text{ cm}^{-1}$. Moreover, the data establish that the weak-field assumption ($S \cdot D \cdot S \gg g\beta B \cdot S$) is valid. We used this assumption in the calculation of g in Table 1.

The concentration of the $S = 9/2$ system is higher than the $S = 1/2$ signal of the $[6\text{Fe-6S}]^{5+}$ state by an order of magnitude. We hypothesize that the $5+$ state is quantitatively accounted for by these two signals, i.e. 10% is $S = 1/2$ and 90% is $S = 9/2$. The situation bears analogy to that in the reduced Fe-protein of nitrogenase, for which we found 20% $S = 1/2$ and 80% $S = 3/2$ [27]. Morgan et al. later showed that these two spin systems in Fe-protein were indistinguishable biochemically, as their intensity ratio is a constant in redox

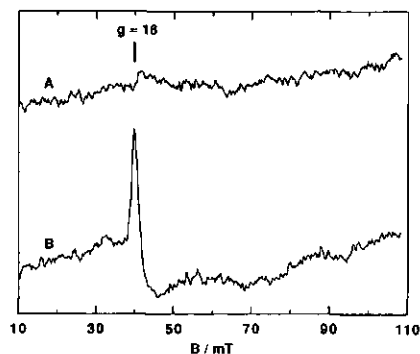


Fig. 10. Dual-mode spectrum of a low-field resonance from *D. vulgaris* prismsane protein reduced with dithionite to the intermediate 4+ state. (A) Magnetic component of the microwave perpendicular to the external magnetic field vector; (B) the two vectors were parallel. EPR conditions, microwave frequencies, 9146 MHz (perpendicular) and 9098 MHz (parallel); microwave power, 200 mW; modulation amplitude, 1.25 mT; temperature, 9 K.

titrations [28]. Meyer and coworkers reached a similar conclusion on the basis of room temperature NMR [29]. We have performed a ratio-titration experiment on a concentrated sample of prismsane protein. Starting from the isolated protein i.e. predominantly in the 5+ form, the prismsane was titrated with small aliquots of Hepes-buffered dithionite. After each addition, the $S = 1/2$ and $S = 9/2$ EPR was measured. In multiple steps, the two signals were titrated away, resulting in the EPR silent $[6\text{Fe-6S}]^{4+}$ state. Throughout this titration, the intensity ratio $[S = 1/2]/[S = 9/2]$ was a constant within experimental error ($\pm 10\%$). The two spin systems are different magnetic ground states from the same biochemical entity with $E_m = +5$ mV at pH 7.5.

Parallel-mode, integer-spin EPR of the 4+ state

The 4+ state is silent in normal-mode EPR. The spin is expected to be integer or zero. Integer spin systems can have forbidden $|\Delta m_s| = 0$ transitions at low field. These transitions within non-Kramers doublets become allowed when the microwave magnetic component is configured parallel, rather than perpendicular, to the static magnetic field. The parallel-mode resonator provides this geometry, which has been proven practical in the EPR detection of $S = 2$ systems in metalloproteins [12].

In Fig. 10, low-temperature dual-mode spectra are presented from concentrated prismsane protein in the 4+ state. We started from the isolated 5+ state and titrated with dithionite to the 4+ state, then to the 3+ state. In the isolated (5+) and in the fully reduced (3+) proteins, there is no parallel-mode signal, consistent with the detection of a quantitative $S = 1/2$ spectrum in normal-mode EPR. Contrarily, the 4+ state exhibits a relatively sharp, asymmetrically shaped feature at low field.

The asymmetric feature has its positive peak at $g \approx 16$ and its width is only a few millitesla. This spectrum is quite different from the $S = 2$ metalloprotein spectra previously reported: the spectra typically had a width of several tens of millitesla, and also had significant intensity in normal-mode EPR [12, 30, 31]. However, we also note a remarkable correspondence in that both the $S = 2$ spectra and the present Fig. 10B are

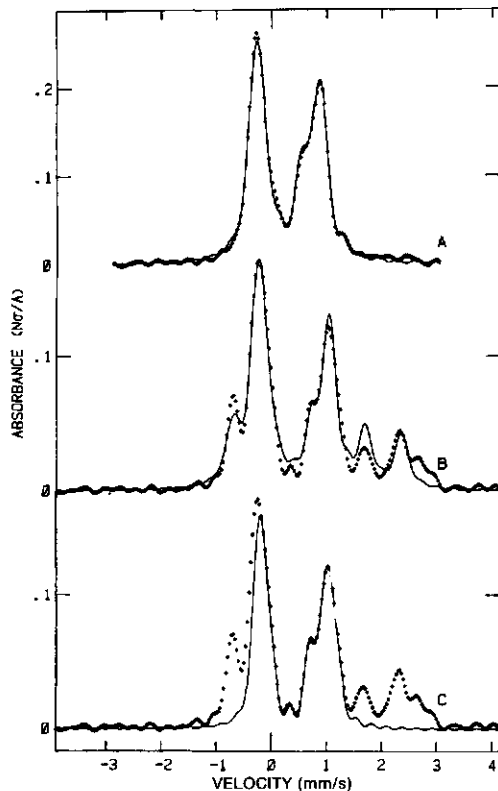


Fig. 11. High temperature, absorption mode, Mössbauer spectra and fits (—) for the prismsane protein in the isolated (5+) and reduced states (3+). (A) Isolated protein, 125 K superimposed by a fit with two sites of occupancy 4 and 2 (see Table 3); (B) dithionite-reduced protein, 125 K superimposed by a four-site fit of occupancy 3, 1, and 1; (C) same data as (B) superimposed by a two-site fit omitting the ferrous atoms.

asymmetric, single-line spectra. The $S = 2$ spectra were interpreted to come from the transition within the highest non-Kramers doublet with approximate g_{eff} of $4S \cdot g_{\text{real}}$, and this gives $g_{\text{eff}} \approx 8$ for $g_{\text{real}} \approx 2$. Extrapolating this model to the present case, we reach the tentative conclusion that $S = 4$.

Mössbauer spectroscopy of the 5+ and 3+ states

In Fig. 11 the absorption-mode, high-temperature Mössbauer spectra are shown for the dithionite-reduced form of the protein (the 3+ state) and for the isolated form of the protein (the 5+ state). These data are superimposed on computer simulations that model the spectra as sums of quadrupole pairs. The fitting parameters for these data are given as for those taken at 175 K (data not shown) are listed in Table 3. Quantitation of the spectra account for all the 5^{2+} atoms in the samples. There are no resonances that are vanishingly small due to the presence of a large and anisotropic internal magnetic field in the atoms, because at these temperatures the magnetic moments from the paramagnetic electrons are averaged to Curie-Law values by the thermal process. Therefore, the hyperfine fields in the $S = 1/2$ state in the reduced enzyme and the $S = 9/2$ state in the resting enzyme

Table 3. A comparison of Mössbauer parameters for prismane and cubane models versus the prismane protein. The data for the model compounds were measured as part of the work described in [19, 32, 33]. For the protein data, the amount of iron is not a free parameter in the analysis, it is fixed by the high-temperature simulations and is identical for the high-field and low-field spectra (and agrees with the ICP-MS value). The Debye temperature for all irons in the protein is 160 K. Valency is the average of the formal valencies (i.e. ferric or ferrous) of all iron atoms.

Sample	Valency	Temperature K	Isomer shift mm/s	Quadrupole splitting	Line width	Occupancy (Fe atoms)
$(\text{C}_4\text{N})_3\text{Fe}_6\text{S}_6(\text{SR})_6$	2.5	125	0.44	1.04	—	6
$(\text{C}_4\text{N})_3\text{Fe}_6\text{S}_6(\text{OR})_6$	2.5	125	0.48	1.03	—	6
$(\text{C}_4\text{N})_3\text{Fe}_6\text{S}_6\text{I}_6$	2.5	125	0.48	1.13	—	6
$(\text{C}_4\text{N})_3\text{Fe}_6\text{S}_6\text{Br}_6$	2.5	125	0.49	1.13	—	6
$(\text{C}_4\text{N})_3\text{Fe}_6\text{S}_6\text{Cl}_6$	2.5	125	0.50	1.10	—	6
$(\text{C}_4\text{N})_2\text{Fe}_6\text{S}_6\text{Cl}_6$	2.67	125	0.43	0.62	—	6
$(\text{C}_4\text{N})_2\text{Fe}_4\text{S}_4(\text{SR})_4$	2.5	125	0.43	0.83	—	4
$(\text{C}_4\text{N})_2\text{Fe}_4\text{S}_4\text{Cl}_4$	2.5	125	0.49	1.04	—	4
Prismane protein (3+)	2.5	125	0.52	1.27	0.27	3
			0.45	0.81	0.27	1
			0.80	2.02	0.27	1
			0.93	3.06	0.27	1
Prismane protein (3+)	2.5	175	0.50	1.24	0.24	3
			0.41	0.79	0.24	1
			0.72	2.02	0.24	1
			0.90	3.03	0.24	1
Prismane protein (5+)	2.83	125	0.40	1.18	0.28	4
			0.32	0.73	0.28	2
Prismane protein (5+)	2.83	175	0.40	1.19	0.26	4
			0.33	0.71	0.26	2
Prismane protein (5+)	2.83	4.2	0.44	1.16	0.28	4 ^a
			0.36	0.7	1	1 ^b
			0.36	0.7	1	1 ^c

Both computer simulations of the diamagnetic irons at this temperature have the same parameters ($\eta = 0$), except for the applied magnetic field.

^a $A_x = A_y = A_z = -11$ mm/s, η is not determined, but is expected to be about 0.6.

^b $A_x = A_y = A_z = -7.3$ mm/s, η is not determined, but is expected to be about 0.6.

which we know to be present due to our previous EPR experiments, are not factors in the Mössbauer spectra shown in Fig. 11. As a consequence, the charge parameters, isomer shift and quadrupole splitting (ΔE_Q), are the only determinants of these spectra. In Table 3, the relevant parameters from a series of prismane model compounds in the 3+ state are also shown. (The inorganic chemists count the exogenous iron atoms as part of the formal charge in the system. For cubanes, their charge is four less than that in the [4Fe-4S] cluster; for prismanes, their charge is six less than that in the [6Fe-6S] cluster.) The reduced form of the protein (3+) has the EPR signature of the 3+ prismane model. Comparing the isomer shifts from the reduced-protein fit to those in Table 3, we find that four of the iron atoms match well (in Fig. 11C, the simulation has only these four iron sites), but an intensity that is up to two iron equivalents is in a form suggestive of a small high-spin ferrous atom such as that found in reduced dithionite or the reduced form of a [2Fe-2S] cluster. The matches in Fig. 11B for these ferrous sites indicate heterogeneity in the protein. Similar effects were reported above for the EPR of the 3+ state. Clearly, there is a difference between the cluster in this protein and that in a $\text{Fe}_6\text{S}_6(\text{SR})_6$ cluster. The [4Fe-4S]²⁺ state and the [6Fe-6S]³⁺ state are isotropic with very similar isomer shifts but unequal quadrupole splittings (Table 3). In both of these clusters, the appropriate interpretation of the formal charge for the irons

is one of partial valence. The six iron atoms (three ferric and three ferrous) in a 3+ prismane model give rise to a single quadrupole pair whose isomer shift changes by about +0.07 mm/s upon single-electron reduction (Table 3). Similarly the 2+ cubane model has a single quadrupole pair whose isomer shift is slightly more sensitive to reduction than the prismane model. This added sensitivity to reduction is expected because the cubane has two less iron atoms/reducing electron than the prismane. The EPR-monitored redox titration has shown that there is a two-electron difference between the isolated and the dithionite-reduced forms of the protein. It is therefore possible that the two ferrous atoms, visible in the spectra from the dithionite-reduced enzyme but absent in those from the protein in the 5+ state, are the active redox center, while the other four iron atoms are part of a [4Fe-4S]²⁺ cluster that is unchanged by this chemistry.

There are, however, several reasons to reject the possibility that a cubane is somehow involved with spectra in Fig. 11. Two of the iron atoms are in the high-spin ferrous state in the dithionite-reduced protein, therefore the other four iron atoms must be in the cubane if one exists. The isomer shift of these four irons agrees well with that of a [4Fe-4S]²⁺ center, which is diamagnetic. Therefore, the $S = 1/2$, prismane-signature EPR spectrum would have to come from the two ferrous atoms; a very unlikely situation. In Fig. 12 the Mössbauer spectra of the dithionite-reduced protein in various temperatures and

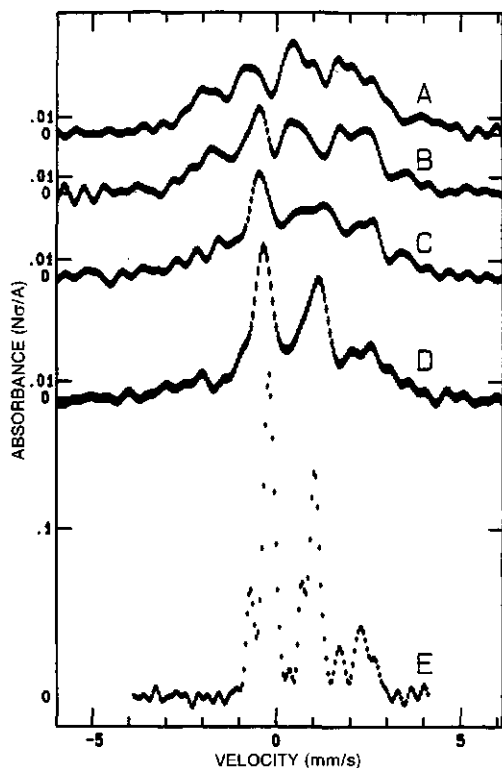


Fig. 12. Absorption-mode Mössbauer spectra of the dithionite-reduced prismane protein at various temperatures and applied magnetic fields. (A) 4.2 K, 5 T applied magnetic field; (B) 4.2 K, 30 mT; (C) 10 K, 30 mT; (D) 20 K, 30 mT; (E) 175 K, 0 mT.

applied magnetic fields are shown. These spectra show that all six of the iron atoms are paramagnetic at low temperature, even at low applied fields. Therefore, all six iron atoms are part of one or more non-integer spin systems. The possibility of a $[4\text{Fe-4S}]^{2+}$ cluster is thereby excluded for this protein. Furthermore, the data in Fig. 12 also require the incorporation of the two ferrous atoms (Fig. 11) into the $S=1/2$ state that quantitates to one electron equivalent by EPR. This conclusion necessitates a situation where the other four iron atoms have an odd number of electrons to account for the paramagnetism ($S=1/2$ EPR) at low temperature.

In Fig. 13, the Mössbauer spectra for the isolated protein ($5+$) at various temperatures and magnetic fields are shown. These spectra have complexities that are not present in the data from the dithionite-reduced protein (Figs 11 and 12). For example, the spectra taken at high temperature (Figs 11A and 13C) fit well to a model with six iron atoms, where the simulations (Table 3) account for all the iron in the protein. However, at low temperature, four of the iron atoms ($2/3$ of the intensity of the spectra) fit well to a model that has a single-iron environment (Fig. 13A and B, Table 3). We interpret this finding to mean that four of the iron atoms are in a regular environment that appears to be nearly diamagnetic, even with the application of very high magnetic fields. The spectral shapes of the central lines in these spectra greatly resemble those of the dithionite-reduced spectra. However, they are

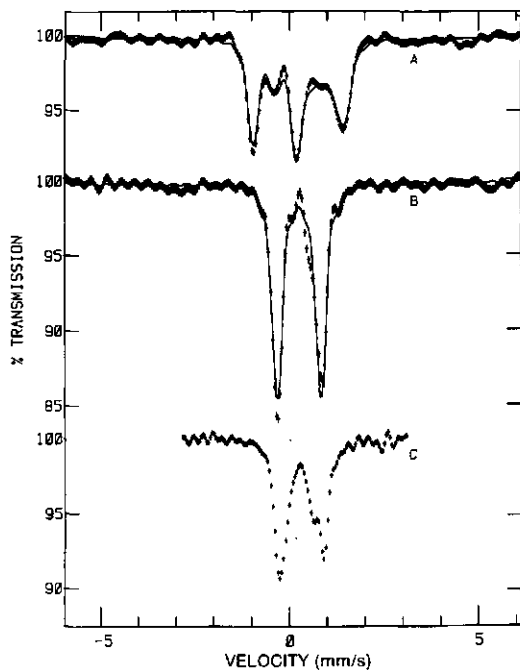


Fig. 13. Transmission-mode Mössbauer spectra and fits (—) of isolated prismane protein (the $5+$ state) at various temperatures and applied magnetic fields. (A) 4.2 K, 5 T applied magnetic field; (B) 4.2 K, 200 mT; (C) 175 K, 0 mT.

shifted to smaller velocities (implying oxidation) by an amount that is greater than the shift characteristic of a single electron oxidation for either the prismanes or cubanes. However, at temperature does one see the presence of the two ferrous iron atoms that were so obvious in the dithionite-reduced protein. We interpret these data to signify that the two-electron difference between these two redox forms of the protein is accounted for by the oxidation of the two ferrous lines and the four-iron cluster. This can only be possible if the two ferrous irons and the four-iron cluster are part of a single cluster. Thus, we conclude that the spectra from both forms of the protein are characteristic of a six-iron cluster. This conclusion leads immediately to the problem of explaining the presence of the $S=9/2$ signal for the six-iron cluster in the resting state of the protein, where four of the iron atoms have just been shown to be diamagnetic. The explanation of this apparent paradox lies in the wings of the spectra shown in Fig. 13A and B. Two of the iron atoms ($1/3$ total intensity) are almost invisible due to the presence of large internal magnetic fields. At 5 T applied magnetic field, the sizes of the induced magnetic fields along the non-easy axes (the perpendicular axes) for this ground state are nearly the size of the 'easy' axis (body-frame z -axis) fields. The electron Zeeman splittings at 5 T are such that the ground state changes its identity with the relative orientation of the protein in the magnetic field. In other words, the Zeeman splitting is sometimes larger than the zero-field splitting depending on field orientation. However, at all orientations the ground state has a large magnetic moment. Therefore, we attribute the lack of electron-spin moment (and magnetic splitting in the Mössbauer spectrum) of four of

ons to very small spin-projection operators ($S_1 \cdot S/S \cdot S$). It also possible that this small moment is due to an asymmetric large distribution over the six-iron cluster such that the spin density is very small over the four near-diamagnetic iron atoms. However, the latter hypothesis is hard to rationalize against the shape of Fig. 13C and the isomer-shift change for the four near-diamagnetic irons that accompanies chemical reduction of the protein (Table 3).

Spin coupling model for the $S = 9/2$ state

In its dithionite-reduced form, the protein has the EPR signal that is thought to be a signature for the 3+ prismane form. Four of the six-iron atoms in the protein mimic the Mössbauer properties of the thiol-prismane very well. Two of the iron atoms seem to be more ionic than those in the thiol-prismane. One structure that would have all of the spectroscopic properties of the protein would be a prismane where four of the six exogenous ligands are thiols and two are more ionic. These two ligands would be located at opposite ends of the prismane so that the other four irons are at geometrically equivalent positions as required by Fig. 13A. The most surprising aspect of this explanation for the spectroscopy is the apparent diamagnetism in the four irons at low temperature (Fig. 13A and B). On the other hand, it is perhaps more surprising that most cubanes and prismanes have demonstrated the property of distributed charge in having equal isomer shifts for their iron atoms while simultaneously demonstrating localized spin by giving large, non-equivalent internal fields. In this protein, we could be seeing for the first time a situation where the ground-state molecular-orbital averages both charge and spin over these four iron atoms.

The computer fit in Fig. 13A gave the best fit for an applied field that is 3% lower than the actual applied magnetic field. This discrepancy is almost an order of magnitude greater than our uncertainty in this measurement. Therefore, the diamagnetic four irons are not diamagnetic when inspected closely, but instead have an extremely low electron-magnetic moment. If we assume that the two high-spin ferrous atoms in the dithionite-reduced center are high-spin ferric atoms in the 5+ center, then it is possible to create an $S = 9/2$ total spin by coupling two $S = 5/2$ ferric atoms with an $S = 1/2$, $3/2$ or $5/2$ effective spin from the ground-state molecular orbital of the near-diamagnetic four iron atoms while maintaining the requirement that these irons have a very small magnetic moment (Fig. 14).

For all three possible combinations of spin vectors in Fig. 14, the ferric ($S = 5/2$) spin vectors have spin-projection operators close to $1/2$. The sum of all spin-projection operators in any spin-coupling scheme is one. We have already hypothesized that the four diamagnetic irons have spin-projection operators near zero. Therefore, if the two ferric irons in the resting enzyme are high-spin ferric ions, they must have spin-projection operators near $1/2$. In Fig. 14, we show a geometrical argument that forces the same conclusion. The geometrical diagram is quantum-mechanically rigorous under the assumptions given in the figure caption. If we further assume that the ionic iron atoms have A values near the ionic limit, 2.2 mT/electron, then we can estimate the shape of their Mössbauer spectra at 4.2 K and 0.04 T applied magnetic field using the EPR data. (The EPR resonance field for the $g \approx 18$ signal at X-band is near 0.04 T.) At 4.2 K, 89% of the spin population is in the $|\pm 9/2\rangle$ Kramers doublet with g values approximately 0, 0 and 18 (Table 1). These g values describe a situation where the electronic spin moment, and

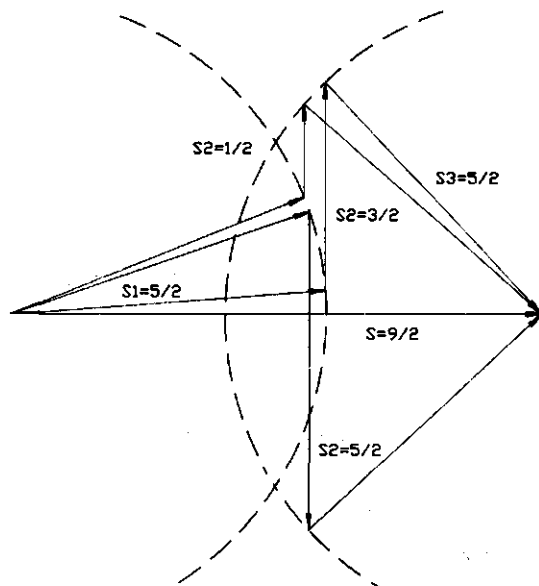


Fig. 14. Hypothetical spin-coupling schemes to obtain $S = 9/2$. The schemes show conservation of momentum constraints on a model where one high-spin ferric ion (S_1), one four-iron cluster (S_2) and one high-spin ferric ion (S_3) are coupled to form a resultant (S), where $S = 9/2$. The vectors are proportional to the magnitudes of the electron-spin moments assuming that the g values of all the components and the resultant are equal; therefore, $S = S_1 + S_2 + S_3$ describes a conservation of energy constraint as well as a type of coupling of angular momenta. S_2 is perpendicular to S , as required by the Mössbauer spectroscopic results. The schemes are drawn from two circles of radius equal to $\sqrt{(35/4)}$ (---) and vector of length $|S_2|$ drawn perpendicular to the resultant. The spin projection operators, $S_i \cdot S/S \cdot S$, for $i = 1, 2, 3$ for the three diagrams are for $S_2 = 1/2, 0.55, 0.00, 0.45$, for $S_2 = 3/2, 0.59, 0.00, 0.41$, and for $S_2 = 5/2, 0.56, 0.00, 0.44$.

therefore the nuclear spin moment, are precessing around the z -axis of a coordinate system fixed with respect to the protein regardless of the orientation of the 0.04-T applied magnetic field. The Mössbauer spectrum is six lines of intensity: 3:2:1:1:2:3. With the above assumptions, the internal field at the ferric irons should be 50 T and give a six-line pattern with a 16-mm/s range.

On the other hand, the Mössbauer spectrum of the two ferric atoms has some complexities above the simple explanation given above. A high-spin ferric atom usually has a magnetic hyperfine interaction that is large (negative) and isotropic and a quadrupole spectrum that is small and rhombic, therefore the nuclear Hamiltonian would seem to be dominated by the magnetic interaction and therefore be a simple pattern. In fact, the electronic Hamiltonian for the $|\pm 9/2\rangle$ Kramers doublet cannot be separated from the nuclear Hamiltonian at low applied magnetic fields. Simulations show that, as the applied magnetic field is increased from the Earth's magnetic field (0.06 mT in our laboratory) to a few tenths of a millitesla, the Mössbauer spectrum changes from an asymmetric four-line pattern to a very symmetric six-line pattern. The g tensor has diagonal values of 0, 0 and 18 (assuming that the $g \approx 18$ signal corresponds to the body-frame z -axis), therefore the electron Zeeman interaction for

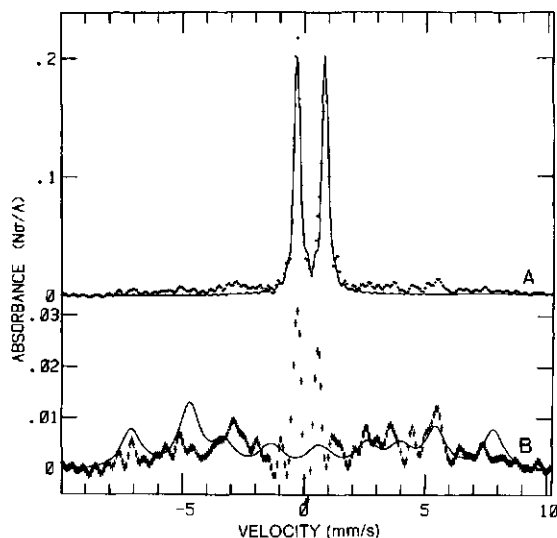


Fig. 15. Low temperature, low-applied-magnetic-field spectra of the isolated prismatic protein. (A) The experimental data at 4.2 K and 0.04 T applied magnetic field superimposed (—) by a single-site model for the four diamagnetic irons (parameters in Table 3); (B) the difference of the spectra in (A) superimposed by the simulation of the two ferric sites (parameters in Table 3). Note the importance of our data reduction methods to the quantitation of these spectra.

various powder orientations is non-zero only to the extent that the body-frame z -axis is along the applied field. When the applied field component along the body-frame z -axis is larger than 2 mT, then the Hamiltonian is so dominated by the electronic terms that only the nuclear terms along this z -axis have an appreciable effect on the spectrum. An example of these effects is given in Appendix. For the orientations where the electronic terms are dominant, the spectra are six-line patterns where only A_z and V_{zz} alter the spectra significantly.

If the applied magnetic field is 0.04 T, then the electronic terms dominate the Hamiltonian in 99% of the body orientations. At 4.2 K, the maximum electronic Zeeman splitting is 0.3 cm^{-1} , so one can ignore the effects of Boltzmann populations at this field other than to realize that 89% of the spin systems are in the $|\pm 9/2\rangle$ Kramers doublet. One should therefore expect a superimposition of two six-line patterns to account for the experimental spectra, with the spectra from the other Kramers doublets making small contributions. Fig. 15B shows the difference spectrum obtained after the subtraction of the diamagnetic four iron atoms previously discussed (Fig. 15A). These four irons are not quite perfectly modelled by the single environment shown in Table 3; therefore, there are two spikes in the center of the spectrum. The difference spectrum has almost exactly the area of two iron equivalents as does the simulation (parameters in Table 3). The simulation has two iron environments, both with large negative A (-11 and -7.3 mm/s) and both with small isomer shifts (0.2 mm/s) and small quadrupole splittings (0.7 mm/s) as expected for high-spin ferric ions. The A difference can be attributed to a difference in the sites, seen in the quadrupole pairs of the ferrous irons in the reduced protein, or to difference in the spin-projection operators. There is no way to separate these

Table 4. Calculated internal magnetic fields (A values) for various spin-coupling models.

S_2	S_1	S_3	
		T (mm/s)	
1/2	-42 (-9.9)	-34 (-8.0)	
3/2	-45 (-10.7)	-31 (-7.3)	
5/2	-43 (-10.2)	-34 (-8.0)	

effects experimentally. By scaling the ionic-limit A values form a best fit to the measured values, we calculate the values in Table 4 (S_2 denotes the spin from four diamagnetic iron atoms). The fit for $S_2 = 3/2$ is exact, but possibly fortuitous because A values for high spin ferric ions in biology can easily vary by 10%.

The computer simulation in Fig. 15 also necessitated an extremely large line width. The only parameter that seemed capable of generating this kind of line-width broadening V_{zz} , therefore we have concluded that either the quadrupole splitting (unlikely) or the direction of the g tensor relative to the quadrupole tensor is distributed for this spin system in the as isolated ($5+$) protein. We have seen heterogeneity in the Mössbauer (Fig. 11B) and EPR (Fig. 1B) spectra of the reduced protein. This may carry over to the as isolated $5+$ state as indicated by the observation of two rhombicities in the $S = 9/2$ EPR. We have not attempted to include heterogeneity in the simulation of Fig. 15. With the above qualifications, we claim that the fit in Fig. 15B accounts for the last two iron in the sample, proves the origin of the coupling to form the $S = 9/2$ multiplet and is an example of a new and unique type of Mössbauer spectrum: that of a widely anisotropic electron spin system in a weak applied magnetic field.

Concluding remarks

In Results and Discussion, we have presented an explanation for many of the spectroscopic properties of the putative prismatic protein at least with respect to EPR and Mössbauer spectroscopies. We now review our conclusions to emphasize their constraints on possible structures for the novel metal cluster of this protein. The emerging picture is a six-iron cluster, where two of the iron atoms are charge-localized (similar to those in a $[2\text{Fe-2S}]$ cluster) and four are similar to those in a $[6\text{Fe-6S}]$ prismatic model cluster. The redox chemistry of the novel cluster is centered about the two ionic irons, but also involves the other four irons. The spin coupling of the $5+$ state gives rise to an $S = 9/2$ ground state with the $|\pm 9/2\rangle$ doublet lowest at low applied magnetic fields. The coupling depends on a ferromagnetic coupling of the two iron atoms. Accordingly, these iron atoms are expected to be separated by the other four-iron atoms to allow the ferromagnetic coupling. A mixed-ligand prismatic, where the ionic irons are at opposite ends of the prismatic with exogenous high Lewis-base ligands (nitrogen or oxygen), has these properties. It is an attractive possibility to identify these ligands with nitrogen ligation that was implicated by multi-frequency EPR from the $S = 1/2$ minor species with all values of $g < 2$. However, any other arrangement compatible with the above constraints would be equally valid.

The unusually high system spin $S = 9/2$ has thus far been tentatively identified in three iron-sulfur enzymes: d

military sulfite reductase [6], carbon-monoxide dehydrogenase [8] and the FeMo-protein of nitrogenase [5]. Several synthetic iron cluster compounds with $S = 9/2$ ground states have also recently been described [34–36]. However, in these models the bridging is $(\mu\text{-OR})_2$ or $(\mu\text{-OH})_3$. Also, their Mössbauer properties are quite distinct from those of the $S = 9/2$ system reported here [35, 36]. Very recently, an $S = 9/2$ protein from *D. desulfuricans* (ATCC 27774), with hydrodynamic and EPR properties comparable to our *D. vulgaris* prismane protein (this paper) [5, 9, 11]), has been briefly described [37]. It is presently not clear how (dis)similar the two proteins are: the Mössbauer data, the redox properties and the metal analysis of the *D. desulfuricans* protein [37] appear to be rather different from those presented here.

We propose that the *D. vulgaris* monomeric prismane protein is a suitable model for the complex iron-sulfur redox enzymes, not only because it carries an iron-sulfur supercluster with associated superspin, but also because this cluster is capable of accepting more than one reducing equivalent within a physiologically relevant potential range. Our ongoing research efforts are presently focussed at obtaining primary and tertiary structural information on this remarkable protein.

APPENDIX

To initiate the calculation, we assume that the zero-field Hamiltonian, $H = D_e[S_z^2 - S(S+1)/3] + E_e(S_x^2 - S_y^2)$, has created the zero-order situation where the electronic ground state is an $m_s = \pm 9/2$ Kramers doublet. It is also assumed that this is the only occupied electronic state and that coupling to all other states can be ignored. The assumptions are consistent with the measured value of $D_e \approx -0.86 \text{ cm}^{-1}$ by EPR. The Kramers doublet has $g \approx 0, 0$ and 18 (for an effective spin one-half), indicating that the electronic spin is precessing around the z -axis of the body-frame exclusively. The Hamiltonian for the combined electronic nuclear transitions

$$H = g\beta_e B_{\text{app}} \cdot \cos\Theta \cdot m_s + A_{xx}I_x S_x + A_{yy}I_y S_y + A_{zz}I_z S_z + 2DI_x^2 + (E-D)I_x^2 + (-E-D)I_y^2, \quad (\text{A1})$$

where $\Delta E_q = 6D(1+\eta^2/3)$, $E = \eta D$, and Θ is the angle between the applied field, B_{app} , and the z -axis of the body coordinate system. If we write the Hamiltonian in the product basis set, $|m_I m_S\rangle$, then the nuclear ground state ($I = 1/2$) matrix is

	$ +1/2, +1/2\rangle$	$ +1/2, -1/2\rangle$	$ -1/2, +1/2\rangle$	$ -1/2, -1/2\rangle$
$\langle +1/2, +1/2 $	$A_x/4 + \alpha/2$	0	0	$A_x/4 - A_y/4$
$\langle +1/2, -1/2 $	0	$-A_x/4 - \alpha/2$	$A_x/4 + A_y/4$	0
$\langle -1/2, +1/2 $	0	$A_x/4 + A_y/4$	$-A_x/4 + \alpha/2$	0
$\langle -1/2, -1/2 $	$A_x/4 - A_y/4$	0	0	$A_x/4 - \alpha/2$

(A2)

where $\alpha = g\beta_e B_{\text{app}} \cdot \cos\Theta$. The corresponding matrix can be solved trigonometrically as

$$\begin{aligned} \Psi_{1,2} &= -(A_x/4) \pm (\alpha/2) \cos(2\Theta_1) \mp [(A_x + A_y)/4] \sin(2\Theta_1), \\ \Psi_1 &= -\sin\Theta_1 | +1/2, -1/2 \rangle + \cos\Theta_1 | -1/2, +1/2 \rangle, \\ \Psi_2 &= +\cos\Theta_1 | +1/2, -1/2 \rangle + \sin\Theta_1 | -1/2, +1/2 \rangle, \end{aligned} \quad (\text{A3})$$

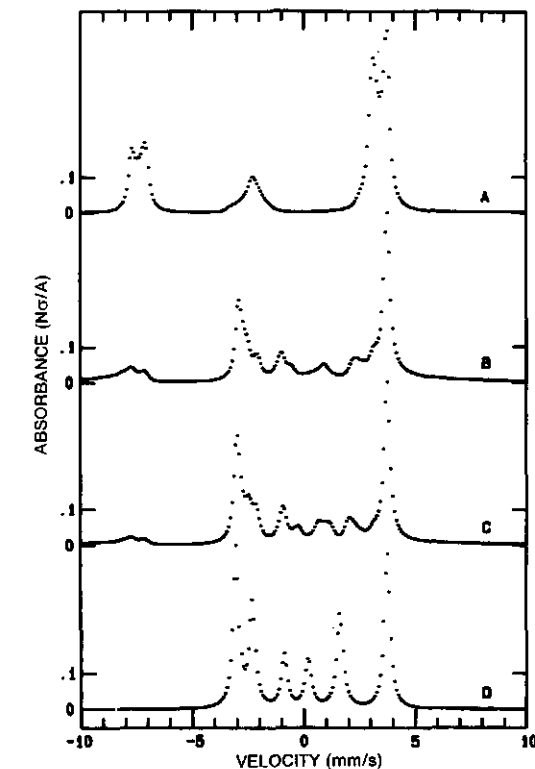


Fig. 16. Computer synthesized spectra of an $S = 9/2$ system at different but small applied magnetic fields. With $\Delta E_q = 0.7 \text{ mm/s}$, $\eta = 0$ and $A_x = A_y = A_z = -5 \text{ mm/s}$, the spectra show the effect of an increasing magnetic field. The applied field is 0 (A), 0.5 mT (B), 1 mT (C) and 40 mT (D).

where $\tan(2\Theta_1) = (A_x + A_y)/(-2\alpha)$, and

$$\begin{aligned} E_{3,4} &= (A_x/4) \pm (\alpha/2) \cos(2\Theta_2) \pm [(A_x - A_y)/4] \cos(2\Theta_2), \\ \Psi_3 &= +\cos\Theta_2 | +1/2, +1/2 \rangle + \sin\Theta_2 | -1/2, -1/2 \rangle, \\ \Psi_4 &= -\sin\Theta_2 | +1/2, +1/2 \rangle + \cos\Theta_2 | -1/2, -1/2 \rangle, \end{aligned} \quad (\text{A4})$$

where $\tan(2\Theta_2) = (A_x - A_y)/(2\alpha)$.

The excited nuclear state ($I = 3/2$) forms an 8×8 matrix with the effective $S = 1/2$ spin system. This matrix blocks into two 4×4 matrices as follows:

	$ +3/2, +1/2\rangle$	$ +1/2, -1/2\rangle$	$ -1/2, +1/2\rangle$	$ -3/2, -1/2\rangle$
$\langle +3/2, +1/2 $	$3A_z/4 + 3D + \alpha/2$	$\sqrt{3}(A_x - A_y)/4$	$\sqrt{3}E$	0
$\langle +1/2, -1/2 $	$\sqrt{3}(A_x - A_y)/4$	$-A_z/4 - 3D - \alpha/2$	$(A_x + A_y)/2$	$\sqrt{3}E$
$\langle -1/2, +1/2 $	$\sqrt{3}E$	$(A_x + A_y)/2$	$-A_z/4 - 3D + \alpha/2$	$\sqrt{3}(A_x - A_y)/4$
$\langle -3/2, -1/2 $	0	$\sqrt{3}E$	$\sqrt{3}(A_x - A_y)/4$	$3A_z/4 + 3D - \alpha/2$

and

	$ +3/2, -1/2\rangle$	$ +1/2, -1/2\rangle$	$ -1/2, -1/2\rangle$	$ -3/2, +1/2\rangle$
$\langle +3/2, -1/2 $	$3A_z/4 + 3D - \alpha/2$	$\sqrt{3}(A_x - A_y)/4$	$\sqrt{3}E$	0
$\langle +1/2, +1/2 $	$\sqrt{3}(A_x - A_y)/4$	$-A_z/4 - 3D + \alpha/2$	$(A_x + A_y)/2$	$\sqrt{3}E$
$\langle -1/2, -1/2 $	$\sqrt{3}E$	$(A_x + A_y)/2$	$-A_z/4 - 3D - \alpha/2$	$\sqrt{3}(A_x - A_y)/4$
$\langle -3/2, +1/2 $	0	$\sqrt{3}E$	$\sqrt{3}(A_x - A_y)/4$	$3A_z/4 + 3D + \alpha/2$

Transition intensities are calculated as in Kundig [38] except that $\Delta m_S = 0$ and the transition dipole operator can be integrated over its azimuth angle (the angle around the propagation vector), but it cannot be integrated over its polar angle because the terms in the Hamiltonian matrices that contain α are not independent of this angle. They depend on Θ ($\alpha = g\beta_e B_{pp} \cdot \cos \Theta$), which happens to be equal to the polar angle because the propagation vector of the radiation field is parallel to the applied-magnetic-field direction. Therefore, the transition intensities containing I_+ and I_- have a factor $(1 + \cos^2 \Theta)/2$ while the intensities containing I_z have a factor $\sin^2 \Theta$. The integration over the angle, Θ , is performed explicitly by incrementing $\cos \Theta$ as described in [39]. An example of the output of this program for increasing values of the applied magnetic field is shown in Fig. 16. When only the Earth's magnetic field is present on the sample (Fig. 16A), the spectrum exemplifies the situation where the nuclear and electronic spins are coupled to form a resultant. This situation is common in paramagnetic proteins [23]. When the electron Zeeman term is much greater than the magnetic hyperfine term (Fig. 16D), the spectrum exemplifies those with a strong magnetic field oriented in body frame [38]. This situation is much different from that encountered in most paramagnetic proteins where the internal magnetic field is oriented along the applied magnetic field.

In the case described here the direction of the internal field (spatial quantization) is determined completely by the zero-field splitting term in creating the effective g tensor with only one non-zero component in its principal-axis (diagonal) representation. It is important to realize that this kind of spatial quantization is usually overlooked by theoreticians because of Kramers theorem: there is a degeneracy in half-integer spin systems (time reversal symmetry) that cannot be removed by zero-field splitting terms. The proof of Kramers theorem seems to prevent spatial quantization. However, we believe that the kind of spatial quantization described here can be generalized to lattice structures, providing both the very large g values and the magnetic anisotropy necessary as a basis for the understanding of hard and soft ferromagnetism.

We are grateful to R. B. G. Wolbert for help in preparing the proteins used in this work. We thank Professor C. Veeger for his

continuing interest and support. Dr. S. P. J. Albracht has kindly provided us access to the parallel-mode and multi-frequency EPR facility at the Department of Biochemistry, The University of Amsterdam. We thank Drs C. Hess-Riechmann and K. Schneider at the University of Bielefeld for the ICP-MS determinations. The iron-sulfur model compounds, referred to in Table 4, were prepared by Professor D. Coucouvanis and his collaborators at The University of Michigan. This investigation was supported by the Netherlands Foundation for Chemical Research (SON) with financial aid from the Netherlands Organization for Scientific Research (NWO) and by the National Institutes of Health (Grant GM-32785 to RHS).

REFERENCES

- Hagen, W. R., van Berkel-Arts, A., Krüse-Wolters, K. M., Dunham, W. R. & Veeger, C. (1986) *FEBS Lett.* **201**, 158-162.
- Hagen, W. R., van Berkel-Arts, A., Krüse-Wolters, K. M., Voordouw, G. & Veeger, C. (1986) *FEBS Lett.* **203**, 59-63.
- Voordouw, G., Hagen, W. R., Krüse-Wolters, K. M., van Berkel-Arts, A. & Veeger, C. (1987) *Eur. J. Biochem.* **162**, 31-36.
- Hagen, W. R., Wassink, H., Eady, R. R., Smith, B. E. & Haaker, H. (1987) *Eur. J. Biochem.* **169**, 457-465.
- Hagen, W. R., Pierik, A. J., Wolbert, R. B. G., Wassink, H., Haaker, H., Veeger, C., Jetten, M. S. M., Stams, A. J. M., Zehnder, A. J. B. (1991) *J. Inorg. Biochem.* **43**, 237.
- Pierik, A. J. & Hagen, W. R. (1991) *Eur. J. Biochem.* **195**, 505-515.
- Jetten, M. S. M., Hagen, W. R., Pierik, A. J., Stams, A. J. M., Zehnder, A. J. B. (1991) *Eur. J. Biochem.* **195**, 385-395.
- Jetten, M. S. M., Pierik, A. J. & Hagen, W. R. (1991) *Eur. J. Biochem.* **202**, 1291-1297.
- Hagen, W. R., Pierik, A. J. & Veeger, C. (1990) *Ital. Biochem. Soc. Trans.* **1**, 85.
- Pierik, A. J., Wolbert, R. B. G., Mutsaers, P. H. A., Hagen, W. R. & Veeger, C. (1992) *Eur. J. Biochem.* **206**, 697-704.
- Hagen, W. R., Pierik, A. J. & Veeger, C. (1989) *J. Chem. Soc. Faraday Trans. 1*, **85**, 4083-4090.
- Hagen, W. R. (1982) *Biochim. Biophys. Acta* **708**, 82-98.
- Albracht, S. P. J. (1973) *J. Magn. Reson.* **13**, 299-303.
- Stevenson, R. C. (1982) *Triplet state EPR: an application three iron-sulfur flavoproteins*, Ph. D. thesis, The University of Michigan.
- Dunham, W. R., Wu, C. T., Polichar, R. M., Sands, R. H., Harding, L. J. (1977) *Nucl. Instrum. Methods* **145**, 537-553.

6. Filter, W. F. (1983) *High-resolution ^{57}Fe Mössbauer spectroscopy*, Ph. D. thesis, The University of Michigan.
7. Dunham, W. R., Hagen, W. R., Braaksma, A., Grande, H. J. & Haaker, H. (1985) *Eur. J. Biochem.* **146**, 497–501.
8. Dunham, W. R., Carroll, R. T., Thompson, J. F., Sands, R. H. & Funk, M. O. (1990) *Eur. J. Biochem.* **190**, 611–617.
9. Kanatzidis, M. G., Hagen, W. R., Dunham, W. R., Lester, R. K. & Coucouvanis, D. (1985) *J. Am. Chem. Soc.* **107**, 953–961.
10. Hagen, W. R. (1989) in *Advanced EPR: applications in biology and biochemistry* (Hoff, A. J., ed.), pp. 785–812, Elsevier, Amsterdam.
11. Dunham, W. R., Fee, J. A., Harding, L. J. & Grande, H. J. (1980) *J. Magn. Reson.* **40**, 351–359.
12. Tsubris, J. C. M., Tsai, R. L., Gunsalus, I. C., Orme-Johnson, W. H., Hansen, R. E. & Beinert, H. (1968) *Proc. Natl Acad. Sci. USA* **59**, 959–965.
13. Sands, R. H. & Dunham, W. R. (1975) *Quart. Rev. Biophys.* **7**, 443–504.
14. Anderson, R. E., Anger, G., Petersson, L., Ehrenberg, A., Cammack, R., Hall, D. O., Mullinger, R. & Rao, K. K. (1975) *Biochim. Biophys. Acta* **376**, 63–71.
15. Hagen, W. R. & Albracht, S. P. J. (1982) *Biochim. Biophys. Acta* **702**, 61–71.
16. Aasa, R. & Vänngård, T. (1975) *J. Magn. Reson.* **19**, 308–315.
17. Hagen, W. R., Eady, R. R., Dunham, W. R. & Haaker, H. (1985) *FEBS Lett.* **189**, 250–254.
18. Morgan, T. V., Prince, R. C. & Mortenson, L. E. (1986) *FEBS Lett.* **206**, 4–6.
19. Meyer, J., Gaillard, J. & Moulis, J.-M. (1988) *Biochemistry* **27**, 6150–6156.
20. Hagen, W. R., Dunham, W. R., Sands, R. H., Shaw, R. W. & Beinert, H. (1984) *Biochim. Biophys. Acta* **765**, 399–402.
21. Hagen, W. R., Dunham, W. R., Johnson, M. K. & Fee, J. A. (1985) *Biochim. Biophys. Acta* **828**, 369–374.
22. Kanatzidis, M. G., Dunham, W. R., Hagen, W. R. & Coucouvanis, D. (1984) *J. Chem. Soc. Chem. Commun.* **1984**, 356–358.
23. Coucouvanis, D., Kanatzidis, M. G., Dunham, W. R. & Hagen, W. R. (1984) *J. Am. Chem. Soc.* **106**, 7998–7999.
24. Snyder, B. S., Patterson, G. S., Abrahamson, A. J. & Holm, R. H. (1989) *J. Am. Chem. Soc.* **111**, 5214–5223.
25. Surerus, K. K., Münck, E., Snyder, B. S. & Holm, R. H. (1989) *J. Am. Chem. Soc.* **111**, 5501–5502.
26. Ding, X.-Q., Bominaar, E. L., Bill, E., Winkler, H. & Trautwein, A. X. (1990) *J. Chem. Phys.* **92**, 178–186.
27. Ravi, N., Moura, I., Tavares, P., LeGall, J., Huynh, B. H. & Moura, J. J. G. (1991) *J. Inorg. Biochem.* **43**, 252.
28. Kundig, W. (1967) *Nucl. Instrum. Methods* **48**, 219–228.
29. Hagen, W. R., Hearshen, D. O., Harding, L. J. & Dunham, W. R. (1985) *J. Magn. Reson.* **61**, 233–244.

Chapter 6

The third subunit of desulfovirdin-type dissimilatory sulfite reductases.

Antonio J. Pierik, Martina G. Duyvis, Joop M.L.M. van Helvoort, Ronnie B.G. Wolbert and Wilfred R. Hagen

(1992) *Eur. J. Biochem.* 205, 111-115.

The third subunit of desulfoviridin-type dissimilatory sulfite reductases

Antonio J. PIERIK, Martina G. DUYVIS, Joop M. L. M. van HELVOORT, Ronnie B. G. WOLBERT and Wilfred R. HAGEN
Department of Biochemistry, Agricultural University, Wageningen, The Netherlands

Received October 25, 1991) – EJB 91 1438

In addition to the 50-kDa (α) and 40-kDa (β) subunits, an 11-kDa polypeptide has been discovered in highly purified *Desulfovibrio vulgaris* (Hildenborough) dissimilatory sulfite reductase. This is in contrast with the hitherto generally accepted $\alpha_2\beta_2$ tetrameric subunit composition. Purification, high-ionic-strength gel-filtration, native electrophoresis and isoelectric focussing do not result in dissociation of the 11-kDa polypeptide from the complex. Densitometric scanning of SDS gels and denaturing gel-filtration indicate a stoichiometric occurrence. A similar 11-kDa polypeptide is present in the desulfoviridin of *D. vulgaris oxamicus* (Monticello), *D. gigas* and *D. desulfuricans* ATCC 27774. We attribute an $\alpha_2\beta_2\gamma_2$ subunit structure to desulfoviridin-type sulfite reductases. N-terminal sequences of the α , β and γ subunits are reported.

A key enzyme in dissimilatory sulfate reduction is sulfite reductase, a complex redox enzyme containing both Fe/S and heme prosthetic groups. Sulfite reductases that are supposed to have a dissimilatory function have been observed in, and isolated from, over 20 species of microorganisms [1–4]. Kinetic parameters and subunit structure of dissimilatory sulfite reductases are markedly different from assimilatory sulfite reductases.

Dissimilatory enzymes are $\alpha_2\beta_2$ proteins (150–230 kDa) that have a millimolar K_m for sulfite, a slightly acidic pH optimum and reduce their substrate to $S_3O_6^{2-}$ and $S_2O_3^{2-}$ [1, 5–8]. The physiological relevance of the *in vitro* observed product composition is a matter of controversy. A number of explanations has been put forward: loss of interaction with the cytoplasmic membrane [9], *in vitro* assay conditions [10], and the possibility that the observed products are *in vivo* intermediates [11]. Partial demetallation of the siroheme is observed in desulfoviridins [2, 12] and is presumably an intrinsic feature of some dissimilatory enzymes. It probably has to do with the formation of $S_3O_6^{2-}$ and $S_2O_3^{2-}$ since desulfoviridin, desulfofuscidin, P582 and desulforubidin-type dissimilatory enzymes have a comparable product composition and specific activity [2–7, 13].

Contrarily, assimilatory sulfite reductases cleanly perform the full six-electron reduction to sulfide. They have a slightly basic pH optimum with a submillimolar K_m for sulfite. The subunit composition, however, is non-uniform: $\alpha_6\beta_4$ [14], α_4-6 [5], or α_2 [16]. This probably reflects differences in the source of reducing equivalents.

A distinct, third, group of sulfite reductases comprises the so-called low-molecular-mass sulfite reductases. These enzymes are presumably assimilatory. They differ from the other two groups in two aspects: they are monomeric (20–30 kDa),

and siroheme iron (III) is fully low spin in the enzyme as isolated [5, 17, 18]. Comparison of the sequences of the low-molecular-mass assimilatory sulfite reductase from *Desulfovibrio vulgaris* (Hildenborough) [19] and the oligomeric assimilatory sulfite reductases from *Escherichia coli* and *Salmonella typhimurium* [20] revealed no significant similarity. Further comparison of primary structures has to await sequencing of dissimilatory enzymes.

We report here that *D. vulgaris* (Hildenborough) desulfoviridin contains a small, hitherto unnoted, γ -subunit in addition to the usual $\alpha_2\beta_2$ motive of dissimilatory enzymes. N-terminal sequences, size and stoichiometry of the subunits have been determined. An immunological comparison of desulfoviridins, the *E. coli* assimilatory enzyme and the low-molecular-mass sulfite reductase of *D. vulgaris* is also presented.

MATERIALS AND METHODS

Growth and purification

Stab-cultures of *Desulfovibrio* were maintained in 10-ml soft-agar tubes [21]. For the isolation of cells, 1-l serum bottles with Saunders medium N [22] were inoculated with 1–2 ml stab culture. Desulfoviridins were purified according to Pierik and Hagen [12]. The electrophoretic 'fast' and 'slow' forms (cf. [23]) of the *D. vulgaris* (Hildenborough) enzyme were separated on a MonoQ HR 5/5 anion-exchange column attached to a Pharmacia FPLC system. A shallow gradient of NaCl in 20 mM Tris/HCl pH 8.0 eluted a major species at ≈ 370 mM NaCl (fast-moving on native gels, $pI \approx 4.5$) and a minor species at ≈ 400 mM NaCl (slow-moving, $pI \approx 4.7$). Rechromatography, a freeze-thaw cycle, and a 48-h incubation at 4°C did not alter the characteristics of the isolated 'fast' or 'slow' form. Experiments with purified desulfoviridin were performed with the 'fast' form (production of antibodies, N-terminal sequences, Figs 1–3 and 5). Purification of the 26-kDa low-molecular-mass assimilatory sulfite reductase

Correspondence to W. R. Hagen, Laboratorium voor Biochemie, Wageningen Universiteit, Dreijenlaan 3, NL-6703 HA Wageningen, The Netherlands

Enzyme. Desulfoviridin or dissimilatory sulfite reductase (EC 1.1.99.1).

from *D. vulgaris* (Hildenborough) and the *E. coli* C600 sulfite reductase holoenzyme closely followed the procedures of Huynh et al. [18] and Siegel and Davis, respectively [14].

Electrophoresis

Polyacrylamide electrophoresis was performed either with a home-built set-up that holds $150 \times 150 \times 1.5$ mm gels or with a Midget system (Pharmacia) holding $8 \times 5 \times 0.75$ mm gels. SDS/polyacrylamide gels according to Laemmli [24] had a 4% T, 2.5% C stacking and a 17.5% T, 0.4% C separating gel. For native electrophoresis SDS was omitted and a 7.5% T, 2.3% C separating gel was used. Desulfovirodin was extracted from excised pieces of the native gel by diffusion. Tricine-buffered gels [25] used a 4% T, 3% C stacking and a 16.5% T, 3% C separating gel. Isoelectric focussing was carried out with Servalyte precoted pI 3–10 gels on a flat-bed Pharmacia Ultraphor electrophoresis unit (4°C). For two-dimensional electrophoresis a single lane of an isoelectric focussing gel was excised and covered with a few drops of SDS-containing sample buffer. After a 5-min room-temperature incubation, the strip was applied onto a denaturing gel. Molecular mass markers were obtained from Pharmacia (14–94-kDa kit and CNBr fragments of horse heart myoglobin). The molecular mass assignment by Kratzin et al. [26] was used for the latter marker mixture.

Antibodies and immunoblotting

The subunits of homogeneous preparations of desulfovirodin and 26-kDa assimilatory sulfite reductase of *D. vulgaris* (Hildenborough) were isolated from $300 \times 150 \times 1.5$ mm Laemmli gels by electroelution. To avoid contamination of the desulfovirodin α -subunit by trailing of the β -subunit, the procedure of electrophoresis and electro-elution was repeated for the α -subunit. The polypeptides purified by this procedure exhibited single bands with a mobility identical to the respective polypeptides present in the preparations before separation and electro-elution.

Antibodies against the SDS-denatured desulfovirodin subunits were induced in mice by subcutaneous injection of two 10- μ g quantities mixed with Freund's complete adjuvant. Antibodies against the SDS-denatured 26-kDa assimilatory sulfite reductase polypeptide were raised in rabbits (100 μ g/injection). Boosts of antigen mixed with Freund's incomplete adjuvant were administered at three-weekly intervals. Sera were used without further purification.

Proteins separated on denaturing Laemmli gels were blotted onto a nitrocellulose support [27]. Goat anti-mouse or anti-rabbit IgG alkaline phosphatase conjugate (Bio-Rad, Richmond, USA and Promega Biotec, Madison, USA, respectively) were used for immunostaining.

N-terminal sequencing

The contents of a $150 \times 150 \times 1.5$ mm Tricine gel [25] loaded with 300 μ g desulfovirodin were blotted onto a polyvinylidene difluoride Immobilon-P support (Millipore). After localization of the subunits by Coomassie R-250 staining, the relevant sections of the blot were excised. Gas-phase sequencing of the polypeptides on the Immobilon support was carried out by the sequencing facility of the Netherlands Foundation for Chemical Research (SON), Leiden.

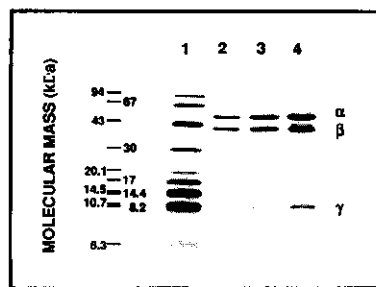


Fig. 1. SDS/PAGE of purified *D. vulgaris* (Hildenborough) desulfovirodin. Lane 1, molecular mass marker mixture; lanes 2–4, 2, 10, and 100 μ g of desulfovirodin, respectively. A Tricine-buffered gel was used [25].

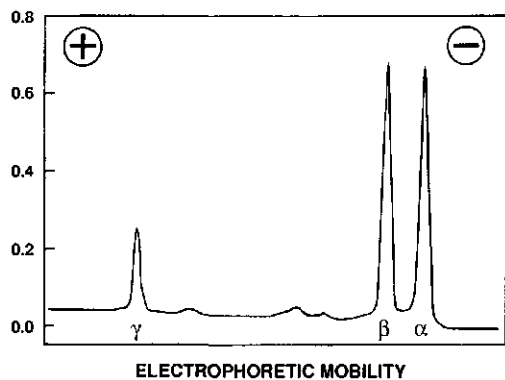
RESULTS AND DISCUSSION

The subunits

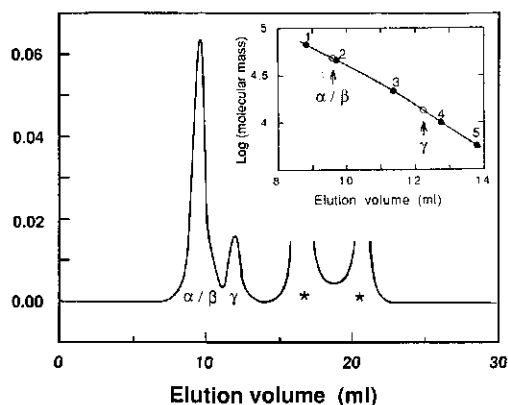
The extent of purification of desulfovirodins is routinely monitored by ultraviolet/visible spectroscopy. This saves time and avoids enzyme-consuming manometric sulfite-dependent hydrogen uptake measurements. Instead of maximization of the specific activity, minimization of the ratio of 280-nm protein absorbance over 628-nm siroporphyrin absorbance is the direct goal of a purification procedure [2, 6, 12, 23, 28, 29]. Similar purity indices, using a different wavelength for the visible absorbance, are routinely employed to follow the purification of ferredoxins, cytochromes and hydrogenases. The major drawback, especially in the case of desulfovirodin, is that the redox state, demetallation, low-spin/high-spin equilibrium and bound substrate or product may influence the purity index. Purity assessment by SDS/PAGE should accompany minimalization of the A_{280}/A_{628} index.

We noted that desulfovirodin preparations of *D. vulgaris* (Hildenborough) with a high purity index A_{280}/A_{628} (4.1–4.5) contained a Coomassie-stainable band with a mobility corresponding to a molecular mass of ≈ 11 kDa in addition to the usual 50-kDa (α) and 40-kDa (β) polypeptides (Fig. 1). The 11-kDa band was not due to the highly charged, fluorescent siroporphyrin, which moved ahead of the bromophenol blue front.

We tried to remove the 11-kDa polypeptide by five techniques: (a) gel filtration in the presence of 1 M KCl; (b) repeated FPLC anion-exchange chromatography; (c) isoelectric focussing; (d) native electrophoresis; (e) two-dimensional electrophoresis. In all cases, the desulfovirodin-containing fractions/bands/spots exhibited the 11-kDa polypeptide on SDS/PAGE. The 11-kDa polypeptide was present in both the 'fast' and the 'slow' form of desulfovirodin. The relative intensity of the Coomassie-stained α , β and γ bands was similar if not identical for the 'fast' and 'slow' form and for the desulfovirodin obtained or separated by the above-specified five techniques. Also, no differences were noted when desulfovirodin was treated with SDS/PAGE sample buffer at room temperature instead of at 100°C. Densitometry of Coomassie-stained SDS/polyacrylamide gels of highly purified samples revealed that polypeptides other than α , β and 11-kDa polypeptides were almost absent (Fig. 2). By integration of the densitometric scan and correction for molecular mass a stoichiometry of 1:1.2:1.1 was obtained (α : β :11-kDa). The tight association and the observed stoichiometry indicate that the 11-kDa polypeptide is an integral part of the de-



2. Laser scanning densitometry of a Coomassie-stained SDS/acrylamide gel of *D. vulgaris* (Hildenborough) desulfoviridin (ng).



3. Denaturing gel filtration of *D. vulgaris* (Hildenborough) desulfoviridin. Desulfoviridin (200 μ g) was separated on a Superose 12 (10/30) support attached to a Pharmacia FPLC system. The flow was 0.25 ml/min using a buffer containing 6 M guanidinium \cdot HCl, 100 mM Tris/Cl, 0.5 mM EDTA, 1 mM dithiothreitol, 1.6. Asterisks denote non-protein peaks due to the liberated prosthetic groups and the dithiothreitol/EDTA excess added to the protein re separation. The inset shows the molecular mass calibration curve. Markers were: 1, bovine serum albumin, 2 and 5, *D. vulgaris* (Hildenborough) Fe-hydrogenase α and β subunit, 3, chymotrypsin, 4, *Megasphaera elsdenii* rubredoxin.

viridin-enzyme complex. Therefore, the subunit composition of desulfoviridin is $\alpha_2\beta_2\gamma_2$, with γ as the hitherto unnoted subunit. The 226-kDa molecular mass of the native *D. vulgaris* (Hildenborough) desulfoviridin holoenzyme determined by sedimentation equilibrium measurements [5] fits better with this corrected subunit composition.

Since molecular-mass determination by SDS/PAGE is sometimes not very reliable, an independent determination by gel filtration under denaturing conditions was made. The elution profile of *D. vulgaris* desulfoviridin (Fig. 3) showed a major peak eluting at 48 ± 3 kDa and a minor one at 13 ± 1 kDa. SDS/PAGE of dialyzed fractions confirmed that the major 48-kDa peak corresponded to the resolved α and β subunits (not shown). The 13-kDa peak

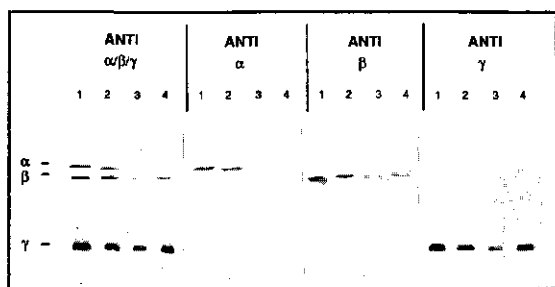


Fig. 4. Detection of desulfoviridin α , β and γ subunits in four *Desulfovibrio* strains by immunostaining of Western blots. Western blots were treated with antisera against the subunits of *D. vulgaris* (Hildenborough) desulfoviridin. Dilutions were $500\times$ (anti- α), $4000\times$ (anti- β) and $2000\times$ (anti- γ); the left-most blot was treated with a mixture of these antisera. Lanes 1 represent *D. vulgaris* (Hildenborough) (NCIB 8303); lane 2, *D. vulgaris oxamicus* (Monticello) (NCIB 9442); lane 3, *D. gigas* (NCIB 9332); and lane 4, *D. desulfuricans* (ATCC 27774) (20 μ g cells per lane, ≈ 50 ng desulfoviridin).

corresponded to the γ -subunit. The elution profile bears additional information on the subunit stoichiometry if we assume that the relative content of aromatic amino acids of the three subunits is identical. Integration and correction for size yields a ratio of 2:1.4 for $(\alpha + \beta) : \gamma$.

By gas-phase sequencing of SDS/PAGE-purified electroblotted subunits, the following N-terminal amino acid sequences were determined (parentheses indicate ambiguous determinations, \times unknown): α : A-K-H-A-T-P-K-L-D-Q-L-E-S-G-P-W-X-S-F-V-(V)-(D)-(I)-(K)-(K); β : A-F-I-S-S-G-Y-N-P-E-K-(P)-(M)-(A)-(N); γ : A-E-X-T-Y-K-G-K-S-F-E-V-X-(D)-(D)-G-F-L-L-I-R-(F)-D.

Literature data on N-terminal sequences of dissimilatory sulfite reductases are very limited. Seki and coworkers [23] reported that the α and β subunit of *D. vulgaris* (Miyazaki) desulfoviridin had N-terminal alanine residues, like all the three subunits of the Hildenborough strain. A sequence corresponding to the mixture of both α and β subunits was presented for desulfofuscin from *Thermodesulfobacterium commune* [4]. It has no apparent similarity with any of the above sequences. Comparison of the above sequences with the sequences of *E. coli*, *S. typhimurium*, *D. vulgaris* (Hildenborough) assimilatory sulfite reductase and spinach nitrite reductase [19, 20] did not reveal significant similarity.

Immunological relationships

Antibodies were raised against the individual α , β and γ subunits of *D. vulgaris* (Hildenborough) desulfoviridin. On immunoblots the antisera exhibited very specific responses with the respective subunits of all four strains investigated [*D. vulgaris* (Hildenborough), *D. vulgaris oxamicus* (Monticello), *D. gigas* and *D. desulfuricans* ATCC 27774 (Fig. 4)]. The responses on immunoblots of the α and β subunits, notably those of the α -subunit of *D. gigas* and *D. desulfuricans* ATCC 27774 are less pronounced than the response of the highly antigenic and strongly cross-reactive γ -subunit. Apparently the γ -subunits of desulfoviridin from different *Desulfovibrio* species share a common highly antigenic epitope. Detection limits for the α , β and γ subunits were approximately 10, 4 and 1 ng, respectively. Since anti- γ antiserum does not cross-react with the α and β subunit, the γ -subunit presumably is

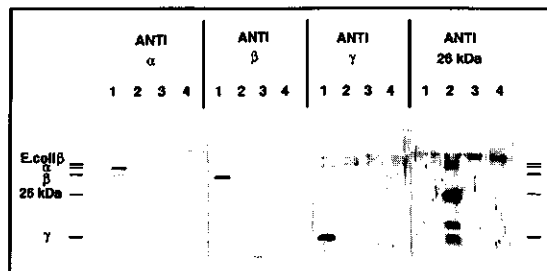


Fig. 5. Comparison of desulfoviridin, low-molecular-mass assimilatory sulfite reductase and *E. coli* assimilatory sulfite reductase by immunostaining of Western blots. Western blots were immunostained after treatment with diluted antisera against the subunits of desulfoviridin: 500 \times anti- α , 4000 \times anti- β or 2000 \times anti- γ and 1000 \times diluted antiserum against 26-kDa *D. vulgaris* (Hildenborough) low-molecular-mass assimilatory sulfite reductase. The positions of the subunits of desulfoviridin, 26-kDa low-molecular-mass sulfite reductase and *E. coli* sulfite reductase β -subunit are indicated on the left. Lane 1 contains 200 ng purified *D. vulgaris* (Hildenborough) desulfoviridin; lane 2, 200 ng purified *D. vulgaris* (Hildenborough) low-molecular-mass assimilatory sulfite reductase; lane 3 and 4, 200 ng *E. coli* sulfite reductase β -subunit and holoenzyme (cf. [14]), respectively.

not a proteolytic fragment of the α or β subunit. The relative response of the subunits on immunoblots of either whole cells (directly treated with SDS/PAGE sample buffer) or purified desulfoviridin was similar. This observation indicates that the *in vivo* subunit composition is also $\alpha_2\beta_2\gamma_2$.

In purified preparations of *D. gigas*, *D. desulfuricans* ATCC 27774 and *D. vulgaris oxamicus* (Monticello) desulfoviridin α , β and γ subunits were observed on Coomassie-stained SDS/PAGE (not shown). These preparations contained some more contaminating polypeptides. The relative staining of the γ -subunit was similar to that of the α and β subunit in Fig. 1. Compared with the *D. vulgaris* (Hildenborough) subunits, minor differences in the size of the polypeptides were observed. The same pattern of minor differences in the electrophoretic mobilities of the Coomassie-staining bands is also seen on immunoblots. Clearly the responses of the antisera with the other *Desulfovibrio* species are not specific but correspond to the three polypeptides of the desulfoviridin.

No significant positive responses of the anti- α , anti- β and anti- γ antisera were obtained with the assimilatory sulfite reductases from *E. coli* and *D. vulgaris* (Hildenborough) (Fig. 5). In addition, desulfoviridin subunits and *E. coli* assimilatory sulfite reductase did not react with the antiserum against the *D. vulgaris* (Hildenborough) 26-kDa low-molecular-mass assimilatory sulfite reductase. Minor cross-reactivity of the anti- α and anti-(26-kDa protein) antiserum, as observed in Fig. 5, is due to higher loads compared to Fig. 4.

In an immunoblot screening of *Desulfovibrio* cell-free extracts with the anti-(26-kDa protein) antiserum a \approx 30-kDa low-molecular-mass assimilatory sulfite reductase was also observed in *D. vulgaris* (Monticello) and *D. desulfuricans* Norway 4 (not shown). Thus, the presence of low-molecular-mass assimilatory sulfite reductases is now indicated in at least five bacterial species: three *Desulfovibrio* strains, *Methanosarcina barkeri* and *Desulfuromonas acetoxidans* [17]. Our results corroborate the previously proposed tripartite nature of the group of (bi)sulfite-reducing enzymes: assimilatory, dissimilatory and low-molecular-mass assimilatory sulfite reductases [2, 5, 17].

CONCLUSIONS

We have found a new subunit in an enzyme that has been studied over at least 20 years. This novel 11-kDa γ -subunit is not a proteolytic fragment of the α or β subunit. It does not dissociate from the $\alpha_2\beta_2\gamma_2$ complex on purification, native electrophoresis, isoelectric focussing, two-dimensional electrophoresis or high-ionic-strength gel filtration. The γ -subunit is present in stoichiometric quantities in whole cells and purified desulfoviridin of at least four *Desulfovibrio* species. Antibodies against the γ -subunit of *D. vulgaris* (Hildenborough) strongly cross-react with the apparently rather homologous and similarly sized γ -subunit in at least four species of *Desulfovibrio*. This ubiquity and cross-reactivity suggest a general role of the γ -subunit in desulfoviridin. As desulfoviridin is a soluble cytoplasmic enzyme [30], a membrane anchoring function of the γ -subunit can be excluded.

Regarding previous work on desulfoviridins [5, 23, 24, 30] we suspect that the relatively small size of the γ -subunit may have complicated an earlier detection by SDS/PAGE. Thus, an explanation for the overlooking of the γ -subunit might be found in the use of a low-percentage cross-linking gel (suitable for α/β separation, but too porous to resolve γ from the front), the fixing/staining procedure, the poor stacking of small polypeptides by the Laemmli system [25] or the use of the relatively insensitive amido black stain [5, 6, 23].

The presence of a γ -subunit in all desulfoviridin-type sulfite reductases is very likely. Its occurrence in P582, desulforubridin and desulfufuscidin-type dissimilatory sulfite reductases has to be demonstrated. Subunit molecular masses for the α and β subunits of desulforubridin and P582-type sulfite reductases have not been published yet. Cloning and sequencing of the genes coding for α , β , and γ subunits of the different types of dissimilatory sulfite reductases will provide a more detailed insight into the structural homology of sulfite reductases. The N-terminal sequences and antisera reported here have already allowed others (R. Karkhoff-Schweizer and Voordouw, personal communication) to identify DNA fragments containing the structural genes of *D. vulgaris* (Hildenborough) desulfoviridin.

Sequence data on the *D. vulgaris* (Hildenborough) assimilatory sulfite reductase were graciously provided prior to publication by J. A. Cowan. We acknowledge Mr J. Haas for his assistance in the handling of animals. We also thank Professor C. Veeger for continuous interest and critical reading. This investigation was supported by the Netherlands Foundation for Chemical Research (SOFON) with the financial aid from the Netherlands Organization for Scientific Research (NWO).

REFERENCES

- Schedel, M. & Trüper, H. G. (1979) *Biochim. Biophys. Acta* 554, 454–467.
- Moura, I., LeGall, J., Lino, A. R., Peck, H. D., Fauque, O., Xavier, A. V., DerVartanian, D. V., Moura, J. J. G. & Henriques, B. H. (1988) *J. Am. Chem. Soc.* 110, 1075–1082.
- Collins, M. D. & Widdel, F. (1986) *System. Appl. Microbiol.* 8, 8–18.
- Hatchikian, E. C. & Zeikus, J. G. (1983) *J. Bacteriol.* 153, 1212–1220.
- Lee, J.-P., LeGall, J. & Peck, H. D. (1973) *J. Bacteriol.* 115, 554–562.
- Kobayashi, K., Takahashi, E. & Ishimoto, M. (1972) *J. Biochem. (Tokyo)* 72, 879–887.
- Akagi, J. M., Chan, M. & Adams, V. (1974) *J. Bacteriol.* 120, 240–244.

- Kobayashi, K., Seki, Y. & Ishimoto, M. (1974) *J. Biochem. (Tokyo)* 75, 519–529.
- Drake, H. L. & Akagi, J. M. (1978) *J. Bacteriol.* 136, 916–923.
- Kobayashi, K., Tachibana S. & Ishimoto, M. (1969) *J. Biochem. (Tokyo)* 65, 155–157.
- Fitz, R. M. & Cypionka, H. (1990) *Arch. Microbiol.* 154, 400–406.
- Pierik, A. J. & Hagen, W. R. (1991) *Eur. J. Biochem.* 195, 505–516.
- Lee, J.-P., Yi, C.-S., LeGall, J. & Peck, H. D. (1973) *J. Bacteriol.* 115, 453–455.
- Siegel, L. M. & Davis, P. S. (1974) *J. Biol. Chem.* 249, 1587–1598.
- Hallenbeck, P. C., Clark, M. A. & Barrett, E. L. (1989) *J. Bacteriol.* 171, 3008–3015.
- Krueger, R. J. & Siegel, L. M. (1982) *Biochemistry* 21, 2892–2904.
- Moura, I., Lino, A. R., Moura, J. J. G., Xavier, A. V., Fauque, G., Peck, H. D. & LeGall, J. (1986) *Biochem. Biophys. Res. Commun.* 141, 1032–1041.
- Huynh, B. H., Kang, L., DerVartanian, D. V., Peck, H. D. & LeGall, J. (1984) *J. Biol. Chem.* 259, 15373–15376.
- Tan, J., Helms, L. R., Swenson, R. P. & Cowan, J. A. (1991) *Biochemistry* 30, 9900–9907.
- Ostrowski, J., Wu, J.-Y., Rueger, D. C., Miller, B. E., Siegel, L. M. & Kredich, N. M. (1989) *J. Biol. Chem.* 264, 15726–15737.
- Postgate, J. R. (1951) *J. Gen. Microbiol.* 5, 714–724.
- Saunders, G. F., Campbell, L. L. & Postgate, J. R. (1964) *J. Bacteriol.* 87, 1073–1078.
- Seki, Y., Kobayashi, K. & Ishimoto, M. (1979) *J. Biochem. (Tokyo)* 85, 705–711.
- Laemmli, U. K. (1970) *Nature* 227, 680–685.
- Schägger, H. & Jagow, G. von (1987) *Anal. Biochem.* 166, 368–379.
- Kratzin, H. D., Wiltfang, J., Karas, M., Neuhoff, V. & Hilschmann, N. (1989) *Anal. Biochem.* 183, 1–8.
- Towbin, H., Staehelin, T. & Gordon, J. (1979) *Proc. Natl Acad. Sci. USA* 76, 4350–4354.
- Seki, Y., Nagai, Y. & Ishimoto, M. (1985) *J. Biochem. (Tokyo)* 98, 1535–1543.
- Aketagawa, J., Kojo, K. & Ishimoto, M. (1985) *J. Agric. Biol. Chem.* 49, 2359–2365.
- Kremer, D. R., Veenhuis, M., Fauque, G., Peck, H. D., LeGall, J., Lampreia, J., Moura, J. J. G. & Hansen, T. A. (1988) *Arch. Microbiol.* 150, 296–301.

Chapter 7

S=9/2 EPR signals are evidence against coupling between the siroheme and the Fe/S cluster prosthetic groups in *Desulfovibrio vulgaris* (Hildenborough) dissimilatory sulfite reductase.

Antonio J. Pierik and Wilfred R. Hagen

(1991) Eur. J. Biochem. 195, 505-516.

$S = 9/2$ EPR signals are evidence against coupling between the siroheme and the Fe/S cluster prosthetic groups in *Desulfovibrio vulgaris* (Hildenborough) dissimilatory sulfite reductase

Onio J. PIERIK and Wilfred R. HAGEN

Department of Biochemistry, Agricultural University, Wageningen, The Netherlands

Received July 24/October 18, 1990) — EJB 90 0898

Sulfite reductases contain siroheme and iron-sulfur cluster prosthetic groups. The two groups are believed to be structurally linked via a single, common ligand. This chemical model is based on a magnetic model for the oxidized enzyme in which all participating iron ions are exchange coupled. This description leads to two serious discrepancies. Although the iron-sulfur cluster is assumed to be a diamagnetic cubane, $[4\text{Fe-4S}]^{2+}$, all iron appears to be paramagnetic in Mössbauer spectroscopy. On the other hand, EPR spectroscopy has failed to detect anything but a single high-spin heme. We have re-addressed this problem by searching for new EPR spectroscopic clues in concentrated samples of dissimilatory sulfite reductase from *Desulfovibrio vulgaris* (Hildenborough). We have found several novel signals with effective g values of 17, 15.1, 11.7, 9.4, 9.0, 4. The signals are interpreted in terms of an $S = 9/2$ system with spin-Hamiltonian parameters $g = 2.00$, $D = -0.56 \text{ cm}^{-1}$, $|E/D| = 0.13$ for the major component. In a reductive titration with sodium borohydride the spectrum disappears with $E_m = -205 \text{ mV}$ at pH 7.5. Contrarily, the major high-spin siroheme component has $S = 5/2$, $g = 1.99$, $D = +9 \text{ cm}^{-1}$, $|E/D| = 0.042$, and $E_m = -295 \text{ mV}$. The sum of all siroheme signals integrates to 0.2 spin/half molecule, indicating considerable demetallation of this prosthetic group. Rigorous quantification procedures for $S = 9/2$ are not available, however, estimation by an approximate method indicates 0.6 $S = 9/2$ spin/half molecule. The $S = 9/2$ system is ascribed to an iron-sulfur cluster. It follows that this cluster is probably not a cubane, is not necessarily exchange-coupled to the siroheme, and, therefore, is not necessarily structurally close to the siroheme. It is suggested that this iron-sulfur prosthetic group has a novel structure suitable for functioning in multiple electron transfer.

Metalloenzymes which catalyze redox reactions are frequently complex bioinorganic systems. They contain more than one prosthetic group in order to be able to function in distinguishable operations. They should be an appropriate sink for a (usually even) number of reducing equivalents. They should also bind and activate substrate(s) for the subsequent combination with stored electrons.

Nature uses the grouping of metal ions into clusters and the grouping of clusters into multi-center systems to increase the versatility of metalloproteins as redox compounds. Specifically, this grouping is to extend drastically the range of available reduction midpoint potentials associated with a particular metal, in order to create the possibility to transfer pairs, multiple pairs, of electrons, and in order to optimize the kinetics of electron transfer. Thus, the topological grouping of metal ions (or, more generally, of entities which carry potentially reactive electrons) results in biologically useful electronic cooperativity.

These electronic interactions are, by necessity, accompanied by their associated magnetic interactions. Although this magnetism is not known to bear any direct relevance to biological functioning, its examination is our

pertinent objective for two reasons. It makes a mirror image of electronic cooperativity; it is also a dominant factor in magnetic resonance spectroscopies. The latter form a major set of practical tools for the study of metalloenzymes.

Magnetic interaction in biological systems is commonly classified into strong, exchange interaction and weak, dipole-dipole interaction. Exchange interaction typically ranges over a distance of one chemical-bond length; i.e. a few tenths of a nanometer. The epithet 'strong' means that the individual magnetism (or angular-momentum properties, or effective spin) of the grouped metal ions, or clusters, is no longer identifiable, but is replaced by a net, overall spin. Contrarily, dipolar interactions have a typical range of one nanometer. The spins of the individual magnets are modified, but they are still identifiable. Exchange coupling and dipolar coupling, though different in their physical origin, have one basic property in common: they both occur between paramagnets. A diamagnet, or an $S = 0$ system, can only be part of a magnetic interaction through transfer of magnetization by polarization; it cannot by itself contribute to a magnetic interaction. However, there appears to be one biological instance of a violation of this rule: the case of a diamagnetic iron-sulfur cluster coupled to a paramagnetic heme iron in sulfite reductases and nitrite reductases.

These enzymes catalyze the six-electron reduction of sulfite to sulfide, and of nitrite to ammonia. To this objective the proteins accommodate siroheme and what appears to be $[4\text{Fe-4S}]$ clusters as prosthetic groups, although they do so with

Correspondence to W. R. Hagen, Laboratorium voor Biochemie, Driekenlaan 3, NL-6703 HA Wageningen, The Netherlands

Enzyme. Desulfoviridin or dissimilatory sulfite reductase (EC 9.1).

widely different quaternary structures: sulfate-reducing bacteria have monomeric assimilatory sulfite reductase [1, 2] as well as $\alpha_2\beta_2$ -tetrameric dissimilatory sulfite reductase [1, 3–5]; spinach leaf contains an $\alpha\beta$ -dimeric nitrite reductase [6–8]. The most intensively studied example is *Escherichia coli* NADPH-sulfite reductase with the subunit structure $\alpha_8\beta_4$ [9]. The hemoprotein β -monomer isolated from this complex has methyl-viologen-linked sulfite-reductase activity and contains one heme and one Fe/S cluster [10]. In the fully oxidized form of the hemoprotein, the iron in the heme is ferric and therefore paramagnetic. The Fe/S cluster has been proposed to be of the $[4\text{Fe-4S}]^{2+;1+}$ ferredoxin type (cf. [11] and references quoted therein); therefore, it should be a diamagnet in the oxidized enzyme at low temperature. Although these assignments would seem rigorously to exclude any possibility for magnetic coupling to occur between the heme and the cubane, a strong exchange coupling has, in fact, been proposed to exist on the basis of a Mössbauer-spectroscopic study [11].

Following this initial proposal, the enzyme (either in its oxidized, uncomplexed form or in other redox and/or ligation states) has been the subject of an extensive series of spectroscopic studies which have all been interpreted in terms of exchange coupling between the heme and a cubane [12–26]. Crystallographic [27] and gene sequencing data [28] also have been claimed to be consistent (or at least not inconsistent) with the existence of a strong coupling.

Mainly on the basis of comparative spectroscopy, this conclusion has been extended to hold also for the monomeric [2, 29] and the $\alpha_2\beta_2$ -tetrameric [29–31] sulfite reductases from sulfate reducers as well as for spinach nitrite reductase [32].

The central argument of Münck and collaborators in their conclusion that a strong exchange coupling exists between a ferric heme ($S = 5/2$) and an oxidized ferredoxin cubane ($S = 0$) in *E. coli* sulfite reductase is the observation that, although the Fe/S cluster is EPR silent, it behaves as a paramagnet in low-temperature Mössbauer spectroscopy [11]. The Mössbauer spectrum for each individual iron site (i.e. the heme iron and all the Fe/S irons) is fitted using a single effective spin Hamiltonian with $S = 5/2$. Münck has also given a first start towards a possible theoretical description of this novel physical phenomenon [33]. The crux of his argument is that coupling of individual Fe/S-iron ion(s) with the heme iron perturbs the Fe/S intra-cluster coupling; this results in the addition of some paramagnetism to the Fe/S ground state from the excited state(s) of the Fe/S spin ladder.

At this point we feel uncomfortable with what we see as a gross physical inconsistency still remaining, namely, of a system which appears to behave as a paramagnet in the Mössbauer spectrometer and as a diamagnet in the EPR spectrometer. We have, therefore, set out to reinvestigate the sulfite reductase system. For convenience we have chosen the sulfate reducing anaerobe *D. vulgaris* (Hildenborough) as the source of enzyme. *Desulfovibrio* species contain large amounts of dissimilatory (bi-)sulfite reductase (up to 7% of the soluble protein, cf. [34]). *D. vulgaris* is regularly cultivated by us in 300-l batch cultures. Thus, the production in millimolar concentrations of the protein on a routine basis allows for a research of, for example, magnetic-spectroscopic clues of low intensity. Below we report on an EPR study which indicates that the oxidized Fe/S cluster in this sulfite reductase at low temperature is not diamagnetic but is paramagnetic. Coupling with the heme is not observed. Furthermore, there is no compelling reason to assign the classical $[4\text{Fe-4S}]$ cubane structure to the Fe/S cluster.

MATERIALS AND METHODS

Desulfovibrio vulgaris, strain Hildenborough, was grown in 300-l batch cultures according to [35] and harvested by means of a Sharples centrifuge. All subsequent steps were carried out at 4°C. Cells were suspended in 10 mM Tris/HCl pH 8.0 and broken in a Manton Gaulin press. Cell-free extract was obtained as the supernatant after a 1-h spin at 100000 × g. With the pH adjusted to 8.0 the conductivity was lowered to 1 mS/cm by dilution with water. The solution was then loaded onto a DEAE-Sephacel column (5 × 20 cm) pre-equilibrated with 10 mM Tris/HCl pH 8.0. After a 1-l wash with 10 mM Tris/HCl plus 20 mM NaCl, pH 8.0, a 3-l gradient of 0–0.5 M NaCl in 10 mM Tris/HCl pH 8.0 was applied. Fractions with a significant 630-nm absorbance were pooled and concentrated over an Amicon YM-100 filter. Gel chromatography of 100-mg protein batches on a S-300 column (4 × 100 cm) equilibrated with 100 mM potassium phosphate yielded desulfovibridin with an A_{630}/A_{280} ratio of 5–6. The last purification step was by FPLC (Pharmacia) at ambient temperature on a 1-ml Mono-Q anion-exchange column. A 0–1 M NaCl gradient in 20 mM Tris/HCl pH 8.0 was used to elute the desulfovibridin at ≈ 0.4 M NaCl. The final preparations had a purity index A_{630}/A_{280} of 4.3. The protein was pure as judged from FPLC rechromatography and from two-dimensional electrophoresis (isoelectric focussing followed by SDS/PAGE, or native PAGE followed by SDS/PAGE). The sulfite-dependent H_2 -uptake activity was 0.15–0.30 $\mu\text{mol} (\text{mg protein})^{-1}$ under conditions identical to those in [1] except that *E. coli* hydrogenase was replaced by 10 μg *D. vulgaris* periplasmic hydrogenase. The iron and acid-labile sulfur content was 22 ± 4 mol/mol. In view of an estimated 10–30% interference of the heme cofactor in the microbial trichloroacetic acid protein determination, we consider the Fe/S values as provisional, and we continue to work on this analytical problem. The reported enzyme concentrations are based on a molecular mass of 220 kDa [1].

Assimilatory sulfite reductase from *D. vulgaris* (Hildenborough) and from *E. coli* C 600 were prepared according to [2] and [9], respectively.

Reductive redox titrations were done at 25°C essentially according to [36] in an anaerobic cell under purified argon with the bulk potential of the stirred solution measured with a Radiometer P-1312 micro-platinum electrode with respect to the potential of a Radiometer K-401 saturated calomel electrode. Reported potentials were recalculated with respect to the normal hydrogen electrode. The freshly prepared reductant was anaerobic NaBH_4 , stabilized with 0.01 M NaOH. Redox equilibrium was obtained as judged by the attainment of a stable potential within a few minutes after the addition of the reductant to the enzyme solution in 50 mM Hepes pH 7.5, preincubated with the following mixture of mediators (each at a final concentration of 40 μM): resorufine, indigo disulfonate, 2-hydroxy-1,4-naphthoquinone, anthraquinone disulfonate, phenosafranin, safranin O, neutral red, benzoquinone, methyl viologen. Samples were drawn and transferred to EPR tubes under a slight overpressure of argon, and directly frozen in liquid nitrogen.

Normal-mode X-band EPR data were taken on a Bruker EPR 200 D spectrometer. The microwave frequency was measured with a Systron Donner frequency counter, model 1292. The modulation frequency was always 100 kHz. The direct current magnetic field was measured with an AEG Kernnanz Magnetfeldmesser, type GA-EPR 11/21-02. The field was modulated with a frequency of 100 kHz. The amplitude

of modulation was calibrated on the modulation broadening of the signal from the Bruker strong-pitch sample. In (de-)population experiments the sample temperature was determined with two 5-k Ω Allen-Bradley carbon resistors immersed in the EPR sample just below and above the measuring area of the TE₁₀₂ cavity. The spectrometer was interfaced with a DASH-16 card to an Olivetti M24 PC with software written in ASYST for 1024-point data acquisition, correction for background signals (with frequency alignment), double integration procedures, and *g*-value determinations. Quantification of spin concentrations from Kramers doublets was according to [37]. The external standard for integration was 0 mM CuSO₄/10 mM HCl/2 M NaClO₄.

Parallel-mode X-band EPR was measured in the laboratory of S. P. J. Albracht (University of Amsterdam) on a Varian E-9 EPR spectrometer equipped with the Varian E-36 bimodal rectangular cavity as previously described [38].

We have previously detailed the method for exactly calculating the effective *g* values of a system with spin *S* using the spin Hamiltonian

$$H_s = D[S_z^2 - S(S+1)/3] + E(S_x^2 - S_y^2) + g\beta B \cdot S$$

and we wrote out [39] the energy matrix for the specific case of *S* = 7/2. In the Appendix to the present paper we list the elements $E(|m_s^i\rangle, |m_s^j\rangle)$ for the cases *S* = 5/2 and *S* = 9/2.

Approximate values for the effective *g* values are obtained in the weak-field (i.e. $D \gg g\beta B$) by substituting in the energy matrix any large number for the quantity *D* (e.g. $D \approx 9 \text{ cm}^{-1}$), and substituting any small number for the external magnetic field *B* (e.g. $B \approx 300 \text{ mT}$).

For low-spin heme signals the tetragonal and rhombic ground field splittings were calculated from the measured *g* values according to Taylor [40]. The rhombicity of the heme has been expressed as the ratio of the tetragonal over the rhombic splitting.

RESULTS

EPR spectra of oxidized desulfovivridin

An overview of EPR signals from *D. vulgaris* desulfovivridin (dissimilatory sulfite reductase) is presented in Fig. 1 in the form of wide-scan spectra of concentrated samples from three different isolations. There is considerable EPR-spectral variation over the different samples; this has been noted before to be the case for dissimilatory sulfite reductases from other sulfate-reducing bacteria [4, 31, 41] and recently also for an activated form of assimilatory sulfite reductase [42]. Several high-spin heme components are observed with *g_x* and *g_y* values centered around *g* \approx 6 in the range 7–8 and with a *g_z* value in the range 2.0–1.9. These components differ in their rhombicity, as reflected in the *g* anisotropy. The spectra are arranged in an increasing order of contributions from the more rhombic components. All the samples also contain a certain amount of low-spin heme, as evidenced by the signals in the *g*-value region from 2.6 to 1.7. The increase in relative intensity from high-spin hemes with the smaller anisotropy in the *g* \approx 6 region is paralleled by a similar decrease from low-spin hemes with the smaller anisotropy in the *g* \approx 2.4 region.

There are minor signals at *g* = 4.3 (*S* = 5/2 spin) presumably from adventitiously bound ferric iron, and at *g* \approx 2 (*S* = 1/2 spin) characteristic for [3Fe-4S]¹⁺. These two signals have not been analyzed in any detail.

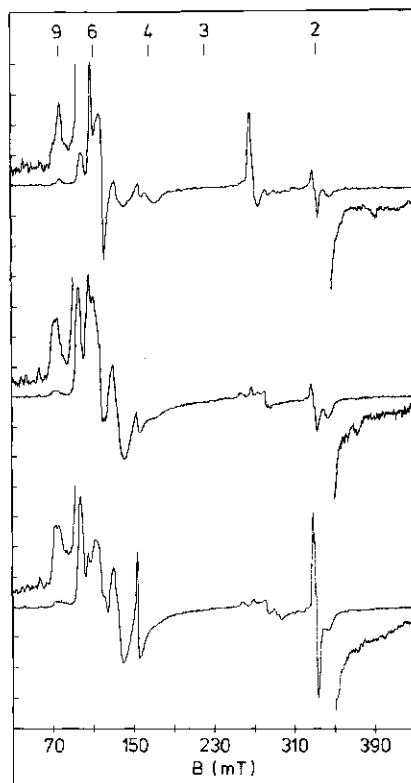


Fig. 1. Wide-scan spectra of three different preparations of *D. vulgaris* desulfovivridin, 125–200 mg/ml in 50 mM Hepes pH 7.5, showing a varying distribution of rhombicities in high-spin and low-spin heme components, and a number of novel signals at very low field. The blow-ups are eightfold amplified compared to the full scans and are five-times averaged. All spectra are base-line corrected with the frequency-adjusted spectrum from a buffer-only sample. EPR conditions: microwave frequency, 9.33 GHz; modulation amplitude, 0.8 mT; microwave power, 13 mW; temperature, 16–17 K.

At the low-field end of the spectra a number of weak, absorption-shaped lines are observed with unusually high effective *g* values in the range from 17 to 9. Another feature is detectable around *g* \approx 4. To our knowledge this set of signals does not readily compare to any system thus far described in the literature. In what follows we attempt to analyze the set of novel signals within the spin-Hamiltonian formalism and we attempt to assign them to a chemical structure.

Limiting the spin to half-integer values by dual-mode EPR spectroscopy

The system is very likely to be high-spin (i.e. $S > 1/2$) in view of the very extreme deviation of the observed *g* values from *g* = 2. Also, the observed temperature dependence (see below) is consistent with $S > 1/2$. It is important to establish early on in the analysis whether the spin is integer or half-integer, because this has major consequences for the choice of the form of the spin-Hamiltonian as well as for quantification procedures, cf. [38, 43]. Desulfovivridin presumably contains only hemes and iron-sulfur clusters as potential paramagnets. At the standard EPR frequency of 9 GHz many

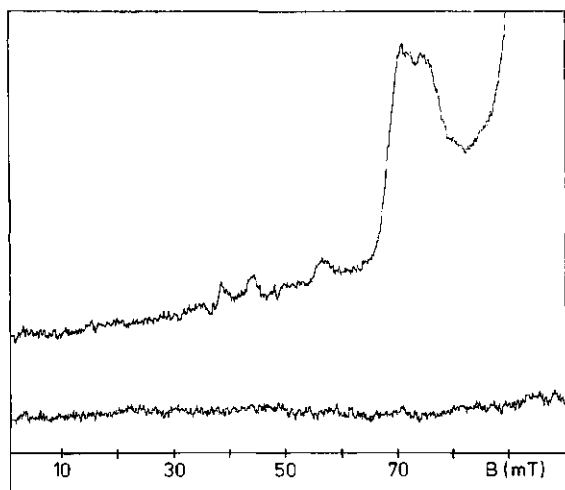


Fig. 2. Dual-mode spectrum of low-field resonances in *D. vulgaris desulfoviridin*, 200 mg/ml in 50 mM Hepes pH 7.5, determines the system spin to be half-integer. The upper trace was obtained with the magnetic component of the microwave perpendicular to the external magnetic field vector; for the lower trace the two vectors were parallel. EPR conditions: microwave frequencies, 9147 MHz in the perpendicular mode and 9108 MHz in the parallel mode; microwave power, 200 mW; modulation amplitude, 1.25 mT; temperature, 16.5 K

high-spin metalloproteins, and specifically all high-spin heme and Fe/S centers, are subject to the weak-field Zeeman effect. This means that the Zeeman splitting is small compared with fine structure splittings. Therefore, integer spin systems exhibit only quasi-forbidden $|\Delta_m| = \text{even}$ transitions. In regular EPR spectrometers, in which the microwave is perpendicular to the static magnetic field, these transitions are allowed for all orientations off the g -tensor axes. However, when the microwave is set parallel to the magnetic field, the transitions become fully allowed also along the g -tensor axes. Practically this means that when the two experiments can be done under a single set of conditions, the features in the parallel-mode spectrum are sharper (at slightly higher effective g -value positions) and roughly twofold more intense than the corresponding ones in the perpendicular-mode spectrum. The use of a bimodal cavity offers precisely this possibility by two subsequent measurements at slightly different frequencies. In Fig. 2 the result of such an experiment is shown for the low-field spectrum of desulfoviridin. Although the bimodal cavity has a lower sensitivity than a comparable, single-mode cavity, all the low-field lines are detectable in the perpendicular-mode spectrum. The observation that none of these lines have detectable intensity in the parallel-mode spectrum, taken under exactly the same conditions, strongly implies that all the observed lines are from $|\Delta_m| = \text{odd}$ transitions. Therefore, the spin is half-integer.

Determination of the minimal spin and the sign of the zero-field splitting

The intensity of the low-field spectrum as a function of temperature is presented in Fig. 3. The four traces have been normalized with respect to microwave power and electronic gain. On the low-field side of the high-spin siroheme spectrum at least four different lines are detected. Three relatively sharp

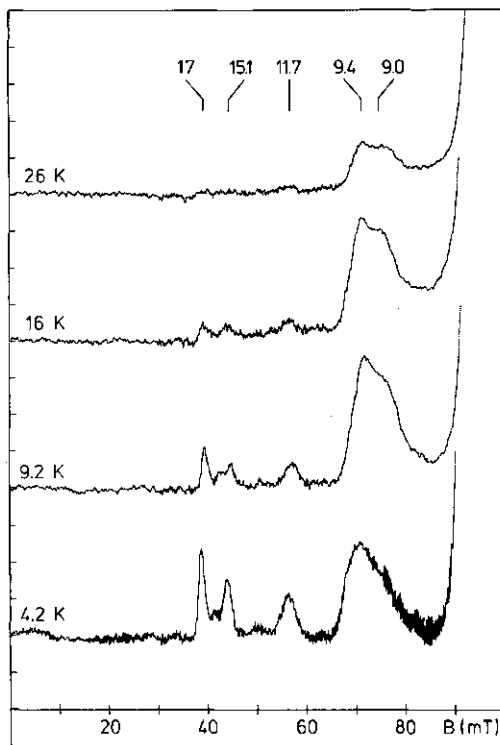


Fig. 3. Temperature dependence of low-field resonances in *D. vulgaris desulfoviridin*, 200 mg/ml in 50 mM Hepes pH 7.5. The spectrum taken at $T = 4.2$ K is nine-times averaged, the other spectra are four-times averaged, and all are corrected with a buffer base line. The traces are replots from stored data with the amplitude adjusted to normalized machine settings. EPR conditions: microwave frequency, 9.33 GHz; microwave powers, 200, 200, 200, 80 mW; modulation amplitudes, 0.8, 0.8, 0.8, 1.0 mT; temperatures, 26, 16, 9.2, 4.2 K

lines with effective g values 17, 15.1 and 11.7, and a broader, composite peak around $g \approx 9$. For half-integer spins in the weak-field limit the rule holds that the highest possible effective g value $g_{\text{max}} \leq 4S$ when the real g value is approximately 2. Thus, the lines at $g = 17$ and 15.1 define the spin $S \geq 9/2$. We take the spin to be $S = 9/2$, and our subsequent g value analysis is consistent with this assumption. For $S = 9/2$ a g value in the range $17.8 \geq g \geq 14$ can only occur for the $|\pm 1/2\rangle$ Kramers doublet as is illustrated in detail in Fig. 4. The highest g value from the spectrum of the $|\pm 9/2\rangle$ doublet is in the range $18 \geq g \geq 17.8$ under the assumption that the system's real g values are 2.00 and $D \gg g\beta B$, and could therefore be close to the observed $g = 17$ if these assumptions were not strictly met. However, a transition within the $|\pm 9/2\rangle$ doublet, with $|\Delta_m| = 9$, will have an extremely low transition probability, as the other two effective g values are virtually zero. The lines at $g = 17$ and 15.1 are, in all likelihood, from the $|\pm 1/2\rangle$ doublets of two $S = 9/2$ systems, with slightly different rhombicity. The intensity of these lines decreases approximately linearly with increasing detection temperature. However, the lines are also seen to broaden with increasing temperature. Thus, the ratio of integrated area over temperature increases with temperature; therefore, the axial zero field splitting parameter, D , has a negative sign. The third sharp

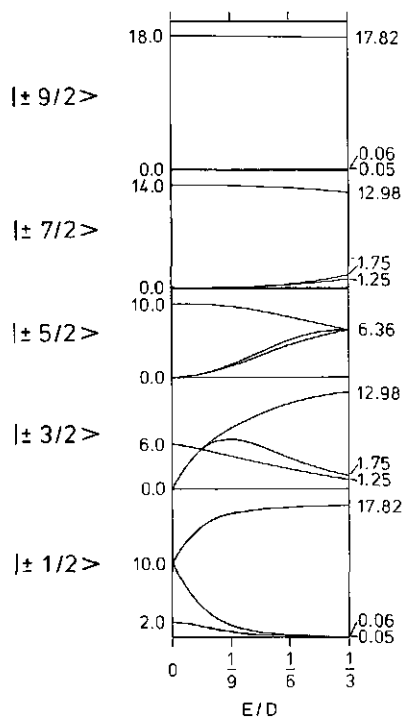


Fig. 4. Relation between the five sets of three effective g values and the rhombicity, $3E/D$, for a system with spin $S = 9/2$, calculated in the weak-field limit (i.e. $D \gg g\beta B$)

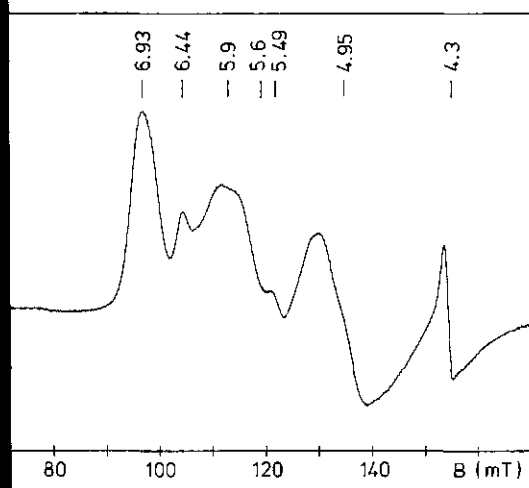


Fig. 5. Low-field part of high-spin ferric siroheme components in *D. vulgaris desulfoviridin*, 200 mg/ml in 50 mM Hepes pH 7.5. EPR conditions: microwave frequency, 9331 MHz; microwave power, 1 mW; modulation amplitude, 1.0 mT; temperature, 17 K

at $g = 11.7$ behaves in concert with the other two in its temperature dependence; this line is probably also from a $|\pm 1/2\rangle$ doublet.

The composite line around $g \approx 9$ as a function of temperature behaves differently from the other three lines in its inten-

Table 1. Calculated and observed effective g values for high-spin siroheme components in *D. vulgaris (Hildenborough) desulfoviridin*. The g values were calculated in the weak-field limit ($D \gg g\beta B$) for the $|\pm 1/2\rangle$ doublet of an $S = 5/2$ system and an isotropic real g value $g = 1.99$; theor. = theoretical; exptl = experimental, obsc. means obscured by [3Fe-4S] signal

E/D		g_x	g_y	g_z
0.0422	theor.	1.932	6.925	4.945
	exptl	1.93	6.93	4.95
0.0200	theor.	1.977	6.435	5.484
	exptl	obsc.	6.44	5.49
0.0015	theor.	1.99	6.00	5.93
	exptl	obsc.	5.9	5.9

sity and broadening. It is probably not from a $|\pm 1/2\rangle$ doublet.

Details of the siroheme spectra

We now proceed by identifying the lines that belong to the high-spin and low-spin siroheme components in order to exclude these from a subsequent g -value analysis of the $S = 9/2$ system and to identify lines which cannot be attributed to siroheme.

Fig. 5 is an expanded run from the sample of Fig. 1, lowest trace, covering the g -perpendicular range of the $S = 5/2$ siroheme spectra. The major component is the most rhombic one with a peak at $g = 6.93$ and a derivative feature with a zero crossing at $g = 4.95$ (the shape of this feature indicates two slightly different components). That these lines go together is easily seen by comparing the three traces of Fig. 1 which exhibit different ratios of this species over less rhombic ones. This conclusion is also borne out by a fit of the effective g values to the $S = 5/2$ spin Hamiltonian in the weak-field limit (see Table 1) which predicts these g values to go together with a third one at $g = 1.93$ and this is indeed what we observe in the high-field region depicted in Fig. 6. A second, minor, less rhombic component can be identified with the lines at $g = 6.44$ and 5.49 with a third g value at 1.98 coincident with (overshadowed by) the near isotropic [3Fe-4S] signal.

The remaining signals around $g \approx 6$ are less readily assigned. The feature at $g = 5.9 \pm 0.1$ might possibly be from a very minor, virtually axial high-spin heme component. Finally, we are unable to match the derivative-shaped line at $g = 5.6$ with any low-field peak into a reasonable combination which would fit the spin Hamiltonian for a high-spin ferric heme spectrum. Therefore, this line may be part of the $S = 9/2$ spectra.

Part of the siroheme is low-spin and this form exhibits a multitude of rhombicities similar to that found for the high-spin state. An expanded scan of the low-spin region is presented in Fig. 6. The g values have been grouped in sets of three by starting from the three-set $g = 2.47, 2.35, 1.78$, which is close to the values ($g = 2.44, 2.36, 1.77$) reported for *D. vulgaris* assimilatory sulfite reductase [2]. The other sets of increased rhombicity have been chosen as reasonable groupings of like intensity. In Table 2 the g values are given together with a corresponding value for the rhombicity, i.e. the ratio of rhombic over axial ligand field splitting within the $d(t_{2g})^5$ configuration. No attempt has been made to assign the g values to particular directions within a molecular frame defined by the siroheme as no single-crystal data are available

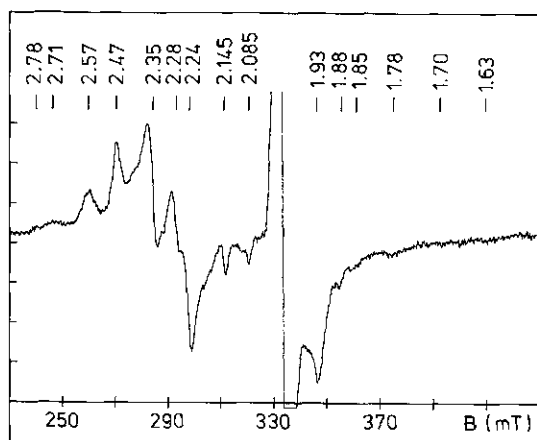


Fig. 6. Details of low-spin siroheme EPR components in *D. vulgaris desulfoviridin*, 200 mg/ml in 50 mM Hepes pH 7.5. The trace is an average of nine spectra corrected with nine buffer base lines. EPR conditions: microwave frequency, 9332 MHz; microwave power, 0.8 mW; modulation amplitude, 1.0 mT; temperature, 17 K

Table 2. Observed g values and rhombicities of low-spin siroheme components in *D. vulgaris* (Hildenborough) *desulfoviridin*. The rhombicity is defined as the absolute ratio of the tetragonal and the rhombic ligand field splitting within the t_{2g} set subject to a strong octahedral field (cf. Taylor [40])

g_1	g_2	g_3	Rhombicity
2.47	2.35	1.78	0.22
2.57	2.28	1.7	0.47
2.57	2.24	1.7	0.54
2.71	2.145	1.6(3)	0.52
2.78	2.085	1.6(3)	0.40

as a reference. There appears to be a rough correspondence in the distribution of rhombicities between the low-spin and high-spin components in that there is a single component of modest rhombicity (the first entry in Table 2 and the second one in Table 1) and a set of slightly different components with about twice this rhombicity.

Only one or two minor features at $g = 1.88$ and, possibly, at $g = 1.85$ remain unassigned.

Magnitude of the zero-field splittings from depopulation

EPR from high-spin hemes is within the $|\pm 1/2\rangle$ doublet and this is commonly the ground doublet, i.e. the zero-field splitting parameter, D , is positive. We want to determine this quantity for spin-quantification purposes as well as to check the validity of the assumption of the weak-field limit, used in the g -value analysis of Table 1. For the hemoprotein β subunit of *E. coli* sulfite reductase, the D value has been determined both by simulation of Mössbauer spectra [11] and by fitting the EPR temperature dependence to a Boltzmann distribution over an $S = 5/2$ multiplet [13]. These two methods resulted in exactly the same answer, $D = 8 \pm 1 \text{ cm}^{-1}$. The small uncertainty claimed in these determinations is rather remarkable in view of the fact that the paramagnetism of the high-spin heme is not very sensitive to changes in D because the zero-field

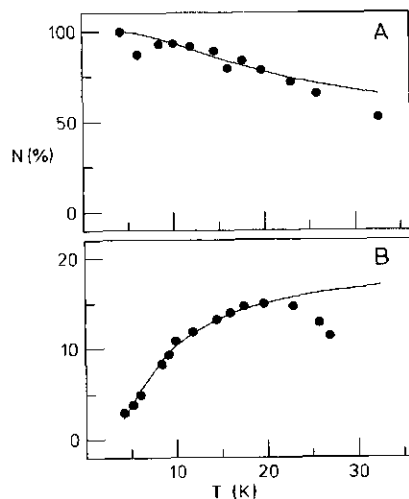


Fig. 7. Thermal (de)population of the lowest doublet of the siroheme $S = 5/2$ multiplet (A) and the one-to-highest doublet of the iron-sulfur $S = 9/2$ multiplet (B). The data points are the area under the absorption-shaped peaks at $g = 6.93$ and $g = 9.0$, respectively, multiplied by the detection temperature (i.e. corrected for Curie-law temperature dependence). The solid traces and the scaling of the ordinate were obtained by fitting the data points to a Boltzmann distribution over the sublevels of an $S = 5/2$ system with $D = +9.1 \text{ cm}^{-1}$, or to the sublevels of an $S = 9/2$ system with $D = -0.56 \text{ cm}^{-1}$, respectively

splittings are considerably larger than the electronic Zeeman interaction created by laboratory fields. A definition of error was not given in [11, 13]. In a determination of the D value for high-spin heme in cytochrome c oxidase one of us [38] found a considerable greater uncertainty ($D = +8.4 \pm 3.1 \text{ cm}^{-1}$). The error was defined as a doubling of the weighted χ -square obtained from a least-squares fit to the EPR depopulation data. We have here used the same definition in determining the error in the D value for high-spin siroheme. Fig. 7A gives the population of the $|\pm 1/2\rangle$ doublet as a function of temperature measured as intensity of the peak at $g = 6.93$. The least-squares fit to the Boltzmann population gives $D = +9.1 \text{ cm}^{-1}$, and a doubling of χ -square defines the range of 4.4 – 15.6 cm^{-1} . Note that the scatter in the data of Fig. 7A is comparable to that in the *E. coli* hemoprotein data reported in [13].

The value of 9 cm^{-1} found for desulfoviridin in usual for high-spin hemes and ensures that we are well into the weak field limit. The data of Fig. 7 also define the temperature range of 4 – 20 K as a reliable one for spin quantification.

For the $S = 9/2$ system, the matter of determining the zero field splitting is more complicated because the low-field signal at $g = 17, 15.1, \text{ and } 11.7$ from $|\pm 1/2\rangle$ doublets rapidly broaden when the temperature is increased from $T = 4 \text{ K}$ (cf. Fig. 3). The line at $g = 9$ is seen to be less sensitive to relaxation broadening near liquid helium temperatures, possibly because the inherent line width is significantly greater than that of the low-field $|\pm 1/2\rangle$ peaks. Inspection of Fig. 7 indicates that the $g = 9$ line is from a $|\pm 3/2\rangle$ doublet. Under this assumption, its intensity as a function of temperature has been fitted to a Boltzmann distribution over an $S = 9/2$ system with the result given in Fig. 7B. The zero-field splitting parameter $D = -0.56 \pm 0.05 \text{ cm}^{-1}$ is much more accurately de-

Table 3. A comparison of calculated and observed effective g values for transitions within the first three doublets of an $S = 9/2$ system in *D. vulgaris* (Hildenborough) desulfoviridin

The theoretical g values indicated by A were calculated in the weak-field limit, i.e. $D \gg g\beta B$ but otherwise D is undetermined. The g values indicated by B were calculated by a full diagonalization of the energy matrix at discrete values of the external magnetic field, and $D = -0.56 \text{ cm}^{-1}$. Both calculations are for a microwave frequency of 9330 MHz and an isotropic real g value of $g = 2.000$. The following abbreviations are used: exptl., experimentally observed g values; outs., resonance line falls outside range of external magnetic field; no det., resonance not detected; obsc., resonance obscured by siroheme spectrum; a question mark indicates that the resonance cannot be identified with certainty

E/D	Doublet	Source	g_x	g_y	g_z
0.133 ($\pm 5\%$)	$ \pm 1/2\rangle$	A	0.53 ± 0.05	17.03 ± 0.08	1.09 ± 0.11
		B	0.37 ± 0.00	17.02 ± 0.08	1.51 ± 0.10
		exptl	outs.	17.0 ± 0.1	not det.
	$ \pm 3/2\rangle$	A	4.02 ± 0.11	8.99 ± 0.24	6.45 ± 0.11
		B	3.98 ± 0.11	8.95 ± 0.24	6.38 ± 0.11
		exptl	4	9.0 ± 0.3	obsc.
	$ \pm 5/2\rangle$	A	9.39 ± 0.07	2.06 ± 0.17	2.34 ± 0.21
		B	9.39 ± 0.07	1.95 ± 0.06	2.55 ± 0.16
		exptl	9.3(5)	?	obsc.
0.058 ($\pm 5\%$)	$ \pm 1/2\rangle$	A	1.37 ± 0.04	15.09 ± 0.15	4.01 ± 0.21
		B	1.11 ± 0.00	15.06 ± 0.15	4.02 ± 0.19
		exptl	not det.	15.1 ± 0.1	4
	$ \pm 3/2\rangle$	A	5.29 ± 0.05	5.53 ± 0.19	5.51 ± 0.16
		B	5.28 ± 0.05	5.08 ± 0.28	5.45 ± 0.15
		exptl	5.6	5.6	5.6
	$ \pm 5/2\rangle$	A	9.91 ± 0.01	0.44 ± 0.05	0.47 ± 0.05
		B	9.90 ± 0.01	0.61 ± 0.01	1.27 ± 0.03
		exptl	not det.	outs.	not det.
0.016 ($\pm 5\%$)	$ \pm 1/2\rangle$	A	1.93 ± 0.01	11.81 ± 0.09	8.06 ± 0.10
		B	1.90 ± 0.01	11.69 ± 0.09	7.87 ± 0.10
		exptl	?	11.7 ± 0.1	8
	$ \pm 3/2\rangle$	A	5.93 ± 0.01	1.85 ± 0.09	1.91 ± 0.10
		B	5.92 ± 0.01	1.82 ± 0.02	2.89 ± 0.04
		exptl	6	?	not det.
	$ \pm 5/2\rangle$	A	9.99 ± 0.00	0.04 ± 0.00	0.04 ± 0.00
		B	9.99 ± 0.00	0.76 ± 0.00	0.93 ± 0.01
		exptl	not det.	not det.	not det.

etermined than in the case of the high-spin siroheme because the temperature dependence is much steeper. The small absolute value of D indicates that the validity of a weak-field approach for our subsequent g -value analysis may break down.

Full g -value analysis of the $S = 9/2$ system

Under the assumption that the lines at $g = 17, 15.1, 11.7$ are the low-field peaks of $|\pm 1/2\rangle$ spectra from three forms of the $S = 9/2$ system of different rhombicities, we have calculated all the corresponding sets of three effective g values for the transitions within the $|\pm 1/2\rangle$, $|\pm 3/2\rangle$, and $|\pm 5/2\rangle$ doublets. We have ignored the $|\pm 7/2\rangle$ and $|\pm 9/2\rangle$ spectra; we expect these to have insignificant transition probability. We have calculated the g values first in the weak-field limit, with variation of the rhombicity parameter E/D . This corresponds to choosing a vertical line through Fig. 4 such that the curve for the highest g value in the $|\pm 1/2\rangle$ panel is intersected at 17, 15.1, or 11.7, respectively. The calculated values are the entries listed as A in Table 3.

We have subsequently also done a complete iterative calculation of the g values without any preset limitation on the relative magnitudes of the zero-field interaction and the electronic Zeeman interaction, as previously detailed [39]. Thus, we have varied the parameter E , while keeping D at the exper-

imentally determined value of -0.56 cm^{-1} . The results are the entries listed as B in Table 3. Table 3 also gives the propagated distribution in the effective g values as a consequence of a 5% distribution in the rhombic zero-field parameter E .

In field-swept EPR spectra, the magnitude of the electronic Zeeman interaction is a constantly varying quantity. Comparison of the effective g values calculated by the two different methods shows that the weak-field limit approach is valid at low magnetic field strength, i.e. for high g values, but becomes increasingly unreliable with increasing magnetic field, i.e. for lower g values. We have previously reached a similar conclusion in relation to the detection of $S = 7/2$ EPR in iron-sulfur proteins [39].

The third class of entries in Table 3, listed as exptl., are the observed, or putatively observed, experimental effective g values. We now proceed to discuss the tentative assignment of these g values to transitions within particular doublets.

For the low-field peak at $g = 17$ two accompanying g values are predicted at 1.1–1.5 and at 0.4–0.5. The last value falls outside the range of our magnet ($B_{\text{max}} \approx 0.9 \text{ T}$; $g_{\text{min}} \approx 0.75$). The middle g value is not experimentally observed which comes as no surprise to us. If the inhomogeneous broadening were from isotropic g strain, then the line widths and intensities at $g = 17$ and 1.5 on a field scale would relate as $(1.5/17)^2$ and $(1.5/17)^{-2}$, respectively (cf. [44]). Thus, the

line at $g = 1.5$ would have a full width at half height of some 0.2 T and an intensity some two orders of magnitude lower than the line at $g = 17$ (i.e. far below the experimental noise level). If there were a contribution from distributed zero-field splitting to the line width, the situation would be even worse as can be seen in Table 3 from the respective g -value distributions at $g = 17$ and 1.5 from a 5% distribution in the quantity E (E -strain or D_E -strain) [44]. This line of reasoning can be equally applied to confirm the essential unobservability of other peaks at intermediate and high-fields which are labeled as 'not detected' in Table 3.

For the transition within the $|\pm 3/2\rangle$ doublet that goes with the $g = 17$ component, a spectrum is predicted with $g \approx 9, 6.4$, and 4. Also, the line at $g \approx 9$ is predicted to be considerably broader on a field scale than the $g = 17$ line for E -strain broadening. This is the line whose intensity we have used to determine the zero-field parameter D . Thus, the value of $D = -0.56 \text{ cm}^{-1}$ applies to the system with $g = 17$ but not necessarily also to the ones with $g = 15.1$ and 11.7. A derivative feature should be at $g = 6.4$; however, this is in the region of the high-spin siroheme spectra and, in fact, it coincides with (i.e. it will be obscured by) the sharp, absorption-shaped siroheme peak at $g = 6.43$. The third peak with the shape of a negative absorption is predicted to be at $g = 4$ and to have an E -strain line width comparable to that of the $g = 9$ line. A spectral feature around $g = 4$ with a width comparable to that of the $g = 9$ line is indeed observed (cf. Fig. 1). However, it is not obvious whether the shape is derivative-like or negative-absorption like. A resonance at $g = 4$ is also predicted as part of the $|\pm 1/2\rangle$ spectrum for the $g = 15.1$ component. Thus, the observed feature at $g = 4$ may be from either one of the above-mentioned sources or from both.

There should be a low-field line at $g = 9.4$ for the $|\pm 5/2\rangle$ doublet and we believe we observe this as a small, sharp shoulder on the $|\pm 3/2\rangle$ $g = 9$ line. This assignment is consistent with the smaller line width compared to that of the $g = 9$ line as predicted from a distribution in the quantity E . The other two lines of the $|\pm 5/2\rangle$ spectrum are not identified.

For the less rhombic form of the $S = 9/2$ system, characterized by the $g = 15.1$ line, an incidental near-isotropy is predicted for the spectrum from the $|\pm 3/2\rangle$ doublet in the region $g \approx 5.1 - 5.5$. We find a feature of considerable intensity at $g \approx 5.6$ in the high-spin siroheme spectral region. This line was left over after assignment of neighbouring lines to siroheme components.

The least rhombic form of the $S = 9/2$ system, with the low-field peak at $g = 11.7$ should have a derivative feature at $g \approx 8$. An imaginative inspector of the $T = 4.2 \text{ K}$ spectrum in Fig. 3 might spot what looks like a zero crossing between the $g = 9$ peak and the first siroheme peak. The $|\pm 3/2\rangle$ spectrum should have a low-field peak at $g = 5.92$. We observe a feature around $g \approx 5.9$ for which we have suggested a possible assignment as a very minor, almost axial, high-spin heme. The alternative interpretation given here is equally plausible.

Three experimental entries in Table 3 are unvalued and marked with a question mark. The predicted g values are in the range 1.8–2.1. We have one or two features in this region left over as unassigned from the analysis of the low-spin siroheme spectra. We have, however, at present insufficient grounds to assign these to one or more of the question marks in Table 3.

In summary, the model of an $S = 9/2$ system of variable rhombicity, corresponding with low-field peaks at $g = 17, 15.1$, and 11.7, has as its main predictions a broad, composite peak around $g \approx 9$ and a near-isotropic spectrum in the range

$g \approx 5.1 - 5.5$, in good agreement with experimental observation. All other predictions are at least not inconsistent with thus far obtained data, and are possibly even partially verified by these.

Spin quantifications

The extensive overlap of the different components in the EPR spectra of oxidized desulfoviridin precludes reliable quantification on the second integrals, except for the isotropic contaminants at $g = 2$ and at $g = 4.3$. We have, therefore, quantified all other components on the basis of the first integral of their low-field absorption-shaped peak using the other two measured or calculated g values in the Aasa-Vännegård intensity correction factor [37].

Quantification of all high-spin and low-spin siroheme components adds up to only 0.22 heme molecule per ha tetramer (Table 4). Although a biochemical interpretation of this number is not obvious to us, the observation is not unexpected. Desulfoviridin from *D. gigas* is known to yield siroporphyrin instead of siroheme upon denaturation [3]. Although early EPR integration for this protein was claimed to give 2.1 siroheme molecules/enzyme molecule [41], this number was more recently redetermined at 0.25/molecule enzyme molecule [30, 31]. An important implication of these findings is that, if the iron-sulfur center is present stoichiometrically, then in a large fraction of the molecules this center cannot be coupled to the siroheme, simply because there is no siroheme to couple with.

In order to check our ability to quantify these signals we have done small-scale purifications of assimilatory sulfite reductases and quantified their siroheme EPR spectra, as specified in the last two entries of Table 4. (In general, the protein amount and concentration of these samples proved to be insufficient positively to identify $S = 9/2$ resonance; however, we have thus far taken one EPR sample of *D. vulgaris* assimilatory sulfite reductase, free of desulfoviridin, down to $T = 4.2 \text{ K}$ and, after extensive averaging, have obtained a spectrum rather similar to the 4.2-K trace in Fig. 3.) Double integration of the low-spin siroheme signal of monomeric, assimilatory sulfite reductase from *D. vulgaris* gave 0.8 spin/optically determined enzyme molecule. This number is identical to the result previously reported by Huyghebaert et al. [2]. For the $\alpha_8\beta_4$ complex from *E. coli*, quantification of the low-field $g = 6.70$ peak resulted in 0.76 high-spin siroheme molecule/ β unit. Siegel et al. [9] previously found a number of 0.83. Christner et al. [11] reported a number of 0.92 on the basis of doubly integrated EPR from the isolated monomeric β subunit. The results of our EPR quantifications on assimilatory sulfite reductases are consistent with literature data.

Spin integration of the $S = 9/2$ system is unprecedented and it poses several major problems. The first question is which feature(s) to base the quantification. All transitions are allowed with the exception of that within the $|\pm 1/2\rangle$ doublet (semi)-forbidden. This type of spectra can be expected to have complicated powder transition probability patterns. They are not usually employed for quantification purposes with the exception of the isotropic $g = 4.3$ line in rhombic $S = 5/2$ systems, and the $\Delta_m = 4$ line in $S = 2$ systems. In the latter case comparison is possible with $S = 2$ model systems of known concentration (cf. [37]), an option which is not available to (yet) for $S = 9/2$ systems. At first sight, it would appear that the transition within the $|\pm 1/2\rangle$ doublet does not carry the problem, but this is probably not altogether true. In assigning the $S = 9/2$ g values we have seen that the relative small

Table 4. Quantification of EPR signals in sulfite reductases

D. vulgaris (Hildenborough) desulfoviridin was 1836 μM in units of $1/2\alpha_2\beta_2$; *D. vulgaris* (Hildenborough) assimilatory sulfite reductase was 58 μM in units of α ; *E. coli* assimilatory sulfite reductase was 33 μM in units of $1/4\alpha_3\beta_4$. All quantifications relative to a 10 mM Cu(II) standard were done on data taken at $T = 17$ K, except for the $S = 9/2$ data which were taken at $T = 4.2$ K. All quantifications are based on the first integral of the low-field absorption-shaped peak, except for those of the [3Fe-4S] and the high-spin Fe(III) signal in desulfoviridin and the low-spin siroheme signal in *D. vulgaris* assimilatory sulfite reductase which are based on the total second integral. Corrections for fractional population of the observed doublet within the spin multiplet are based on $D = 9.1$ cm^{-1} (high-spin siroheme in desulfoviridin), $D = -0.56$ cm^{-1} ($S = 9/2$ system in desulfoviridin), and $D = 8.0$ cm^{-1} (high-spin siroheme in *E. coli* sulfite reductase)

Spectral component	g values	Spins	Stoichiometry	
		μM		
<i>D. vulgaris</i> desulfoviridin high-spin siroheme	6.93; 4.95; 1.93	294	0.17	
	6.44; 5.48; 1.98	14		
	low-spin siroheme	2.78–2.71; 2.145–2.085; 1.63	19	0.05
		2.57; 2.28–2.24; 1.70	36	
		2.47; 2.35; 1.78	28	
	[3Fe-4S] ¹⁺	2.0215; 2.001	23	0.01
high-spin Fe(III)	4.3	10	< 0.01	
$S = 9/2$ Fe/S	17.0; (1.10); (0.53)	1036	0.61	
	15.1; (4.01); (1.37)	72		
	11.7; (8.06); (1.93)	17		
<i>D. vulgaris</i> assimilatory sulfite reductase low-spin siroheme	2.43; 2.37; 1.78	48	0.81	
<i>E. coli</i> assimilatory sulfite reductase high-spin siroheme	6.70; 5.27; 1.97	25	0.76	

of the zero-field parameter $D = -0.56$ cm^{-1} implies that the weak-field condition is not met at intermediate and high fields. An implication of this statement is that the $|\pm 1/2\rangle$ spectrum is not a true $S' = 1/2$ system in the sense used by Aasa and Vänngård in their development of the quantification algorithm for biological EPR [37]. In other words, the $|\pm 1/2\rangle$ doublet is not a pure $|\pm 1/2\rangle$ doublet at all as it is mixed with the other doublets by the zero-field interaction term. Therefore, the transition within this $|\pm 1/2\rangle$ doublet becomes less than fully allowed. Reliable quantification of such a system would require an application of the appropriate time-independent spin-Hamiltonian onto the full basis set of the $S = 9/2$ multiplet. Unfortunately, a workable solution to this problem is not available at this time.

We want to settle for an approximate solution by using the Aasa/Vänngård high-field approach on the $|\pm 1/2\rangle$ data. The problem is still not straightforwardly solved as only one of the three g values from these spectra is observed. We choose to use the other two values as calculated in the high-field approach to be consistent with the assumption underlying the quantification formalism. We want, however, to indicate to the reader that our choice is one of limitation and that the final result will be rather sensitive to the g values employed as a consequence of the extreme anisotropy of these spectra. Finally, we realize that we may presently be ignoring yet another problem in as far as the line shape and line width are likely to at least partially reflect a distribution in rhombicities (E-strain). Therefore, the anisotropy and transition probability may significantly vary even over a single, inhomogeneously broadened resonance line.

The results of quantifications on the peaks at $g = 17, 15.1,$ and 11.7 are given in Table 4. With the above developed restrictions in mind, we draw the tentative conclusion that the concentration of $S = 9/2$ spin system is comparable to the concentration of half-enzyme molecules. Thus, we propose as working hypothesis that there are two $S = 9/2$ systems per β_2 tetramer.

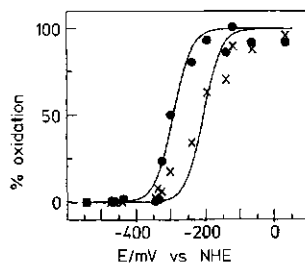


Fig. 8. Reductive titration at pH 7.5 of high-spin components in *D. vulgaris* desulfoviridin with sodium borohydride in the presence of mediators. The $S = 9/2$ putative iron-sulfur cluster was monitored at $g = 9.0$ (X) and the $S = 5/2$ siroheme at $g = 6.93$ (●). The solid traces and the ordinate scaling were obtained by fitting the EPR intensities to $n = 1.0$ Nernst curves in the absence of interaction. EPR conditions were as for Fig. 1

Reduction potentials of the siroheme and the $S = 9/2$ system

A reductive titration with sodium borohydride in the presence of mediators is presented in Fig. 8. Dithionite has not been used in order to avoid the production of sulfite during the titration [4]. The rhombic high-spin siroheme reduces as an $n = 1$ acceptor with a potential $E_m = -295$ mV at pH 7.5. Hall et al. [4] reported $E_m = -310$ mV for the mediated reduction with dithionite of *D. gigas* desulfoviridin at pH 9.0. For the β subunit of *E. coli* assimilatory sulfite reductase, a value of $E_m = -340$ mV was reported at pH 7.7 by Siegel et al. [12].

The peak at $g = 9$, corresponding to the $|\pm 3/2\rangle$ spectrum from the most rhombic $S = 9/2$ component, titrates with a significantly higher reduction potential of $E_m = -205$ mV, and approximately $n = 1$.

At the end point of the titration only a very weak ferredoxin-like signal ($g = 2.07; 1.93; 1.90$) was developed

which integrated to 0.01 $S = 1/2$ spin/ $\alpha\beta$ unit. Prolonged incubation of a second preparation with excess dithionite maximally gave 0.06 spin/unit. This is in contrast to the number of 0.85 reported by Hall et al. for the *D. gigas* desulfoviridin [4]. It is, however, consistent with the negligible intensity that Liu et al. found in the *D. gigas* enzyme [41] and with the low intensities repeatedly reported for the *E. coli* hemoprotein β monomer (e.g. [12]).

DISCUSSION

The active site for the biological six-electron reduction of sulfur(IV) in sulfite was modeled by Siegel and coworkers as a double prosthetic group: a siroheme and a [4Fe-4S] cluster are supposedly electromagnetically linked by strong exchange coupling, and physically linked by a common bridging ligand (cf. [11] and references quoted therein). In spite of its novel character, the model has never been challenged during the decade following its initial formulation. On the contrary, a number of studies have appeared which have all provided added support [12–28]. Furthermore, the model which was originally proposed to describe the active site of assimilatory sulfite reductase from *E. coli* has subsequently been generalized to hold also for sulfite and nitrite reductase from other sources [2, 29–32]. We now want to bring the double-group model to an issue as we see possibilities for its falsification from a chemical, a physical, and an enzymological point of view.

The chemical identity of the iron-sulfur cluster has not been established. The double-group model is based on the premise that the cluster is a [4Fe-4S] $^{(2+;1+)}$ cubane. This was a reasonable assumption in its historical perspective of the knowledge of that time on biological iron-sulfur structures. In recent years, however, evidence has been obtained indicating that other, more complex (i.e. with a larger number of iron ions), structures may occur in proteins [39, 45–48]. The total of available analytical data on iron and acid-labile sulfur content of sulfite reductases is insufficient to choose a particular structure. Early determinations on the *E. coli* enzyme gave 20–21 Fe and 14–15 S^{2-} per 3–4 siroheme molecules in the $\alpha_8\beta_4$ complex [9], and 5.8 Fe and 4.5 S^{2-} per 0.6 siroheme molecule in the isolated β subunit [10]. Extrapolation of these data, would fix the number of non-heme iron atoms to between four and nine/siroheme molecule. In a later determination, only 5.1 Fe and 3.4 S^{2-} atoms were found/ β monomer in protein which contained a stoichiometric amount of siroheme [12]. For the *D. vulgaris* assimilatory sulfite reductase, Huynh et al. reported 4.7 Fe and 4.6 S^{2-} atoms/monomer, where the EPR spectrum integrated to 0.8 siroheme molecule/monomer [2]. Although the authors conclude on the existence of a cubane bridged by a fifth S^{2-} to the siroheme, it seems to us equally valid to extrapolate these numbers to $Fe_{4.5}S_{5.8}$ per siroheme (1.0 Fe), again an inconclusive result. Even more intriguing is the result of Moura et al. who find 18 Fe atoms in a molecule of *D. gigas* desulfoviridin where only 0.25 siroheme molecule/molecule is detected by EPR spectroscopy [30, 31]; they report 21 Fe atoms for another $\alpha_2\beta_2$ dissimilatory sulfite reductase, 'desulfurubidin' from *D. baculatus*, strain DSM 1743 [31]. For both enzymes the authors conclude on the presence of one isolated cubane and one cubane-siroheme complex per $\alpha\beta$ unit (i.e. ≤ 18 Fe expected per tetrameric complex) mainly on the basis of Mössbauer spectroscopic data. Under this model we would expect to find 16.4 Fe in *D. vulgaris* desulfoviridin, taking into account the observed

0.2 spin of siroheme per $\alpha\beta$ unit. In fact, we find some 22 ± 4 Fe and acid-labile sulfur atoms/220-kDa tetrameric molecule.

Although the analytical data are equivocal regarding the identification of the iron-sulfur cluster(s) with the [4Fe-4S] $^{(2+;1+)}$ cubane structure, our present EPR results on *D. vulgaris* desulfoviridin provide explicit arguments against that assignment. An $S = 9/2$ spin is certainly not a fingerprint for a cubane. The observed paramagnetism in the oxidized state of the enzyme is plainly inconsistent with a [4Fe-4S] $^{2+}$ diamagnetic structure. Resonances similar to those reported here have been observed by Moura et al. in the enzymes from *D. baculatus* and *D. gigas* [31]. The authors have proposed an interpretation very different from ours. Notably, a line at $g = 5.8$ was assigned to 'the excited state' of the siroheme, and a line at $g = 9.7$ 'may represent' a high-spin Fe(III) species (ibidem). Both assignments appear to us to be unlikely: excited-state EPR has never yet been observed for $S = 5/2$ heme (the zero-field splitting is too large); a high-spin Fe(III) species with $g = 9.7$ should exhibit a much stronger line at $g = 4.3$, and this is not observed. We propose that the lines at $g = 9.7$ and 5.8, together with a resonance at even higher g value not commented on by the authors but clearly observable in their spectra (cf. Fig. 2 in [31]), are so similar to the set of resonances reported here that they are likely to come from analogous $S = 9/2$ systems. While these last conclusions cannot at this time be generalized to also hold for comparable systems (notably, for the *E. coli* sulfite reductase), they do together with the considerable uncertainty in the analytical data, provide a warning that it is at least premature to use the cubane structure (without protein sequence data) in the interpretation of a 0.3-nm electron density map [27] or to reach cubane ligation from DNA sequence data [28].

An essential element of the double-group model is the strong exchange coupling between the paramagnetic siroheme and a diamagnetic cubane [11, 33]. Our failure to envisage exchange coupling between paramagnets and diamagnets as a real physical possibility was the incentive to initiate the present work. From our observation that the/an iron-sulfur structure, at least in *D. vulgaris* desulfoviridin, is not diamagnetic in the oxidized enzyme, we conclude that the question of the nature of the coupling has now lost much of its practical relevance. Furthermore, the fact that the two spin systems, the $S = 5/2$ siroheme and the $S = 9/2$ iron-sulfur cluster, are independent entities both in their paramagnetism and in their redox chemistry, implies that there are no experimentally based grounds to model the two prosthetic groups as being spatially adjacent.

Our reinterpretation of the paramagnetism of sulfite reductase implies that the iron-sulfur cluster is a novel structure in biology. One datum appears to be at variance with this conclusion, namely, the observation of a ferredoxin-like ' $g = 1.93$ ' spectrum in the reduced enzyme. We have only observed trace amounts of this spectrum in terms of $S = 1/2$ spin concentration/enzyme concentration (the model of Moura et al. [31] would predict four spins/enzyme molecule). However, others have succeeded in boosting this intensity in the *E. coli* enzyme to near stoichiometry in samples in which the siroheme was previously complexed with CO or with CN^- [12]. In the light of our present-day knowledge, we think that these observations are worthy of extension in follow-up studies with the following considerations in mind.

a) It is known from work on iron-sulfur model compounds that the [4Fe-4S] cubane structure is a thermodynamically sink into which other structures can 'spontaneously' be converted [49, 50].

b) The regeneration of active enzyme from the complexed form has not been reported.

c) The complete spectral and redox properties of the putative novel Fe/S structure are yet to be established.

From an enzymological point of view, the one-electron-transferring cubane structure would appear to be a less fortunate choice as part of a biological machinery involved in six-electron-reduction reactions. Two sirohemes plus four iron atoms together would, in principle, provide the capacity for storage of six electrons. However, for the monomeric assimilatory sulfite reductases this capacity would be limited to two electrons only. We have recently provided evidence for the presence of a novel iron-sulfur cluster with the putative core structure $[6\text{Fe}-6\text{S}]$ in a protein of unknown function [48]. This cluster can undergo three subsequent reduction steps within a physiologically compatible range of reduction potentials (see below). We have now also observed $S = 9/2$ EPR signals of considerable integrated intensity from this protein in its one-highest redox state (our unpublished observations). A further iron-sulfur grouping with associated multi-electron transfer capacity would obviously be a useful attribute for the iron-reducing enzyme system.

We hope that the results and considerations presented here will prove to be a first step towards a re-evaluation of the existing blocks for biological six-electron reductions. We also expect them to be a first step towards the development of magnetic resonance methods on very-high-spin systems in biology and, specifically, towards practical solutions of the problems which come with their quantitative spectroscopic analysis.

APPENDIX

For an $S = 5/2$ spin the non-zero elements $E(\langle m_s^i |, |m_s^j \rangle)$ (the upper triangular portion of the) hermitian energy matrix are

$$\begin{aligned} E(5/2, +5/2) &= 10D/3 + 5Z \\ E(5/2, +3/2) &= \sqrt{5} X^- \\ E(5/2, +1/2) &= \sqrt{10} E \\ E(5/2, -5/2) &= 10D/3 - 5Z \\ E(5/2, -3/2) &= \sqrt{5} X^+ \\ E(5/2, -1/2) &= \sqrt{10} E \\ E(3/2, +3/2) &= -2D/3 + 3Z \\ E(3/2, +1/2) &= 2\sqrt{2} X^- \\ E(3/2, -1/2) &= 3\sqrt{2} E \\ E(3/2, -3/2) &= -2D/3 - 3Z \\ E(3/2, +1/2) &= 3\sqrt{2} E \\ E(3/2, -1/2) &= 2\sqrt{2} X^+ \\ E(1/2, +1/2) &= -8D/3 + Z \\ E(1/2, -1/2) &= 3X^- \\ E(1/2, -1/2) &= -8D/3 - Z \end{aligned}$$

in which

$$\begin{aligned} 1/2 g_x^i g_x^j \beta\beta \\ + 1/2 g_x^i g_x^j \beta\beta + i/2 g_y^i g_y^j \beta\beta \\ + 1/2 g_x^i g_x^j \beta\beta - i/2 g_y^i g_y^j \beta\beta. \end{aligned}$$

Similarly, for $S = 9/2$ the elements of the energy matrix

$$\begin{aligned} E(9/2, +9/2) &= 12D + 9Z \\ E(9/2, +7/2) &= 3X^- \\ E(9/2, +5/2) &= 6E \\ E(9/2, -9/2) &= 12D - 9Z \\ E(9/2, -7/2) &= 3X^+ \\ E(9/2, -5/2) &= 6E \\ E(7/2, +7/2) &= 4D + 7Z \\ E(7/2, +5/2) &= 4X^- \\ E(7/2, +3/2) &= 2\sqrt{21} E \\ E(7/2, -7/2) &= 4D - 7Z \end{aligned}$$

$$\begin{aligned} E(-7/2, -5/2) &= 4X^+ \\ E(-7/2, -3/2) &= 2\sqrt{21} E \\ E(+5/2, +5/2) &= -2D + 5Z \\ E(+5/2, +3/2) &= \sqrt{21} X^- \\ E(+5/2, +1/2) &= 3\sqrt{14} E \\ E(-5/2, -5/2) &= -2D - 5Z \\ E(-5/2, -3/2) &= \sqrt{21} X^+ \\ E(-5/2, -1/2) &= 3\sqrt{14} E \\ E(+3/2, +3/2) &= -6D + 3Z \\ E(+3/2, +1/2) &= \sqrt{24} X^- \\ E(+3/2, -1/2) &= 5\sqrt{6} E \\ E(-3/2, -3/2) &= -6D - 3Z \\ E(-3/2, +1/2) &= 5\sqrt{6} E \\ E(-3/2, -1/2) &= \sqrt{24} X^+ \\ E(+1/2, +1/2) &= -8D + Z \\ E(+1/2, -1/2) &= 5X^- \\ E(-1/2, -1/2) &= -8D - Z. \end{aligned}$$

We have previously described in [39] how these matrices can be used for the computation of effective g values.

We thank Dr S. P. J. Albracht for providing access to the parallel-mode EPR facility at the Department of Biochemistry, The University of Amsterdam. We are grateful to R. B. G. Wolbert for help in preparing the enzymes used in this work. We thank Professor C. Veeger for his continuous interest and support. This investigation was supported by the Netherlands Foundation for Chemical Research (SON) with financial aid from the Netherlands Organization for Scientific Research (NWO).

REFERENCES

- Lee, J.-P., Le Gall, J. & Peck, H. D. (1973) *J. Bacteriol.* **115**, 529–542.
- Huynh, B. H., Kang, L., DerVartanian, D. V., Peck, H. D. & LeGall, J. (1984) *J. Biol. Chem.* **259**, 15373–15376.
- Murphy, M. J. & Siegel, L. M. (1973) *J. Biol. Chem.* **248**, 6911–6919.
- Hall, M. H., Prince, R. H. & Cammack, R. (1979) *Biochim. Biophys. Acta* **581**, 27–33.
- Hall, M. H. & Prince, R. H. (1981) *J. Inorg. Nucl. Chem.* **43**, 815–823.
- Vega, J. M. & Kamin, H. (1977) *J. Biol. Chem.* **252**, 896–909.
- Lancaster, J. R., Vega, J. M., Kamin, H., Orme-Johnson, N. R., Orme-Johnson, W. H., Krueger, R. J. & Siegel, L. M. (1979) *J. Biol. Chem.* **254**, 1268–1272.
- Hirasawa-Saga, M., Horie, S. & Tamura, G. (1982) *Agric. Biol. Chem.* **46**, 1319–1328.
- Siegel, L. M., Murphy, M. J. & Kamin, H. (1973) *J. Biol. Chem.* **248**, 251–264.
- Siegel, L. M. & Davis, P. S. (1974) *J. Biol. Chem.* **249**, 1587–1598.
- Christner, J. A., Münck, E., Janick, P. A. & Siegel, L. M. (1981) *J. Biol. Chem.* **256**, 2098–2101.
- Siegel, L. M., Rueger, D. C., Barber, M. J., Krueger, R. J., Orme-Johnson, N. R. & Orme-Johnson, W. H. (1982) *J. Biol. Chem.* **257**, 6343–6350.
- Janick, P. A. & Siegel, L. M. (1982) *Biochemistry* **21**, 3538–3547.
- Janick, P. A., Rueger, D. C., Krueger, R. J., Barber, M. J. & Siegel, L. M. (1983) *Biochemistry* **22**, 396–408.
- Janick, P. A. & Siegel, L. M. (1983) *Biochemistry* **22**, 504–515.
- Christner, J. A., Münck, E., Janick, P. A. & Siegel, L. M. (1983) *J. Biol. Chem.* **258**, 11147–11156.
- Christner, J. A., Janick, P. A., Siegel, L. M. & Münck, E. (1983) *J. Biol. Chem.* **258**, 11157–11164.
- Christner, J. A., Münck, E., Kent, T. A., Janick, P. A., Salerno, J. C. & Siegel, L. M. (1984) *J. Am. Chem. Soc.* **106**, 6786–6794.
- Cline, J. F., Janick, P. A., Siegel, L. M. & Hoffman, B. M. (1985) *Biochemistry* **24**, 7942–7947.
- Cline, J. F., Janick, P. A., Siegel, L. M. & Hoffman, B. M. (1986) *Biochemistry* **25**, 4647–4654.

21. Day, E. P., Peterson, J., Bonvoisin, J. J., Young, L. J., Wilkerson, J. O. & Siegel, L. M. (1988) *Biochemistry* 27, 2126–2132.
22. Young, L. J. & Siegel, L. M. (1988) *Biochemistry* 27, 2790–2800.
23. Young, L. J. & Siegel, L. M. (1988) *Biochemistry* 27, 5984–5990.
24. Han, S., Madden, J. F., Thompson, R. G., Strauss, S. H., Siegel, L. M. & Spiro, T. G. (1989) *Biochemistry* 28, 5461–5471.
25. Madden, J. F., Han, S., Siegel, L. M. & Spiro, T. G. (1989) *Biochemistry* 28, 5471–5477.
26. Han, S., Madden, J. F., Siegel, L. M. & Spiro, T. G. (1989) *Biochemistry* 28, 5477–5485.
27. McRee, D. E., Richardson, D. C., Richardson, J. S. & Siegel, L. M. (1986) *J. Biol. Chem.* 261, 10277–10281.
28. Ostrowski, J., Wu, J.-Y., Rueger, D. C., Miller, B. E., Siegel, L. M. & Kredich, N. M. (1989) *J. Biol. Chem.* 264, 15726–15737.
29. Huynh, B. H., Kang, L., DerVartanian, D. V., Peck, H. D. & LeGall, J. (1985) *Rev. Port. Quim.* 27, 23–24.
30. Moura, I., Lino, A. R., Moura, J. J. G., Xavier, A. V., Fauque, G., DerVartanian, D. V., Peck, H. D., LeGall, J. & Huynh, B. H. (1987) *Recl. Trav. Chim. Pays-Bas* 106, 284.
31. Moura, I., LeGall, J., Lino, A. R., Peck, H. D., Fauque, G., Xavier, A. V., DerVartanian, D. V., Moura, J. J. G. & Huynh, B. H. (1988) *J. Am. Chem. Soc.* 110, 1075–1082.
32. Wilkerson, L. O., Janick, P. A. & Siegel, L. M. (1983) *Biochemistry* 22, 5048–5054.
33. Münck, E. (1982) in *Iron-sulfur proteins* (Spiro, T. G., ed.) pp. 165–175, John Wiley & Sons, New York.
34. Peck, H. D. & LeGall, J. (1982) *Phil. Trans. R. Soc. Lond. B* 298, 443–466.
35. Van der Westen, H. M., Mayhew, S. G. & Veeger, C. (1978) *FEBS Lett.* 86, 122–126.
36. Dutton, P. L. (1978) *Methods Enzymol. Vol. 54*, pp. 411–435.
37. Aasa, R. & Vänngård, T. (1975) *J. Magn. Reson.* 19, 308–311.
38. Hagen, W. R. (1982) *Biochim. Biophys. Acta* 708, 82–98.
39. Hagen, W. R., Wassink, H., Eady, R. R., Smith, B. E. & Haak, H. (1987) *Eur. J. Biochem.* 169, 457–465.
40. Taylor, C. P. S. (1977) *Biochim. Biophys. Acta* 491, 137–149.
41. Liu, C. L., DerVartanian, D. V. & Peck, H. D. (1979) *Biochim. Biophys. Res. Commun.* 91, 962–970.
42. Young, L. J. & Siegel, L. M. (1988) *Biochemistry* 27, 4991–4999.
43. Hagen, W. R., Dunham, W. R., Sands, R. H., Shaw, R. W., Beinert, H. (1984) *Biochim. Biophys. Acta* 765, 399–402.
44. Hagen, W. R. (1981) *J. Magn. Reson.* 44, 447–469.
45. Hagen, W. R., van Berkel-Arts, A., Krüse-Wolters, K. M., Voordouw, G. & Veeger, C. (1986) *FEBS Lett* 203, 59–63.
46. Voordouw, G., Hagen, W. R., Krüse-Wolters, K. M., van Berkel-Arts, A. & Veeger, C. (1987) *Eur. J. Biochem.* 162, 31–36.
47. George, G. N., Prince, R. C., Stockley, K. E. & Adams, M. W. (1989) *Biochem. J.* 259, 597–600.
48. Hagen, W. R., Pierik, A. J. & Veeger, C. (1989) *J. Chem. Soc. Faraday Trans. 1*, 85, 4083–4090.
49. Hagen, K. S., Reynolds, J. G. & Holm, R. H. (1981) *J. Am. Chem. Soc.* 103, 4054–4064.
50. Kanatzidis, M. G., Hagen, W. R., Dunham, W. R., Lester, K. & Coucouvanis, D. (1985) *J. Am. Chem. Soc.* 107, 959–961.

Chapter 8

Redox properties and EPR spectroscopy of the P clusters of the *Azotobacter vinelandii* MoFe protein.

Antonio J. Pierik, Hans Wassink, Huub Haaker and Wilfred R. Hagen

(1993) Eur. J. Biochem. 212, 51-61.

Redox properties and EPR spectroscopy of the P clusters of *Azotobacter vinelandii* MoFe protein

Antonio J. PIERIK, Hans WASSINK, Huub HAAKER and Wilfred R. HAGEN

Department of Biochemistry, Wageningen Agricultural University, The Netherlands

Received September 7, 1992) – EJB 92 1281

In *Azotobacter vinelandii* MoFe protein the oxidation of the P clusters to the $S = 7/2$ state is associated with a redox reaction with $E_{m,7.5} = +90 \pm 10$ mV (vs the normal hydrogen electrode), $n = 1$. A concomitant redox process is observed for a rhombic $S = 1/2$ EPR signal with $g = 1.97$, 1.88 and 1.68. This indicates that both $S = 1/2$ and $S = 7/2$ signals are associated with oxidized P clusters occurring as a physical mixture of spin states. The maximal intensity of the $S = 1/2$ and $S = 7/2$ signals in the mediated equilibrium redox titration is similar if not identical to that of solid-thionine-treated samples. Summation of the spin concentration of the $S = 1/2$ spin state (0.25 ± 0.03 spin/ $\alpha_2\beta_2$) and the $S = 7/2$ spin state (1.3 ± 0.2 spin/ $\alpha_2\beta_2$) confirms that the MoFe protein has absolutely no more than two P clusters. In spectra of enzyme fixed at potentials around -100 mV a very low-intensity $g = 12$ EPR signal was discovered. In parallel-mode EPR the signal sharpened and increased > 10 -fold in intensity which allowed us to assign the $g = 12$ signal to a non-Kramers system (presumably $S = 3$). In contrast with the non-Kramers EPR signals of various metalloproteins and inorganic compounds, the sharp absorption-shaped $g = 12$ signal is not significantly broadened into zero field, implying that the zero field splitting of the non-Kramers doublet is smaller than the X-band microwave quantum. The temperature dependence of this $g = 12$ EPR signal indicates that it is from an excited state within the integer spin multiplet. A bell-shaped titration curve with $E_{m,7.5} = -307 \pm 30$ mV and $+81 \pm 30$ mV midpoint potentials is found for the $g = 12$ EPR signal. We propose that this signal represents an intermediate redox state of the P clusters between the diamagnetic, dithionite-reduced and the fully oxidized $S = 7/2$ and $S = 1/2$ state. Redox transitions of two electrons (-307 ± 30 mV) and one electron ($+90 \pm 10$ mV) link the sequence $S = 0 = S = 3 = (S = 7/2 \text{ and } S = 1/2)$. We propose to name the latter paramagnetic oxidation states of the P clusters in nitrogenase P^{ox1} and P^{ox2} , and to retain P^N for the diamagnetic native redox state. The magnetic circular dichroism and Mössbauer data on thionine-oxidized MoFe protein have to be re-evaluated bearing in mind that the oxidized P clusters can exist in two redox-states. Finally, an account is given of the EPR spectroscopic properties of $S = 9/2$ and other systems obtained upon superoxidation of the MoFe protein.

Nitrogenase is the biological catalyst for the activation of the dinitrogen molecule in aqueous solution. The enzyme complex consists of two dissociable metalloproteins, the 30-kDa $\alpha_2\beta_2$ tetrameric MoFe protein and the homodimeric ≈ 62 -kDa Fe protein. Substrate binding, activation and reduction takes place on the MoFe protein, presumably

on the unique iron-molybdenum cofactor centres (FeMoco). The Fe protein is not only an electron carrier to the MoFe protein but also couples ATP hydrolysis to the substrate reduction.

During the last two decades the extensive spectroscopic and kinetic characterisation of nitrogenase (reviewed in [1]) has been focussed on the component proteins from *Azotobacter vinelandii*, *Clostridium pasteurianum* and *Klebsiella pneumoniae*. In addition to the Mo-containing nitrogenases some organisms like *Rhodobacter capsulatus*, *A. vinelandii* and *A. chroococcum* also have alternative nitrogenase systems [1, 2]. The most significant difference from the Mo nitrogenase system is the absence of molybdenum in the MoFe protein. The vanadium system contains vanadium instead of molybdenum [3, 4], while in the 'third' nitrogenase system apparently an Fe-only protein activates dinitrogen [5].

The MoFe protein, containing 2 Mo, ≈ 30 Fe and acid-labile sulphide ions, is one of the most complex [Fe-S] proteins. On the basis of extensive Mössbauer studies [6–15]

Correspondence to W. R. Hagen, Laboratorium voor Biochemie, Wageningen Universiteit, Dreijenlaan 3, NL-6703 HA, Wageningen, The Netherlands

Fax: +31-8370-84801.

Abbreviations. MoFe protein, the molybdenum-iron protein of nitrogenase; FeMoco, iron-molybdenum cofactor; MCD, magnetic circular dichroism; NHE, normal hydrogen electrode; Av1, Av2, Ac2, Kp1, Kp2, Cp1, Cp2, the MoFe protein and Fe protein of *Azotobacter vinelandii*, *A. chroococcum*, *Klebsiella pneumoniae* and *Clostridium pasteurianum*, respectively; P^N , P^{ox1} , P^{ox2} , P^{EROX} , the iron-sulfur P cluster in different redox states, namely, native (i.e. dithionite-reduced), one-step-oxidized, two-steps-oxidized, beyond two-steps-oxidized, respectively.

Enzyme. Nitrogenase (EC 1.18.6.1).

the Fe ions of the MoFe protein have been grouped into two types of clusters: the FeMoco and the 'P' clusters [9]. The most thoroughly investigated type is the FeMoco centre containing, tightly associated, a single Mo atom, some 5–8 Fe/S²⁻ ions and (R)-homocitrate (see [1] and references therein). The FeMoco centre is extractable [16] and reconstitutable [13]. In the dithionite-reduced protein it exhibits $S = 3/2$ EPR signals with $g = 4.3, 3.7, 2.0$ for the ground doublet [7, 17]. This dithionite-reduced FeMoco centre can be oxidized by a one-electron process with $E_m \approx -100$ mV in the protein [18] to a diamagnetic redox state [9, 15]. From the double integration of the $S = 3/2$ EPR signal [7], the molybdenum content [19] and the Mössbauer spectroscopy, it has been inferred that two FeMoco centres are present in the $\alpha_2\beta_2$ MoFe protein.

With two FeMoco centres containing 5–8 Fe/S²⁻ ions and a total content of some 30 Fe/S²⁻ ions/protein, an approximate 14–20 Fe and S²⁻ are to be accounted for by the P clusters. While the extractability and $S = 3/2$ EPR signals have been used to define the FeMoco centres in reasonable detail, the stoichiometry, spin state and redox potential(s) of the P clusters are controversial. Two models have been formulated. In the Mössbauer-derived model [9] a P cluster is a special form of the [4Fe-4S] cubane structure, namely, with one Fe atom distinguishable from the other three as it has a pure high-spin ferrous character in the dithionite-reduced form. In this model the tetrameric MoFe protein contains four P clusters. These clusters would further differ from the classical cubanes in that, upon oxidation with thionine, they have an 'EPR-silent' uniaxial doublet ground state within a $S = 3/2, 5/2, 7/2$ or $9/2$ multiplet [9, 12]. Support for this model was found by low-temperature magnetic circular dichroism (MCD) studies, from which it was concluded that the ground state was an electronic doublet with an estimated $g_{||} \approx 11-12$ [20–22].

In the alternative model of Hagen and coworkers [23] the 4×4 -Fe P cluster concept was redefined after the discovery of $S = 7/2$ EPR signals in solid-thionine-oxidized MoFe proteins. On the basis of an observed stoichiometry of approximately two $S = 7/2$ spin/protein, it was proposed that a P cluster may be a larger grouping of some eight Fe atoms; this implies a MoFe protein with only two P clusters/tetramer. Each P cluster would have the capacity to accept more than one reducing equivalent. This view was subsequently challenged by Münck and collaborators who claimed the $S = 7/2$ EPR to be an artifact resulting from the use of solid thionine as the oxidant [24]. However, the low-resolution X-ray structure of *C. pasteurianum* MoFe protein indicated a spatial arrangement with two supercluster-like P clusters rather than four isolated cubanes [25].

Supported by the observation of $S = 7/2$ EPR signals after treatment with soluble oxidants other than thionine [26], we determined the redox properties of this EPR signal by a mediated equilibrium titration. These experiments led to the discovery of several novel EPR signals with associated redox transitions, which will also be described and discussed in this paper.

MATERIALS AND METHODS

Azotobacter vinelandii ATCC 478 was grown and nitro-genase MoFe protein assayed and purified by standard procedures [27]. After the final precipitation step with MgCl₂, the MoFe protein was dissolved in 25 mM Tes/NaOH

pH 7.5, 250 mM NaCl, 0.5 mM Na₂S₂O₄. Centrifugation $20000 \times g$ (15 min) removed a minor, not readily dissolvable precipitate. Dithionite and residual MgCl₂ were removed anaerobically by filtration on a Bio-Gel P6DG column equilibrated with 25 mM Tes/NaOH pH 7.5, 250 mM NaCl. The MoFe protein solution (≈ 25 mg/ml) was finally concentrated fivefold with a 50-ml-capacity Amicon device equipped with a YM-100 filter. No significant precipitates were observed after a $20000 \times g$ (10-min) centrifugation step. The preparation had the following characteristics: protein concentration, 97 mg/ml; specific activity, 2300 nmol ethylene produced $\times \text{min}^{-1} \times \text{mg}^{-1}$ (Av_2/Av_1 ratio ≈ 30); Mo content, 1.7 mol ion/mol. Analytical procedures for the determination of protein (microbiuret) and molybdenum (dithiol method) were as described [28]. The molar protein concentration, EPR spin quantitation and molybdenum stoichiometry were calculated using a molecular mass of 229344 Da for the $\alpha_2\beta_2$ complex, determined from the DNA-derived amino acid sequence of *Azotobacter vinelandii* OP (ATCC 13905) [29].

For acetylene reduction assays of samples from the redox titration microliter quantities were diluted with 25 mM Tes/NaOH pH 7.5, 250 mM NaCl containing excess dithionite. Within the experimental error of 5–10% caused by the dilution, full catalytic activity of MoFe protein was maintained. This applies to comparison of (a) the original dithionite-reduced MoFe protein (97 mg/ml); (b) samples with mediators, withdrawn directly from the titration cell; and (c) EPR samples thawed anaerobically.

Dye-mediated redox titrations (cf. [30]) of MoFe proteins were performed in an anaerobic cell under purified argon. The MoFe protein/mediator mixture was in 25 mM Tes/NaOH pH 7.5, 250 mM NaCl. Methyl and benzyl viologen, neutral red, safranin O, phenosafranin, anthraquinone-2-sulfonate, 2-hydroxy-1,4-naphthoquinone, indigo disulfonate, resorufin, methylene blue, phenazine ethosulfate, 2,6-dichloroindophenol and *N,N,N',N'*-tetramethyl-*p*-phenylenediamine mediators were used at a final concentration of 40 μM . The redox potential was adjusted with freshly prepared 50 mM sodium dithionite and potassium ferricyanide solutions in 0.5 M Tes/NaOH pH 7.5 containing 250 mM NaCl. Potentials reported in this paper refer to potentials with respect to the normal hydrogen electrode (NHE) and were obtained by using a potential of +246 mV vs NHE for the saturated calomel reference electrode at 22°C [30]. Media containing MoFe protein mixtures with a stable potential could be maintained in the -450 mV to +250 mV range (vs NHE). Stabilization of the potential usually required 1–5 min. This probably corresponds to the attainment of a redox equilibrium between titrant, mediating dyes and MoFe protein. At redox potentials higher than +250 mV vs NHE considerable deactivation occurred (i.e. > 2 mV/min) with concomitant loss of activity. As will be discussed in Results, a likely explanation for this phenomenon is breakdown of the clusters.

As a check, redox titration samples were re-reduced by sixfold dilution with 100 mM dithionite, 500 mM Tes/NaOH pH 7.5. Samples were incubated for 10 min at room temperature prior to freezing and the intensity of the $g = 3.7$ $S = 7/2$ FeMoco EPR signal was compared with the starting material.

Solid-thionine-oxidation was according to Hagen et al. [23]: 150 μl dithionite-free MoFe protein solution (97 mg/ml) was anaerobically incubated with 1.5 mg thionine (Ludox Eastman). Samples oxidized with stoichiometric amounts of dissolved thionine (cf. [24]) were prepared by mixing dithionite-free MoFe protein solution with thionine solution in demineralized water ($\epsilon_{602\text{nm}} = 56000 \text{ M}^{-1} \text{ cm}^{-1}$, 2 electro-

onine molecule). The thionine solution was filtered through a 0.22- μm Millex filter to remove undissolved dye prior to vacuum/argon cycles.

EPR instrumentation, calibration, spin quantitation and software were as in [31]. Effective g -values for the subpeaks of the doublets of the $S = 9/2$ multiplet, assuming validity of the weak-field approach, were calculated (see [32]) with the program RHOMBO (available upon request).

RESULTS AND DISCUSSION

Equilibrium-mediated titration of the FeMoco $S = 3/2$ EPR signal

In spectroscopic studies on the P clusters, the redox state of the FeMoco centre is usually used as a convenient internal standard to monitor the degree of oxidation of the MoFe protein [9, 20, 23]. Fig. 1A shows the mediated redox titration of the $S = 3/2$ signal as a reference to both previous and new EPR spectroscopic results on the P clusters. Corrected for the minor depopulation of the EPR-active $|\pm 1/2\rangle$ doublet, 1.7 ± 0.2 spin/ $\alpha_2\beta_2$ was determined by double integration (2–12 K). As a benchmark for the single integration method of Aasa and Vänngård [33], the absorption-shaped $g = 3$ and $g = 2.0$ signals were also used to calculate the spin concentration. Relative deviations from the values derived from double integration were 2–8%.

The observed $E_{m,7.5} = -42 \pm 10$ mV for the FeMoco centre in our *A. vinelandii* preparation is in good agreement with those published for *A. vinelandii* and *A. chroococcum* MoFe proteins, $E_{m,7.9} = -48$ mV and -46 mV [18]. Midpoint potentials in MoFe protein of other bacteria range from 177 mV to 0 mV [18, 34, 35].

Equilibrium redox titration of the $S = 7/2$ EPR signal

Hagen and coworkers have shown that *A. vinelandii* MoFe protein exhibits $S = 7/2$ EPR signals after treatment with solid thionine [23]. To demonstrate whether solid thionine induces these signals by binding or by oxidation, we performed a mediated equilibrium redox titration of the $S = 7/2$ EPR signals of *A. vinelandii* MoFe protein (Fig. 1C). At liquid nitrogen boil-off temperatures were found to give the best reproducible readings for the $g = 10.4$ amplitude, although the optimal temperature for the $g = 10.4$ EPR signal of the $|\pm 1/2\rangle$ doublet is some 40 K [23]. At 94 K the detection limit for the $g = 10.4$ $S = 7/2$ EPR signal corresponded to a MoFe protein concentration of 1 mg/ml (5 μM). The $g = 10.4$ $S = 7/2$ signals titrated with a bell-shaped curve, attaining maximum intensity around +200 mV, and with midpoint potentials of $+90 \pm 10$ mV and $+345 \pm 30$ mV for an assumed one-electron process. Within the experimental errors imposed by the reproducibility of the titration and solid thionine treatment, the maximal amplitude of $S = 7/2$ signals after the titration and solid thionine treatment were identical. Apparently the $S = 7/2$ signals are not due to adsorption of thionine on MoFe protein to thionine particles, since thionine was not present in the mediator mixture. Also since the mediators were each present at 40 μM , compared to the 0.6 mM concentration of P clusters, binding of mediators to the protein is an unlikely explanation for the presence of stoichiometric $S = 7/2$ signals. This is in agreement with the observation that $S = 7/2$ EPR signals can also be generated in Kp1 by soluble non-dye oxidants like ferricyanide [26]. The effectiveness of solid thionine must reside in the combined

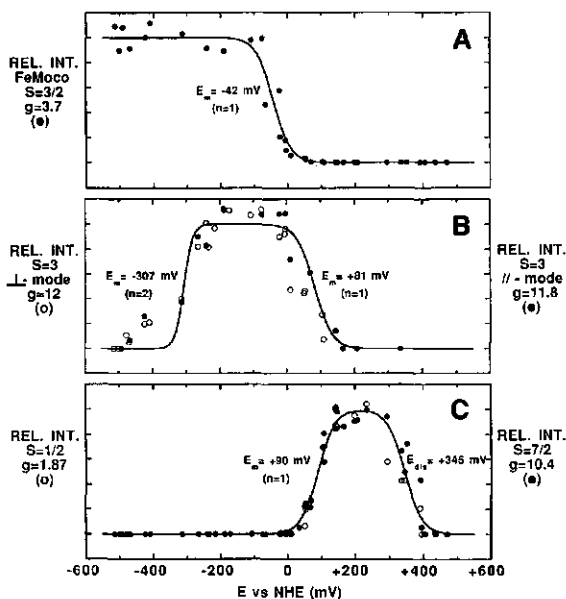


Fig. 1. Mediated redox titration of the $S = 3/2$, $S = 3$, $S = 7/2$ and $S = 1/2$ EPR signals of *A. vinelandii* MoFe protein. Relative intensities (REL. INT.) of EPR signals associated with the MoFe protein are plotted as a function of the equilibrium redox potential in the presence of mediators (see Materials and Methods). The solid lines are least-squares fits to fixed- n -value Nernst equations with E_m and n values as indicated using the closed dots. For convenience data points for potentials $> +300$ mV are presented and a $+345$ -mV, $n = 1$ curve is drawn for the right half of the bell-shaped curve in C. This presentation is artificial: the solution potential is probably not in equilibrium with the protein as complex non-Nernstian changes and inactivation of the MoFe protein occur (*vide infra*). EPR conditions: (A, ●) $S = 3/2$, amplitude of the $g = 3.7$ zero-crossing feature; modulation amplitude, 1.6 mT; microwave power, 20 mW; temperature, 14 K; (B, ○) $S = 3$, $g \approx 12$, recorded with a normal EPR spectrometer (i.e. microwave magnetic field perpendicular to the magnetic field), surface enclosed by the absorption-shaped feature; modulation amplitude, 1.6 mT; microwave power, 200 mW; temperature, 20 K; (B, ●) $S = 3$, $g = 11.8$, recorded with a dual-mode cavity operating in the parallel mode, amplitude of the $g = 11.8$ peak; modulation amplitude, 1.25 mT; microwave power, 200 mW; temperature, 20 K; (C, ○) $S = 1/2$, amplitude of the $g = 1.87$ zero-crossing feature; modulation amplitude, 1.6 mT; microwave power, 200 mW; temperature, 20 K; (C, ●) $S = 7/2$, amplitude of the $g = 10.4$ peak; modulation amplitude, 0.8 mT; microwave power, 200 mW; temperature, 94 K. All spectra were recorded with a 100-kHz modulation frequency and 9.29–9.32-GHz microwave frequency (except for parallel mode: 9.09 GHz).

properties of redox potential and solubility, as already noted by Münck and collaborators [24] in order to explain their failure to produce $S = 7/2$ signals with other oxidation procedures. The absence of $S = 7/2$ signals in their preparations might be due to the inability of dissolved thionine to oxidize MoFe to the top of the bell-shaped curve of Fig. 1C.

Why are the 6–10 equivalents of thionine added not able to oxidize the MoFe protein to the $S = 7/2$ state? Although the measured potentials of a thionine solution and suspension are almost identical [24], the solution potential after mixing with MoFe protein is quite different. With stoichiometric amounts of (dissolved) thionine the $\ln([\text{thionine ox}]/[\text{thio-}$

nine red]) term in the Nernst equation dramatically changes. With 6–10 equivalents added and consumption of 2–4 equivalents, the solution potential will be close to the midpoint potential of thionine (+42 mV at pH 7.5 [36]). Residual amounts of dithionite would further lower the solution potential in the dissolved-thionine procedure. With an excess solid thionine present, the drop of the solution potential will be less, since the formation of some reduced thionine does not change the large excess oxidized thionine (solid thionine will come into solution).

Additional evidence supporting this interpretation was obtained from experiments with dithionite free MoFe protein in 50 mM Tes/NaOH, 250 mM NaCl, pH 7.5, treated with graded amounts of aqueous-thionine solution. $S = 3/2$ FeMoco signals were abolished with 3–5 equivalents. As anticipated from the above considerations, 0–10 equivalents did not produce $S = 7/2$ signals. But 10–30 equivalents gradually yielded $S = 7/2$ signals with a maximum amplitude of $\approx 90\%$ of a parallel sample treated with solid thionine (data not shown).

Evidence for a $S = 1/2$ and $S = 7/2$ physical spin mixture

In a number of studies on MoFe proteins substoichiometric $S = 1/2$ EPR signals have been observed. These $S = 1/2$ signals can be divided into four main groups, according to the redox state and catalytic activity of the MoFe protein: (I) axial $S = 1/2$ signals ($g_{\parallel} = 2.05$, $g_{\perp} = 1.92$), associated with the reduced state of the catalytically inactive 'demolybdo' form, $E_m \approx -400$ mV [17, 34, 37]; (II) axial $S = 1/2$ signals ($g_{\parallel} = 2.09$, $g_{\perp} = 2.00$), associated with an oxidized form of the oxygen or excess ferricyanide inactivated MoFe protein [17, 38]; (III) rhombic $S = 1/2$ signals ($g_{av} > 2$, g_z between 2.07 and 2.17), which can be observed only during turnover [39–41]; (IV) rhombic $S = 1/2$ signals ($g_{av} < 2$, g_z between 1.6 and 1.8), which are associated with oxidized MoFe protein [2, 17, 24, 42, 43].

The nitrogenase preparation used in our study was almost totally devoid of the group I and II axial species in the -500 mV to $+300$ mV range (< 0.02 spin/protein). Also, no group III $S = 1/2$ signals were observed. In the 0 to $+400$ mV range of the mediated redox titration of *A. vinelandii* MoFe protein group IV $S = 1/2$ signals were observed (Fig. 2). The g -values of the main rhombic species were typical for MoFe protein group IV type signals. They were all below the g -value of the free electron ($g = 1.97$, 1.88 and 1.68) and were almost identical to those of oxidized Kp1 [42], solid-thionine-oxidized Kp1 [24], controlled- O_2 -exposed Av1 [43] and similar to ferricyanide-oxidized Cp1 [17, 38]. The appearance and disappearance of the rhombic $S = 1/2$ EPR signal was concomitant with that of the $S = 7/2$ signals (Fig. 1C). This was confirmed by the observation that solid or soluble (10–30 equivalents) thionine-treated samples also exhibited this rhombic $g < 2$ $S = 1/2$ EPR signal. The observed midpoint potential of $+90 \pm 10$ mV is almost identical to the $+85$ mV measured by O'Donnell for similar EPR signals of Kp1 [42].

It seems likely that the $S = 1/2$ and $S = 7/2$ spin states are degenerate electronic ground states of P clusters with the same level of oxidation. For [4Fe-4S]⁺ model compounds [44] the term 'physical spin mixture' is used to describe this phenomenon. An alternative model is that the $S = 7/2$ state is a low-lying excited electronic state of the $S = 1/2$ ground state. If a P cluster is composed of some eight spin-coupled d^5 and d^6 iron ions, the number of possible spin coupling

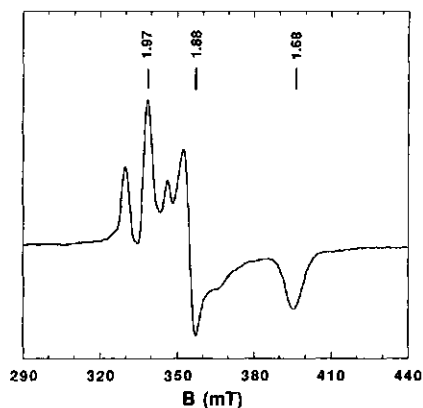


Fig. 2. The rhombic $S = 1/2$ EPR signal of *A. vinelandii* MoFe protein, which co-titrated with the $S = 7/2$ EPR signals. The equilibrium redox potential of MoFe protein (64 mg/ml; 0.28 mM), 50 mM Tes/NaOH, 250 mM NaCl, pH 7.5 was adjusted $+236$ mV vs NHE by addition of buffered ferricyanide solution in the presence of redox mediators (see Materials and Methods). The g -values of the main rhombic $S = 1/2$ species are indicated. With the 200-mW incident power, the intense radical signal derived from the redox mediator mixture is heavily saturated and appears as absorption-shaped peak at $g \approx 2$. EPR conditions: microwave frequency, 9.31 GHz; modulation frequency, 100 kHz; modulation amplitude 1.6 mT; microwave power, 200 mW; temperature, 20 K.

schemes is large. It is therefore possible that an oxidized cluster can indeed have more than one energetically favourable spin state. Our observations indicate that the magnetic properties of the oxidized P clusters are best described as physical spin mixture (cf. [44]). If the $S = 7/2$ spin state were a low-lying electronic excited state of the $S = 1/2$ state, marked deviation of Curie's law should have been observed for the $S = 1/2$ EPR signals. However, the rhombic $S = 1/2$ signals followed Curie's law over the 4.2–28 K temperature range: namely, the product of the signal's second integral and the absolute temperature was a constant $\pm 10\%$ over the range. A second piece of evidence can be found in the temperature dependence of the population of the $|\pm 1/2\rangle$ and $|\pm 3/2\rangle$ doublets of the $S = 7/2$ multiplet. Hagen and coworkers showed that for $D = -3.7$ cm⁻¹ the amplitude of the $g = 10.4$ EPR signal from the $|\pm 1/2\rangle$ doublet perfectly obeyed a $S = 7/2$ Boltzmann distribution function in the 4.2–100 K range [23]. Although not stated in [23], the temperature dependence of the $g = 5.8$ EPR signal from the $|\pm 3/2\rangle$ doublet can be used to obtain a similar D value with a normal $S = 7/2$ Boltzmann distribution function. The temperature dependence of two doublets thus indicates that the $S = 7/2$ multiplet is energetically isolated from both lower and higher electronic spin states.

Two or four P clusters: incorporation of the $S = 1/2$ EPR signals

In the solid-thionine oxidation of Av1, Kp1 and Ac1 [24] 1–2 $S = 7/2$ systems were observed. If $S = 7/2$ and $S = 1/2$ form a physical spin mixture of the oxidized P clusters the spin count should be reevaluated. The amplitudes of spectral shape of $S = 1/2$ and $S = 7/2$ EPR signals were almost identical for solid-thionine-treated samples and sampl

poised at redox potentials around +200 mV. Double integration of the full 300–400-mT part of the EPR spectrum recorded under non-saturating conditions gave $0.25 \pm 0.03 = 1/2\alpha_2\beta_2$ (4.2–25 K). A 5–20% correction was made for the contribution of the overmodulated and heavily saturated radical signal around $g = 2.00$. From comparison of this double integration of the full spectrum with single integration [33] of the absorption-shaped $g = 1.97$ or $g = 1.68$ peaks, it was estimated that the main rhombic species accounts for 5% of the spin concentration of the $g = 1.6$ – 2.0 region. Spectral features that contribute to the residual 15% (i.e. $0.04 = 1/2\alpha_2\beta_2$) are visible in Fig. 2 as a peak at $g = 1.91$, a trough at $g = 1.82$ and a broad shoulder at $g = 1.60$. We have presented the titration of the $g = 1.88$ amplitude of the main rhombic $S = 1/2$ species in Fig. 1. The $g = 1.91$, 1.82 and 1.61 features titrate in an almost identical way (not shown). An occasional sample exhibited a somewhat higher contribution of the minor species, with a concomitant increase of a $g = 2.02$ shoulder on the low-field side of the radical signal. Multiple $S = 1/2$ forms with different g -tensors, but with similar average g -value and line-widths are so known to occur in Kp1 [24, 42]. The forms interconvert with pH [42] and are dependent on the preparation [24] and organism [17, 24, 38, 41, 42] (and this study).

In agreement with previous work, spin quantitation of the $S = 7/2$ species by single integration [33] of the $g = 10.4$ signal amounted to some 1.3 ± 0.2 spin/ $\alpha_2\beta_2$. The 33% uncertainty in our previous quantitation was considerably reduced by recording spectra at 90 K. The estimated uncertainty of 7 cm^{-1} in the D value then propagates an uncertainty of less than 10%, which is comparable to the combined error of values for the single integration, protein concentration etc. The broadening of the $g = 10.4$ feature might have led to a minor underestimation. From summation of the spin counts $S = 7/2$ and $S = 1/2$ (to a total of 1.5 ± 0.25 spin/ $\alpha_2\beta_2$), it is clear that the MoFe protein has absolutely no more than two P clusters. We assume that this spin count extrapolates two P clusters based on the observation of Braaksmas et al. [27] that Av1 preparations can have an even higher specific activity of up to 3000 nmol ethylene produced $\times \text{mg}^{-1}$. The top of the bell-shaped titration curve is broad enough to allow a full generation of the $S = 1/2$ and $S = 7/2$ physical spin mixture before further oxidation of this redox state takes place. We will discuss the oxidative half of the bell-shaped titration curve of the $S = 1/2$ $S = 7/2$ spin mixture in a later section.

Novel $g = 12$ EPR signal from MoFe protein

At intermediate redox potentials we found a small absorption-shaped peak with a maximal amplitude at $g = 6 \pm 0.4$ ($g \approx 12$) superimposed on a very broad feature extending into zero field (Fig. 3). The unusual $g \approx 12$ signal could only be detected in a narrow temperature window, with the highest microwave power and modulation amplitude settings. At liquid helium temperature the levels between which the EPR transition occurs were apparently not sufficiently modulated to result in a detectable signal, while relaxational broadening and Curie-law behaviour prohibited detection at higher temperature. It is obvious from the low signal/noise ratio of the 68-mg/ml sample in Fig. 3 why the $g \approx 12$ signal escaped attention in previous studies. For comparison, the amplitude of this $g \approx 12$ signal is 20-fold, 100-fold and 10-fold less intense than the maximal amplitudes of the $g =$

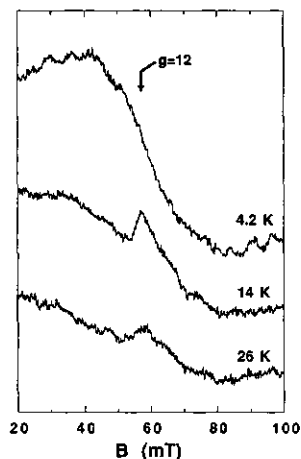


Fig. 3. Temperature dependence of the $g \approx 12$ (normal-mode) EPR signal of *A. vinelandii* MoFe protein poised at -190 mV vs NHE. The redox potential of MoFe protein (68 mg/ml; 0.30 mM) in 50 mM Tes/NaOH, 250 mM NaCl, pH 7.5, was set in the presence of redox mediators (see Materials and Methods). EPR conditions: microwave frequency, 9.32 GHz; modulation frequency, 100 kHz; modulation amplitude 1.6 mT; microwave power, 200 mW.

10.4 ($S = 7/2$), $g = 3.7$ ($S = 3/2$) and $g = 1.88$ ($S = 1/2$) EPR signals, respectively.

A direct experiment to prove the Kramers or non-Kramers origin of an EPR signal is the application of dual-mode EPR spectroscopy [32, 45, 46]. By the use of a dual-mode cavity attached to normal EPR spectrometer, the orientation of the microwave field compared to the magnetic field can be changed. While with the normal X-band EPR spectrometer (microwave \perp magnetic field) in principle only microwave-induced transitions with $|\Delta_{m1}| = 1$ can be observed (i.e. Kramers systems), this dual-mode spectrometer can also be operated with a parallel microwave and magnetic field. This selectively enhances the transition probability of microwave transitions with $|\Delta_{m1}| = 0$ (non-Kramers systems), and almost totally abolishes the $|\Delta_{m1}| = 1$ transitions. The usefulness of the dual-mode EPR spectrometer for the discrimination between Kramers and non-Kramers EPR signals is demonstrated in Fig. 4. In the perpendicular mode (Fig. 4, lowest trace) the $g \approx 12$ signal is almost invisible, due to the reduced sensitivity of the dual-mode spectrometer; in the parallel mode however a $g = 12$ (maximal amplitude at 11.9 ± 0.2) signal has a >10 -fold intensity. No saturation of the $g = 12$ signal was observed in the parallel mode at any detection temperature up to the maximal incident microwave power level of 200 mW. With optimized settings the sharp $g = 12$ parallel mode EPR signal is even detectable with 20 μM MoFe protein (not shown). The increased intensity and the fourfold sharpening of the $g = 12$ line to 1.7 mT (full width at half height at 10 K) proves that this EPR signal must be associated with microwave-induced transitions with $|\Delta_{m1}| = 0$, i.e. within a non-Kramers system [32, 45, 46]. A number of observations rule out an adventitious correlation between the $g \approx 12$ normal-mode EPR signal and the sharp $g = 12$ parallel-mode EPR signal. Both temperature dependence (Figs 3 and 4), titration behaviour (Fig. 1B) and position in the EPR spectrum leave no doubt that these signals are associated with the same non-Kramers paramagnet.

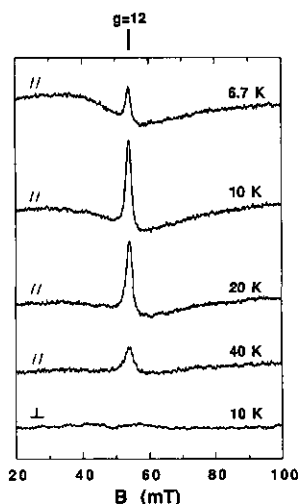


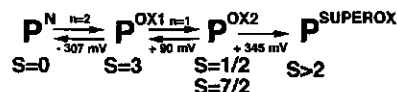
Fig. 4. Temperature dependence of the $g = 11.8$ parallel-mode EPR signal of *A. vinelandii* MoFe protein poised at -190 mV vs NHE. The equilibrium redox potential of MoFe protein (68 mg/ml; 0.30 mM) in 50 mM Tes/NaOH, 250 mM NaCl, pH 7.5, was set in the presence of redox mediators (see Materials and Methods). Spectra were recorded with an EPR spectrometer with a dual-mode cavity operating in the parallel mode (upper four traces, //) or perpendicular mode (\perp , lower trace). EPR conditions: microwave frequency, 9.09 GHz (//) and 9.14 GHz (\perp); modulation frequency, 100 kHz; modulation amplitude 1.25 mT; microwave power, 200 mW.

In addition to the absorption-shaped $g = 12$ EPR signal, a wide 0–80-mT feature with a different temperature dependence was observed (Figs 3 and 4). Like the $g = 12$ signal, the intensity in the parallel mode increased (10-K traces of Fig. 4), defining a non-Kramers origin. The signal does not change significantly over the complete titration. We assume that it represents a minor contaminant, possibly ferrous ions.

The $g = 12$ EPR signal is associated with the P clusters

Although normal-mode EPR amplitudes have been presented in Fig. 1B, one could argue, that with the 10–20 K optimal temperature for the $g = 12$ signal, $g = 10.4$ $S = 7/2$ EPR signals might have interfered. Actually, with the 56-mT ($g \approx 12$) and 64-mT ($g = 10.4$) positions and ≈ 6 -mT line-widths, the absorption-shaped EPR signals were resolved only for the 10–15-K range or for samples with low $g = 10.4$ amplitudes. The tenfold enhanced sensitivity and the complete removal of the $g = 10.4$ signal in the parallel mode, made it possible to measure the redox properties of the $g = 12$ signal in a very reliable way in the full redox window. In Fig. 1B a tentative fit to the Nernst equation is presented using the amplitudes of the 16 parallel-mode data points. Since a redox transition between the diamagnetic dithionite-reduced state and $g \approx 12$ integer spin state requires an even number of electrons, we have assumed $n = 2$ for this step. A precise n value for this transition is not borne out by the data, whose curvature (Fig. 1B) is suggestive of a slow redox equilibrium and/or an anticooperative effect. A fit to a three-redox-states Nernst curve gave midpoint potentials of -307 ± 30 mV (assuming $n = 2$) and $+81 \pm 30$ mV ($n = 1$). The similarity of the $S = 1/2/S = 7/2$ midpoint potential

($+90 \pm 10$ mV) and the (approximate) midpoint potential of the $g = 12$ signal suggests that these processes might be linked. This would identify the $g = 12$ non-Kramers system with the P clusters in a more reduced state than the $S = 1/2$ $S = 7/2$ state. Scheme 1 summarizes the redox behaviour of the P clusters, including the disappearance of the $g = 12$ signal at low potentials and the non-reversible loss of $S = 1/2$ $S = 7/2$ EPR signals at high redox potentials (apparent $E_m = +345$ mV):



Scheme 1.

in which P^{N} is the $S = 0$ native dithionite-reduced redox state, P^{OX1} is the first oxidized redox state exhibiting the non-Kramers $g = 12$ EPR signal, P^{OX2} is the second oxidized redox state occurring as a physical mixture of $S = 1/2$ and $S = 7/2$ spin states and $\text{P}^{\text{SUPEROX}}$ is a superoxidized redox state with magnetic properties, which will be discussed below. Scheme 1 unifies our EPR results and a number of Mössbauer, MCD and susceptibility observations, but at the same time poses questions with regard to the spin state of P^{OX1} . We summarize our evidence for this scheme below.

Smith and coworkers have monitored dye-mediated redox titrations of Kp1 with Mössbauer spectroscopy. They found that oxidation of Kp1 to what they call the 'M1 species' was associated with a one- or two-electron redox process with $E_{m,8,7} = -340$ mV [11]. In the nomenclature used by Münck and coworkers for Av1 and Cp1, this corresponds to oxidation of the P clusters from the redox state P^{N} (diamagnetic) to the state P^{OX} (paramagnetic) [7, 9, 12]. The close similarity between the P-cluster midpoint potential of Kp1 (-340 mV) and the -307 -mV midpoint potential of the low-potential side of the bell-shaped titration curve for the $g = 12$ EPR signal of Av1 (Fig. 1) suggests that these redox processes reflect the same redox transition in the P clusters. Since the $S = 1/2$ midpoint potential of Kp1 [42] is also identical to the $S = 1/2/S = 7/2$ midpoint potential of Av1 (Fig. 1) the frameworks of Av1 and Kp1 P-cluster redox processes appear to be mutually consistent. The observation of P-cluster oxidation before FeMoco oxidation in Mössbauer monitored thionine titrations of Av1 (Figs 1 and 2 in [9] confirms that our EPR-defined $\text{P}^{\text{N}} = \text{P}^{\text{OX1}}$ redox process matches the ' $\text{P}^{\text{N}} = \text{P}^{\text{OX}}$ ' transition. The identification of the paramagnetic M1 Mössbauer species with P^{OX1} rather than P^{OX2} is also supported by experiments with dissolved thionine discussed above. Av1 samples treated with 0–10 equivalents of dissolved thionine exhibited the $g = 12$ EPR signal and no $g = 10.4$ EPR signal from the P^{OX2} redox state (not shown).

The above analysis can be supplemented with a tentative estimation for the midpoint potential of the $\text{P}^{\text{N}} = \text{P}^{\text{OX1}}$ transition of Av1. In the description of their sample pretreatment Zimmermann and coworkers mentioned that adjustment -325 mV left both P and FeMoco centres of Av1 for at least 95% in the 'native' (i.e. reduced) state [9]. It seems to us that the choice of this potential might have reflected a threefold for oxidation to the 'M1' state. Since FeMoco oxidizes after the P clusters, the upper boundary for the midpoint potential of the $\text{P}^{\text{N}} = \text{P}^{\text{OX1}}$ transition must be well below

-42 mV. These Mössbauer observations are in reasonable agreement with the -307 mV reported here. The sluggishness of the $P^{N} = P^{OX1}$ redox transition as observed by Mössbauer experiments [6, 9] might explain the discrepancy. The pronounced non-Nernstian behaviour of the left half of the bell-shaped titration curve (Fig. 1C) seems to reflect the same kinetic bottleneck, even in the presence of 40 μ M mediating dyes.

Tentative assignment of the $g = 12$ signal to an $S = 3$ spin system

A $g = 12$ signal does not indicate a triplet ($S = 1$) non-Kramers' system, which rather would have exhibited $g \approx 2$ and $g \approx 4$ EPR signals (see [47]). The current reference collection of $S \neq 11$ non-Kramers EPR signals is composed of $S = 2$, $S = 3$ and $S = 4$ systems [32, 45, 46, 48, 49] (and references therein). In the relevant biological systems with large D and $E \ll D$ zero-field splitting parameters, the $2S+1$ levels are split into a singlet ($|0\rangle$) and S 'non-Kramers doublets' ($|1^{\pm}\rangle$ to $|S^{\pm}\rangle$) in zero field. Non-Kramers EPR signals predominantly originate from the transition between the two levels of the 'non-Kramers doublets' and obey the resonance condition of Eqn (1) [50]:

$$(h\nu)^2 = \Delta^2 + (g\beta B)^2 \quad (1)$$

which $h\nu$ is the microwave quantum (0.3 cm^{-1} in X-band), Δ is the zero field splitting of the doublet and $g = g_{\text{eff}} \cos \alpha$ where α is the angle between the applied magnetic field B and the molecular z axis.

Usually a so-called 'broadening into zero field' is observed because the resonance Eqn (1) could only be met for low magnetic fields with the typical Δ ($\ll 1 \text{ cm}^{-1}$). In addition, the distribution of the D and E zero-field splitting parameters resulted in a spread of Δ [32, 45, 46, 48, 49]. Contrarily, extensive broadening into zero-field of the $g = 12$ parallel-mode EPR signal is absent. This defines a magnitude of Δ which is much smaller than the microwave quantum (0.3 cm^{-1} in X-band). In non-Kramers systems in which the condition $\Delta < h\nu$ could be met by measurement at P or V-band frequencies [46, 48, 51], the linewidth of the low-field EPR signals was an order of magnitude larger than that of the $g = 12$ EPR signal in Av1 (1.7 mT linewidth). This indicates that, in addition to its small magnitude, Δ has a very narrow distribution.

Since a small Δ in Eqn (1) can only slightly shift the observed EPR feature to a lower field, we infer that g_{eff} is close to but smaller than 12. Combined with the assumption that $g_{\text{real}} \approx 2$, the EPR signal thus represents a transition within a $|2^{\pm}\rangle$ or $|3^{\pm}\rangle$ non-Kramers doublet. From the temperature dependence of the $g = 12$ EPR signal both in normal and parallel-mode EPR (Figs 3 and 4), it is clear that this doublet is an excited doublet. In Fig. 5 we have presented the Curie-law-corrected surface enclosed by the $g = 12$ EPR signal to visualize the thermally-induced population. The relatively shallow onset of population in the 4.2–8-K range confirms the existence of one or more levels below the EPR-active doublet, in agreement with the assignment of the EPR signal to a $|2^{\pm}\rangle$ or $|3^{\pm}\rangle$ doublet. If the $g = 12$ signal is from a $|2^{\pm}\rangle$ doublet, $D \approx +2 \text{ cm}^{-1}$ for $S = 2$ or $|D| \approx 1 \text{ cm}^{-1}$ for $S > 2$ and $g_{\text{eff}} = 8$ is shifted to 12 by Δ . However the presence of extensive broadening into zero field seems to be in conflict with $\Delta = 0.23 \text{ cm}^{-1}$, required by Eqn (1) to shift g to 12. An $S = 4$ or higher system spin seems to be less likely: EPR signals with $g_{\text{eff}} = 16, 20$, etc. from $|4^{\pm}\rangle, |5^{\pm}\rangle,$

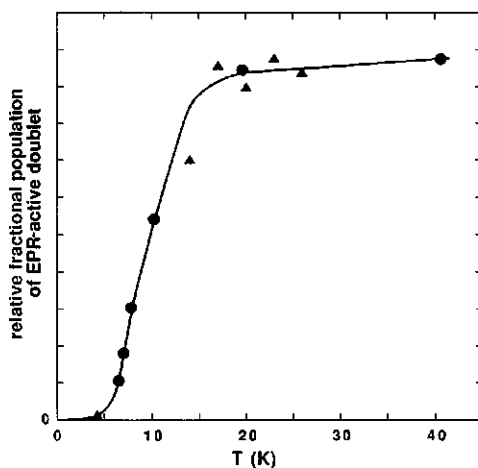


Fig. 5. Relative fractional population of the non-Kramers doublet giving rise to the $g = 12$ EPR signal of *A. vinelandii* MoFe protein. The surface enclosed by the $g = 12$ peak, corrected for the Curie-law temperature dependence, is presented as a function of the temperature, recorded with (▲) a normal-mode EPR spectrometer (cf. Fig. 3); (●) with an EPR spectrometer with a dual-mode cavity operating in the parallel mode (cf. the upper four traces of Fig. 4). The solid line is not a fit to a Boltzmann distribution but a curve presenting the approximate shape of the temperature dependence of the relative fractional population. The vertical scale of the normal-mode EPR signal has been adjusted to give a comparable relative population to the parallel mode at high temperatures.

etc. doublets were not observed. Such signals should have been sharper than the $g = 12$ signal (i.e. easier to detect), since by approximation the splitting Δ of a 'non-Kramers doublet' $|n^{\pm}\rangle$ is a function of $|D|^* (E/D)^n$ [45, 48, 49]. An assignment to the $|3^{\pm}\rangle$ doublet of an $S = 3$ system with a small positive D value seems to be most consistent from the EPR results. The unusually small amplitude of the $g = 12$ EPR signal in the perpendicular mode can also be explained with this interpretation. In perpendicular mode, microwave-induced transitions are strictly forbidden for the principal molecular axes, including the $\alpha = 0$ orientation giving rise to the $g = 12$ EPR signal in parallel mode. The very small but broad $g = 12$ EPR signal in perpendicular mode is presumably due to intermediate orientations.

Oxidation beyond +200 mV

We observed that $S = 1/2$ and $S = 7/2$ EPR signals were lost upon incubation at redox potentials higher than +200 mV. The results of a survey of the high-redox-potential window by normal and parallel-mode EPR spectroscopy have been summarized in Figs 6 and 7. Starting from the P^{OX2} redox state, oxidation proceeds by successive development of three discrete EPR signals, which we will label Superox1–3.

Superox1. An absorption-shaped parallel-mode EPR signal at $g = 15$ (≈ 8 mT full width at half height), observable only at $T < 15$ K. It did not saturate at 200 mW incident power. Since the temperature-corrected amplitude decreases in the range where relaxational broadening does not yet oc-

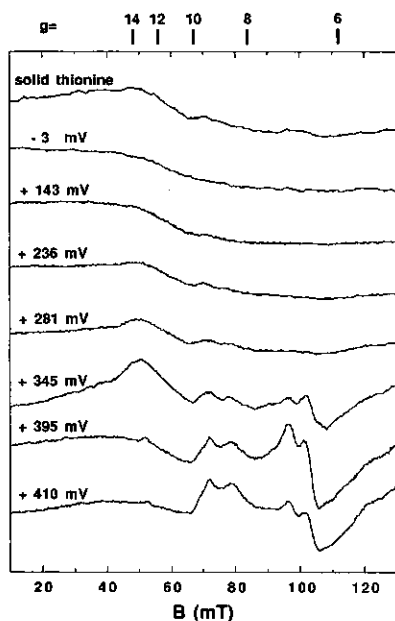


Fig. 6. EPR spectra of *A. vinelandii* MoFe protein equilibrated at high redox potentials. MoFe protein (60 mg/ml; 0.26 mM) in 50 mM Tes/NaOH, 250 mM NaCl, pH 7.5, was oxidatively titrated with buffered ferricyanide in the presence of redox mediators as described in Materials and Methods. Amplitudes of the spectra have been scaled to that of a 60-mg/ml solution, as addition of ferricyanide gradually diluted the MoFe protein to 32 mg/ml at +410 mV vs NHE. For comparison, the EPR spectrum of a solid-thionine-treated sample is shown in the upper trace. EPR conditions: microwave frequency, 9.29–9.31 GHz; modulation frequency, 100 kHz; modulation amplitude 1.6 mT; microwave power, 20 mW; temperature, 4.2 K. Note that due to the low-temperature, the $S = 7/2 \pm 1/2$ and $|\pm 3/2\rangle$ doublets are not sufficiently populated to give rise to sizeable $g = 10.4, 5.8$ and 5.5 EPR signals (cf. [23], Fig. 4).

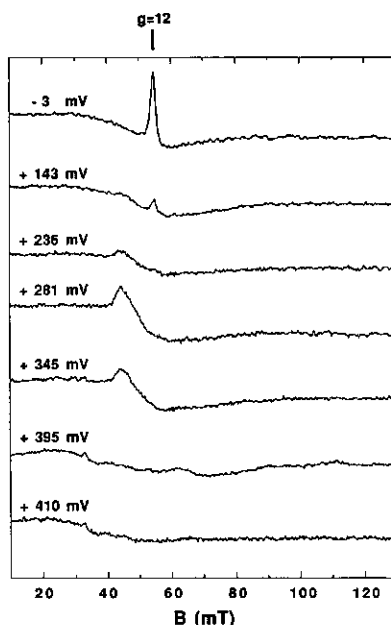


Fig. 7. Parallel-mode EPR spectra of *A. vinelandii* MoFe protein equilibrated at high redox potentials: evidence for a second integer spin paramagnetic species. MoFe protein, (60 mg/ml; 0.26 mM) in 50 mM Tes/NaOH, 250 mM NaCl, pH 7.5, was oxidatively titrated with buffered ferricyanide in the presence of redox mediators as described in Materials and Methods. Spectra were recorded with an EPR spectrometer with a dual-mode cavity operating in the parallel mode. Amplitudes of the spectra have been scaled to that of a 60-mg/ml solution, as addition of ferricyanide gradually diluted the MoFe protein to 32 mg/ml at +410 mV vs NHE. EPR conditions: microwave frequency, 9.06–9.09 GHz; modulation frequency, 100 kHz; modulation amplitude 1.25 mT; microwave power, 160 mW; temperature, 12 K.

cur, the signal is probably from a ground state of a non-Kramers system (possibly $S = 4$). The intensity in parallel mode is relatively weak and explains why, in normal mode, no corresponding signals were detected.

Superox2. A broad absorption-shaped normal-mode EPR signal at $g = 13$. It can be observed in the 4.2–15 K range. The Curie-law-corrected intensity increased threefold in this temperature range. No saturation was observed with 200 mW microwave power. In the perpendicular mode of the dual-mode EPR spectrometer the Superox2 signal was detectable, but was lost in the parallel mode. It thus should represent the low-field inflection of a very anisotropic excited doublet within an $S \approx 7/2$ Kramers system.

Superox3. A relatively intense EPR signal composed of a $g = 6.41$ zero-crossing and $g = 6.91$ absorption-shaped feature with a $g = 7.3$ shoulder. The origin of these signals can only be explained in the framework of an $S = 9/2$ spin system, because possible solutions for $S = 5/2$ or $S = 7/2$ require additional g -values. Calculation of g -values as outlined in [31] provides two possible solutions for the origin of the $g = 6.91$ and $g = 6.41$ EPR signals: $S = 9/2$ with $|E/D| = 0.082$ (calculated g -values 6.90, 6.43 and 4.86) or $S = 9/2$ with $|E/D| \approx 0.30$ (calculated g -values 6.8, 6.3 and 5.9).

Maximal amplitudes for the Superox1, 2 and 3 EPR signals were obtained by poisoning the redox potential at +300, +340 and +370 mV, respectively. The present study indicates that the tentative assignment [23] of the very weak $g \approx 14$ EPR signal of solid-thionine-oxidized Av1 to the $|\pm 5/2\rangle$ doublet was not correct. The line shape, spectra position and temperature dependence establishes that the EPR signal in Fig. 6 of [23] is the same as the Superox1 signal. However, the relative amount in solid-thionine-oxidized Av1 in [23] is some tenfold lower than the maximal intensity of the Superox2 signal. From the intensities of Superox EPR signals we estimate that the solid-thionine treatment poises Av1 at an apparent potential of $+280 \pm 30$ mV with a maximal (super)oxidation of the P^{ox2} redox state of some 5–10%. The decline of the $S = 7/2$ EPR signal as a function of the incubation time with solid thionine [23] agrees with the further oxidation as estimated by the generation of the Superox2 and Superox3 EPR signals.

Because the Superox1–3 EPR signals appeared when $S = 1/2$ and $S = 7/2$ EPR signals were lost, the EPR signal should represent P clusters oxidized beyond P^{ox2} or are generated on breakdown of the P clusters. Although the ox

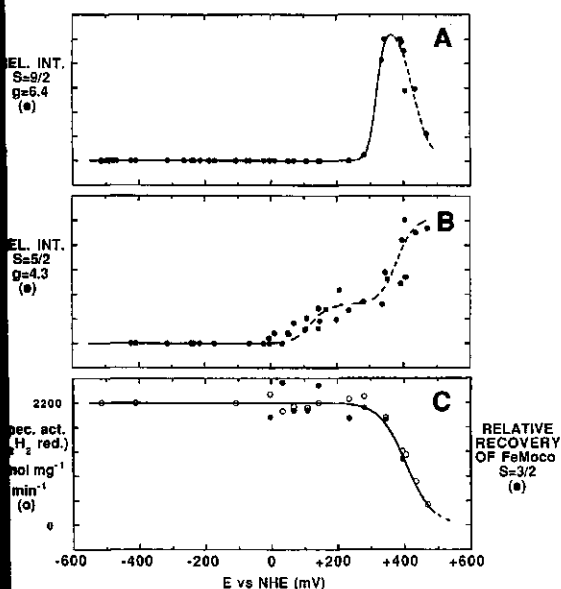


Fig. 8. The behaviour of *A. vinelandii* MoFe protein at high redox potentials: $S = 9/2$, $S = 5/2$ ($g = 4.3$) EPR signals, acetylene reduction activity and FeMoco $S = 3/2$ recovery indicate the onset of breakdown of the [Fe-S] clusters at redox potentials higher than +300 mV vs NHE. In A and B relative intensities (REL. INT.) EPR signals present in and/or generated during the redox-potential-dependent breakdown are plotted as a function of the applied reduction potential in the presence of mediators (see Materials and Methods). In C the specific activity in the acetylene reduction (Spect. C, H_2 red.) assay (\circ) and the amplitude of the $S = 3/2$ FeMoco EPR signal (\bullet) are shown after dilution with excess sodium dithionite. The potential axis of C refers to the observed solution potential prior to addition of the dithionite. EPR conditions: (A) $S = 9/2$, amplitude of the $g = 6.4$ zero-crossing feature; modulation amplitude, 1.6 mT; microwave power, 200 mW; temperature, 10 K; (B) $S = 5/2$, amplitude of the $g = 4.3$ feature; modulation amplitude, 1.6 mT; microwave power, 200 mW; temperature, 4.2 K; (C) $S = 3/2$, amplitude of the $g = 3.7$ zero-crossing feature; modulation amplitude, 1.6 mT; microwave power, 20 mW; temperature, 14 K. All spectra were recorded with a 100-kHz modulation frequency and 9–9.32-GHz microwave frequency.

tion of P^{OX2} seemed to obey a $n = 1$ Nernst curve with an apparent $E_m \approx +345$ mV, the superoxidized signals titrated with steep bell-shaped non-Nernst curves. It seems appropriate at this stage to discuss whether oxidation of the MoFe protein beyond P^{OX2} is still reversible. While in the low-potential range reversibility was easily established by repositing the potential, the drift of the redox potential was considerable at potentials higher than +250 mV. Instead of repositing potentials to the top of the bell-shaped curve of the $S = 1/2$ and $S = 7/2$ signals, we have followed the high-potential behavior by addition of an excess dithionite. The results of acetylene reduction measurements and the recovery of $S = 3/2$ EPR signals of FeMoco in these samples are depicted in Fig. 8C. For comparison, the relative amplitudes of the intense $g = 6.4$ Superox3 signal is also presented. Loss of activity and FeMoco $S = 3/2$ recovery coincided with the generation of these EPR signals. The complexity of the transition Superox1–3 signals and their dependence on the applied

redox potential thus must reflect gradual destruction of [Fe-S] clusters in the MoFe protein. The apparent 'midpoint potential' of destruction of Av1 was +400 mV (Fig. 8), almost identical to that of Cp1 [38]. The 'midpoint potential' of destruction is considerably lower in Kp1 (+280 mV) [43, 52], which is in line with our previous observation that solid-thionine-superoxidized Kp1 more rapidly than Av1.

The process of superoxidation can also be followed by measuring the intensity of the $g = 4.3$ EPR signal (Fig. 8B). The $g = 4.3$ signal is typical for the $|\pm 3/2\rangle$ doublet of rhombic high-spin ferric ions ($E/D > 0.25$, $|D| \approx 1 \text{ cm}^{-1}$). We have omitted this part of the EPR spectrum in Fig. 6 for clarity since the $g = 4.3$ signal has large amplitude due to the isotropic nature of the effective g -tensor. Starting with reduced MoFe protein the $g = 4.3$ EPR signal titrated in two distinct stages. The first (reversible) step at +120 mV was associated with $0.1\text{--}0.2 \text{ spin}/\alpha_2\beta_2$ (from double integration, assuming $|D| = 1 \text{ cm}^{-1}$). It seems likely that this step represents oxidation of substoichiometric amounts of adventitiously bound iron ions. A second step was observed at potentials where superoxidized EPR signals started to develop. The number of spins associated with the second step is some 2–6-fold higher than the first stage. In such samples the $|\pm 1/2\rangle$ and $|\pm 5/2\rangle$ doublets of the $S = 5/2$ spin multiplet are also discernible as $g = 9.4$ and $g = 9.8$ peaks (the 75-mT part of the lowest traces of Fig. 6). This second step represents the liberation of stoichiometric amounts of ferric ions from degraded [Fe-S] clusters.

Conclusions

By means of EPR spectroscopy of *A. vinelandii* MoFe protein oxidized to well-defined redox states, we have determined the redox properties of the P clusters. The complex redox behaviour clearly implicates that definition of the redox state by a mere mixing of MoFe protein with oxidants will not yield P clusters in a single well-defined redox state. In our opinion, in previous studies a number of considerations have been neglected. In particular, the 'electron counting' by addition of 2–12 equivalents is prone to errors, since kinetics of oxidation, accumulation of reduced oxidants and the presence of apoprotein or contaminant reducing equivalents ($S_2O_8^{2-}$) introduce uncertainties in the number of electrons actually taken up by the MoFe protein. Particularly, mixing with high-potential oxidants without redox-potential-buffering mediators could produce an overshoot of the redox potential before reversible oxidation to the P^{OX1} or P^{OX2} states has fully developed.

Since thionine has been extensively used in the past, we have compared EPR signals and amplitudes of thionine-treated samples with equilibrium dye-mediated redox-titration samples. This comparison clearly points out that the Mössbauer and MCD experiments [7, 9, 12, 20–22] must have been performed with P clusters oxidized to the P^{OX1} state. The dual-mode EPR spectroscopic evidence for the non-Kramers nature of this P^{OX1} redox state strongly suggests that efforts should be made to interpret the M1 paramagnetic Mössbauer spectrum with a spin Hamiltonian formalism for a non-Kramers system. From magnetic susceptibility measurements with the NMR method [53], it can be (re)calculated (molecular mass 230 kDa [29] and two instead of four P clusters) that in the P^{OX1} redox state there is no room for $S \geq 3/2$ paramagnets in addition to one $S = 3$ paramagnet/P cluster. Since P^{OX1} interconverts with the P^{OX2} redox state quantitating to $1.75 \pm 0.25 \text{ spin/active MoFe protein}$, the evi-

dence that all subcomponents of the M1 Mössbauer spectrum are derived from the P cluster $S = 3$ paramagnets seems to be likely.

It has long been known that hydrogen evolution activity of nitrogenase is not sensitive to carbon monoxide, although the nitrogen fixation reaction itself is strongly inhibited [54, 55]. It seems to us that of all the redox transitions identified in the present work, only one can reasonably be associated with the production of molecular hydrogen, namely, the reduction of the P clusters at $E_{m,7.5} = -307$ mV corresponding to the transition from $S = 3$ to $S = 0$. This assignment would implicate the P cluster as a possible site for hydrogen production. Interestingly, we have recently determined a very similar reduction potential, $E_{m,7.0} = -307$ mV, for the H cluster (i.e. the putative site of hydrogen activation) in the bidirectional Fe-hydrogenase from *Desulfovibrio vulgaris* [56].

Remarkably, low-temperature MCD experiments have been interpreted in terms of a ground state doublet with $g_{\parallel} \approx 12$ [20–22]; contrarily, we find a $g = 12$ EPR signal from an excited state. The apparent discrepancy might be due to field-induced mixing of the levels of the non-Kramers spin multiplet. A detailed investigation of Kp1 by EPR and MCD spectroscopy is currently in progress (S. Marritt, A. J. Thomson and B. E. Smith, personal communication). Alternatively, the EPR and MCD measurements might be fully consistent if the P^{OX1} redox state occurs as a physical mixture of non-Kramers spin states.

We are very grateful to Dr S. P. J. Albracht for providing us ample access to, and help with, the parallel-mode EPR facility at the Department of Biochemistry, University of Amsterdam. We thank Drs B. E. Smith and R. R. Eady at the Nitrogen Fixation Laboratory of the University of Sussex for sharing with us much unpublished material and for many discussions (EC project SC1-0179-c/TT: Energy transduction in biological nitrogen fixation). We thank Professor C. Veeger for his continuous interest and support. This investigation was supported by the Netherlands Foundation for Chemical Research (SON) with financial aid from the Netherlands Organization for Scientific Research (NWO).

REFERENCES

- Smith, B. E. & Eady, R. R. (1992) *Eur. J. Biochem.* **205**, 1–15.
- Pau, R. N. (1989) *Trends Biochem. Sci.* **14**, 183–186.
- Morningstar, J. E. & Hales, B. J. (1987) *J. Am. Chem. Soc.* **109**, 6854–6855.
- Eady, R. R., Robson, R. L., Richardson, T. H., Miller, R. W. & Hawkins, M. (1987) *Biochem. J.* **244**, 197–207.
- Müller, A., Schneider, K., Knüttel, K. & Hagen, W. R. (1992) *FEBS Lett.* **303**, 36–40.
- Smith, B. E. & Lang, G. (1974) *Biochem. J.* **137**, 169–180.
- Münck, E., Rhodes, H., Orme-Johnson, W. H., Davis, L. C., Brill, W. J. & Shah, V. K. (1975) *Biochim. Biophys. Acta* **400**, 32–53.
- Rawlings, J., Shah, V. K., Chisnell, J. R., Brill, W. J., Zimmermann, R., Münck, E. & Orme-Johnson, W. H. (1978) *J. Biol. Chem.* **253**, 1001–1004.
- Zimmermann, R., Münck, E., Brill, W. J., Shah, V. K., Henzl, M. T., Rawlings, J. & Orme-Johnson, W. H. (1978) *Biochim. Biophys. Acta* **537**, 185–207.
- Huynh, B. H., Münck, E. & Orme-Johnson, W. H. (1979) *Biochim. Biophys. Acta* **527**, 192–203.
- Smith, B. E., O'Donnell, M. J., Lang, G. & Spartalian, K. (1980) *Biochem. J.* **191**, 449–455.
- Huynh, B. H., Henzl, M. T., Christner, J. A., Zimmermann, R., Orme-Johnson, W. H. & Münck, E. (1980) *Biochim. Biophys. Acta* **623**, 124–138.
- McLean, P. A., Papaefthymiou, V., Orme-Johnson, W. H. & Münck, E. (1987) *J. Biol. Chem.* **262**, 12900–12903.
- Dunham, W. R., Hagen, W. R., Braaksma, A., Grande, H. J. & Haaker, H. (1985) *Eur. J. Biochem.* **146**, 497–501.
- Newton, W. E., Gheller, S. F., Sands, R. H. & Dunham, W. R. (1989) *Biochem. Biophys. Res. Commun.* **162**, 882–891.
- Shah, V. K. & Brill, W. J. (1977) *Proc. Natl. Acad. Sci. USA* **74**, 3249–3253.
- Palmer, G., Multani, J. S., Cretney, W. C., Zumft, W. G. & Mortenson, L. E. (1972) *Arch. Biochem. Biophys.* **153**, 325–332.
- O'Donnell, M. J. & Smith, B. E. (1978) *Biochem. J.* **173**, 831–839.
- Eady, R. R. (1980) *Methods Enzymol.* **69**, 753–778.
- Johnson, M. K., Thomson, A. J., Robinson, A. E. & Smith, B. E. (1981) *Biochim. Biophys. Acta* **671**, 61–70.
- Robinson, A. E., Richards, A. J. M., Thomson, A. J., Hawkes, T. R. & Smith, B. E. (1984) *Biochem. J.* **219**, 495–503.
- Morningstar, J. E., Johnson, M. K., Case, E. E. & Hales, B. J. (1987) *Biochemistry* **26**, 1795–1800.
- Hagen, W. R., Wassink, H., Eady, R. R., Smith, B. E. & Haaker, H. (1987) *Eur. J. Biochem.* **169**, 457–465.
- Lindahl, P. A., Papaefthymiou, V., Orme-Johnson, W. H. & Münck, E. (1988) *J. Biol. Chem.* **263**, 19412–19418.
- Bolin, J. T., Ronco, A. E., Mortenson, L. E., Morgan, T. V., Williamson, M. & Xuong, N.-H. (1990) in *Nitrogen fixation: achievements and objectives* (Gresshoff, P. M., Roth, L. E., Stacey, G. & Newton, W. E., eds) pp. 117–124, Chapman and Hall, New York.
- Smith, B. E. (1990) in *Nitrogen fixation: achievements and objectives* (Gresshoff, P. M., Roth, L. E., Stacey, G. & Newton, W. E., eds) pp. 3–13, Chapman and Hall, New York.
- Braaksma, A., Haaker, H., Grande, H. J. & Veeger, C. (1982) *Eur. J. Biochem.* **121**, 483–491.
- Pierik, A. J., Wolbert, R. B. G., Hagen, W. R. & Veeger, C. (1992) *Eur. J. Biochem.* **206**, 697–704.
- Brigle, K. E., Newton, W. E. & Dean, D. R. (1985) *Gene* **37**, 37–44.
- Dutton, P. L. (1978) *Methods Enzymol.* **54**, 411–435.
- Pierik, A. J. & Hagen, W. R. (1991) *Eur. J. Biochem.* **195**, 505–526.
- Hagen, W. R. (1992) in *Advances in inorganic chemistry 38: iron-sulfur proteins* (Cammack, R. & Sykes, A. G., eds) pp. 165–222, Academic Press, San Diego.
- Aasa, R. & Vänngård, T. (1975) *J. Magn. Res.* **19**, 308–315.
- Albrecht, S. L. & Evans, M. C. W. (1973) *Biochem. Biophys. Res. Commun.* **55**, 1009–1014.
- Zumft, W. G., Mortenson, L. E. & Palmer, G. (1974) *Eur. J. Biochem.* **46**, 525–535.
- Clark, W. M. (1960) *Oxidation-reduction potentials of organic systems*, pp. 420–423, Williams & Wilkins Co., Baltimore.
- Zumft, W. G. & Mortenson, L. E. (1973) *Eur. J. Biochem.* **35**, 401–409.
- Gomez-Moreno, C. & Ke, B. (1979) *Mol. Cell. Biochem.* **26**, 111–118.
- Lowe, D. J., Eady, R. R. & Thorneley, R. N. F. (1978) *Biochem. J.* **173**, 277–290.
- Davis, L. C., Henzl, M. T., Burris, R. H. & Orme-Johnson, W. H. (1979) *Biochemistry* **18**, 4860–4869.
- Hawkes, T. R., Lowe, D. J. & Smith, B. E. (1983) *Biochem. J.* **211**, 495–497.
- O'Donnell, M. J. (1978) Thesis, University of Sussex, Falmer.
- Wang, Z.-C., Burns, A. & Watt, G. D. (1985) *Biochemistry* **24**, 214–221.
- Carney, M. J., Papaefthymiou, G. C., Spartalian, K., Frankel, B. & Holm, R. H. (1988) *J. Am. Chem. Soc.* **110**, 6084–6092.
- Hagen, W. R. (1982) *Biochim. Biophys. Acta* **708**, 82–98.
- Hendrich, M. P. & Debrunner, P. G. (1989) *Biophys. J.* **56**, 489–506.
- Stevenson, R. C. (1984) *J. Magn. Res.* **57**, 24–42.
- Hendrich, M. P., Pearce, L. L., Que, L., Chasteen, N. D. & Day, E. P. (1991) *J. Am. Chem. Soc.* **113**, 3039–3044.

9. Juarez-Garcia, C., Hendrich, M. P., Holman, T. R., Que, L. & Münck, E. (1991) *J. Am. Chem. Soc.* **113**, 518-525.
10. Bleaney, B. & Scovil, H. E. D. (1952) *Philos. Mag.* **43**, 999-1000.
11. Hagen, W. R., Dunham, W. R., Johnson, M. K. & Fee, J. A. (1985) *Biochim. Biophys. Acta* **828**, 369-374.
12. O'Donnell, M. J. & Smith, B. E. (1980) *FEBS Lett.* **120**, 251-254.
13. Smith, J. P., Emptage, M. H. & Orme-Johnson, W. H. (1982) *J. Biol. Chem.* **257**, 2310-2313.
14. Hardy, R. W. F., Knight, E., Jr. & D'Eustachio, A. J. (1965) *Biochem. Biophys. Res. Commun.* **20**, 539-544.
15. Hwang, J. C., Chen, C. H. & Burris, R. H. (1973) *Biochim. Biophys. Acta* **292**, 256-270.
16. Pierik, A. J., Hagen, W. R., Redeker, J. S., Wolbert, R. B. G., Boersma, M., Verhagen, M. F. J. M., Grande, H. J., Veeger, C., Mutsaers, P. H. A., Sands, R. H. & Dunham, W. R. (1992) *Eur. J. Biochem.* **209**, 63-72.

Chapter 9

Nigerythrin and rubrerythrin from *Desulfovibrio vulgaris* each contain two mononuclear iron centers and two dinuclear iron clusters.

Antonio J. Pierik, Ronnie B.G. Wolbert, Gerrit L. Portier, Marc F.J.M. Verhagen and Wilfred R. Hagen

(1993) Eur. J. Biochem. 212, 237-245.

Nigerythrin and rubrerythrin from *Desulfovibrio vulgaris* both contain two mononuclear iron centers and two dinuclear iron clusters

Antonio J. PIERIK, Ronnie B. G. WOLBERT, Gerrit L. PORTIER, Marc F. J. M. VERHAGEN and Wilfred R. HAGEN
Department of Biochemistry, Wageningen Agricultural University, The Netherlands

Received September 28, 1992) – EJB 92 1371

The trivial name 'rubr-erythrin' is a contraction of two other trivial names: rubredoxin (ruber, red) and hemerythrin. It names a protein of undetermined biological function which putatively carries rubredoxin-like mononuclear iron and hemerythrin-like dinuclear iron. The name 'nigerythrin' (niger, black) is an analogy of rubrerythrin. It identifies a second protein of undetermined function which has prosthetic groups similar to rubrerythrin. Rubrerythrin was initially described [LeGall, J., Prickril, B. C., Moura, I., Xavier, A. V., Moura, J. J. G. & Huynh, B.-H. (1988) *Biochemistry* 27, 1636–1642] as a homodimer with four iron ions arranged into two rubredoxin sites and one inter-subunit dinuclear cluster. Nigerythrin is a novel protein. Here, we report that both proteins are homodimers, each dimer carrying not four but six iron ions in two mononuclear centers and two dinuclear clusters. Rubrerythrin and nigerythrin are probably both located in the cytoplasm; they are differentially characterized with respect to molecular mass, pI, N-terminal sequence, antibody cross-reactivity, optical absorption, EPR spectroscopy, and reduction potentials. All three reduction potentials in both proteins are $> +200$ mV. These appear too high to be of practical relevance in the cytoplasm of the sulfate reducer *Desulfovibrio vulgaris* (Hildenborough). We suggest the possibility of a non-redox role for both proteins with all six iron ions in the ferrous state.

Sulfate reducers, especially *Desulfovibrio* spp., are the source of a variety of proteins carrying novel metal centers and novel arrangements of metal centers [1, 2]. From these proteins have recently been purified which exemplify three distinct variations to the rubredoxin structural theme of distorted tetrahedral coordination by four cysteinate sulfur atoms to a single Fe(II) or Fe(III) ion. Desulfurodoxin has a different Cys motif, namely two Cys adjacent. This is thought to result in a strained iron site, which is reflected in a drastically different EPR and visible spectrum [3]. Desulfurodoxin has a similarly strained FeS₄ site but in addition an (N, O) octahedrally coordinated iron site [4]. Finally, rubrerythrin appears to have a 'regular' FeS₄ site (in EPR spectroscopy) but with an unusually high reduction potential. In addition, it contains a putative μ -oxo bridged dinuclear iron cluster [5]. Rubredoxin has been thoroughly studied for several decades now (cf. [6, 7]). Data on the other proteins is limited as only one or two examples for each class have been described. Here, we re-evaluate and extend the data on rubrerythrin and we report on a second example from this class.

The trivial name rubr-erythrin is a contraction of rubredoxin plus hemerythrin. The name was chosen on the basis of spectroscopic investigations, which indicated that the protein contains a mononuclear rubredoxin-like iron and a dinuclear

iron cluster not unlike that found in hemerythrin [5]. Hemerythrin is the O₂ transport protein in the blood of marine invertebrates [8]. Subsequently, however, the amino-acid sequence of rubrerythrin was determined both directly [9] and by inference from the structural gene sequence [10]. The sequence proved to have regional similarity to the E-X-X-H binding domain for the dinuclear iron cluster in *Escherichia coli* ribonucleotide reductase [11]. X-ray crystallographic studies have revealed that the structure and ligation of the dinuclear iron cluster in ribonucleotide reductase is rather different from that of hemerythrin [10, 12]. Of course, a renaming of rubr-erythrin (rubr-ribonucleotide reductase) would now not only be difficult to pronounce but would also suggest an enzymic function where none has yet been established. Thus, the trivial name rubrerythrin is presently retained. In fact, we propose a similar name, nigerythrin (niger = black) for a novel protein also purified from *D. vulgaris* (Hildenborough) and with spectroscopic and other properties similar to those of rubrerythrin.

The published sequence data of rubrerythrin pose two other problems. Firstly, in the original description of the isolation of rubrerythrin by LeGall et al. it was claimed that the protein resides in the periplasmic space of *D. vulgaris* [5]. However, comparison of the gene sequence with the amino-acid sequence of the mature protein gives no indication for a processable export sequence [9, 10]. The second problem is that of the stoichiometries of the prosthetic groups. Again, in the original work of LeGall et al., the iron count and the EPR and Mössbauer spectroscopic data were interpreted in terms of two rubredoxin-like centers and one dinuclear cluster/rubrerythrin homodimer [5]. However, Kurtz and Prickril have noticed that the protein sequence of each monomer has two

Correspondence to W. R. Hagen, Laboratorium voor Biochemie, Wageningen Universiteit, Dreijenlaan 3, NL-6703 HA Wageningen, The Netherlands.

Fax: +31 8370 84801.

Note. The novel amino acid sequence data published here have been deposited with the EMBL sequence data bank.

E-X-X-H motives comprising a complete putative binding site for one dinuclear cluster. This suggests that, just as in the homodimeric R2 subunit of ribonucleotide reductase, rubrerythrin may also carry two dinuclear iron clusters [11]. Exactly this problem has clouded the ribonucleotide reductase field until the three-dimensional structure of the R2 dimer was solved by X-ray crystallography [12]. Below, we will specifically address these problems for rubrerythrin and for the novel nigerythrin.

MATERIALS AND METHODS

Growth of organism and preparation of crude extracts

The sulfate reducer *Desulfovibrio vulgaris* (Hildenborough) NCIB 8303 was maintained on Postgate's medium [13]; large-scale growth at 35°C on lactate/sulfate was in modified Saunders' medium [14]. Stirred batch cultures of 240 l were grown under nitrogen to $A_{600} \approx 0.8$ in 60 h from a 1% inoculum in a home-built anaerobic glass fermentor. With a Sharpless continuous-flow centrifuge 150–200 g wet cells were collected over a 10-h period and directly processed after completing the harvesting.

For the isolation of both nigerythrin and rubrerythrin a whole-cell extract was prepared anaerobically. The cells were resuspended in three volumes standard buffer (10 mM Tris/HCl pH 8.0) and were then disrupted by three passages through a chilled Manton-Gaulin press at 84 MPa. A spatula of DNase, RNase, and the protease inhibitor phenylmethylsulfonyl fluoride each was added and the suspension was centrifuged at $10000 \times g$ for 20 min. The supernatant was freed of membranes by centrifugation at $100000 \times g$ for 60 min. The pH was adjusted to 8.0 with 1 M Tris/HCl pH 9 and the supernatant was diluted with water to yield a conductivity of 1.2 mS/cm.

For the localization of nigerythrin, periplasmic extracts were prepared which were increasingly contaminated with the cytoplasm by prolonged extraction. The cells were resuspended in three volumes water at 4°C and the periplasm was extracted essentially according to [14] by gentle disintegration of the cell wall with EDTA (1:1 dilution to a final concentration of 50 mM Na₂ EDTA plus 50 mM Tris/HCl pH 9) with the temperature raised to 32°C while stirring. Samples were then taken as a function of incubation time from 0 to 60 min and immediately centrifuged ($10000 \times g$, 10 min). The supernatants were checked for desulfoviridin by $A_{630}/(A_{610} - A_{650})$ and, after dithionite-reduction, for cytochromes *c* by $A_{553} - A_{570}$. The nigerythrin content was estimated by Western blotting.

Initial detection of nigerythrin

We have recently described the purification and characterization of the prismane protein, a putative [6Fe-6S]-cluster-containing protein from the cytoplasm of *D. vulgaris* [15]. The last step of that purification involves anion-exchange chromatography at ambient temperature on a FPLC-Mono Q 5/5 column with a 0–1 M NaCl gradient in 20 mM Tris/HCl pH 8.0. In this step the prismane protein eluted at 130 mM NaCl and was resolved from several other proteins that predominantly eluted in the 160–250 mM NaCl concentration range [15]. A minor, black, protein fraction eluted just before the prismane protein at ≈ 100 mM NaCl. This fraction was pooled, dialyzed against 25 mM Hepes pH 7.5 and concentrated (Amicon/YM-30) to make a single 100- μ l EPR

sample. The EPR spectrum at 13 K indicated the presence of mononuclear iron ($g \approx 4.3$) and a dinuclear, non-Fe/S iron cluster ($g \approx 1.5-2.0$) as in the *D. vulgaris* rubrerythrin described by LeGall et al. [5]. However, the ultraviolet/visible spectrum (notably, a peak at 590 nm; see below) was different from that described for rubrerythrin [5]. SDS/PAGE indicated a molecular mass some 25% greater than that reported for the rubrerythrin subunit (excluding the possibility that the protein is a proteolytic fragment of rubrerythrin). Therefore the remaining protein was used to prepare polyclonal antibodies in mice (see below). The antiserum was subsequently used to set up a purification scheme specifically for nigerythrin by monitoring chromatography fractions with Western blotting.

Purification of nigerythrin

All columns were run at 4°C with a computerized Pharmacia FPLC system. The whole-cell extract (0.5 l) was applied onto a DEAE Sepharose Fast Flow column (volume, 0.3 l; flow rate, 20 ml/min) equilibrated with standard buffer. Cytochromes were eluted with the standard buffer. After washing with one column volume of standard buffer (10 mM Tris/HCl pH 8.0 at 4°C), a 0–1 M NaCl gradient in standard buffer (15 column volumes) was applied. Western blotting revealed that the nigerythrin eluted around 170 mM NaCl. The pooled 350 ml was concentrated (Amicon YM-30), centrifuged at $14000 \times g$ for 15 min. The supernatant was split for two subsequent runs on a Superdex 75 'prep grade' gel-filtration column (volume, 0.33 l; flow rate, 2 ml/min) equilibrated with 20 mM Tris/HCl pH 8.0 plus 150 mM NaCl. With the same buffer the nigerythrin was eluted around 106 ml. A total pool of 125 ml, identified with Western blotting, was concentrated on Amicon YM-30, centrifuged at $14000 \times g$ for 15 min and diluted to 0.3 l (final conductivity, 1.5 mS/cm). This sample was applied onto a Bio-Gel HT hydroxyapatite column (volume, 40 ml) equilibrated with 10 mM potassium phosphate pH 7.5 (flow rate, 1.5 ml/min). The column was washed with this buffer. Then a 10–500 mM potassium phosphate gradient (15 column volumes) was applied at a flow rate of 2 ml/min. Nigerythrin was found, with Western blotting, to elute at the very end of the gradient. A pool of 65 ml was concentrated to 2.5 ml. The buffer was exchanged with 10 mM Mes pH 6.0 by passing the sample through a Mes-buffered Sephadex G-25 column of 30 ml volume, and the eluate was concentrated again to 2.5 ml and was centrifuged at $14000 \times g$ for 15 min. The supernatant was applied (flow rate, 0.25 ml/min) onto a MonoQ HR 5/5 anion exchanger (volume, 1 ml). This column was washed with 5 ml Mes buffer and the protein was eluted with a 0–0.4 M NaCl gradient in 10 mM Mes pH 6.0 (45 column volumes). Nigerythrin content of eluting fractions was now determined by absorbance on the purity index (see below) of $R \equiv A_{280}/A_{590}$. From a starting material of 135 g wet cells, a final yield of approximately 0.5–1 g nigerythrin was obtained with $R < 9$.

Purification of rubrerythrin

The rubrerythrin was purified essentially as described by LeGall et al. [5], with the exception that here whole-cell extract was used as the starting material. The final preparation had a purity index (cf. [5]) of $A_{280}/A_{492} = 7.2$.

Analytical methods

Protein was determined in some cases with the microbiological method [16] after trichloroacetic acid/deoxycholate precipitation [17] or with Coomassie staining according to Bradford [18]; bovine serum albumin was the standard. The following methods have been recently detailed in our previous work [15]: colorimetric iron determination as the ferene complex; SDS gel electrophoresis; isoelectric focussing; relative molecular mass determination by gel filtration (on Superdex 75 prep grade); the raising of antibodies in Balb/C mice and their subsequent use in immunoblotting.

N-terminal analysis of freeze-dried protein was carried out by gas-phase sequencing (R. Amons and R. H. Karssies, Medizin University).

Activity tests were literature procedures for ribonucleotide reductase [19], nitrate reductase [20], superoxide dismutase [21], catalase [22], and phosphate [23] from pyrophosphatase. These activities were all found to be absent.

EPR spectroscopies and potentiometry

Ultraviolet/visible absorption data were recorded on an Aminco DW-2000 spectrophotometer. EPR spectra were recorded on a Bruker ER-200 D spectrometer with peripheral equipment and data handling as we have described before [24]. The setup and the ingredients for the mediated ox titrations were also given there. The reductant was sodium dithionite, the oxidant was potassium ferricyanide.

RESULTS

Heterogeneity, molecular mass and iron content

Both nigerythrin and rubrerythrin exhibited a single band on Coomassie-blue-stained SDS/PAGE gels. The apparent molecular mass for SDS-denatured rubrerythrin was 22 kDa, identical to the number reported previously by LeGall et al. [5] and consistent with the mass of 21544 Da deduced from the amino acid sequence [9] or the gene nucleotide sequence [10]. The electrophoretic mobility of SDS-denatured nigerythrin indicated a significantly higher molecular mass, 27 ± 2 kDa.

Flat-bed isoelectric focussing at 4°C also gave a single band for both proteins. The position of rubrerythrin corresponded to a $pI = 7.0 \pm 0.1$, which is close to the value of 7.0 reported by LeGall et al. [5]. Nigerythrin proved to be significantly more acidic, $pI = 5.1 \pm 0.1$.

The native molecular mass of nigerythrin was determined by gel filtration. On Superdex 75, equilibrated with 20 mM Tris/HCl pH 8.0 plus 150 mM NaCl, the protein elution profile (280-nm detection) was a single symmetrical peak corresponding to a molecular mass of 54 ± 3 kDa. Thus, nigerythrin is an α_2 -homodimer of 2×27 kDa.

Le Gall et al. reported some four iron atoms/dimer in two preparations of α_2 -rubrerythrin [5]. We found approximately four iron atoms/dimer in a single preparation of rubrerythrin. Nigerythrin samples purified from five different batch cultures we determined 5–8 iron atoms/ α_2 -dimer. These findings suggest that the Fe stoichiometry in these two proteins may be higher than four; therefore, the prosthetic group stoichiometry may be different from that originally proposed by Le Gall et al. However, these determinations are indicative only, as they have necessarily been made on small amounts of protein.

	1	5	10	15											
Rubrerythrin	M	K	S	L	K	G	S	R	T	E	K	N	I	L	T
Nigerythrin	M	K	V	R	A	Q	V	P	T	V	K	N	A	T	N
NarH / NarY	M	K	I	R	S	Q	V	G	M	V	L	N	L	D	K

Fig. 1. A comparison of the N-terminal sequences of *D. vulgaris* rubrerythrin, nigerythrin, and the β -subunit of *E. coli* nitrate reductase. The sequence from rubrerythrin has been taken from [9, 10]; the nigerythrin sequence was determined in this work; the third sequence is the product of *NarY* or *NarH* encoding respectively for the β -subunit of nitrate reductase A or Z (which have identical N-termini) [25, 26]. All sequences have a conspicuous surplus of positive and of uncharged polar groups.

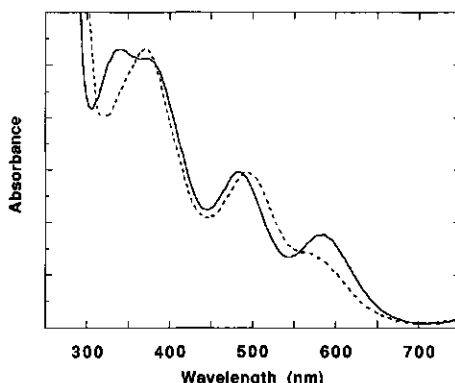


Fig. 2. A comparison of the ultraviolet/visible spectra from nigerythrin (—) and rubrerythrin (---) as isolated from *D. vulgaris*. The protein concentrations were 96 μ g/ml (nigerythrin) and 63 μ g/ml (rubrerythrin) in 10 mM Hepes pH 7.0. The amplitudes have been adjusted to match the 486-nm peak of nigerythrin with the 492-nm peak of rubrerythrin (see Table 1 for absorption coefficients).

N-terminal sequence

The amino-terminal sequence of nigerythrin was determined with gas-phase sequencing. A first attempt on 1.8 pmol protein sample blotted onto an Immobilon-P (Millipore) support gave very low yields in the sequencer. Therefore, 1.1 nmol of water-dialyzed protein was freeze-dried and, without further treatment, used for the gas-phase sequencing. The first 15 residues are given in Fig. 1 and are compared with the N-terminus of rubrerythrin [9, 10] and of the β -subunit of *Escherichia coli* nitrate reductase complex [25, 26]. There is some similarity to the rubrerythrin N-terminal sequence but this was not picked up when the nigerythrin data was subjected to the FASTA sequence comparison program [27]. Instead, the only similar sequence identified was the N-terminus of the β -subunits from *E. coli* nitrate reductases A and Z. Directly following the 15th residue in the nitrate reductase β -subunit there is the first Cys motif for the putative binding of an iron-sulfur cluster [25, 26, 28]. Rubrerythrin and nigerythrin carry no iron-sulfur clusters. No sequence similarity was detected between rubrerythrin and nitrate reductase β -subunit, and none is expected between nigerythrin and nitrate reductase β -subunit beyond the one shown in Fig. 1. All three amino-terminal sequences are

Table 1. A comparison of physico-chemical and biochemical properties of nigerythrin and rubrerythrin from *D. vulgaris* (Hildborough). The rubrerythrin data in the first two sections (protein and ultraviolet/visible spectroscopy) have been taken from the work LeGall et al. [5, 9, 10]. All other data are from this work.

	Property	Value for		
		nigerythrin	rubrerythrin	
Protein	putative localization	cytoplasmic	uncertain	
	subunit composition	α_2	α_2	
	subunit mass/kDa	27	21.544	
	pI	5.1	7.1	
Ultraviolet/visible spectroscopy (as isolated protein)	λ_{max}/nm ($\epsilon/mM^{-1} cm^{-1}$) for peak	1	280 (59)	280 (73)
		2	335 (20.8)	350 (17.9)
		3	382 (20.0)	365 (18.3)
		4	486 (10.7)	492 (10.4)
		5	590 (6.6)	570 (4.7)
EPR of FeS_4 site	g_1 ($\pm 1/2 >$)	9.28	9.4	
	g_1 ($\pm 3/2 >$)	≈ 3.8	≈ 4.0	
	g_2 ($\pm 3/2 >$)	4.29	4.29	
	g_3 ($\pm 3/2 >$)	≈ 4.8	≈ 4.6	
	g_1 ($\pm 5/2 >$)	9.86	9.6	
	g-real	1.97–2.07	1.97–2.03	
	$ E/D $ D/cm^{-1}	0.26 ≈ -1	0.29 $\approx +1$	
EPR of dinuclear cluster	g_1	1.964	1.958	
	g_2	1.74	1.739	
	g_3	1.53	1.54	
	$P_{1/2}$ at $T = 4.2 K/mW$	47	4	
Reduction potentials	$E_{m,7}$ mononuclear Fe/mV	+213	+281	
	1st $E_{m,7}$ dinuclear cluster/ mV	+300	+339	
	2nd $E_{m,7}$ dinuclear cluster/ mV	+209	+246	
Stoichiometries (as isolated protein)	Fe/dimer	5–8	≈ 5	
	EPR integral FeS_4	0.81	0.84	
	EPR integral dinuclear Fe	0.20	0.14	
Stoichiometry from maximal amplitudes corrected for disproportionation	EPR ratio $[FeS_4]/[dinuclear Fe]$	0.98	0.99	

characterized by a conspicuous surplus of positive and of non-charged polar groups.

Antibodies, localization

The polyclonal antibody preparation, which was used to monitor the purification of nigerythrin, was mouse serum without further purification. On Western blots immunostained after treatment with 2000-fold diluted mouse anti-nigerythrin a single 27-kDa band was obtained either with *D. vulgaris* cell extract or with the purified nigerythrin. No response was detected with purified rubrerythrin.

Localization of the nigerythrin was inferred from time-dependent extraction data. Extracts of *D. vulgaris* cells were made as described in the Materials and Methods section. The procedure employed has been devised to prepare a periplasmic fraction; however, upon prolonged incubation, the cytoplasmic membrane also disintegrated and cytoplasmic proteins appeared in the extract. Markers detected by optical absorbance for the periplasmic fraction were *c*-type cytochromes [29–31], with dissimilatory sulfite reductase or desulfoviridin for the cytoplasmic fraction [32]. The cytochrome absorption increased with extraction time up to 10 min and subsequently remained constant. The desulfoviridin absorption increased constantly from 0 to 60 min.

Nigerythrin was detectable by visual inspection of Wes blots after only a 5-min extraction and the response increased constantly with time up to 60 min. We suggest therefore that the readily soluble nigerythrin has a cytoplasmic location.

Ultraviolet/visible spectroscopy

Fig. 2 shows the ultraviolet/visible absorption spectra of the as isolated nigerythrin and rubrerythrin. The peak positions and absorption coefficients are given in Table 1. The spectrum for rubrerythrin is essentially identical to that reported by LeGall et al. (cf. [5] and Table 1). The spectrum of nigerythrin has similar features but it is quantitatively different. Whereas rubrerythrin exhibits three peaks (280, 492 nm) and two shoulders (350, 570 nm), nigerythrin shows four resolved peaks (280, 335, 486, 590 nm) and a shoulder (382 nm). The pronounced peak at 590 nm is especially characteristic of nigerythrin and has been used to monitor the protein in the final purification step.

LeGall et al. have made the point that the optical spectrum of rubrerythrin is rather similar to that of a plain rubredoxin (times two), except for the region around 350 nm; suggest that the additional absorption in the rubrerythrin spectrum 'bears some resemblance to that of met-hemoglobin' [5]. We suggest that the additional absorption arc

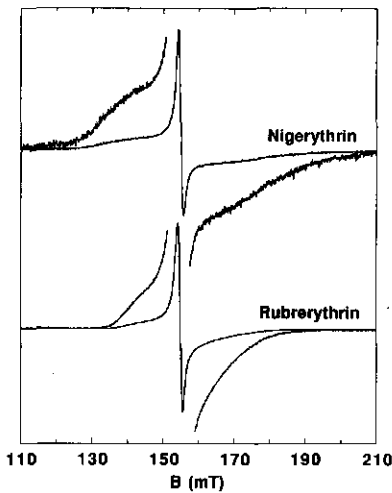


Fig. 3. EPR spectra of the $g = 4.3$ signal from the mononuclear ferric site in *D. vulgaris* nigerythrin and rubrerythrin. The signal from the $|\pm 3/2\rangle$ doublet of an $S = 5/2$ system. The 'wings' have been magnified $8\times$. The protein concentrations were 1.1 mg/ml (nigerythrin) and 3.9 mg/ml (rubrerythrin) in 10 mM Mes pH 7.0. EPR conditions: microwave frequency, 9303 MHz; microwave power, 2 mW; modulation amplitude, 0.6 mT; temperature, 4.2 K.

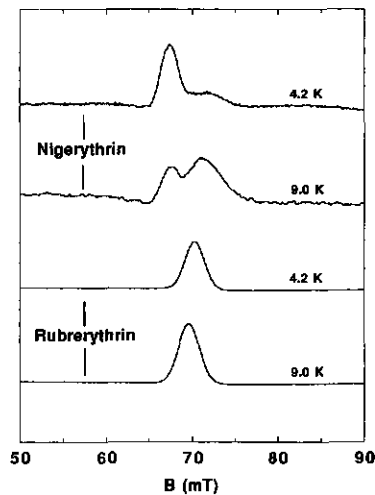


Fig. 4. Temperature-dependent low-field EPR spectra ($g = 9-10$) from the mononuclear ferric site in *D. vulgaris* nigerythrin and rubrerythrin. The protein concentrations were as in Fig. 3. The signal at lowest field is from the $|\pm 5/2\rangle$ doublet and the one at higher field is from the $|\pm 1/2\rangle$ doublet. The amplitude of the $T = 9$ K spectrum has been increased compared to the 4.2 K spectrum to compensate for Curie-law temperature dependence. EPR conditions: microwave frequency, 9.30 GHz; microwave power, 200 mW; modulation amplitude, 2 mT.

0 nm in the spectrum of both nigerythrin and rubrerythrin are equally well compared to that of the ribonucleotide reductase β_2 -homodimer. Preparations of that protein with one to four irons (i.e. two dinuclear clusters) have peaks at 350 nm ($\epsilon = 9.3 \text{ mM}^{-1} \text{ cm}^{-1}$) and at 365 nm ($\epsilon = 7.4 \text{ mM}^{-1} \text{ cm}^{-1}$) [33, 34].

A useful purity index was defined by LeGall et al. for rubrerythrin, $R = A_{280}/A_{492} = 7.0$. Similarly, for purified nigerythrin we find on the basis of five different preparations, $R = A_{280}/A_{486} = 6.0 \pm 0.2$, $R_2 = A_{280}/A_{590} = 8.9 \pm 0.5$.

Reduction with dithionite of nigerythrin or rubrerythrin results in a complete bleaching of the visible spectrum of both proteins at the high-wavelength side of the dithionite peak.

EPR spectroscopy

The mononuclear iron site is detected in the oxidized state with EPR spectroscopy as a low-symmetry, high-spin ferric complex (Figs 3 and 4). Such a system is described by the usual spin Hamiltonian [35]

$$H = D[S_z^2 - S(S+1)/3] + E(S_x^2 - S_y^2) + \beta \mathbf{B} \cdot \mathbf{g} \cdot \mathbf{S}. \quad (1)$$

High-spin Fe(III) is $3d^5$; therefore, the system is subject to quenching of orbital angular momentum, and the g -tensor is usually found to be a scalar close to the free-electron value $g_e = 2.00$ [36]. For metalloproteins it is commonly observed that $D \gg h\nu$, the latter being the microwave energy, 0.3 cm^{-1} for regular X-band EPR [37]. Under these conditions the six magnetic sublevels of the $S = 5/2$ system arrange into three well-separated Kramers doublets. Three complete spectra can in principle be observed from the three a -doublet EPR transitions. In the limit of maximal rhombicity, defined by $|E/D| = 1/3$, the predicted three spectra are as follows. The lower and the upper doublet ($|\pm 1/2\rangle$ and $|\pm 5/2\rangle$) give identical spectra with effective g -values 9.69,

0.86, 0.61; the latter two 'lines' are usually inhomogeneously broadened beyond detection [37]. The transition within the middle doublet has, by mathematical coincidence, its three effective g -values coinciding into an isotropic value $g = 4.29$, which defines an easily detectable spectrum. With a decreased rhombicity, i.e. $|E/D| < 1/3$, the $g = 4.29$ line from the $|\pm 3/2\rangle$ doublet splits up into three lines, the $g = 9.69$ line from the $|\pm 1/2\rangle$ doublet moves to lower values, and the $g = 9.69$ line from the $|\pm 5/2\rangle$ doublet moves to higher values (with a maximum at $g = 10$).

The theoretical spectrum just described is approximately that observed for rubredoxin [38] but for this protein a significant anisotropy in the real g -tensor must be invoked for a precise data analysis [39]. The deviation from the free-electron g -value is much larger than predicted on the basis of generally accepted theory [36]. We now meet this problem again in the EPR of the mononuclear iron of nigerythrin and rubrerythrin. The spectra from the $|\pm 3/2\rangle$ middle doublet are given in Fig. 3. Three distinct features are observed, which indicates that the rhombicity E/D is slightly less than the maximal value of $1/3$. The low-field peaks from the $|\pm 1/2\rangle$ and from the $|\pm 5/2\rangle$ doublets are given in Fig. 4. The effective g -values for the two doublets are not identical, which again indicates E/D to be slightly less than $1/3$. All effective g -values obtained from the spectra of Figs 3 and 4 are listed in Table 1. These values can be fitted (see [37]) to Eqn (1) but only if we assume a considerable deviation of the real g -value from the free-electron value and also a considerable anisotropy in this deviation. The fitted values for E/D and ranges for the real g -values are also in Table 1.

From the relative intensities of the low-field peaks from the $|\pm 1/2\rangle$ and $|\pm 5/2\rangle$ doublets as a function of temperature (Fig. 4) it is readily seen that the ground state for nigerythrin is $|\pm 5/2\rangle$, therefore D is negative. Contrarily,

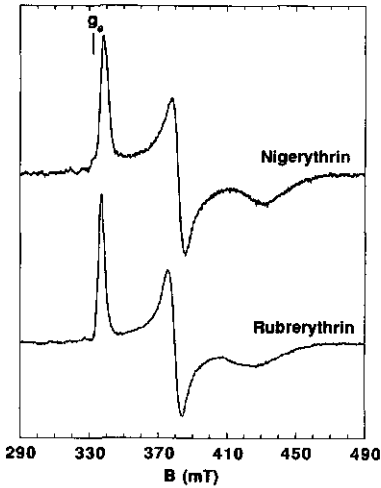


Fig. 5. EPR spectra from the mixed-valence dinuclear iron cluster in nigerythrin and rubrerythrin as isolated from *D. vulgaris*. The protein concentrations were as in Fig. 3. EPR conditions: microwave frequency, 9.30 GHz; microwave power, 200 mW; modulation amplitude, 1.6 mT; temperature, 12 K.

the ground state for rubrerythrin is $|\pm 1/2\rangle$, therefore D is positive. The absolute value of D in rubredoxin-type systems is of the order of the Boltzmann constant; an accurate determination requires intensity data at temperatures lower than 4 K (cf. [38]). From our data at $T \geq 4$ K we estimate $|D| \approx 1 \text{ cm}^{-1}$ for both proteins.

EPR spectra at 12 K from the dinuclear iron cluster in the proteins as isolated are presented in Fig. 5. The spectra have all three g -values below g_e and an average g -value of 1.74. This type of spectrum was first observed from the mixed-valence dinuclear iron cluster in hemerythrin [40]; it has subsequently been observed from the dinuclear cluster in purple-acid phosphatases (reviewed in [41]), in methane monooxygenase hydroxylase [42], and in ribonucleotide reductase [43].

Bertrand et al. have proposed a semi-quantitative ligand-field model to explain the g -values of these spectra [44]. The model is a variation of the Gibson model for $[2\text{Fe-2S}]^{1+}$ clusters [45, 46]. The two models differ only in that the environment of the ferrous ion in the Fe/S clusters is distorted tetrahedral, while in the non-sulfur, dinuclear clusters considered here the ferrous ion environment is distorted octahedral. The model of Bertrand et al. satisfactorily explains why all g -values are less than g_e and why the deviation from g_e is considerable. An interesting prediction of the model is that the g -values of the non-Fe/S cluster are very sensitive to distortion of the octahedral ferrous site. This suggests that the small differences in g -values observed here between nigerythrin and rubrerythrin (Fig. 5 and Table 1) correspond to only a very minor difference in chemical structure around the respective ferrous ions. We have, however, found these differences to be reproducible over different preparations. A more pronounced difference is found in the microwave power saturation at 4.2 K. From the saturation curve in Fig. 6 it is apparent that the spin-lattice relaxation for the cluster in nigerythrin is considerably faster than for the one in rubrerythrin. The nominal power level required for a 50% ampli-

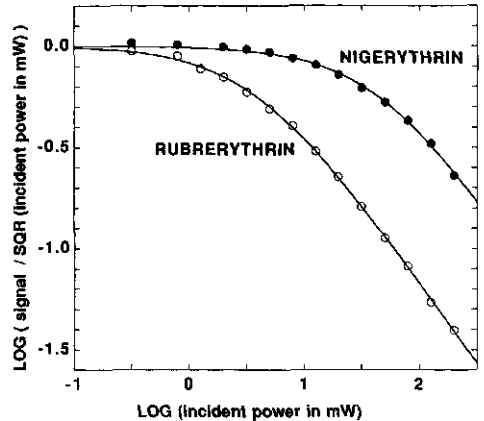


Fig. 6. Saturation plot of the mixed-valence dinuclear iron signals at a temperature of 4.2 K. SQR = square root.

tude reduction by saturation is 47 mW for nigerythrin, while it is only 4 mW for rubrerythrin.

Redox titrations and ratio quantifications

Quantification at 12 K of the $S = 1/2$ signals from the dinuclear cluster in the proteins as isolated gives stoichiometric numbers, namely, 0.2 (nigerythrin) and 0.14 (rubrerythrin) spin/protein monomer. Both proteins, as isolated, are presumably not in a single, well defined redox state. Quantification of the $m_s = \pm 3/2$ subspectrum from the $S = 5/2$ rubredoxin-like, mononuclear ferric ion centers (Fig. 7) is suitably done at or above a temperature of 20 K, where the fractional population of the $|\pm 3/2\rangle$ doublet (for $|D| = 1 \text{ cm}^{-1}$) is virtually maximal, i.e. close to 1/3. The concentration is some 0.8 $S = 5/2$ spins per monomer for both proteins as isolated (Table 1). The fact that this number is short of unity indicates that the mononuclear iron may be fully oxidized and/or that the preparations contain some apoprotein.

Oxido-reductive titrations were done as described previously [24]. The mononuclear iron was monitored at $g = 4.3$ with the sample at 105 K, while the dinuclear cluster was detected at $g = 1.74$ with the sample at 12 K. The results are presented in Fig. 7. The data from the mononuclear iron from the dinuclear cluster have been fit to Nernstian, single electron ($n = 1$) transitions with an amplitude scaling factor being part of the fitting. The resulting reduction potentials are given in Table 1. The combination of the spin stoichiometry number for the mononuclear iron and that for the dinuclear cluster of the protein as isolated does not correspond to a single potential in the graph of Fig. 7 either for nigerythrin or for rubrerythrin. Therefore, the preparations contain some apoprotein and/or the different redox groups are not in equilibrium with each other in the proteins as isolated. This problem is not easy to address as it requires very accurate knowledge of the proteins' iron contents. A perhaps more relevant question from a biological point of view is what is the ratio of mononuclear/dinuclear centers. It was originally reported to be 2:1 [5] but a correction to 1:1 was later suggested on the basis of sequence data [11]. We now solve this question by inspection of Fig. 7. Comparing the spin concentration of the $S = 5/2$ ferric sites in

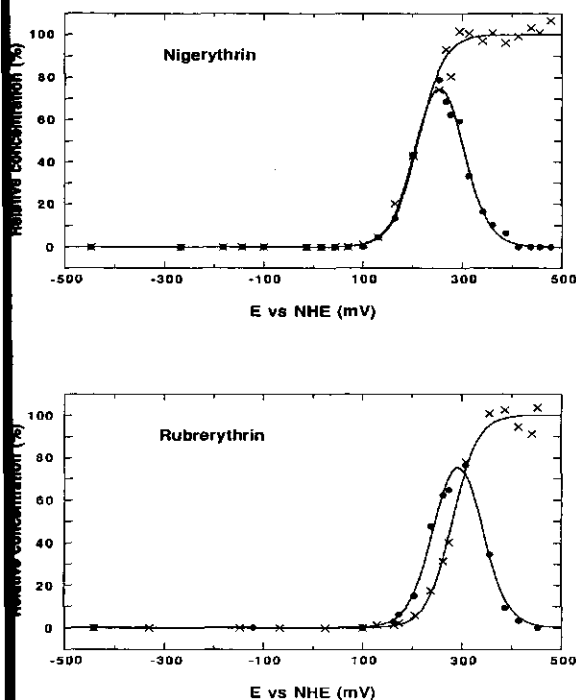


Fig. 7. Oxido-reductive titration of the mononuclear iron (x) and the dinuclear cluster (●) of *D. vulgaris* nigerythrin and rubrerythrin. The mononuclear iron was monitored at $g = 4.3$ with a detection temperature of 105 K; the dinuclear cluster was monitored at $g = 1.74$ with a detection temperature of 12 K. Other EPR conditions: microwave frequency, 9.30 GHz; microwave power, 100 mW; modulation amplitude, 1.6 mT. The solid lines are fits for $n = 1$ redox transitions with the midpoint potentials given in Table 1. NHE = Normal hydrogen electrode.

+350 mV samples with the maximal spin concentration of the mixed-valence state of the dinuclear center we find that the ratio $[S = 1/2]/[S = 5/2]$ is approximately 0.73. Fitting the amplitudes of the $S = 1/2$ signal to Eqn (2) (in which F is the Faraday constant and R is the gas constant),

$$100\%/[S = 1/2] = 1 + \exp\{(E_1 - E)nF/RT\} + \exp\{(E - E_2)nF/RT\} \quad (2)$$

the appropriate correction for loss of spin intensity due to disproportionation can be made [47-49]. This leads to an actual concentration ratio very close to unity for both proteins (Table 1). We conclude from these observations that both nigerythrin and rubrerythrin contain one mononuclear and one dinuclear center per subunit. Therefore, the holoproteins should carry six iron ions/ α_2 -dimer.

DISCUSSION

Non-heme, non-Fe/S, dinuclear iron proteins form a small but diverse class with respect to catalytic activity, nature of the bridges between the two Fe ions and reduction potentials of the individual Fe ions. The two proteins described here add to this diversity. The biological functions of nigerythrin and rubrerythrin are unknown; however, they are isolated from an anaerobe, therefore oxygen-transport (cf.

hemerythrin) or monooxygenase (cf. methane monooxygenase) are not likely. We have considered superoxide dismutase and catalase activity (as part of a protection mechanism against oxygen toxicity); activity tests were negative. Pyrophosphatase activity (cf. purple acid phosphatase) has been reported for rubrerythrin [50] but later proved not to be reproducible [11]. We have not found any pyrophosphatase activity. In the dinuclear-iron-containing ribonucleotide reductase from aerobic species the cluster supposedly acts in the stabilization of the tyrosine radical (i.e. a peroxidase activity [51]), again not a likely function in an anaerobe. It has been argued in a recent review that dinuclear iron proteins match, or even outdo, hemoproteins in versatility, and in this comparison rubrerythrin was juxtaposed to the cytochromes to suggest a role in electron transfer [52]. We have now determined that the redox potentials of all iron in rubrerythrin and in nigerythrin are $E_{m,7} > 200$ mV. It seems to us that these numbers make it unlikely that the two proteins act in electron transfer in *Desulfovibrio*. We suggest that the proteins may play a non-redox role different from functions for dinuclear iron proteins which have been established thus far.

Assignment of a function to these proteins may be helped by knowledge of their localization in the cell. In their first description of rubrerythrin, LeGall et al. claimed this protein to be periplasmic [5]. However, in subsequent sequencing work, no processable export sequence was identified [9, 10]. The genes for other periplasmic proteins in *D. vulgaris*, namely hydrogenase and three different cytochromes, in all cases do code for export sequences [31, 53]. It is possible that the localization of rubrerythrin proved ambiguous because of the nature of the starting material used by LeGall and coworkers. They isolated the protein from cells that were stored at -80°C and thawed at room temperature for 14 h. [5]. We have recently argued that this procedure may well lead to rupture of the periplasmic membrane and that the resulting material is not optimal for the isolation of active Fe-hydrogenase [54]. With antibodies against nigerythrin we have shown that this protein is obtained upon prolonged extraction of freshly harvested *D. vulgaris* cells together with a marker enzyme for the cytoplasm, i.e. the dissimilatory sulfite reductase.

The N-terminal sequence of nigerythrin shows some similarity to that of rubrerythrin; however, there is a much stronger similarity to the N-terminal sequence from the β -subunit of the *E. coli* nitrate reductase complex. It is unlikely that this similarity reflects a similarity in catalytic function because, from the 16th residue, onwards the *E. coli* protein carries Cys-rich motifs for the coordination of four Fe/S clusters [25, 26, 28]. Also, we have not found any nitrate reductase activity with nigerythrin or rubrerythrin. All three N-terminal sequences are rich in positively charged and in uncharged, polar groups. We suggest that these sequences may carry a recognition motif to target and associate the respective proteins to a receptive complementary structure, e.g. a protein partner or a membrane (notably, the inner side of the cytoplasmic membrane).

The precise structure of the dinuclear cluster in the two proteins is yet to be established. The amino-acid sequence of nigerythrin is unknown, except for the first 15 residues. Kurtz and Prickril noted that the rubrerythrin subunit contains a pair of E-X-X-H sequences, which is also found in methane monooxygenase and in ribonucleotide reductase [11]. From the X-ray structure of the latter enzyme we know that this pair provides one bridging carboxylate and three external ligands to the dinuclear cluster [12]. Whether the

clusters in nigerythrin and rubrerythrin are μ -oxo bridged is not established. With the sequence known, rubrerythrin is an attractive candidate for X-ray crystallography. Sieker et al. described preliminary crystallization results on rubrerythrin several years ago [55] but no follow-up has been reported yet. We suggested above that some apoprotein may be present in the purified proteins and this may have frustrated the crystallization work.

A previous Mössbauer spectroscopic study led to the conclusion that rubrerythrin contains a single dinuclear iron cluster/two mononuclear iron [5]. This is at variance with the 1:1 ratio that we derive from our present EPR analysis. However, the optical spectra of the two preparations are apparently identical. We suggest that the Mössbauer analysis may be incorrect because the rubrerythrin was not in a precisely defined redox state. This is certainly the case for the protein as isolated (cf. Table 1). To obtain Mössbauer data on all-ferrous rubrerythrin, LeGall et al. used ascorbate-reduced protein [5]. We have, however, observed that reduction kinetics of the dinuclear cluster in these proteins by ascorbate or by dithionite is very slow in the absence of redox mediator. Similar behaviour (i.e. complete reduction takes at least several hours) is apparently exhibited by the dinuclear iron cluster in ribonucleotide reductase [34].

An $E_{m,7.6} = +230$ mV in phosphate buffer was originally found with EPR for the mononuclear iron in rubrerythrin [5]. In a subsequent preliminary report the detection of redox cooperativity between the mononuclear iron and the dinuclear cluster was claimed [56] but no substantiation has been provided yet. Our present findings are not consistent with the previous. We find $E_{m,7.0} = +281$ mV using Hepes buffer to avoid pH-shift artifacts upon freezing (cf. [57]). We also find that all three redox transitions both in rubrerythrin and in nigerythrin are well described as Nernstian half reactions with $n = 1$ without cooperativity. This has been an important datum in our subsequent determination of the unit stoichiometry of mononuclear/dinuclear centers. However, the question of cooperativity may not be of biological relevance for redox transitions that appear to be outside the practical range of potentials for the cytoplasm of a sulfate reducer.

We thank A. H. Westphal for help with the sequence comparisons. We thank Professor C. Veeger for his continuous interest and support. This investigation was supported by the Netherlands Foundation for Chemical Research (SON) with financial aid from the Netherlands Organization for Scientific Research (NWO).

REFERENCES

- Moura, I., Macedo, A. & Moura, J. J. G. (1989) in *Advanced EPR: applications in biology and biochemistry* (Hoff, A. J., ed.) pp. 813–838, Elsevier, Amsterdam.
- Cammack, R. (1992) in *Advances in inorganic chemistry*, vol. 38: *Iron-sulfur proteins* (Cammack, R. & Sykes, A. G., eds) pp. 281–322, Academic Press, London.
- Moura, I., Huynh, B.-H., Hausinger, R. P., LeGall, J., Xavier, A. V. & Münck, E. (1980) *J. Biol. Chem.* 255, 2493–2498.
- Moura, I., Tavares, P., Moura, J. J. G., Ravi, N., Huynh, B.-H., Liu, M.-Y. & LeGall, J. (1990) *J. Biol. Chem.* 265, 21596–21602.
- LeGall, J., Prickril, B. C., Moura, I., Xavier, A. V., Moura, J. J. G. & Huynh, B.-H. (1988) *Biochemistry* 27, 1636–1642.
- Eaton, W. A. & Lovenberg, W. (1973) in *Iron-sulfur proteins*, vol. 2: Molecular properties (Lovenberg, W., ed.) pp. 131–162, Academic Press, New York.
- LeGall, J., Moura, J. J. G., Peck, H. D. Jr & Xavier, A. V. (1982) in *Iron-sulfur proteins* (Spiro, T. G., ed.) pp. 177–248, John Wiley & Sons, New York.
- Holmes, M. A., Letrong, I., Turley, S., Sieker, L. C. & Stenkamp, R. E. (1991) *J. Mol. Biol.* 218, 583–593.
- van Beumen, J. J., van Driessche, G., Liu, M.-Y. & LeGall, J. (1991) *J. Biol. Chem.* 266, 20645–20653.
- Prickril, B. C., Kurtz, D. M., LeGall, J. & Voordouw, G. (1991) *Biochemistry* 30, 11118–11123.
- Kurtz, D. M. & Prickril, B. C. (1991) *Biochem. Biophys. Res. Commun.* 181, 337–341.
- Nordlund, P., Sjöberg, B. M. & Eklund, H. (1990) *Nature* 345, 593–598.
- Postgate, J. R. (1951) *J. Gen. Microbiol.* 5, 714–724.
- van der Westen, H. M., Mayhew, S. G. & Veeger, C. (1978) *FEBS Lett.* 86, 122–126.
- Pierik, A. J., Wolbert, R. B. G., Mutsaers, P. H. A., Hagen, W. R. & Veeger, C. (1992) *Eur. J. Biochem.* 206, 697–704.
- Goa, J. (1953) *Scand. J. Clin. Lab. Invest.* 5, 218–222.
- Bensadoun, A. & Weinstein, D. (1976) *Anal. Biochem.* 70, 241–250.
- Bradford, M. M. (1976) *Anal. Biochem.* 72, 248–254.
- Brown, N. C., Eliasson, R., Reichard, P. & Thelander, L. (1969) *Eur. J. Biochem.* 9, 512–518.
- Jones, R. W. & Garland, P. B. (1977) *Biochem. J.* 164, 199–211.
- McCord, J. M. & Fridovich, I. (1969) *J. Biol. Chem.* 244, 6049–6055.
- Rørth, M. & Jensen, P. K. (1967) *Biochim. Biophys. Acta* 139, 171–173.
- Ottolenghi, P. (1975) *Biochem. J.* 151, 61–66.
- Pierik, A. J. & Hagen, W. R. (1991) *Eur. J. Biochem.* 195, 505–516.
- Blasco, F., Iobbi, C., Giordano, G., Chippaux, M. & Bonnefoy V. (1989) *Mol. Gen. Genet.* 218, 249–256.
- Blasco, F., Iobbi, C., Ratouchniak, J., Bonnefoy, V. & Chippaux M. (1990) *Mol. Gen. Genet.* 222, 104–111.
- Pearson, W. (1990) *Methods Enzymol.* 183, 63–98.
- Guigliarelli, B., Asso, M., More, C., Augier, V., Blasco, F., Pommier, J., Giordano, G. & Bertrand, P. (1992) *Eur. J. Biochem.* 207, 61–68.
- Voordouw, G. & Brenner, S. (1986) *Eur. J. Biochem.* 159, 347–351.
- van Rooijen, G. J. H., Bruschi, M. & Voordouw, G. (1989) *Bacteriol.* 171, 3575–3578.
- Pollock, W. B. R., Louffi, M., Bruschi, M., Rapp-Giles, B. J., Wall, J. D. & Voordouw, G. (1991) *J. Bacteriol.* 173, 220–228.
- Kremer, D. R., Veenhuis, M., Fauque, G., Peck, H. D. Jr, LeGall, J., Lampreia, J., Moura, J. J. G. & Hansen, T. A. (1988) *Arch. Microbiol.* 150, 296–301.
- Ehrenberg, A. & Reichard, P. (1972) *J. Biol. Chem.* 247, 3485–3488.
- Lynch, J. B., Juarez-Garcia, C., Münck, E. & Que, L. Jr (1989) *J. Biol. Chem.* 264, 8091–8096.
- Wickman, H. H., Klein, M. P. & Shirley, D. A. (1965) *J. Chem. Phys.* 42, 2113–2117.
- Abraham, A. & Bleaney, B. (1970) *Electron paramagnetic resonance of transition ions*, pp. 436–442, Clarendon Press Oxford, 1970.
- Hagen, W. R. (1992) in *Advances in inorganic chemistry*, vol. 38: *Iron-sulfur proteins* (Cammack, R. & Sykes, A. G., ed) pp. 165–222, Academic Press, London.
- Peisach, J., Blumberg, W. E., Lode, E. T. & Coon, M. J. (197) *J. Biol. Chem.* 246, 5877–5881.
- Hearshen, D. O., Hagen, W. R., Sands, R. H., Grande, H. J., Crespi, H. L., Gunsalus, I. C. & Dunham, W. R. (1986) *Magn. Reson.* 69, 440–459.
- Muhoberac, B. B., Wharton, D. C., Babcock, L. M., Harrington, P. C. & Wilkins, R. G. (1980) *Biochim. Biophys. Acta* 62, 337–345.
- Doi, K., Antanaitis, B. C. & Aisen, P. (1988) *Struct. Bonding* 70, 1–26.
- Woodland, M. P., Patil, D. S., Cammack, R. & Dalton, H. (198) *Biochim. Biophys. Acta* 873, 237–242.

3. Gerez, C., Atta, M., Fontecave, M., Gaillard, J., Scheer, C. & Latour, J. M. (1991) *J. Inorg. Biochem.* 43, 536.
4. Bertrand, P., Guigliarelli, B. & Gayda, J.-P. (1986) *Arch. Biochem. Biophys.* 245, 305-307.
5. Gibson, J. F., Hall, D. O., Thornley, J. H. M. & Whatley, F. R. (1966) *Proc. Natl. Acad. Sci USA* 56, 987-990.
6. Bertrand, P. & Gayda, J.-P. (1979) *Biochim. Biophys. Acta* 579, 107-121.
7. Clark, W. M. (1960) *Oxidation-reduction potentials of organic systems*, ch. 7, Williams & Wilkins, Baltimore, MD.
8. Liu, K. E. & Lippard, S. J. (1991) *J. Biol. Chem.* 266, 12836-12839.
9. Liu, K. E. & Lippard, S. J. (1991) *J. Biol. Chem.* 266, 24859.
10. Liu, M.-Y. & LeGall, J. (1990) *Biochem. Biophys. Res. Commun.* 171, 313-318.
11. Fontecave, M., Gerez, C., Mansuy, D. & Reichard, P. (1990) *J. Biol. Chem.* 265, 10919-10924.
12. Stubbe, J. (1991) *Curr. Opin. Struct. Biol.* 1, 788-795.
13. Prickril, B. C., Czechowski, M. H., Przybyla, A. E., Peck, H. D. Jr & LeGall, J. (1986) *J. Bacteriol.* 167, 722-725.
14. Pierik, A. J., Hagen, W. R., Redeker, J. S., Wolbert, R. B. G., Boersma, M., Verhagen, M. F. J. M., Grande, H. J., Veeger, C., Mutsaers, P. H. A., Sands, R. H. & Dunham, W. R. (1992) *Eur. J. Biochem.* 209, 63-72.
15. Sieker, L. C., Turley, S., Stenkamp, R. E. & LeGall, J. (1987) *Recl. Trav. Chim. Pays-Bas* 106, 281.
16. Moura, I., Moura, J. J. G., LeGall, J. & Huynh, B.-H. (1989) *J. Inorg. Biochem.* 36, 228.
17. Williams-Smith, D. L., Bray, R. C., Barber, M. J., Tsopanakis, A. D. & Vincent, S. P. (1977) *Biochem. J.* 167, 593-600.

Chapter 10

The occurrence of high-spin states in iron-sulfur proteins.

In Table 1 and 2 a comprehensive review is presented summarizing all currently known iron-sulfur proteins with $S \geq 3/2$ ground states. For comparison a selection of relevant iron containing proteins and inorganic transition metal compounds with $S \geq 3/2$ spin states is also included. Since the axial zero-field splitting parameter D and the rhombicity (E/D) for non-integer spin systems are easily determined in particular by EPR spectroscopy (see Chapter 4, 7, 8 and 9) these values have also been listed in Table 1. Occasionally the D and E/D parameters are available for more than one source or by a combination of EPR, Mössbauer, MCD and/or ENDOR spectroscopic measurements (for instance $S=3/2$ of $[4\text{Fe-4S}]^{1+}$ model compounds and the FeMo cofactor in the *Klebsiella pneumoniae* MoFe protein). Table 1 provides those data or the range of data which were quoted with the highest accuracy in the original references. Some D and E/D values were not actually mentioned in the quoted publication(s), but have been estimated from temperature dependence of spectra and/or g -values.

Contrary to the comparatively easy determination of both spin state, D and E/D parameters for Kramers systems the extraction of spin Hamiltonian parameters of Non-Kramers systems (Table 2) is considerably more difficult. Due to faster relaxation, inherently weaker intensity or even absence of (parallel-mode) EPR signals the determination of spin state and spin Hamiltonian parameters is not straightforward, and might necessitate Mössbauer and MCD measurements. For a number of cases accurate data are either fully absent or spectroscopic measurements give conflicting results [85,151,158,161]. The representation of spin Hamiltonian parameters has therefore been omitted from Table 2. Judged from the rapid expansion of publications on spin integer systems and the renewed interest in parallel mode EPR spectroscopy more theoretically oriented research will certainly be aimed at simulation of spin-integer spectra, the distribution of Spin Hamiltonian parameters and the use of high order terms.

A concluding remark with respect to the applicability and biological relevance of the listed spin states and parameters has to be made. Since the direct relation between 1) biological function and spin state, 2) three-dimensional structure and spin state [105], 3) three-dimensional structure and E and D values is not clear, the subdivision is partially superficial. The actual spin state of the clusters might even be different at biologically relevant temperatures, because spectroscopic measurements (necessarily) have been performed between 1.5 and 200 K. Nonetheless the biologically oriented reader should be aware that the low temperature spectroscopic measurements on superspin paramagnets provide an indispensable probe for the identification and characterization of unusual iron-sulfur clusters in proteins. This justifies a partially phenomenological approach.

Table 1: Kramers Spin systems with S=3/2, S=5/2, S=7/2 and S=9/2 in iron-sulfur and iron containing proteins and some relevant model compounds

nd: The D or E/D value was not determined and could not be estimated from the data in the quoted reference(s).

var: A number of compounds have been characterized with variable D or E/D values.

Protein or model compound	Spin state	D cm ⁻¹	E/D	References
Iron-Sulfur proteins				
[4Fe-4S] ⁺ in ferredoxin <i>Pyrococcus furiosus</i>	S=3/2	3.3	0.22	[1-4]
2*[4Fe-4S] ⁺ in ferredoxin <i>Desulfovibrio africanus</i>	S=3/2	nd	0.27	[5,6]
2*[4Fe-4Se] ⁺ in ferredoxin	S=3/2	3	0.08	[7-9]
[4Fe-4S] ⁺ in glutamine amidotransferase	S=3/2	>3	0.02	[10,11]
[4Fe-4S] ⁺ in Fe-hydrogenase	S=3/2	-3	0.15	[12,13]
[4Fe-4S] ⁺ in aldehyde Fd oxidoreductase	S=3/2	4.3	0.135	[14]
[4Fe-4S] ⁺ in CO dehydrogenase	S=3/2	1	1	[15]
[Ni3Fe4S] ⁺ in ferredoxin	S=3/2	-2.2	0.18	[16]
[Ni3Fe4S] ⁺ CN ⁻ complex in ferredoxin	S=3/2	>0	0.06	[16]
Cofactor of nitrogenase comp. 1	S=3/2			
Mo-containing systems				
<i>Azotobacter chroococcum</i>		nd	0.05	[17,18]
<i>Azotobacter vinelandii</i>		6.1	0.053	[18-27], Chapter 8
<i>Bacillus polymyxa</i>		nd	0.05	[18]
<i>Chromatium vinosum</i>		nd	0.05	[28]
<i>Clostridium pasteurianum</i>		5.2	0.042	[18,26,27,29-32]
<i>Klebsiella pneumoniae</i>		6.2	0.055	[18,25,33,34]
V-containing systems				
<i>Azotobacter chroococcum</i>		<0	0.26	[35]
<i>Azotobacter vinelandii</i>		-0.74	0.26	[36-38]
Fe-only-containing systems				
<i>Azotobacter vinelandii</i>		nd	nd	[39]
<i>Rhodobacter capsulatus</i>		nd	0.33	[40]
Nitrogenase Fe protein				
<i>Azotobacter chroococcum</i>	S=3/2	nd	nd	[41]
<i>Azotobacter vinelandii</i>		-5	0.12	[41-45]
<i>Clostridium pasteurianum</i>		nd	nd	[44-46]
<i>Klebsiella pneumoniae</i>		nd	nd	[41]
<i>Azotobacter chroococcum</i> (V-system)		nd	nd	[47]
<i>Azotobacter vinelandii</i> (V-system)		nd	0.15	[48]
Reduced prismane protein	S=3/2	>1	0.24	[49,50]
[Fe-S] in <i>E. coli</i> sulfite reductase	S=3/2	nd	0.30	[51]

Table 1 continued

Protein or model compound	Spin state	D cm ⁻¹	E/D	References
Iron-Sulfur proteins continued				
Oxidized rubredoxin	S=5/2	1.5-2	0.28	[52-58]
Oxidized desulforedoxin	S=5/2	+2.2	0.08	[59,60]
Oxidized rubrerythrin	S=5/2	+1.5	0.29	[61], Chapter 9
Oxidized nigerythrin	S=5/2	-1	0.26	Chapter 9
Oxidized desulferodoxin	S=5/2	+2	0.08	[62]
[3Fe-4S] ⁺ in purple aconitase	S=5/2	+1.5	0.31	[63,64]
Nitrogenase Fe protein	S=5/2			
<i>Azotobacter vinelandii</i>		2	0.32	[45]
[4Fe-4S] ⁺ in glutamine amidotransferase	S=5/2	<0	0.31	[11]
[Zn3Fe4S] ⁺ in ferredoxin	S=5/2	-2.7	0.25	[65,66]
[Cd3Fe-4S] ⁺ in ferredoxin	S=5/2	nd	0.30	[65]
Oxidized CO dehydrogenase	S=5/2	+2	0.27	[67-69]
Semiox. P-clusters nitrogenase comp. 1	S=5/2			
<i>Azotobacter vinelandii</i>		-3	0.02	[70,71]
<i>Klebsiella pneumoniae</i>		-3	0.02	[72]
<i>Azotobacter chroococcum</i> (V system)		nd	0.1	[71,73]
Oxid. P ^{ox2} P-clusters nitrogenase comp. 1	S=7/2			
<i>Azotobacter vinelandii</i>		-3.7	0.04	[74,75], Chapter 8
<i>Klebsiella pneumoniae</i>		-3.3	0.04	[74-76]
<i>Azotobacter chroococcum</i>		nd	0.04	[74]
Selenium subst. ferredoxin	S=7/2	-2.1	0.12	[77]
Dissimilatory sulfite reductase	S=9/2	-0.6	0.02-0.13	Chapter 7
Oxidized prismane protein	S=9/2	-0.9	0.06&0.11	[49,78,79], Ch. 5
Oxidized CO dehydrogenase	S=9/2	<0	0.05	[69]
Superox. P-clusters nitrogenase comp.1	S=9/2			
<i>Azotobacter vinelandii</i>		nd	nd	Chapter 8
<i>Klebsiella pneumoniae</i>		nd	nd	[76]
Gamma-irrad. ribonucleotide reductase	S=9/2	≈4	0.03	[80]
Iron-containing proteins				
Lipoxygenase-Fe ²⁺ -NO complex	S=3/2	15	0.1-0.3	[81]
Metmyoglobin	S=5/2	9	0	[82,83]
Metmyoglobin fluoride	S=5/2	6	0	[82,83]
Methemoglobin	S=5/2	10.7	0	[82,84]
Heme in cytochrome c oxidase	S=5/2	+8	0-0.02	[85]
Siroheme in sulfite reductases	S=5/2	+9	0-0.05	[51,86], Ch. 7
Superoxide dismutase	S=5/2	-2	0.24	[87-89,195]
Fe ³⁺ in lipoxygenase	S=5/2	1.7	0.01	[90]
Phenylalanine hydroxylase	S=5/2	nd	nd	[91]
Protocatechuate dioxygenase	S=5/2	±2	0.03	[92,93]
Fe ³⁺ in conalbumin/transferrin	S=5/2	nd	0.30	[94]

Table 1 continued

Protein or model compound	Spin state	D cm ⁻¹	E/D	References
Model compounds				
Extracted FeMoco	S=3/2	7.5	0.11	[95,96]
Extracted FeVaco	S=3/2	nd	nd	[97]
Fe ³⁺ in model compound	S=3/2	nd	nd	[98]
Cr ³⁺ in models	S=3/2	0.4-0.5	0.02-0.2	[99,100]
Mo ³⁺ in models	S=3/2	<0	0	[100,101]
[4Fe4S] ⁺ model compounds	S=3/2	var	var	[102-106]
Co ²⁺ substituted proteins	S=3/2	var	var	[107-111]
Fe ³⁺ -Ni ²⁺ model compound	S=3/2	nd	0.33	[112]
Fe ³⁺ -2Cu ²⁺ model compound	S=5/2	7.2	0.07	[113]
Fe ³⁺ in models	S=5/2	var	>0.25	[114-116]
Linear [3Fe4S] ¹⁺ model compound	S=5/2	+0.7	0.33	[117,118]
Mn ²⁺ in models	S=5/2	0.03-0.9	0-0.33	[119-121]
Mn ²⁺ in superoxide dismutase	S=5/2	0.5	0.027	[122]
Gd ³⁺ in soda-silica-ytria glass	S=7/2	var	var	[123]
Fe ₂ dinuclear model	S=9/2	var	var	[124-126]
Dinuclear Mn ²⁺ -Mn ³⁺ complex	S=9/2	nd	nd	[127]
Cu ²⁺ -Gd ³⁺ -Cu ²⁺ complex	S=9/2	nd	nd	[128]
Mn ²⁺ -Cu ²⁺ -Mn ²⁺ complex	S=9/2	nd	nd	[129]
Mn ⁴⁺ -3Mn ³⁺ complex	S=9/2	+0.3	0	[130]

Table 2: Non-Kramers Spin systems with $S \geq 2$ in iron-sulfur and iron-containing proteins and some relevant model compounds

MB	Mössbauer spectroscopy
MCD	Magnetic Circular Dichroism spectroscopy
//EPR	parallel-mode EPR spectroscopy
EPR	EPR spectroscopy

Protein or model compounds	Spin state	Spectroscopy	References
Iron-Sulfur proteins			
Fe ²⁺ in reduced rubredoxin	S=2	MB,MCD	[60,131,132]
Fe ²⁺ in reduced desulforedoxin	S=2	MB	[60]
Fe ²⁺ in reduced rubrerythrin	S=2	MB	[61]
Fe ²⁺ in reduced desulfoferrodoxin	S=2	MB	[62]
[3Fe-4S] ⁰ in ferredoxin	S=2	EPR,MB,MCD	[133-149]
[3Fe-4S] ⁰ in aconitase	S=2	EPR,MB	[150,151]
[3Fe-4S] ⁰ in [NiFe]hydrogenase	S=2	EPR,MB	[152,153]
[3Fe-4S] ⁰ in glutamate synthase	S=2	EPR,MCD	[154,155]
[Zn3Fe-4S] ²⁺ in ferredoxin	S=2	MB,MCD	[65,66]
[Cd3Fe-4S] ²⁺ in ferredoxin	S=2	MB,MCD	[65,66]
Proton reoxidized Fe-hydrogenase	S=2	EPR	[25,156,157]
Oxid. P ^{OX1} P-clusters nitrogenase	S=3		
<i>Azotobacter vinelandii</i>		//EPR,MB	[158],Chapter 8
<i>Klebsiella pneumoniae</i>		//EPR,MB,MCD	[158-160]
<i>Clostridium pasteurianum</i>		//EPR,MB	[158]
<i>Xanthobacter autotrophicus</i>		//EPR,MB	[158]
<i>Azotobacter chroococcum</i> (V system)		//EPR,MCD	[73]
[6Fe-6S] ⁴⁺ in prismane protein	S=4	//EPR	Chapter 5
Iron-containing proteins			
Fe ²⁺ in reduced myoglobin (CO)	S=2	//EPR,MB	[161,162]
Fe ²⁺ in reduced cytochrome P450	S=2	MB	[163]
Reduced cytochrome c oxidase	S=2	MCD	[164]
Oxid. cytochrome c oxidase	S=2	//EPR	[85,165-168]
Cytochrome bo formate compl.	S=2	EPR	[169]
Fe ²⁺ in transferrin/haemosiderin	S=2	//EPR	[85,170]
Fe ²⁺ in protocatechuate dioxygenase	S=2	MB	[171]
Fe ²⁺ in superoxide dismutase	S=2	MB	[172]
Fe ²⁺ subst. alcoholdehydrogenase	S=2	EPR,MB	[173]
Fe ²⁺ in metallothionein	S=2	EPR,MB	[174]
Fe ²⁺ -Fe ²⁺ in ribonucleotide reductase	S=4	EPR,MB	[175]
Fe ²⁺ -Fe ²⁺ azide complex in hemerythrin	S=4	//EPR,MCD	[176,177]
Fe ²⁺ -Fe ²⁺ in methane monooxygenase	S=4	//EPR	[178-182]

Table 2 continued

Protein or model compound	Spin state	Spectroscopy	References
Model compounds			
Fe ²⁺ (EDTA)	S=2	//EPR	[85,151]
Fe ²⁺ (H ₂ O) ₆	S=2	//EPR	[85,151]
Fe ²⁺ S ₄ models	S=2	EPR,MB	[183]
[4Fe-4S] ⁺ in model	S=2	MB	[184]
Fe ²⁺ -doped zinc fluosilicate	S=2	//EPR	[151]
Fe ²⁺ in porphyrin	S=2	//EPR	[151,161]
Ni ²⁺ -dimer	S=2	//EPR	[112]
Fe ³⁺ -Cu ²⁺ model	S=3	//EPR,MB	[185,186]
Ni ²⁺ acetylacetonate trimer	S=3	EPR	[187]
di-Co ²⁺ -substituted hemocyanin	S=3	EPR,MCD	[188]
Fe ²⁺ -Fe ²⁺ binuclear model	S=4	//EPR,MB	[189-191]
4Mn ⁴⁺ -Mn ³⁺ model	S=10	EPR	[192]
6Mn ²⁺ nitronyl nitroxide model	S=12	EPR	[193]
8Mn ³⁺ -4Mn ⁴⁺ model	S=14	---	[194]

References

- Conover, R.C., Kowal, A.T., Fu, W., Park, J.-B., Aono, S., Adams, M.W.W. & Johnson, M.K. (1990) J. Biol. Chem. **265**, 8533-8541.
- Park, J.-B., Fan, C., Hoffman, B.M. & Adams, M.W.W. (1991) J. Biol. Chem. **266**, 19351-19356.
- Conover, R.C., Park, J.-B., Adams, M.W.W. & Johnson, M.K. (1991) J. Am. Chem. Soc. **113**, 2799-2800.
- Adams, M.W.W. (1992) In: Advances in Inorganic Chemistry 38: Iron-Sulfur Proteins (Cammack, R. & Sykes, A.G., eds), pp. 341-396, Academic Press, San Diego.
- George, S.J., Armstrong, F.A., Hatchikian, E.C. & Thomson, A.J. (1989) Biochem. J. **264**, 275-284.
- Armstrong, F.A. (1992) In: Advances in Inorganic Chemistry 38: Iron-Sulfur Proteins (Cammack, R. & Sykes, A.G., eds), pp. 117-163, Academic Press, San Diego.
- Moulis, J.-M., Auric, P., Gaillard, J. & Meyer, J. (1984) J. Biol. Chem. **259**, 11396-11402.
- Auric, P., Gaillard, J., Meyer, J. & Moulis, J.-M. (1987) Biochem. J. **242**, 525-530.
- Meyer, J., Moulis, J.-M., Gaillard, J. & Lutz, M. (1992) In: Advances in Inorganic Chemistry 38: Iron-Sulfur Proteins (Cammack, R. & Sykes, A.G., eds), pp. 73-115, Academic Press, San Diego.
- Vollmer, S.J., Switzer, R.L. & Debrunner, P.G. (1983) J. Biol. Chem. **258**, 14284-14293.
- Oñate, Y.A., Vollmer, S.J., Switzer, R.L. & Johnson, M.K. (1989) J. Biol. Chem. **264**, 18386-18391.
- Zambrano, I.C., Kowal, A.T., Adams, M.W.W., Mortenson, L.E. & Johnson, M.K.

- (1987) Rec. Trav. Chim. Pays-Bas **106**, 235.
13. Zambrano, I.C., Kowal, A.T., Mortenson, L.E., Adams, M.W.W. & Johnson, M.K. (1989) J. Biol. Chem. **264**, 20974-20983.
 14. Mukund, S. & Adams, M.W.W. (1990) J. Biol. Chem. **265**, 11508-11516.
 15. Lindahl, P.A., Münck, E. & Ragsdale, S.W. (1990) J. Biol. Chem. **265**, 3873-3879.
 16. Conover, R.C., Park, J.-B., Adams, M.W.W. & Johnson, M.K. (1990) J. Am. Chem. Soc. **112**, 4562-4564.
 17. Yates, M.G. & Planqué, K. (1975) Eur. J. Biochem. **60**, 467-476.
 18. O'Donnell, M.J. & Smith, B.E. (1978) Biochem. J. **173**, 831-839.
 19. Münck, E., Rhodes, H., Orme-Johnson, W.H., Davis, L.C., Brill, W.J. & Shah, V.K. (1975) Biochim. Biophys. Acta **400**, 32-53.
 20. Huynh, B.H., Münck, E. & Orme-Johnson, W.H. (1979) Biochim. Biophys. Acta **527**, 192-203.
 21. Hoffman, B.M., Roberts, J.E. & Orme-Johnson, W.H. (1982) J. Am. Chem. Soc. **104**, 860-862.
 22. Hoffman, B.M., Venters, R.A., Roberts, J.E., Nelson, M. & Orme-Johnson, W.H. (1982) J. Am. Chem. Soc. **104**, 4711-4712.
 23. Euler, W.B., Martinsen, J., McDonald, J.W., Watt, G.D. & Wang, Z.-C. (1984) Biochemistry **23**, 3021-3024.
 24. Scott, D.J., May, H.D., Newton, W.E., Brigle, K.E. & Dean, D.R. (1990) Nature **343**, 188-190.
 25. Hagen, W.R. (1987) in Cytochrome systems (Papa, S., Chance, B. & Ernster, L., eds), pp. 459-466, Plenum Press, New York.
 26. Morgan, T.V., Mortenson, L.E., McDonald, J.W. & Watt, G.D. (1988) J. Inorg. Biochem. **33**, 111-120.
 27. Venters, R.A., Nelson, M.J., McLean, P.A., True, A.E., Levy, M.A., Hoffman, B.M. & Orme-Johnson, W.H. (1986) J. Am. Chem. Soc. **108**, 3487-3498.
 28. Albrecht, S.L. & Evans, M.C.W. (1973) Biochem. Biophys. Res. Comm. **55**, 1009-1014.
 29. Palmer, G., Multani, J.S., Cretney, W.C., Zumft, W.G. & Mortenson, L.E. (1972) Arch. Biochem. Biophys. **153**, 325-332.
 30. Walker, M. & Mortenson, L.E. (1973) Biochem. Biophys. Res. Comm. **54**, 669-676.
 31. Zumft, W.G., Mortenson, L.E. & Palmer, G. (1974) Eur. J. Biochem. **46**, 525-535.
 32. Gurbiel, R.J., Bolin, J.T., Ronco, A.E., Mortenson, L. & Hoffman, B.M. (1991) J. Magn. Res. **91**, 227-240.
 33. Smith, B.E., Lowe, D.J. & Bray, R.C. (1973) Biochem. J. **135**, 331-341.
 34. Kent, H.M., Ioannidis, I., Gormal, C., Smith, B.E. & Buck, M. (1989) Biochem. J. **264**, 257-264.
 35. Eady, R.R., Robson, R.L., Richardson, T.H., Miller, R.W. & Hawkins, M. (1987) Biochem. J. **244**, 197-207.
 36. Hales, B.J., Case, E.E., Morningstar, J.E., Dzeda, M.F. & Mauterer, L.A. (1986) Biochemistry **25**, 7251-7255.
 37. Hales, B.J., True, A.E. & Hoffman, B.M. (1989) J. Am. Chem. Soc. **111**, 8519-8520.
 38. Morningstar, J.E. & Hales, B.J. (1987) J. Am. Chem. Soc. **109**, 6854-6855.
 39. Pau, R.N., Eldridge, M.E., Lowe, D.J., Mitchenall, L.A. & Eady, R.R. (1993) Biochem. J. **293**, 101-107.
 40. Müller, A., Schneider, K., Knüttel, K. & Hagen, W.R. (1992) FEBS Lett. **303**, 36-40.
 41. Hagen, W.R., Eady, R.R., Dunham, W.R. & Haaker, H. (1985) FEBS Lett. **189**, 250-254.
 42. Lindahl, P.A., Day, E.P., Kent, T.A., Orme-Johnson, W.H. & Münck, E. (1985) J. Biol. Chem. **260**, 11160-11173.
 43. Watt, G.D. & McDonald, J.W. (1985) Biochemistry **24**, 7226-7231.

44. Vance Morgan, T., Prince, R.C. & Mortenson, L.E. (1986) FEBS Lett. **206**, 4-8.
45. Lindahl, P.A., Gorelick, N.J., Münck, E. & Orme-Johnson, W.H. (1987) J. Biol. Chem. **262**, 14945-14953.
46. Meyer, J., Gaillard, J. & Moulis, J.-M. (1988) Biochemistry **27**, 6150-6156.
47. Eady, R.R., Richardson, T.H., Miller, R.W., Hawkins, M. & Lowe, D.J. (1988) Biochem. J. **256**, 189-196.
48. Hales, B.J., Langosch, D.J. & Case, E.E. (1986) J. Biol. Chem. **261**, 15301-15306.
49. Moura, I., Tavares, P., Moura, J.J.G., Ravi, N., Huynh, B.H., Liu, M.Y. & LeGall, J. (1992) J. Biol. Chem. **267**, 4489-4496.
50. Pierik, A.J. & Hagen, W.R., unpublished results.
51. Janick, P.A. & Siegel, L.M. (1982) Biochemistry **21**, 3538-3547.
52. Peisach, J., Blumberg, W.E., Lode, E.T. & Coon, M.J. (1971) J. Biol. Chem. **246**, 5877-5881.
53. Lovenberg, W. & Walker, M.N. (1978) Methods Enzymol. **53**, 340-346.
54. Moura, I., Moura, J.J.G., Santos, H.H., Xavier, A.V. and LeGall, J. (1979) FEBS Lett. **107**, 419-421.
55. Palmer, G. & Brintzinger, H. (1966) Nature **211**, 189-190.
56. Schulz, C.E. & Debrunner, P.G. (1976) J. Phys. Colloque **37 (suppl. 6)**, 163-165.
57. Schulz, C.E. (1979) PhD Thesis, Univ. of Illinois at Urbana-Champaign.
58. Bennett, D.E. & Johnson, M.K. (1987) Biochim. Biophys. Acta **911**, 71-80.
59. Moura, I., Xavier, A.V., Cammack, R., Bruschi, M. and LeGall, J. (1978) Biochim. Biophys. Acta **533**, 156-162.
60. Moura, I., Huynh, B.H., Hausinger, R.P., LeGall, J., Xavier, A.V. & Münck, E. (1980) J. Biol. Chem. **255**, 2493-2498.
61. LeGall, J., Prickril, B.C., Moura, I., Xavier, A.V., Moura, J.J.G. & Huynh, B.-H. (1988) Biochemistry **27**, 1636-1642.
62. Moura, I., Tavares, P., Moura, J.J.G., Ravi, N., Huynh, B.H., Liu, M.-Y. & LeGall, J. (1990) J. Biol. Chem. **265**, 21596-21602.
63. Kennedy, M.C., Kent, T.A., Emptage, M.H., Merkle, H., Beinert, H. & Münck, E. (1984) J. Biol. Chem. **259**, 14463-14471.
64. Richards, A.J.M., Thomson, A.J., Holm, R.H. & Hagen, K.S. (1990) Spectrochim. Acta **46A**, 987-993.
65. Butt, J.E., Armstrong, F.A., Breton, J., George, S.J., Thomson, A.J. & Hatchikian, E.C. (1991) J. Am. Chem. Soc. **113**, 6663-6670.
66. Surerus, K.K., Münck, E., Moura, I., Moura, J.J.G. & LeGall, J. (1987) J. Am. Chem. Soc. **109**, 3805-3807.
67. Bonam, D. & Ludden, P.W. (1987) J. Biol. Chem. **262**, 2980-2987.
68. Stephens, P.J., McKenna, M.-C., Ensign, S.A., Bonam, D. & Ludden, P.W. (1989) J. Biol. Chem. **264**, 16347-16350.
69. Jetten, M.S.M., Pierik, A.J. & Hagen, W.R. (1991) Eur. J. Biochem. **202**, 1291-1297.
70. Pierik, A.J. & Hagen, W.R. (1993) unpublished results.
71. Tittsworth, R. & Hales, B.J. (1993) In: New Horizons in Nitrogen Fixation (Palacios, R., Mora, J. & Newton, W.E., eds.), Nijhoff/Junk, Dordrecht (The Netherlands), 138.
72. Pierik, A.J., Howes, B.D. & Smith, A.J. (1993) unpublished results.
73. Pierik, A.J., Lowe, D.J., Eldridge, M.E., Marritt, S., Farrar, J.A., Thomson, A.J. & Eady, R.R. (1993) In: New Horizons in Nitrogen Fixation (Palacios, R., Mora, J. & Newton, W.E., eds.), Nijhoff/Junk, Dordrecht (The Netherlands), 147.
74. Hagen, W.R., Wassink, H., Eady, R.R., Smith, B.E. & Haaker, H. (1987) Eur. J. Biochem. **169**, 457-465.
75. Lindahl, P.A., Papaefthymiou, V., Orme-Johnson, W.H. & Münck, E. (1988) J. Biol. Chem. **263**, 19412-19418.

76. Pierik, A.J., Marritt, S., Thomson, A.J. & Smith, B.E. (1993) unpublished results.
77. Gaillard, J., Moulis, J.-M., Auric, P. & Meyer, J. (1986) Biochemistry **25**, 464-468.
78. Stokkermans, J.P.W.G., Houba, P.H.J., Pierik, A.J., Hagen, W.R., Van Dongen, W.M.A.M. & Veeger, C. (1992) Eur. J. Biochem. **210**, 983-988.
79. Ravi, N., Moura, I., Tavares, P., LeGall, J., Huynh, B.H. & Moura, J.J.G. (1991) J. Inorg. Biochem. **43**, 252.
80. Hendrich, M.P., Elgren, T.E. & Que, L. (1991) Biochem. Biophys. Res. Commun. **176**, 705-710.
81. Salerno, J.C. & Siedow, J.N. (1979) Biochim. Biophys. Acta **579**, 246-251.
82. Peisach, J., Blumberg, W.E., Ogawa, S., Rachmilewitz, E.A. & Oltzik, R. (1971) J. Biol. Chem. **246**, 3342-3355.
83. Yim, M.B., Kuo, L.C. & Makinen, M.W. (1982) J. Magn. Res. **46**, 247-256.
84. Alpert, Y., Couder, Y., Tuchendler, J. & Thomé, H. (1973) Biochim. Biophys. Acta **322**, 34-37.
85. Hagen, W.R. (1982) Biochim. Biophys. Acta **708**, 82-98.
86. Siegel, L.M., Rueger, D.C., Barber, M.J., Krueger, R.J., Orme-Johnson, N.R. & Orme-Johnson, W.H. (1982) J. Biol. Chem. **257**, 6343-6350.
87. Yost, J.F. & Fridovich, I. (1973) J. Biol. Chem. **248**, 4905-4908.
88. Hatchikian, E.C. & Henry, Y.A. (1977) Biochimie **59**, 153-161.
89. Fee, J.A., McClune, G.J., Lees, A.C., Zidovetzki, R. & Pecht, I. (1981) Israel J. Chem. **21**, 54-58.
90. Zhang, Y., Gebhard, M.S. & Solomon, E.I. (1991) J. Am. Chem. Soc. **113**, 5162-5175.
91. Martínez, A., Andersson, K.K., Haavik, J. & Flatmark, T. (1991) Eur. J. Biochem. **198**, 675-682.
92. Que, L., Lipscomb, J.D., Zimmermann, R., Münck, E., Orme-Johnson, N.R. & Orme-Johnson, W.H. (1976) Biochim. Biophys. Acta **452**, 320-334.
93. Que, L. (1980) Structure Bonding **40**, 39-72.
94. Price, E.M. & Gibson, J.F. (1972) J. Biol. Chem. **247**, 8031-8035.
95. Rawlings, J., Shah, V.K., Chisnell, J.R., Brill, W.J., Zimmermann, R., Münck, E. & Orme-Johnson, W.H. (1978) J. Biol. Chem. **253**, 1001-1004.
96. Burgess, B.K., Stiefel, E.I. & Newton, W.E. (1980) J. Biol. Chem. **255**, 353-356.
97. Smith, B.E., Eady, R.R., Lowe, D.J. & Gormal, C. (1988) Biochem. J. **250**, 299-302.
98. Hoskins, B.F., Martin, R.L. & White, A.H. (1966) Nature **211**, 627-628.
99. Hempel, J.C., Morgan, L.O. & Lewis, W.B. (1970) Inorg. Chem. **9**, 2064-2072.
100. Jarrett, H.S. (1957) J. Chem. Phys. **27**, 1298-1304.
101. Averill, B.A. & Orme-Johnson, W.H. (1980) Inorg. Chem. **19**, 1702-1705.
102. Laskowski, E.J., Reynolds, J.G., Frankel, R.B., Foner, S., Papaefthymiou, G.C. & Holm, R.H. (1979) J. Am. Chem. Soc. **101**, 6562-6570.
103. Carney, M.J., Holm, R.H., Papaefthymiou, G.C. & Frankel, R.B. (1986) J. Am. Chem. Soc. **108**, 3519-3521.
104. Carney, M.J., Papaefthymiou, G.C., Spartalian, K., Frankel, R.B. & Holm, R.H. (1988) J. Am. Chem. Soc. **110**, 6084-6095.
105. Carney, M.J., Papaefthymiou, G.C., Whitener, M.A., Spartalian, K., Frankel, R.B. & Holm, R.H. (1988) Inorg. Chem. **27**, 346-352.
106. Carney, M.J., Papaefthymiou, G.C., Frankel, R.B. & Holm, R.H. (1989) Inorg. Chem. **28**, 1497-1503.
107. Kennedy, F.S., Hill, H.A.O., Kaden, T.A. & Vallee, B.L. (1972) Biochem. Biophys. Res. Comm. **48**, 1533-1539.
108. Cockle, S.A., Lindskog, S. & Grell, E. (1974) Biochem. J. **143**, 703-715.
109. Good, M. & Vašák, M. (1986) Biochemistry **25**, 3328-3334.
110. Moura, I., Teixeira, M., LeGall, J. & Moura, J.J.G. (1991) J. Inorg. Biochem. **44**, 127-

- 139.
111. Bubacco, L., Magliozzo, R.S., Beltramini, M., Salvato, B. & Peisach, J. (1992) Biochemistry **31**, 9294-9303.
 112. Holman, T.R., Hendrich, M.P. & Que, L. (1992) Inorg. Chem. **31**, 937-939.
 113. Morgenstern-Badarau, I. & Wickman, H.H. (1985) Inorg. Chem. **24**, 1889-1892.
 114. Wickman, H.H., Klein, M.P. & Shirley, D.A. (1965) J. Chem. Phys. **42**, 2113-2117.
 115. Dowsing, R.D. & Gibson, J.F. (1969) J. Chem. Phys. **50**, 294-303.
 116. Lang, G., Aasa, R., Garbett, K. & Williams, R.J.P. (1971) J. Chem. Phys. **55**, 4539-4548.
 117. Hagen, K.S., Watson, A.D. & Holm, R.H. (1983) J. Am. Chem. Soc. **105**, 3905-3913.
 118. Gierd, J.-J., Papaefthymiou, G.C., Watson, A.D., Gamp, E., Hagen, K.S., Edelstein, N., Frankel, R.B. & Holm, R.H. (1984) J. Am. Chem. Soc. **106**, 5941-5947.
 119. Dowsing, R.D., Gibson, J.F., Goodgame, D.M.L., Goodgame, M. & Hayward, P.J. (1969) J. Chem. Soc. **1969A**, 1242-1248.
 120. Dowsing, R.D., Gibson, J.F., Goodgame, M. & Hayward, P.J. (1969) J. Chem. Soc. **1969A**, 187-193.
 121. Hoffman, B.M., Weschler, C.J. & Basolo, F. (1976) J. Am. Chem. Soc. **98**, 5473-5482.
 122. Peterson, J., Fee, J.A. & Day, E.P. (1991) Biochim. Biophys. Acta **1079**, 161-168.
 123. Nicklin, R.C., Johnstone, J.K., Barnes, R.G. & Wilder, D.R. (1973) J. Chem. Phys. **59**, 1652-1668.
 124. Snyder, B.S., Patterson, G.S., Abrahamson, A.J. & Holm, R.H. (1989) J. Am. Chem. Soc. **111**, 5214-5223.
 125. Surerus, K.K., Münck, E., Snyder, B.S. & Holm, R.H. (1989) J. Am. Chem. Soc. **111**, 5501-5502.
 126. Ding, X.-Q., Bominaar, E.L., Bill, E., Winkler, H., Trautwein, A.X., Drüeke, S., Chaudhuri, P. & Wieghardt, K. (1990) J. Chem. Phys. **92**, 178-186.
 127. Schake, A.R., Schmitt, E.A., Conti, A.J., Streib, W.E., Huffman, J.C., Hendrickson, D.N. & Christou, G. (1991) Inorg. Chem. **30**, 3192-3199.
 128. Bencini, A., Benelli, C., Caneschi, A., Dei, A. & Gatteschi, D. (1986) Inorg. Chem. **25**, 572-575.
 129. Pei, Y., Journaux, Y. & Kahn, O. (1988) Inorg. Chem. **27**, 399-404.
 130. Hendrickson, D.N., Christou, G., Schmitt, E.A., Libby, E., Bashkin, J.S., Wang, S., Tsai, H.-L., Vincent, J.B., Boyd, P.D.W., Huffmann, J.C., Folting, K., Li, Q. & Streib, W.E. (1992) J. Am. Chem. Soc. **114**, 2455-2471.
 131. Winkler, H., Schultz, C. & Debrunner, P.G. (1979) Phys. Lett. **69A**, 360-363.
 132. Johnson, M.K., Robinson, A.E. & Thomson, A.J. (1982) In: Iron Sulfur Proteins (Spiro, T.G., ed.) pp. 367-406.
 133. LeGall, J., Ljungdahl, P.O., Moura, I., Peck, H.D., Xavier, A.V., Moura, J.J.G., Teixeira, M., Huynh, B.H. & DerVartanian, D.V. (1982) Biochem. Biophys. Res. Comm. **106**, 610-616.
 134. Thomson, A.J., Robinson, A.E., Johnson, M.K., Moura, J.J.G., Moura, I., Xavier, A.V. & LeGall, J. (1981) Biochim. Biophys. Acta **670**, 93-100.
 135. Huynh, B.H., Moura, J.J.G., Moura, I., Kent, T.A., LeGall, J., Xavier, A.V. & Münck, E. (1980) J. Biol. Chem. **255**, 3242-3244.
 136. Emptage, M.H., Kent, T.A., Huynh, B.H., Rawlings, J., Orme-Johnson, W.H. & Münck, E. (1980) J. Biol. Chem. **255**, 1793-1796.
 137. Thomson, A.J., Robinson, A.E., Johnson, M.K., Cammack, R., Rao, K.K. & Hall, D.O. (1981) Biochim. Biophys. Acta **637**, 423-432.
 138. Bell, S.H., Dickson, D.P.E., Johnson, C.E., Cammack, R., Hall, D.O. & Rao, K.K. (1982) FEBS Lett. **142**, 143-146.
 139. Kent, T.A., Moura, I., Moura, J.J.G., Lipscomb, J.D., Huynh, B.H., LeGall, J., Xavier,

- A.V. & Münck, E. (1982) FEBS Lett. **138**, 55-58.
140. Münck, E. (1982) in: Iron-Sulfur Proteins (Spiro, T.G., ed.), pp. 147-175.
141. Hille, R., Yoshida, T., Tarr, G.E., Williams, C.H., Ludwig, M.L., Fee, J.A., Kent, T.A., Huynh, B.H. & Münck, E. (1983) J. Biol. Chem. **258**, 13008-13013.
142. George, S.J., Richards, A.J.M., Thomson, A.J. & Yates, M.G. (1984) Biochem. J. **224**, 247-251.
143. Hagen, W.R., Dunham, W.R., Johnson, M.K. & Fee, J.A. (1985) Biochim. Biophys. Acta **828**, 369-374.
144. Papaefthymiou, V., Girerd, J.-J., Moura, I., Moura, J.J.G. & Münck, E. (1987) J. Am. Chem. Soc. **109**, 4703-4710.
145. Johnson, M.K., Bennett, D.E., Fee, J.A. & Sweeney, W.V. (1987) Biochim. Biophys. Acta **911**, 81-94.
146. Day, E.P., Peterson, J., Bonvoisin, J.J., Moura, I., Moura, J.J.G. (1988) J. Biol. Chem. **263**, 3684-3689.
147. Armstrong, F.A., George, S.J., Cammack, R., Hatchikian, E.C. & Thomson, A.J. (1989) Biochem. J. **264**, 265-273.
148. Conover, R.C., Kowal, A.T., Fu, W., Park, J.-B., Aono, S., Adams, M.W.W. & Johnson, M.K. (1990) J. Biol. Chem. **265**, 8533-8541.
149. Stephens, P.J., Jensen, G.M., Devlin, F.J., Morgan, T.V., Stout, C.D., Martin, A.E. & Burgess, B.K. (1991) Biochemistry **30**, 3200-3209.
150. Kent, T.A., Dreyer, J.-L., Kennedy, M.C., Huynh, B.H., Emptage, M.H., Beinert, H. & Münck, E. (1982) Proc. Natl Acad. Sci. USA **79**, 1096-1100.
151. Hendrich, M.P. & Debrunner, P.G. (1989) Biophys. J. **56**, 489-506.
152. Teixeira, M., Moura, I., Xavier, A.V., Moura, J.J.G., LeGall, J., DerVartanian, D.V., Peck, H.D. & Huynh, B.-H. (1989) J. Biol. Chem. **264**, 16345-16450.
153. Asso, M., Guigliarelli, B., Yagi, T. & Bertrand, P. (1992) Biochim. Biophys. Acta **1122**, 50-56.
154. Knaff, D.B., Hirasawa, M., Ameyibor, E., Fu, W. & Johnson, M.K. (1991) J. Biol. Chem. **266**, 15080-15084.
155. Vanoni, M.A., Edmondson, D.E., Zanetti, G. & Curti, B. (1992) Biochemistry **31**, 4613-4623.
156. Hagen, W.R., Van Berkel-Arts, A., Krüse-Wolters, K.M., Dunham, W.R. & Veeger, C. (1986) FEBS Lett. **201**, 158-162.
157. Voordouw, G., Hagen, W.R., Krüse-Wolters, K.M., Van Berkel-Arts, A. & Veeger, C. (1987) Eur. J. Biochem. **162**, 31-36.
158. Surerus, K.K., Hendrich, M.P., Christie, P.D., Rottgardt, D., Orme-Johnson, W.H. & Münck, E. (1992) J. Am. Chem. Soc. **114**, 8579-8590.
159. Marritt, S., Pierik, A.J., Thomson, A.J., Hagen, W.R., Lowe, D.J., Albracht, S.P.J. & Smith, B.E. (1993) In: New Horizons in Nitrogen Fixation (Palacios, R., Mora, J. & Newton, W.E., eds.), Nijhoff/Junk, Dordrecht (The Netherlands), 153.
160. Marritt, S., Faridooon, K.Y., Pierik, A.J., Gormal, C., Howes, B.D., Buck, M., Lowe, D.J., Thomson, A.J. & Smith, B.E. (1993) In: New Horizons in Nitrogen Fixation (Palacios, R., Mora, J. & Newton, W.E., eds.), Nijhoff/Junk, Dordrecht (The Netherlands), 144.
161. Hendrich, M.P. & Debrunner, P.G. (1988) J. Magn. Res. **78**, 133-141.
162. Lang, G. & Marshall, W. (1966) Proc. Phys. Soc. (London) **87**, 3-34.
163. Champion, P.M., Lipscomb, J.D., Münck, E., Debrunner, P.G. & Gunsalus, I.C. (1975) Biochemistry **14**, 4151-4158.
164. Thomson, A.J. & Johnson, M.K. (1980) Biochem. J. **191**, 411-420.
165. Hagen, W.R. (1984) Biochim. Biophys. Acta **765**, 399-402.
166. Brudvig, G.W., Stevens, T.H., Morse, R.H. & Chan, S.I. (1981) Biochemistry **20**, 3912-

- 3921.
167. Cooper, C.E., Moody, A.J., Rich, P.R., Wigglesworth, J.M. & Ioannidis, N. (1991) Biochem. Soc. Transact. **19**, 259S.
168. Dunham, W.R., Sands, R.H., Shaw, R.W. & Beinert, H. (1983) Biochim. Biophys. Acta **748**, 73-85.
169. Calhoun, M.W., Gennis, R.B. & Salerno, J.C. (1992) FEBS Lett. **309**, 127-129.
170. Weir, M.P., Peters, T.J. & Gibson, J.F. (1985) Biochim. Biophys. Acta **828**, 298-305.
171. Que, L. (1980) Structure Bonding **40**, 39-72.
172. Whittaker, J.W. & Solomon, E.I. (1988) J. Am. Chem. Soc. **110**, 5329-5339.
173. Bill, E., Haas, C., Ding, X.-Q., Maret, W., Winkler, H. & Trautwein, A. Zeppezauer, M. (1989) Eur. J. Biochem. **180**, 111-121.
174. Werth, M.T. & Johnson, M.K. (1989) Biochemistry **28**, 3982-3988.
175. Lynch, J.B., Juarez-Garcia, C., Münck, E. & Que, L. (1989) J. Am. Chem. Soc. **264**, 8091-8096.
176. Reem, R.C. & Solomon, E.I. (1987) J. Am. Chem. Soc. **109**, 1216-1226.
177. Hendrich, M.P., Pearce, L.L., Que, L., Chasteen, N.D. & Day, E.P. (1991) J. Am. Chem. Soc. **113**, 3039-3044.
178. Fox, B.G. & Lipscomb, J.D. (1988) Biochem. Biophys. Res. Comm. **154**, 165-170.
179. Fox, B.G., Surerus, K.K., Münck, E. & Lipscomb, J.D. (1988) J. Biol. Chem. **263**, 10553-10556.
180. Fox, B.G., Froland, W.A., Dege, J.E. & Lipscomb, J.D. (1989) J. Biol. Chem. **264**, 10023-10033.
181. Hendrich, M.P., Münck, E., Fox, B.G. & Lipscomb, J.D. (1990) J. Am. Chem. Soc. **112**, 5861-5865.
182. Liu, K.E. & Lippard, S.J. (1991) J. Biol. Chem. **266**, 12836-12839 & correction in **266**, 24859.
183. Werth, M.T., Kurtz, D.M., Howes, B.D. & Huynh, B.H. (1989) Inorg. Chem. **28**, 1357-1361.
184. Weigel, J.A., Holm, R.H., Surerus, K.K. & Münck, E. (1989) J. Am. Chem. Soc. **111**, 9246-9247.
185. Juarez-Garcia, C., Hendrich, M.P., Holman, T.R., Que, L. & Münck, E. (1991) J. Am. Chem. Soc. **113**, 518-525.
186. Holman, T.R., Andersen, K.A., Anderson, O.P., Hendrich, M.P., Juarez-Garcia, C., Münck, E. & Que, L. (1990) Angew. Chem. Int. Ed. Engl. **29**, 921-923.
187. Boyd, P.D.W. & Martin, R.L. (1979) J. Chem. Soc. Dalton **1979**, 92-95.
188. Bubacco, L., Magliozzo, R.S., Beltramini, M., Salvato, B. & Peisach, J. (1992) Biochemistry **31**, 9294-9303.
189. Snyder, B.S., Patterson, G.S., Abrahamson, A.J. & Holm, R.H. (1989) J. Am. Chem. Soc. **111**, 5214-5223.
190. Borovik, A.S., Hendrich, M.P., Holman, T.R., Münck, E., Papaefthymiou, V. & Que, L. (1990) J. Am. Chem. Soc. **112**, 6031-6038.
191. Stassinopoulos, A., Schulte, G., Papaefthymiou, G.C. & Caradonna, J.P. (1991) J. Am. Chem. Soc. **113**, 8686-8697.
192. Caneschi, A., Gatteschi, D. & Sessoli, R. (1991) J. Am. Chem. Soc. **113**, 5873-5874.
193. Caneschi, A., Gatteschi, D., Laugier, J., Rey, P., Sessoli, R. & Zanchini, C. (1988) J. Am. Chem. Soc. **110**, 2795-2799.
194. Boyd, P.D.W., Li, R., Vincent, J.B., Folting, K., Chang, H.R., Streib, W.E., Huffmann, J.C., Christou, G. & Hendrickson, D.N. (1988) J. Am. Chem. Soc. **110**, 8537-8539.
195. Verhagen, M.F.J.M. & Hagen, W.R. (1993) unpublished results.

Chapter 11

Summary.

Summary

Iron-sulfur clusters are present in a large number of proteins. So far structures of four types of protein-bound iron-sulfur clusters have been determined by X-ray diffraction: rubredoxin-like, [2Fe-2S], [3Fe-4S] and [4Fe-4S] centers. The presence of any of these clusters in a protein can be predicted by comparison of spectroscopic properties. However a number of multiple-electron transferring enzymes, like the Fe-only hydrogenase, sulfite reductase and nitrogenase MoFe protein have enigmatic iron-sulfur clusters with spectroscopic properties unlike those of the known structures. These enzymes share a high iron and acid-labile sulfur content and the presence of superspin systems with $S \geq 5/2$. In this thesis biochemical and spectroscopic studies are presented on the above-mentioned iron-sulfur proteins and two unusual newly discovered iron-sulfur proteins, the 'prismane' protein and nigerythrin.

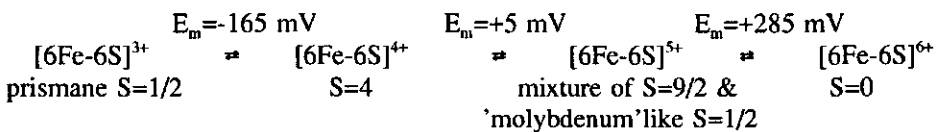
Chapter 2 summarizes new findings on the Fe-only hydrogenase and the redox properties of its cubanes and hydrogen activating iron-sulfur H-cluster. The hydrogenase, aerobically isolated from the sulfate-reducing bacterium *Desulfovibrio vulgaris* (Hildenborough) was shown to be composed of a mixture of high and low activity charge conformers, which can be isolated and discriminated by chromatographic and electrophoretic techniques. The redox properties of the rhombic $S=1/2$ EPR signals associated with the H-cluster of hydrogenase preactivated with dithionite or hydrogen were considerably more simple than those reported by Patil and coworkers for the (oxygen-insensitive) resting enzyme. Instead of sequential bell-shaped curves for the rhombic $g=2.07$ ($g=1.96$ and $g=1.89$) and $g=2.11$ ($g=2.05$ and $g=2.00$) EPR signals in reductive dye-mediated titrations, a simple behaviour with two redox states was observed both in reductive and oxidative titrations. The interconversion between the diamagnetic reduced and the oxidized redox state of the H-cluster exhibiting the $g=2.11$ $S=1/2$ EPR signal occurred at -307 mV. The bell-shaped nature and the occurrence of the $g=2.07$ rhombic EPR signal thus was due to the activation process of the H-cluster. By equilibration with H_2/H^+ of activated hydrogenase a midpoint potential of -330 mV was determined for the cubanes. A similar midpoint potential was observed in a dye-mediated titration of a recombinant hydrogenase lacking the H-cluster. In these experiments no evidence for redox interaction between the two cubanes was seen.

In the course of extensive purification procedures of the Fe-hydrogenase it was recognized that an iron-sulfur protein with novel EPR spectroscopic properties occasionally contaminated hydrogenase preparations (Chapter 3). The as isolated form had a substoichiometric $S=1/2$ EPR signal with $g=1.97$, $g=1.95$ and $g=1.90$. Chemical analysis showed that, although such g -values are typical for Mo^{5+} (or W^{5+}) no metals other than iron were present. The 'molybdenum'-like EPR spectrum disappeared both on reduction and oxidation. In the dithionite reduced form an almost stoichiometric $S=1/2$ EPR signal was observed. The g -values ($g=2.00$, 1.82 and 1.32) were reminiscent of those of prismane model compounds in the $[6Fe-6S]^{3+}$ redox state. Therefore the protein was proposed to be a prismane-containing protein, in agreement with the chemical analysis indicating ≈ 6 Fe/protein. The occurrence of $S=1/2$ EPR signals in the as isolated state and dithionite reduced state could be explained by the assumption that the 'prismane protein' had four redox states: the fully reduced $[6Fe-6S]^{3+}$ state with the fingerprint prismane signal, an $[6Fe-6S]^{4+}$ redox state with unknown spin state ($S=0$ or integer), the $[6Fe-6S]^{5+}$ state with the molybdenum-like $S=1/2$ EPR signal and the fully oxidized $[6Fe-6S]^{6+}$ redox state ($S=0$ or integer).

The purification, chemical analysis and biochemical characterization of this 'prismane protein' are described in Chapter 4. The 'prismane' protein is a monomeric, cytoplasmic protein with a molecular mass of 52 kDa as estimated by sedimentation-equilibrium centrifugation. The protein contained 6.3 ± 0.4 Fe and 6.2 ± 0.7 S^2 per polypeptide. With

polyclonal antibodies similar 'prismane' proteins were detected in *Desulfovibrio vulgaris* (Monticello) and *Desulfovibrio desulfuricans* (ATCC 27774). Using the N-terminal sequence and antibodies against this prismane protein Stokkermans and coworkers have sequenced the gene coding for this prismane protein as well as the homologous protein of *Desulfovibrio desulfuricans* (ATCC 27774).

Further spectroscopic evidence for a new iron-sulfur cluster and strong support for the presence of a prismane core is presented in Chapter 5. The discovery that the $[6\text{Fe-6S}]^{5+}$ redox state exhibited a spin mixture of approximately stoichiometric $S=9/2$ and substoichiometric molybdenum-like $S=1/2$ EPR signals confirmed the earlier hypothesis of four redox states of the prismane protein. Dye-mediated redox titrations and the observation of a $g=16$ signal with increased intensity in parallel-mode EPR for the $[6\text{Fe-6S}]^{4+}$ redox state completed the following scheme:



Multiple frequency EPR spectroscopy of the $S=1/2$ EPR signals showed that additional broadening indicative of nitrogen ligation was present. The line broadening caused by enrichment of the prismane protein with ^{57}Fe was in agreement with ≈ 6 Fe per cluster. Quantitative high-resolution Mössbauer spectroscopy of the ^{57}Fe enriched prismane protein revealed that both in the $[6\text{Fe-6S}]^{3+}$ and the $[6\text{Fe-6S}]^{5+}$ form the iron ions were inequivalent. A 4:2 ratio of quadrupole doublets was observed. The quadrupole splitting and isomer shift of the four iron ions were relatively invariant to the redox change of the cluster, while the two apparently more ionic iron ions had a more pronounced change from Fe^{2+} to Fe^{3+} character. Mössbauer spectroscopy at low temperatures and with applied magnetic fields indicated that the four and two iron ions were present in the same magnetically coupled structure. This led to a model in which the prismane structure is composed of a central set of four iron ions with a more ionic iron ion on each side. The more ionic iron ions could correlate with the nitrogen ligation as inferred from EPR studies.

The unique EPR spectroscopic properties of the 'prismane protein' prompted investigation of dissimilatory sulfite reductase (desulfoviridin), a readily available iron-sulfur enzyme obtained during the isolation of Fe-hydrogenase from *Desulfovibrio vulgaris* (Hildenborough). The scrutiny for pure and electrophoretic homogeneous preparations of the desulfoviridin for EPR spectroscopic studies unexpectedly led to the discovery of a third, hitherto unrecognized 11 kDa subunit in this enzyme (Chapter 6). The γ subunit appeared to be tightly bound in the desulfoviridin complex for which a subunit composition of $\alpha_2\beta_2\gamma_2$ was determined. N-terminal sequences and polyclonal antibodies against the α , β and γ subunits were obtained. The polyclonal antibodies allowed demonstration of the presence of homologous α , β and γ subunits in desulfoviridin-type dissimilatory sulfite reductases of three other *Desulfovibrio* species.

Chapter 7 delineates the redox and spectroscopic results on the siroheme and $S=9/2$ EPR signals of desulfoviridin. By summation of the $S=1/2$ and $S=5/2$ EPR signals of the siroheme group it was shown that only 20% of the siroheme groups were metallated. The midpoint potential for the $\text{Fe}^{2+}/\text{Fe}^{3+}$ transition of the main species of the siroheme was -295 mV. No significant amounts of EPR signals of normal iron-sulfur clusters were observed. Instead, several novel EPR signals with $g=17$, $g=15.1$, $g=11.7$ and $g=9.0$ were found in the as isolated oxidized form of the protein. These EPR signals were from a paramagnet with $S=9/2$. A stoichiometry of approximately 0.6 spin per $\alpha\beta\gamma$ was estimated. In a reductive redox titration the $S=9/2$ EPR signals disappeared with $E_m = -205$ mV. It was proposed that in the

desulfoviridin-type dissimilatory sulfite reductase larger iron-sulfur clusters are present which give rise to the $S=9/2$ EPR signals. The demetallation of the siroheme and the $S=9/2$ EPR signals from an iron-sulfur cluster were in contradiction with the model of Siegel and coworkers for the sulfite reductase of *Escherichia coli*, in which coupling between a regular $[4\text{Fe}-4\text{S}]^{2+}$ cubane and the $\text{Fe}^{2+/3+}$ ion of the siroheme is proposed to explain spectroscopic properties.

In Chapter 8 the redox and EPR spectroscopic properties of the nitrogenase MoFe protein from *Azotobacter vinelandii* are described. By controlled oxidation with dye-mediated redox titrations the long lasting controversy on the spin and redox states of the oxidized P-cluster iron-sulfur centers was solved. It turned out that oxidation of the P clusters could lead to two consecutive redox states, P^{OX1} and P^{OX2} . On oxidation of the dithionite reduced P-clusters by two electrons ($E_m \approx -307$ mV) first the P^{OX1} state is obtained with a weak $g=12$ EPR signal, which increased in intensity at higher temperature and sharpened and intensified >10 fold in parallel-mode EPR. This allowed assignment of the $g=12$ EPR signal to an excited state of a non-Kramers spin system (presumably $S=3$). Previous Mössbauer and MCD spectroscopic measurements appeared to have been made with this redox state. A second oxidation by one electron ($E_m = +90$ mV) led to the P^{OX2} redox state, which occurred as a spin mixture of $S=1/2$ and $S=7/2$ species. This redox state corresponded to the form obtained by the solid thionine oxidation procedure of Hagen and coworkers. Further oxidation of P^{OX2} redox state caused destruction of the iron-sulfur clusters and concomitant formation of $S=9/2$ and other high spin EPR signals.

During the efforts to obtain highly-purified Fe-hydrogenase and prismane protein from *Desulfovibrio vulgaris* (Hildenborough) a black protein with an ultraviolet-visible spectrum reminiscent of rubredoxin-like iron-sulfur centers was obtained. Subsequent biochemical and EPR spectroscopic characterization (Chapter 9) indicated that this protein was similar but not identical to the protein rubrerythrin isolated by Moura and coworkers. The new protein was called nigerythrin due to its black color and hemerythrin-like EPR signal. Although rubrerythrin was originally reported to contain two rubredoxin-like and one dinuclear iron center, metal analyses and spin quantitation revealed that rubrerythrin and nigerythrin each contain two rubredoxin-like and two dinuclear iron centers per homodimer. The three redox transitions in both proteins had midpoint potentials higher than $+200$ mV. This suggested that both proteins have a non-redox role with all six iron ions in the ferrous state.

In Chapter 10 a literature survey of non-integer and integer high spin systems in iron-sulfur proteins is presented. In contrast to the well-documented occurrence of $S=3/2$ and $S=2$ spin states in $[4\text{Fe}-4\text{S}]^{1+}$ and $[3\text{Fe}-4\text{S}]^0$, respectively, the characterization of other, unusual iron-sulfur clusters with high spin states has not yet reached full maturity. The recent crystal structure of the MoFe protein of *Azotobacter vinelandii*, in which the FeMoco and P-clusters appeared to be larger clusters shows that the correlation between high spin states with structures other than the four basic iron-sulfur clusters indeed holds. The diversity of redox and spin states as observed for the prismane protein, desulfoviridin, carbonmonoxide dehydrogenase and Fe-hydrogenase indicates that besides the FeMoco and P-clusters other larger iron-sulfur clusters are present in biological systems.

Samenvatting

De chemische reacties die plaatsvinden in levende wezens worden gekatalyseerd door enzymen. Enzymen zijn eiwitten die door hun ruimtelijke structuur van gekoppelde aminozuren in staat zijn chemische reacties te katalyseren. Uitgaande van een basale set van 20 aminozuren kunnen door variatie in samenstelling en relatieve positie een groot aantal verschillende enzymen gemaakt worden. Naast aminozuren komen ook andere biomoleculen en metaalionen voor in eiwitten. Het belang van metaalionen is bekend door de fel-rode aanwezigheid van de aan hemoglobine gebonden ijzer-ionen in ons bloed. Hoewel hemoglobine eigenlijk het enige metaalionen bevattende eiwit is waarmee we geconfronteerd worden, zijn op onzichtbare wijze vele andere metalen zoals koper, mangaan, magnesium, zink, nikkel, molybdeen en vanadium betrokken bij essentiële biochemische processen in bacteriën, planten, dieren en de mens. Door opname van metaalionen in de door aminozuren of met andere biomoleculen gevormde bindingsplaatsen kan het scala van chemische reacties van levende wezens aanzienlijk uitgebreid worden.

Door het bestuderen van deze metaalionen kan in veel gevallen informatie verkregen worden over het functioneren van het hele metallo-eiwit. Dit kan omdat meestal alleen de metaalionen en hun directe omgeving betrokken zijn bij katalytische en structurele functies. De studie wordt aanzienlijk vergemakkelijkt omdat veel voorkomende metaalionen zoals ijzer en koper specifieke eigenschappen hebben die eenvoudig zijn te observeren zelfs te midden van de duizenden andere atomen in het metallo-eiwit. Door met daarvoor geschikte spectroscopische instrumenten de interactie van de metaalionen met allerlei vormen van elektromagnetische straling te bestuderen, worden de niet direct met het oog zichtbare eigenschappen, zoals het magnetisme van de elektronen of kernen van de metaalionen blootgelegd. Dit heeft geleid tot een gedegen inzicht in het functioneren van eiwitten en enzymen met ijzer en andere metaalionen. Toch is uiteindelijk opheldering van de drie-dimensionale structuur met bijvoorbeeld röntgendiffractie nodig om de exacte configuratie van de metaalionen te beschrijven. Momenteel is van ongeveer honderd verschillende metalloeiwitten de drie-dimensionale structuur bekend. In deze referentie collectie blijken niet alleen eiwit structuren met geïsoleerde metaalionen voor te komen, maar ook structuren met geclusterde eenheden van meerdere metaalionen.

De meest unieke groep eiwitten met metallo-clusters wordt gevormd door de zogenaamde ijzer-zwavel eiwitten. Dit zijn eiwitten waarin de ijzer ionen zijn verankerd aan voornamelijk cysteine en S^2 ionen. Ijzer-zwavel clusters zijn betrokken bij een groot aantal belangrijke processen in alle levende organismen. Een alom bekende en bestudeerde functie is het transport van elektronen. Bepaalde kleine eiwitten kunnen door opname (reductie) of afstaan (oxidatie) van een electron het te langzame transport van elektronen tussen grote en/of membraan-gebonden eiwitten versnellen. Reductie en oxidatie (redox) reacties zijn de energetisch gezien cruciale onderdelen van alle respiratoire en metabole processen. De biologisch gezien meest relevante voorbeelden hiervan zijn te vinden in de mitochondriale ademhalingsketen en het fotosynthetische systeem. Hierin zijn meerdere ijzer-zwavel clusters betrokken bij electrontransport binnenin eiwit-complexen die met de celmembraan geassocieerd zijn. Een tweede functie houdt verband met de eigenschap van sommige ijzer-zwavel clusters om niet alleen elektronen te transporteren maar deze ook direct over te dragen of te onttrekken aan andere moleculen of ionen onder vorming van nieuwe verbindingen (redox-katalyse). Het ijzer-zwavel clusters bevattende enzym nitrogenase is bijvoorbeeld in staat om het chemische gezien inerte stikstof uit de lucht om te zetten in twee ammonium ionen. In een niet door kunstmest beïnvloed ecosysteem is dit enzym een belangrijke schakel in de stikstof-kringloop. De derde functie van ijzer-zwavel clusters heeft in tegenstelling tot electron-transport en redox-katalyse niets te maken met redox-eigenschappen. Het

belangrijkste voorbeeld hiervan is te vinden in de bij de afbraak van glucose betrokken citroenzuur cyclus. Eén van de enzymen van de citroenzuur cyclus, het aconitase, heeft een ijzer-zwavel cluster dat de omzetting van citroenzuur in iso-citroenzuur katalyseert.

Momenteel zijn de drie-dimensionale structuren bekend van een viertal verschillende basale typen ijzer-zwavel clusters die in eiwitten voorkomen. De eenvoudigste structuur wordt gevormd door een ijzer ion dat met vier cysteines is verankerd aan het eiwit. Formeel gesproken is dit eigenlijk geen ijzer-zwavel cluster, omdat slechts één ijzer ion en geen zuur-labiele zwavel aanwezig is. Een eiwit met zo'n centrum is het bacteriële eiwit rubredoxine (een contractie van *ruber*=rood, redox proteïne). Het ijzer ion kan door wisselen van lading van 2+ naar 3+ en vice versa dienst doen als transportmiddel voor electronen. Een tweede structuur komt voor in de planten ferredoxines (contractie van *ferrum*=ijzer, redox proteïne). De cluster is opgebouwd uit twee ijzer ionen met twee zuur-labiele zwavel ionen die tussen de ijzer ionen liggen. Deze twee ijzer twee zwavel cluster (verkort genoteerd als [2Fe-2S]) wordt aan elke zijde door twee cysteine residuen van het eiwit vastgehouden. In de zogenaamde 'Rieske' centra van de ademhalingsketen zijn de twee cysteines van één ijzer ion vervangen door twee histidine liganden. In principe kan de [2Fe-2S] cluster in drie toestanden voorkomen (d.w.z. met twee Fe²⁺, één Fe²⁺ en één Fe³⁺, of twee Fe³⁺). In eiwitten is de vorm met twee Fe²⁺ ionen echter niet stabiel. De [2Fe-2S] cluster kan alleen met een 1+ of 2+ lading voorkomen, verkort weergegeven als [2Fe-2S]^{1+/2+} (verkregen door sommatie van de ladingen van de twee ijzer ionen met de 2- lading van de zuur-labiele zwavels). Net als rubredoxine kan de [2Fe-2S] cluster functioneren in het electronen transport. Een derde structuur, de cubaan ofwel de [4Fe-4S] cluster, is opgebouwd uit een structuur van vier ijzer en vier zuur-labiele zwavel ionen die alternerend op de hoekpunten van een cubus liggen. De cubus wordt meestal door vier en soms door drie cysteines gebonden. In bacteriële ferredoxines en een groot aantal andere ijzer-zwavel eiwitten is de cubaan stabiel in de 1+ en 2+ vorm: [4Fe-4S]^{1+/2+}. In de zogenaamde 'High Potential Iron-sulfur Proteins' (HiPIP's) zijn alleen de 2+ en 3+ lading stabiel onder normale condities, [4Fe-4S]^{2+/3+}. Bij de meeste eiwitten functioneren de [4Fe-4S] clusters als transportmiddel voor electronen. In een aantal niet-redox enzymen zoals aconitase heeft de cubaan in de [4Fe-4S]²⁺ vorm een katalytische functie. De vierde basale ijzer-zwavel structuur, [3Fe-4S]^{0/1+}, kan worden beschouwd als een cubaan waaruit één ijzer ion is verwijderd. Sommige eiwitten die (oorspronkelijk) een cubaan bevatten, worden zelfs geïsoleerd met een [3Fe-4S] cluster. Door Fe²⁺ toe te voegen aan de [3Fe-4S]⁰ vorm kan de cubaan structuur hersteld worden. Een mogelijk biologische functie van deze 'cluster-conversie' is nog niet geheel duidelijk.

De identificatie van de ijzer-zwavel clusters van eiwitten waar nog geen drie dimensionale structuur van bekend is, wordt gewoonlijk gedaan door het vergelijken van de chemische en spectroscopische eigenschappen met die van de vier bekende basale ijzer-zwavel clusters. Met name de zogenaamde Electron Paramagnetische Resonantie (EPR) spectroscopie levert een belangrijke bijdrage omdat de vier typen ijzer-zwavel clusters op eenvoudige wijze kunnen worden gedetecteerd en gedetermineerd. Om EPR spectroscopie en de toepassing voor de identificatie van ijzer-zwavel clusters te kunnen begrijpen, is het noodzakelijk magnetisme en de magnetische eigenschappen van ijzer ionen in ijzer-zwavel clusters iets nader toe te lichten. Magnetisme vindt zijn oorsprong in de ongepaarde electronen van metaalionen. Het zogenaamde (ferro)magnetisme waar we normaal mee te maken hebben wordt veroorzaakt door het optreden van ordening van deze elementaire magneetjes op grotere schaal. In de meeste materialen is echter effectief geen magnetisme waar te nemen door uitmiddeling van de individuele magneetveldjes. Dit fenomeen wordt paramagnetisme genoemd. Het magnetische karakter van zo'n schijnbaar netto 'niet-magnetisch' materiaal komt slechts tot uitdrukking onder condities die de wanordelijke oriëntatie wijzigen (bijv. verlaging van temperatuur of het aanleggen van een extern magneetveld). Twee relevante voorbeelden van elementaire magneetjes zijn het Fe²⁺ en Fe³⁺ ion. In deze ionen zijn respectievelijk 5 en 6

electronen aanwezig in de buitenste electronenschil. De sterkte van de elementaire magneetjes zoals een electron wordt aangeduid met het begrip spin. De spin S van een electron heeft een grootte van $1/2$. De spins van de 5 of 6 electronen kunnen door parallele of anti-parallele oriëntatie elkaar versterken of uitmiddelen. Voor de 5 electronen van het Fe^{3+} ion zijn er drie mogelijkheden: $\uparrow\downarrow\uparrow\downarrow$ (netto $S=1/2$), $\uparrow\downarrow\uparrow\uparrow$ (netto $S=3/2$) en $\uparrow\uparrow\uparrow\uparrow$ ($S=5/2$). Het blijkt dat in ijzer-zwavel clusters $S=5/2$ voor Fe^{3+} en $S=2$ voor Fe^{2+} energetisch gezien het gunstigst is. In ijzer-zwavel clusters zijn de ijzer ionen voldoende dicht bij elkaar om een zeer intense magnetische interactie aan te gaan. Net als bij de spins van de individuele electronen in de losse ionen kunnen, bijvoorbeeld in $[2\text{Fe}-2\text{S}]^+$ de $S=5/2$ van Fe^{3+} en de $S=2$ van Fe^{2+} koppelen tot $S=1/2$ en $S=9/2$. Het blijkt dat ook de tussenliggende spins toegestaan zijn ($S=3/2$, $S=5/2$ en $S=7/2$). Hoewel er meerdere spin toestanden mogelijk zijn, wordt voor $[2\text{Fe}-2\text{S}]^{1+}$ alleen de $S=1/2$ toestand waargenomen. Ook in de $[2\text{Fe}-2\text{S}]^{2+}$ vorm is de waargenomen spin grondtoestand eenvoudig. De $S=5/2$ spins van de Fe^{3+} ionen zijn antiparallel gekoppeld en de cluster heeft netto geen spin ($S=0$ ofwel diamagnetisch). De koppeling in $[4\text{Fe}-4\text{S}]^{1+}$, $[4\text{Fe}-4\text{S}]^{3+}$ en $[3\text{Fe}-4\text{S}]^{1+}$ is zodanig dat $S=1/2$ meestal de grondtoestand is, terwijl $[4\text{Fe}-4\text{S}]^{2+}$ diamagnetisch is. Hoewel er een sterke koppeling is tussen de ijzer-ionen in deze clusters, blijken de afzonderlijke clusters zich magnetisch nagenoeg onafhankelijk te gedragen.

Het feit dat ijzer-zwavel clusters zich als afzonderlijke paramagneten gedragen maakt het mogelijk de interactie met een extern magneetveld op eenvoudige wijze te beschrijven. Een geïsoleerde paramagneet kan zich namelijk in een extern magneetveld op twee manieren oriënteren. Deze twee oriëntaties hebben een lineair van het aangelegde magneetveld (B) afhankelijk energieverval (ΔE):

$$\Delta E = g \cdot \beta \cdot B$$

waarin de g -waarde een voor de ijzer-zwavel cluster specifieke constante is en β een natuurconstante met vaste waarde (Bohr magneton). Bij in het laboratorium gemakkelijk te verkrijgen magneetvelden blijkt microgolfstraling het energie verschil tussen de twee oriëntaties te kunnen overbruggen. Dit is de basis van Electron Paramagnetische Resonantie (EPR) spectroscopie waarin de absorptie van microgolfstraling van constante energie wordt gevolgd als functie van een te variëren magneetveld. Omdat de gevoeligheid omgekeerd evenredig is met de temperatuur en bij hoge temperatuur de signalen verbreden, moeten de (bevroren) oplossingen van ijzer-zwavel eiwitten tussen -269 en -150 °C bestudeerd worden. Door invullen van de energie van de microgolfstraling en het geobserveerde resonantie magneetveld kan de g -waarde van een paramagnetisch ijzer-zwavel cluster bepaald worden. Ten gevolge van de willekeurige oriëntatie van de ijzer-zwavel clusters in een bevroren oplossing zijn er soms meerdere g -waarden waar te nemen. De g -waarden herbergen informatie over de aard van het paramagnetisme. IJzer-zwavel clusters met $S=1/2$ vertonen pieken met g -waarden rondom 2, terwijl $S > 1/2$ g -waarden sterk van 2 afwijkende g -waarden kunnen hebben. Hoewel in bepaalde opzichten formule (1) ook correct is voor $S \neq 1/2$, is de theoretische beschrijving ingewikkelder. De waargenomen g -waarden kunnen met quantummechanische berekeningen gerelateerd worden aan de spin en de zogenaamde D en E parameters (de axiale en rhombische nul-velds splitsingsparameters). De waarden van D en E voor vele paramagneten met heeltallige spins ($S=1$, $S=2$ en hoger) zijn zo ongunstig dat er geen of slechts brede pieken in het normale EPR spectrum zijn waar te nemen. Daarentegen zijn er in de EPR spectra van nagenoeg alle halftallige 'high spin' systemen ($S=3/2$, $S=5/2$, $S=7/2$ en $S=9/2$) wel duidelijke pieken waarneembaar. Het blijkt dat in de meeste gevallen de g -waarden alleen afhankelijk zijn van het quotient van E en D (de rhombiciteit). De quantummechanische berekeningen voorspellen dat de spin altijd groter is dan een kwart van de g -waarde. Met rhombogrammen, grafieken van de theoretisch berekende g -waarden als functie van de rhombiciteit, kan de spin toestand en E/D van de halftallige high spin systemen

gemakkelijk afgelezen worden. Door de grootte van D met de temperatuurs afhankelijkheid van de EPR signalen te bepalen kan, met de uit de rhombogrammen afgelezen quotiënt E/D , de waarde van E berekend worden. De grootte van D en E (uitgedrukt in de hiervoor geschikte eenheid van energie, cm^{-1}) en de spin toestand zijn net als de g -waarden bij een $S=1/2$ systeem de karakteristieke grootheden. Door de oppervlakte onder de pieken in het EPR spectrum te bepalen kan voor alle halfvallige spin systemen een schatting gemaakt worden van het aantal spin systemen per eiwit (spin quantisatie). Voor $S \neq 1/2$ halfvallige spin systemen zijn voor de berekening de E en D parameters cruciaal.

Met een speciaal type EPR spectrometer kan de magnetische component van de microgolffstraling en het magneetveld van de loodrechte naar de parallele oriëntatie gewijzigd worden. Dit verhoogt de waarschijnlijkheid (d.w.z. de intensiteit) van overgangen in heeltallige spin systemen en reduceert die van de halfvallige spins nagenoeg tot nul. Dit is een waterdicht bewijs voor halfvalligheid, terwijl in sommige gevallen heeltalligheid aangetoond kan worden door de toegenomen intensiteit in de 'parallele mode'. Spin quantisatie voor heeltallige spin systemen is zelfs met intense parallele mode EPR signalen moeilijk. De theorie is namelijk nog niet voldoende ontwikkeld.

Omdat het aantal Fe^{2+} en Fe^{3+} ionen en de drie-dimensionale structuur de magnetische eigenschappen van ijzer-zwavel clusters zeer sterk beïnvloeden, kunnen de diverse soorten ijzer-zwavel clusters met EPR spectroscopie gedetermineerd worden. De identificatie wordt gebruikelijkerwijs ondersteund door analyse van het Fe/S gehalte en het gedrag van het EPR spectrum als functie van intensiteit van de microgolffstraling en temperatuur.

De affiniteit van een cluster voor electronen, uitgedrukt in de zogenaamde redox halfwaarde potentiaal, kan worden bepaald met door EPR spectroscopie gevolgde redox-titraties. Hiertoe wordt een mengsel van organische kleurstoffen en het ijzer-zwavel eiwit met een kalium ferricyanide of natrium dithioniet oplossing getitreerd, terwijl de redox-potentiaal van de oplossing wordt gemeten met electrodes. Deze redox-potentiaal beschrijft de sterkte waarmee in de oplossing electronen worden aangeboden. De kleurstoffen bufferen de redox potentiaal en zorgen tegelijkertijd voor het redox-evenwicht tussen de meet-electrode en de geoxideerde en gereduceerde ijzer-zwavel clusters in het eiwit. Door de amplitude van de EPR signalen van de geoxideerde of gereduceerde cluster als functie van de gemeten redox potentiaal te volgen, kan de redox potentiaal bepaald worden waarbij de cluster voor de helft in de geoxideerde en voor de helft in de gereduceerde vorm aanwezig is (de halfwaarde potentiaal). Een lage halfwaarde potentiaal geeft aan dat het moeilijk is om de cluster electronen te laten opnemen (=reduceren), een hoge halfwaarde potentiaal houdt in dat de cluster gemakkelijk electronen opneemt. De halfwaarde potentialen van ijzer-zwavel clusters in eiwitten variëren van -500 tot $+400$ mV. De halfwaarde potentiaal vormt in combinatie met de spin toestand en de g -waarden een belangrijk determinatie kenmerk van ijzer-zwavel clusters.

Hoewel de mogelijkheden van EPR spectroscopie zeer uitgebreid zijn, is complementatie met andere spectroscopische technieken noodzakelijk. Met name informatie over diamagnetische ijzer-zwavel clusters en de exacte koppeling en valentie van de ijzer ionen in een cluster kan niet worden verkregen met EPR spectroscopie. Mössbauer spectroscopie is gebaseerd op de absorptie van γ -straling door ijzer-kernen. Omdat de afzonderlijke ijzer-kernen kunnen worden gedetecteerd, complementeert dit de met EPR spectroscopie verkregen waarnemingen. Helaas treedt de absorptie van γ -straling alleen op met de kern van de ^{57}Fe isotoop, die slechts in 2% van alle ijzer ionen voorkomt. De gevoeligheid van Mössbauer spectroscopie kan echter verhoogd worden door het ijzer-zwavel eiwit te verrijken met dit (kostbare) isotoop.

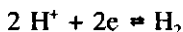
Toch zijn EPR en Mössbauer spectroscopie niet in staat om alle ijzer-zwavel clusters te identificeren. De magnetische eigenschappen van een aantal eiwitten wijken namelijk zo dramatisch af van de bekende clusters, dat het verondersteld wordt dat er andere nog

onbekende ijzer-zwavel clusters moeten bestaan. Dit is niet alleen duidelijk geworden maar ook bewezen voor het zogenaamde molybdeen-ijzer eiwit uit het nitrogenase enzym complex. Dit molybdeen-ijzer eiwit is de feitelijke katalysator van de volgende reactie:

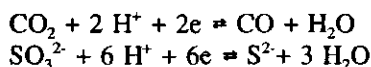


Het molybdeen-ijzer eiwit bevat 4 zeer ongewone ijzer-zwavel clusters met aparte magnetische eigenschappen. Twee clusters zijn met een organisch oplosmiddel uit het eiwit te extraheren en bevatten elk één molybdeen ion, 7 ijzer en 8-9 zuur-labele zwavel ionen. De samenstelling van de cofactor impliceert dat deze cluster een grotere ijzer-zwavel cluster is. Deze zogenaamde FeMo cofactor clusters hebben een uniek $S=3/2$ EPR signaal, dat geheel anders is dan dat van $[4\text{Fe}-4\text{S}]^{1+}$ clusters. Er zijn duidelijke aanwijzingen dat de reductie van stikstof plaatsvindt met deze clusters. De andere twee (proteïne gebonden of 'P') clusters verzorgen de aanvoer van electronen naar de FeMo cofactor centra. Ook de P-clusters hebben een ongewoon paramagnetisme met een spin $S \geq 5/2$ in de geoxideerde vorm. Bij oxidatie met vast thionine zijn zelfs $S=7/2$ EPR signalen waar te nemen. De spin quantisatie van deze $S=7/2$ EPR signalen en de recentelijk gepubliceerde drie-dimensionale structuur laten zien dat de P-clusters net als de FeMo cofactor grote ijzer-zwavel clusters zijn.

Voor andere ijzer-zwavel eiwitten zijn de bewijzen minder hard. Een van die enzymen is het ijzer-hydrogenase uit de bacterie *Desulfovibrio vulgaris* (Hildenborough). Dit hydrogenase heeft in tegenstelling tot nikkel-ijzer bevattende hydrogenases alleen ijzer ionen. Net als nitrogenase katalyseert hydrogenase een ongewone redox-reactie:



Het ijzer-hydrogenase bevat twee met EPR spectroscopie te identificeren $[4\text{Fe}-4\text{S}]^{1+/2+}$ cubanen. De eigenschappen van de twee cubanen zijn vergelijkbaar met die van normale electronen transporterende ferredoxines. Naast de cubanen zijn er ongeveer 6 ijzer en zuur-labele zwavel ionen aanwezig in de waterstof activerende H-cluster. In 1986 werd door Hagen de hypothese opgesteld dat deze H-cluster zou kunnen overeenkomen met een door anorganisch chemici gesynthetiseerd $[6\text{Fe}-6\text{S}]$ prismaan cluster. Naast het nitrogenase molybdeen-ijzer eiwit en het hydrogenase komt de correlatie tussen hoge spin, een relatief hoog Fe/S gehalte en redox-reacties met meerdere electronen in nog minstens 3 andere eiwitten voor. Dit zijn de enzymen koolmonoxide dehydrogenase en sulfiet reductase, die de volgende reacties katalyseren:



en een in hoofdstuk 3, 4 en 5 beschreven nieuw ijzer-zwavel eiwit. Het hoge gehalte aan ijzer en zuur-labele zwavel ionen, de aanwezigheid van (super)spin systemen met $S > 5/2$ en de multi-electronen overdragende eigenschappen van deze eiwitten doen suggereren dat er, net als in het molybdeen-ijzer eiwit van nitrogenase, grotere ijzer-zwavel (super)clusters aanwezig zijn. Deze 'supercluster-superspin' werk-hypothese vormt de basis van de in dit proefschrift vastgelegde resultaten. Een sleutelrol werd vertolkt door het in hoofdstuk 3, 4 en 5 beschreven 'prismaan eiwit', een nieuw ijzer-zwavel eiwit dat dienst heeft gedaan als een model voor de andere eiwitten. In de hoofdstukken 2, 3, 5, 7 en 8 wordt de supercluster-superspin hypothese getoetst door beschrijving van de redox en EPR spectroscopische eigenschappen van dit prismaan eiwit, hydrogenase, sulfiet reductase en het nitrogenase molybdeen-ijzer eiwit. Naast de spectroscopische karakterisering zijn in hoofdstuk 2, 4 en 6 de isolatie en biochemische karakteristieken van deze eiwitten beschreven. Naast de ontdekking van het prismaan eiwit

wordt in dit proefschrift nog een tweede nieuw ijzer-zwavel eiwit beschreven, het zogenaamde nigerythrine. De biochemische en spectroscopische karakterisering geeft aan dat dit eiwit geen ijzer-zwavel superclusters, maar andere ongebruikelijke clusters bevat.

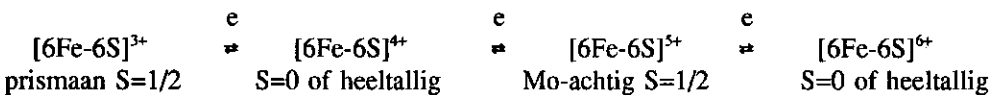
In hoofdstuk 2 worden de redox eigenschappen van het enzym hydrogenase uit de bacterie *Desulfovibrio vulgaris* (Hildenborough) beschreven. Door scheiding van verschillende ladingsvormen van het enzym werd aangetoond dat een hydrogenase enzym preparaat bestaat uit een mengsel van species met hoge en lage katalytische activiteit. In de preparaten met een hoge activiteit werden 12-15 ijzer ionen waargenomen. Met behulp van een aantal geavanceerde element-analyse methoden werd het gehalte van andere metaalionen en selenium bepaald. Deze elementen waren in zeer lage hoeveelheden aanwezig en correleerden niet met enzymatische activiteit. Het kan daarom uitgesloten worden dat er metaalionen anders dan ijzer betrokken zijn bij de katalyse.

De studie van het redox-gedrag van de twee cubanen en de H-cluster van het hydrogenase door Patil en medewerkers leverde moeilijk te interpreteren resultaten op. Zij namen waar dat bij een reductieve redox-titratie van het aerob geïsoleerde hydrogenase zich eerst een EPR signaal met $g=2.07$ ($g=1.96$ en $g=1.89$) ontwikkelde, dat vervolgens verdween onder simultane vorming van een EPR signaal met $g=2.11$ ($g=2.05$ en $g=2.00$). Bij verdere reductie verdween ook dit signaal, gevolgd door een abrupte ontwikkeling van EPR signalen van de twee $[4Fe-4S]^{1+}$ clusters. EPR signalen vergelijkbaar met de $g=2.07$ en $g=2.11$ $S=1/2$ EPR signalen worden ook in andere ijzer-hydrogenases waargenomen en zijn afkomstig van de H-cluster. In hoofdstuk 2 wordt beschreven dat het door hen waargenomen complexe redox-gedrag van de H-cluster signalen een gevolg was van het activeringsproces van het aerob geïsoleerde enzym. In titraties van met waterstof of natrium dithioniet geactiveerd hydrogenase werd namelijk geen $g=2.07$ signaal waargenomen en bleef het $g=2.11$ EPR signaal ook bij hogere redox potentiaal bestaan. Deze waarnemingen geven aan dat de H-cluster van het normaal geïsoleerde hydrogenase voorkomt in een speciale zuurstof stabiele vorm, die bij reductieve activatie wordt omgezet in de normale tijdens de katalyse actieve vorm. Het $g=2.07$ EPR signaal is geen aparte redox-vorm van de H-cluster, maar is een artificiële intermediaire vorm die optreedt tijdens het activeringsproces. Eenmaal geactiveerd kan de H-cluster voorkomen in twee redox toestanden, een gereduceerde vorm zonder EPR signaal en een geoxideerde vorm met het $g=2.11$ EPR signaal (de halfwaarde potentiaal is ongeveer -307 mV). De spin integratie gaf aan dat 40% van het hydrogenase een H-cluster met een $g=2.11$ EPR signal bezat. Omdat geen andere EPR signalen werden waargenomen wordt aangenomen dat de resterende 60% van de hydrogenase moleculen geen H-cluster of een inactieve H-cluster had. Dit is vermoedelijk een gevolg van het feit dat de voor de titraties gebruikte enzym preparaten met een middelmatige activiteit bestonden uit een mengsel van H-cluster bevattende actieve en H-cluster missende inactieve species.

Naast de karakterisering van de H-cluster werden met twee speciale titraties de redox eigenschappen van de $[4Fe-4S]^{1+/2+}$ cubanen van het hydrogenase bestudeerd. Een probleem dat zich bij een normale titratie voordoet is dat bij de halfwaarde potentiaal van de cubanen door de katalytische activiteit van het hydrogenase het redox evenwicht verstoord wordt. Het hydrogenase gaat namelijk waterstof produceren uit de in het water aanwezige protonen en de in de kleurstoffen aanwezige electronen. Door de redox toestand met waterstof en de pH te controleren heerst er wel evenwicht. De corresponderende redox potentiaal van de oplossing kan worden berekend uit de partiële waterstofdruk en de pH. Een tweede methode om de halfwaarde potentiaal van de cubanen te kunnen bepalen maakte gebruik van een 'recombinant' hydrogenase met cubanen en zonder H-cluster. Dit hydrogenase wordt aangemaakt als het gen voor het hydrogenase eiwit tot overproductie wordt aanzet in de bacterie *Escherichia coli*. Zonder H-cluster vindt geen katalyse plaats en is de redox potentiaal stabiel. De met waterstof/pH equilibratie en met het 'recombinant' hydrogenase gemeten halfwaarde potentiaal van de cubanen was -335 ± 10 mV. Er werd bij de hier omschreven

experimenten onder de correcte evenwichts condities geen coöperativiteit van de cubanen geobserveerd: de twee cubanen gedroegen zich als nagenoeg identieke losse één-electron donerende of accepterende redox-groepen.

In hoofdstuk 3, 4 en 5 worden de ontdekking, biochemische en spectroscopische eigenschappen van het 'prismaan eiwit' beschreven. Dit eiwit werd ontdekt bij de isolatie van het hydrogenase uit *Desulfovibrio vulgaris* (Hildenborough). Bij de electroforetische scheiding in de aanwezigheid van het denaturende agens natrium dodecylsulfaat, werd in een onzuivere fractie van het hydrogenase een eiwit-bandje met een molecuulmassa van 59000 waargenomen. Een allereerste gedachte was dat dit eiwit misschien het hydC eiwit zou kunnen zijn. Dit eiwit is het hypothetische produkt van het aan hydrogenase gerelateerde hydC gen. Op grond van de op de DNA sequentie gebaseerde aminozuur volgorde zou het hydC eiwit een ijzer-zwavel cluster bevattend eiwit met een molecuulmassa van 66000 moeten zijn. Spoedig bleek echter uit experimenten met antilichamen tegen artificieel geproduceerd hydC eiwit dat het nieuwe eiwit niet overeenkwam met het hydC eiwit. De eigenschappen van het nieuwe eiwit waren zo ongewoon dat een verdere studie zinvol leek. In het circa zes ijzer en zuur-labiele zwavel ionen bevattende eiwit werden namelijk noch in de onbehandelde en noch in de gereduceerde vorm EPR signalen waargenomen die leken op enig ander bekend ijzer-zwavel eiwit. De onbehandelde vorm vertoonde een $S=1/2$ EPR signaal met $g=1.97$, $g=1.95$ en $g=1.90$. Hoewel deze g -waarden ook voorkomen in Mo^{5+} en W^{5+} ionen moest het signaal van een ijzer-zwavel cluster afkomstig zijn omdat met chemische analyse geen andere metaalionen werden waargenomen. De spin-integratie van dit 'molybdeen-achtige' signaal gaf aan dat slechts 10% van het eiwit dit signaal vertoonde. Omdat dit signaal verdween bij oxidatie en bij reductie werd vermoed dat het afkomstig was van intermediaire redox toestand, die in de onbehandelde vorm maar voor een deel aanwezig was. In de gereduceerde vorm werd een zeer uitzonderlijk nieuw $S=1/2$ EPR signaal met $g=2.00$, 1.82 en 1.32 geobserveerd. Spin quantisatie gaf aan dat het signaal correspondeerde met ongeveer $0.6-0.9 S=1/2$ paramagneet per eiwit. De grote mate van overeenkomst van het EPR spectrum van de gereduceerde vorm met de door anorganisch chemici gesynthetiseerde $[6Fe-6S]^{3+}$ prismaan cluster, gecombineerd met de chemische analyse van het eiwit, suggereerde dat een prismaan-bevattend-eiwit geïsoleerd was. Uitgaande van de herkenbare $[6Fe-6S]^{3+}$ toestand werd een schema opgesteld om de redox toestanden en EPR signalen van het prismaan eiwit te verklaren:



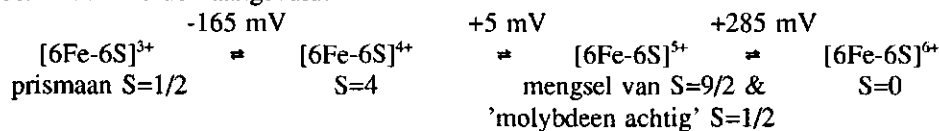
De naam 'prismaan eiwit' en dit schema moeten beschouwd worden als een werkmodel.

In Hoofdstuk 4 worden de biochemische eigenschappen en isolatie van dit prismaan eiwit uit de bacterie *Desulfovibrio vulgaris* (Hildenborough) beschreven. Omdat tot op heden nog geen katalytische activiteit is gevonden voor het slechts in kleine hoeveelheden voorkomende prismaan eiwit moest de zuivering met immuno-enzymatische kleuring gevolgd worden. Hiertoe werden de eiwit ketens van een te analyseren eiwit fractie met electroforese in aanwezigheid van natriumdodecylsulfaat op grootte gescheiden. Na overbrengen op een membraan kan met antilichamen de aanwezigheid van het prismaan eiwit met een kleur zichtbaar gemaakt worden. De scheiding op molecuul massa zorgt voor een positieve identificatie omdat sommige andere eiwitten ook een lichte kleurreactie kunnen geven. Na elk van de vier tot zes zuiveringsstappen werden de prismaan eiwit bevattende fracties met immunoenzymatische kleuring opgespoord. Op deze wijze kan uitgaande van 200 gram cellen (300 liter bacterie cultuur) 0.005 gram zuiver prismaan eiwit verkregen worden.

Het prismaan eiwit bleek te bestaan uit een enkele aminozuur keten. De molecuulmassa werd op verschillende manieren bepaald. De meest betrouwbaar geachte

sedimentatie evenwichts centrifugatie techniek bepaalde een molecuulmassa van 52000 ± 900 . De chemische analyse toonde aan dat 6.3 ± 0.4 ijzer, 6.2 ± 0.7 zuur-labele zwavel en minder dan 0.05 atoom van andere metalen en selenium aanwezig was. Er waren geen andere organische moleculen zoals heem of flavine aanwezig. Het zichtbare absorptie spectrum van het prismaan eiwit vertoonde de voor ijzer-zwavel eiwitten gebruikelijke brede absorptieband bij 400 nanometer. Door immunoenzymatische kleuring van eiwit-fractionen van de celcompartimenten werd aangetoond dat het prismaan eiwit in het cytoplasma van *Desulfovibrio vulgaris* (Hildenborough) voorkwam. In de nauw verwante bacterie *Desulfovibrio vulgaris* Monticello en *Desulfovibrio desulfuricans* (ATCC 27774) bleek ook een prismaan eiwit voor te komen dat kennelijk voldoende homoloog was om met de antilichamen tegen prismaan eiwit uit *Desulfovibrio vulgaris* (Hildenborough) te reageren.

Hoofdstuk 5 beschrijft de vervolgstudie van de redox en spin toestanden van het prismaan eiwit met EPR en Mössbauer spectroscopie. De drie halfwaarde potentialen van de overgangen tussen de redox toestanden werden bepaald met kleurstof gemedieerde redox titraties van de twee bekende $S=1/2$ EPR signalen. Gecombineerd met de ontdekking van $S=9/2$ EPR signalen in de $[6\text{Fe-6S}]^{3+}$ vorm en een $g=16$ EPR signaal van een heeltallig spin systeem (vermoedelijk $S=4$) in de $[6\text{Fe-6S}]^{4+}$ vorm kon het schema voor de redox en spin toestanden worden aangevuld:

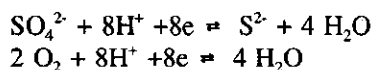


Het bewijs dat de $S=9/2$ en de 'molybdeenachtige' $S=1/2$ EPR signalen afkomstig waren van dezelfde redox toestand werd geleverd door een stapsgewijze reductieve titratie. De $S=9/2$ en $S=1/2$ EPR signalen bleken simultaan te verdwijnen onder vorming van het in de parallele mode waarneembare $g=16$ EPR signaal. Met de uit de g -waarden en temperatuursafhankelijkheid bepaalde E/D en D waarden van de $S=9/2$ EPR signalen kon geschat worden dat in de $[6\text{Fe-6S}]^{5+}$ vorm $95 \pm 35\%$ van het eiwit een ijzer-zwavel cluster met $S=9/2$ had. Binnen de experimentele fout complementeerde dit de substoichiometrische 10% van de clusters die een 'molybdeen-achtig' $S=1/2$ signaal hadden. Bij discussie van de in Hoofdstuk 7 en 8 beschreven resultaten zal blijken dat mengsels van spin toestanden en van species met dezelfde spin ook in andere ijzer-zwavel eiwitten voorkomen.

Met EPR spectrometers werkend bij diverse microgolffrequenties werd de lijnvorm van de $S=1/2$ EPR signalen van het gewone en het in het ^{57}Fe isotoop verrijkte prismaan eiwit bestudeerd. De door de kernspin van de ^{57}Fe ionen veroorzaakte verbreding van de EPR signalen was in overeenstemming met de aanwezigheid van ongeveer zes ijzer ionen in de cluster. Naast de met ^{57}Fe te introduceren verbreding bleek er een tweede microgolffrequentie onafhankelijke verbreding van de $S=1/2$ EPR signalen te zijn. De enige voor de hand liggende verklaring hiervoor is de aanwezigheid van direct aan de ijzer ionen gebonden stikstof atomen. Mössbauer spectroscopie van het met ^{57}Fe verrijkte prismaan eiwit gaf aan dat de ijzer ionen in het prismaan eiwit inequivalent waren. Zowel in de $[6\text{Fe-6S}]^{3+}$ als de $[6\text{Fe-6S}]^{4+}$ vorm werd een 4:2 verhouding van pieken waargenomen. De parameters die de chemische omgeving van de ijzer ionen omschrijven, de zogenaamde quadrupool splitsing en de 'isomer shift' waren in beide redox toestanden vrij constant voor de groep van de vier ijzer ionen. Twee ijzer ionen vertoonden echter een veel duidelijkere verandering van een Fe^{2+} naar een Fe^{3+} karakter. Mössbauer spectroscopie bij lage temperaturen en in aanwezigheid van aangelegde magneetvelden liet zien dat de vier en twee ijzer ionen in dezelfde spin gekoppelde paramagnetische structuur aanwezig waren. Dit leidde tot een model van een prismaan achtige structuur met een centrale set van vier ijzer ionen met twee aan weerszijde liggende meer ionogene ijzer ionen. De twee meer ionogene ijzer ionen zouden bijvoorbeeld

door histidine gebonden kunnen worden, in overeenstemming met de waargenomen lijnverbreding van de EPR signalen. De uitzonderlijke Mössbauer spectroscopische eigenschappen van de $S=9/2$ spin toestand van de $[6\text{Fe-6S}]^{3+}$ vorm konden worden verklaard met een spin koppelingsmodel waarin de twee meer ionogene $S=5/2$ Fe^{3+} ionen gekoppeld zijn met nagenoeg diamagnetische vier ijzer ionen.

In hoofdstuk 6 en 7 worden de resultaten van onderzoek naar nieuwe eigenschappen van het enzym sulfiet reductase beschreven. Dit enzym katalyseert de omzetting (dissimilatie) van sulfiet in zwavelwaterstof bij een op sulfaat-reductie gebaseerde ademhalingsketen. Sulfaat vervangt namelijk zuurstof als electronen acceptor voor de verbranding van substraten bij de strikt anaëroob bacterie *Desulfovibrio vulgaris* (Hildenborough):



Naast in sulfaat-reducerende bacteriën voorkomende dissimilatieve sulfiet reductases zijn er in sommige organismen ook assimilatieve sulfiet reductases, die betrokken zijn bij de productie van zwavelwaterstof voor de opbouw (assimilatie) van zwavel-bevattende verbindingen in de cel. In *Desulfovibrio vulgaris* (Hildenborough) komt zowel een dissimilatief als een assimilatief sulfiet reductase voor. Vermoedelijk kan dus het bij de dissimilatie vrijgekomen zwavelwaterstof niet gebruikt worden voor de assimilatie. De cel bevat echter veel meer dissimilatief sulfiet reductase omdat de voor de productie van energie noodzakelijke om te zetten hoeveelheid sulfiet groter is.

Alle sulfiet reductases bevatten ijzer-zwavel clusters en siroheem, een organisch molecuul dat een $\text{Fe}^{2+/3+}$ ion gebonden kan hebben aan zijn vier stikstof atomen. Echter het aantal siroheem groepen, de metallering van het siroheem, de hoeveelheid ijzer en zuur labiele zwavel en het aantal en soort eiwitketens van de sulfiet reductases uit *Desulfovibrio* en andere organismen verschillen sterk. De dissimilatieve sulfiet reductases zijn door het hoge gehalte in de cel, de aanwezigheid van ≈ 20 Fe/S en de betrekkelijk uniforme molecuulmassa en samenstelling van de eiwitketens gemakkelijk te onderscheiden. Op grond van het zichtbare spectrum worden de dissimilatieve sulfiet reductases onderverdeeld in vier klassen die aangeduid worden met de triviale namen desulfovridine, desulforubidine, desulfofuscidine en P582.

In hoofdstuk 6 wordt de ontdekking van een nieuwe eiwitketen in dissimilatieve sulfiet reductases van het desulfovridine type beschreven. Tot dusver werd aangenomen dat desulfovridine en de andere dissimilatieve sulfiet reductases twee α en twee β eiwitketens hadden (afgekort als $\alpha_2\beta_2$). De α en β ketens hebben molecuul massa's van ≈ 55000 en ≈ 45000 en zijn gemakkelijk te scheiden met gelelectroforese in aanwezigheid van natrium dodecylsulfaat. De kleurloze eiwitketens kunnen door behandeling met de Coomassie kleurstof blauw gekleurd worden. Bij de controle van de zuiverheid van desulfovridine uit *Desulfovibrio vulgaris* (Hildenborough) werd naast de gebruikelijke twee blauwe bandjes van de α en β ketens steeds een derde eiwitbandje met een molecuulmassa van 11000 waargenomen. Hoewel aanvankelijk vermoed werd dat dit derde bandje afkomstig was van een onzuiverheid of afbraak-product, bleek in meerdere preparaten een vrij constante hoeveelheid van de derde eiwitketen aanwezig te zijn. Pogingen met diverse scheidingsmethoden resulteerden niet in de verwijdering. De verhouding ten opzichte van de α en β ketens bleef zelfs nagenoeg stoichiometrisch. Daarom werd geconcludeerd dat de eiwitketen samenstelling van desulfovridine niet $\alpha_2\beta_2$ maar $\alpha_2\beta_2\gamma_2$ was, met derde keten als γ . De mogelijkheid bestond dat de γ eiwit keten was gevormd door splitsing van de α of β eiwit keten en aan het enzym gebonden bleef. Hiertoe werd met immuno-enzymatische kleuring de reactie van antilichamen tegen de afzonderlijke eiwitketens met de eiwitketens onderzocht. De antilichamen gaven echter alleen kleur-reacties met de respectievelijke

eiwitketens. Dit toonde aan dat de α , β en γ inderdaad verschillende eiwitketens waren en dat de kleinere β en γ ketens niet uit de α keten gevormd. De mogelijkheid om met de antilichamen ook in nog niet gezuiverde preparaten α , β en γ aan te tonen kwam in een aantal experimenten uitstekend van pas. Er kon aangetoond worden dat de verhouding tussen de α , β en γ ketens tijdens de zuiverings procedure niet wijzigde. Met de gemeten stoichiometrie voor het gezuiverde desulfovirdine vormt dit een belangrijk bewijs dat het enzym onder fysiologische condities ook drie ketens bevat. Ten tweede kon met de antilichamen op gemakkelijke wijze worden aangetoond dat ook in drie andere *Desulfovibrio* stammen een γ keten in desulfovirdine aanwezig is. Door gedeeltelijke zuivering van de desulfovirdines uit de andere stammen werd bevestigd dat de γ keten ook daadwerkelijk aan het desulfovirdine gebonden was. De antilichamen tegen de eiwitketens van desulfovirdine gaven geen kleurreactie met de assimilatieve sulfiet reductases uit *Desulfovibrio vulgaris* (Hildenborough) en *Escherichia coli*. Antilichamen tegen het assimilatieve sulfiet reductase uit *Desulfovibrio vulgaris* (Hildenborough) reageerden met geen van de andere sulfiet reductases. Dit geeft aan dat hoewel de assimilatieve en dissimilatieve sulfiet reductases dezelfde reactie katalyseren er op eiwitniveau grote verschillen bestaan.

De aminozuur volgorden van de N-terminale uiteinden van de α , β en de nieuwe γ eiwitketen werden bepaald om identificatie van de volledige aminozuur volgorde uit de DNA volgorde in de toekomst mogelijk te maken. Recentelijk is mede met behulp van de hier beschreven antilichamen en de N-terminale aminozuur volgorde, de volledige aminozuur volgorde van de γ keten opgehelderd door Voordouw en medewerkers.

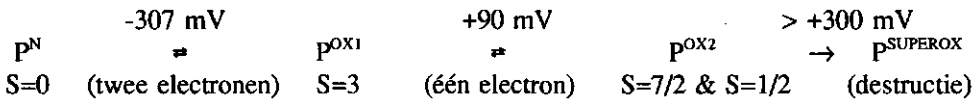
De EPR spectroscopische studie van het dissimilatieve sulfiet reductase uit *Desulfovibrio vulgaris* (Hildenborough) wordt beschreven in Hoofdstuk 7. Dit enzym vertoonde een grote verscheidenheid aan EPR signalen. De eenvoudigst te interpreteren signalen waren afkomstig van verschillende $S=5/2$ en $S=1/2$ species van de siroheem groepen in Fe^{3+} vorm. Sommatie van de spin quantisaties van de EPR signalen van de siroheem groepen gaf aan dat slechts 20% van de siroheem groepen een ijzer ion bevatte. In overeenstemming met het zichtbare absorptie spectrum was de overige 80% van de siroheem aanwezig in de gedemetalleerde vorm, d.w.z. als siroporfyrine. Dit bevestigde de waarnemingen van Moura en medewerkers die het desulfovirdine uit *Desulfovibrio gigas* bestudeerden. De betekenis van de demetallering in desulfovirdine is onduidelijk, vooral omdat andere dissimilatieve sulfiet reductases zoals desulforubidine wel volledig gemetalleerde siroheem groepen bevatten.

Naast de van de siroheem afkomstige EPR signalen werden er in het geïsoleerde enzym zeer uitzonderlijke EPR signalen geobserveerd met g-waarden van $g=17$, 15.1, 11.7 en 9.0. Omdat de signalen verdwenen bij EPR spectroscopie in de parallele mode moesten de signalen afkomstig zijn van een halfvallig spin systeem. De temperatuursafhankelijkheid van de signalen en de theoretisch berekende g-waarden gaven aan dat de signalen afkomstig waren van paramagneten met $S=9/2$. Er kon worden berekend dat ≈ 0.6 paramagneet met $S=9/2$ per $\alpha\beta\gamma$ eenheid aanwezig was. Met een kleurstof-gemedieerde titratie werd aangetoond dat de paramagnetische centra met $S=9/2$ een van de gemetalleerde siroheem centra onafhankelijk redox-gedrag hadden.

In het door Siegel opgestelde model bevat het assimilatieve sulfiet reductase uit *Escherichia coli* een diamagnetische $[4Fe-4S]^{2+}$ cubaan die magnetisch gekoppeld is met het paramagnetische $Fe^{2+/3+}$ ion in de siroheem groep. Afgezien van de ons inziens moeilijk voor te stellen koppeling tussen een paramagnetische met een niet-magnetische groep gaven de hier beschreven bevindingen aan dat het door Siegel opgestelde model niet toepasbaar is voor desulfovirdine. Allereerst is in desulfovirdine 80% van de siroheem gedemetalleerd en kan dus niet koppelen. Bovendien zijn er in de gereduceerde vorm geen EPR signalen van 'ontkoppelde' $[4Fe-4S]^{1+}$ cubanen waarneembaar. Desulfovirdine moet dus andere ijzer-zwavel clusters hebben. Gecombineerd met de bevindingen met high spin signalen in andere

eiwitten wijst de aanwezigheid van een $S=9/2$ spin systeem eerder op een ongebruikelijk ijzer-zwavel (super)cluster in desulfovirdine.

In Hoofdstuk 8 worden de resultaten van het onderzoek aan de P-clusters van het molybdeen-ijzer eiwit van het nitrogenase uit *Azotobacter vinelandii* beschreven. Door gecontroleerde oxidatie met kleurstof gemedieerde redox titraties konden de P-clusters in drie goed gedefinieerde redox toestanden worden verkregen. In de volledig gereduceerde natieve toestand P^N zijn de P-clusters diamagnetisch. Oxidatie met twee electronen leidt tot de eerste geoxideerde toestand (P^{OX1}), waarin de P-clusters een in de parallele mode intenser wordend $g=12$ EPR signaal vertonen. Dit signaal is waarschijnlijk afkomstig van een $S=3$ spin systeem. Door oxidatie van P^{OX1} met één electron wordt de tweede geoxideerde vorm van de P-clusters verkregen. In deze P^{OX2} toestand komen de P-clusters voor als een mengsel van species met $S=7/2$ en $S=1/2$. Verdere 'super'-oxidatie van de P^{OX2} toestand destrueerde het enzym onder vorming van $S=9/2$ en andere high spin EPR signalen. Het volgende schema vat de halfwaarde potentialen, redox en spin toestanden van de P clusters samen:



Dit schema verklaart de schijnbare tegenstrijdigheid van de Mössbauer spectroscopische metingen door de groep van Münck met de EPR spectroscopische metingen door Hagen. De Mössbauer metingen bleken uitgevoerd te zijn met de P^{OX1} toestand, terwijl Hagen en medewerkers de P^{OX2} vorm hadden bestudeerd. De correctheid van de met EPR spectroscopie afgeleide heeltaligheid van de spintoestand van de P^{OX1} vorm werd recentelijk bevestigd door een herinterpretatie van de Mössbauer spectroscopie.

In Hoofdstuk 9 worden de biochemische en spectroscopische eigenschappen van de eiwitten rubrerythrine en het hier voor het eerst beschreven nigerythrine uit de bacterie *Desulfovibrio vulgaris* (Hildenborough) vergeleken. De namen van deze eiwitten zijn samenvoegsels van rubredoxine-hemerythrine (tot rubre-rythrine) en niger(zwart)-hemerythrine (tot niger-ythrine). Het eerste deel van de naam wijst op de rubredoxine-achtige ijzer centra en de daarmee geassocieerde kleur, terwijl het tweede deel gebruikt is omdat de spectroscopische eigenschappen van de beide eiwitten verwant zijn met die van hemerythrine, een zuurstof transportierend eiwit uit mariene ongewervelde dieren. Hemerythrine bevat een dinucleair ijzer cluster: twee door zuurstof verbonden en door zuurstof en stikstof omringde ijzer ionen, die in de $Fe^{2+}-Fe^{2+}$ ($S=0$ of $S=4$), $Fe^{3+}-Fe^{2+}$ ($S=1/2$) en $Fe^{3+}-Fe^{3+}$ vorm ($S=0$) kunnen voorkomen. De verwantschap met hemerythrine berust op het voor dinucleaire ijzer clusters karakteristieke EPR signaal met $g < 2$ in de redox toestand met de gemengde valentie.

Rubrerythrine en nigerythrine zijn beide opgebouwd uit twee identieke eiwitketens. Hoewel er verschillen waren tussen de molecuulmassa's van de eiwitketens, de iso-electrische punten en de N-terminale aminozuur sequentie van rubrerythrine en nigerythrine bleken de EPR spectra van de rubredoxine-achtige en de dinucleaire ijzer centra nagenoeg identiek te zijn. Dit werd bevestigd door kleurstof gemedieerde redox titraties waarin de $g=4.3$ EPR signalen van de Fe^{3+} vorm ($S=5/2$) van de rubredoxine-achtige centra en de $S=1/2$ EPR signalen van $Fe^{3+}-Fe^{2+}$ vorm van de dinucleaire centra gevolgd werden. De halfwaarde potentialen voor de $Fe^{2+} \rightleftharpoons Fe^{3+}$ overgang van de rubredoxine-achtige centra was $+281$ mV voor rubrerythrine en $+213$ mV voor nigerythrine. De halfwaarde potentialen voor de $Fe^{2+}-Fe^{2+} \rightleftharpoons Fe^{3+}-Fe^{2+}$ en $Fe^{3+}-Fe^{2+} \rightleftharpoons Fe^{3+}-Fe^{3+}$ overgangen, respectievelijk $+246$ en $+339$ mV voor rubrerythrine en $+209$ en $+300$ mV voor nigerythrine, lagen zo dichtbij elkaar dat verdere reductie of oxidatie van de $Fe^{3+}-Fe^{2+}$ vorm optrad voordat alle dinucleaire centra in deze vorm waren. Na correctie voor dit effect bleek dat de met EPR spin quantisatie geobserveerde verhouding tussen de rubredoxine achtige en dinucleaire centra zowel in rubrerythrine als in

nigerythrine gelijk was. Deze spin quantisatie en het ijzer gehalte van 5-8 per eiwit tonen aan dat rubrerythrine en nigerythrine twee rubredoxine-achtige en twee dinucleaire centra hebben. De foutieve interpretatie van LeGall en medewerkers dat rubrerythrine twee rubredoxine-achtige centra en slechts één dinucleair centrum had, werd verklaard door de inhomogeniteit van de redox toestand van de door hen bestudeerde preparaten. Gezien de halfwaarde potentialen wordt verwacht dat rubrerythrine en nigerythrine in de bacterie actief zijn in de volledig gereduceerde vorm. Ondanks pogingen om voor dinucleaire ijzer clusters relevante katalytische activiteiten aan te tonen kon geen biologische functie worden waargenomen.

Het overzicht in hoofdstuk 10 vormt een inventarisatie van het voorkomen van high spin systemen. Hieruit blijkt dat high spin systemen in ijzer-zwavel clusters minder uitzonderlijk zijn dan in het verleden werd aangenomen. De diversiteit van de redox en spin toestanden van de ijzer-zwavel clusters van de multi-electronen overdragende eiwitten maakt het op dit moment nog niet mogelijk om tot een classificatie te komen.

Curriculum vitae

Antonius Johannes Pierik werd op 30 september 1964 geboren in Wageningen. Na de basisschool behaalde hij op 4 juni 1982 het Atheneum B diploma aan het Marnix College te Ede.

Zijn scheikunde studie aan de Rijksuniversiteit Utrecht werd op 21 september 1987 met lof afgesloten. Tijdens deze studie werden afstudeervakken gedaan bij de vakgroepen Synthetische Organische Chemie (Synthese van chirale cyclische bis-fosfinen, bij Dr. J. Boersma en Dr. P. Vermeer) en Biochemie (Voorkomen en werking van Ca^{2+} -onafhankelijke fosfolipase A_2 in de rat, bij Prof. Dr. H. van den Bosch).

Terug in zijn geboortestad begon hij op 1 oktober 1987 gefinancierd door NWO als Onderzoeker-in-Opleiding (OIO) bij de vakgroep Biochemie van de Landbouwniversiteit Wageningen. In 1991 ontving hij een Koninklijke/Shell Studiereis. De resultaten van het onderzoek tot mei 1992 zijn vastgelegd in dit proefschrift.

Vanaf 1 mei 1992 verrichte hij in Brighton (Engeland) in het kader van een EEG 'Twinning' project tussen de Landbouwniversiteit Wageningen en het Nitrogen Fixation Laboratory onderzoek naar de structuur en functie van de P-clusters van nitrogenase. Vanaf september 1993 zal dit onderzoek met ondersteuning van de University of East-Anglia (Norwich, Engeland) en de Medizinische Universität (Lübeck, Duitsland) worden gecontinueerd met een twee-jarige beurs van het Human Capital and Mobility Programma van de EEG.

List of publications

1. Pierik, A.J., Nijssen, J.G., Aarsman, A.J. & Van den Bosch, H. (1988) Biochim. Biophys. Acta **962**, 345-353. Calcium-independent phospholipase A₂ in rat tissue cytosols.
2. Pierik, A.J., Hagen, W.R., Redeker, J.S. & Veeger, C. (1988) Abstr. Second Int. Symp. Mol. Biol. Hydrogenase (Helen, Georgia, U.S.A). FPLC purification and elemental analysis of *Desulfovibrio vulgaris* (Hildenborough) iron hydrogenase.
3. Hagen, W.R., Pierik, A.J. & Veeger, C. (1989) J. Chem. Soc., Faraday Trans. I **85**, 4083-4090. Novel Electron Paramagnetic Resonance Signals from an Fe/S Protein containing Six Iron Atoms.
4. Hagen, W.R., Pierik, A.J. & Veeger, C. (1990) Metal Active Sites in Biology and their Synthetic Analogues (SAMBAS III, Bostalsee, Saarland, Germany), 54. Iron-sulfur superclusters in biological redox catalysis.
5. Pierik, A.J., Hagen, W.R. & Veeger, C. (1990) EBEC Reports **6** (Sixth European Bioenergetics Conference, Noordwijkerhout, The Netherlands), 16. The redox states of the prismane protein.
6. Hagen, W.R., Pierik, A.J. & Veeger, C. (1990) Ital. Biochem. Soc. Trans. **1** (Joint Symp. Ital./Dutch/Yugosl. Biochem. Soc., Bari, Italy.), 85. Iron-sulfur superclusters in biological redox catalysis.
7. Jetten, M.S.M., Hagen, W.R., Pierik, A.J., Stams, A.J.M. & Zehnder, A.J.B. (1991) Eur. J. Biochem. **195**, 385-391. Paramagnetic centers and acetyl-coenzyme A / CO exchange activity of carbon monoxide dehydrogenase from *Methanothrix soehngenii*.
8. Pierik, A.J. & Hagen, W.R. (1991) Eur. J. Biochem. **195**, 505-516. S=9/2 EPR signals are evidence against coupling between the siroheme and the Fe/S cluster prosthetic groups in *Desulfovibrio vulgaris* (Hildenborough) dissimilatory sulfite reductase.
9. Hagen, W.R., Pierik, A.J., Wolbert, R.B.G., Wassink, H., Haaker, H., Veeger, C., Jetten, M.K., Stams, A.J.M. & Zehnder, A.J.B. (1991) Biofactors **3** (Int. Symp. Peter Hemmerich, Konstanz, Germany), 144. Superclusters with superspins in iron-sulfur redox enzymes.
10. Hagen, W.R., Pierik, A.J., Wolbert, R.B.G., Wassink, H., Haaker, H., Veeger, C., Jetten, M.K., Stams, A.J.M. & Zehnder, A.J.B. (1991) J. Inorg. Biochem. **43** (Fifth Int. Conf. Bioinorg. Chem., Oxford, U.K.), 237. S=9/2 EPR of iron-sulfur clusters in the prismane protein, sulfite reductase, CO dehydrogenase, and nitrogenase.
11. Hagen, W.R., Pierik, A.J., Wolbert, R.B.G., Verhagen, M.F.J.M. & Veeger, C. (1991) Abstr. Third Int. Conf. Molec. Biol. Hydrogenases, Troia, Portugal, pp. 72-75. A reinvestigation of the redox properties of the periplasmic Fe-hydrogenase from *Desulfovibrio vulgaris* (Hildenborough).

12. Jetten, M.S.M., Pierik, A.J. & Hagen, W.R. (1991) Eur. J. Biochem. **202**, 1291-1297. EPR characterization of a high-spin system in carbon monoxide dehydrogenase from *Methanotheroxobrevibacter*.
13. Pierik, A.J., Duyvis, M.G., Van Helvoort, J.M.L.M., Wolbert, R.B.G. & Hagen, W.R. (1992) Eur. J. Biochem. **205**, 111-115. The third subunit of desulfoviridin-type dissimilatory sulfite reductases.
14. Link, T.A., Hagen, W.R., Pierik, A.J., Assmann, C. & Von Jagow, G. (1992) Abstr. EUROBIC I, Newcastle-upon-Tyne, U.K., P5. Determination of the redox properties of the "Rieske" [2Fe-2S] cluster of bovine heart *bc₁* complex by direct electrochemistry of a water soluble fragment.
15. Pierik, A.J., Wassink, H. Haaker, H. & Hagen, W.R. (1992) Abstr. EUROBIC I, Newcastle-upon-Tyne, U.K., P14. EPR spectroscopy of the P-clusters of *Azotobacter vinelandii* MoFe protein.
16. Pierik, A.J., Wolbert, R.B.G., Portier, G.L. & Hagen, W.R. (1992) Abstr. EUROBIC I, Newcastle-upon-Tyne, U.K., P19. Rubrerythrin and nigerythrin from *Desulfovibrio vulgaris*: two homodimers each with two dinuclear iron centers and two rubredoxin-like iron centers.
17. Pierik, A.J., Wolbert, R.B.G., Mutsaers, P.H.A., Hagen, W.R. & Veeger, C. (1992) Eur. J. Biochem. **206**, 697-704. Purification and biochemical characterization of a putative [6Fe-6S] prismane-cluster-containing protein from *Desulfovibrio vulgaris* (Hildenborough).
18. Pierik, A.J., Hagen, W.R., Dunham, W.R. & Sands, R.H. (1992) Eur. J. Biochem. **206**, 705-719. Multi-frequency EPR and high-resolution Mössbauer spectroscopy of a putative [6Fe-6S] prismane-cluster-containing protein from *Desulfovibrio vulgaris* (Hildenborough): characterization of a supercluster and superspin model protein.
19. Stokkermans, J.P.W.G., Pierik, A.J., Wolbert, R.B.G., Hagen, W.R., Van Dongen, W.M.A.M. & Veeger, C. (1992) Eur. J. Biochem. **208**, 435-442. The primary structure of a protein containing a putative [6Fe-6S] prismane cluster from *Desulfovibrio vulgaris* (Hildenborough).
20. Link, T.A., Hagen, W.R., Pierik, A.J., Assmann, C. & Von Jagow, G. (1992) Eur. J. Biochem. **208**, 685-691. Determination of the redox properties of the Rieske [2Fe-2S] cluster of bovine heart *bc₁* complex by direct electrochemistry of a water-soluble fragment.
21. Pierik, A.J., Hagen, W.R., Redeker, J.S., Wolbert, R.B.G., Boersma, M., Verhagen, M.F.J.M., Grande, H.J., Veeger, C., Mutsaers, P.H.A., Sands, R.H. & Dunham, W.R. (1992) Eur. J. Biochem. **209**, 63-72. Redox properties of the iron-sulfur clusters in activated Fe-hydrogenase from *Desulfovibrio vulgaris* (Hildenborough).
22. Stokkermans, J.P.W.G., Houba, P.H.J., Pierik, A.J., Hagen, W.R., Van Dongen, W.M.A.M. & Veeger, C. (1992) Eur. J. Biochem. **210**, 983-988. Overproduction of prismane protein in *Desulfovibrio vulgaris* (Hildenborough): evidence for a second S=1/2-spin system in the one-electron reduced state.

23. Pierik, A.J., Wassink, H., Haaker, H. & Hagen, W.R. (1993) Eur. J. Biochem. **212**, 51-61. Redox properties and EPR spectroscopy of the P clusters of the *Azotobacter vinelandii* MoFe protein.
24. Pierik, A.J., Wolbert, R.B.G., Portier, G.L., Verhagen, M.F.J.M. & Hagen, W.R. (1993) Eur. J. Biochem. **212**, 237-245. Nigerythrin and rubrerythrin from *Desulfovibrio vulgaris* each contain two mononuclear iron centers and two dinuclear iron clusters.
25. Pierik, A.J., Lowe, D.J., Eldridge, M.E., Marritt, S., Farrar, J.A., Thomson, A.J. & Eady, R.R. (1993) In: *New Horizons in Nitrogen Fixation* (Palacios, R., Mora, J. & Newton, W.E., eds.), Nijhoff/Junk, Dordrecht (The Netherlands), 147. EPR and MCD spectroscopic characterisation of the VFe-cofactor and P-cluster centres of the VFe protein from *Azotobacter chroococcum*.
26. Marritt, S., Pierik, A.J., Thomson, A.J., Hagen, W.R., Lowe, D.J., Albracht, S.P.J. & Smith, B.E. (1993) In: *New Horizons in Nitrogen Fixation* (Palacios, R., Mora, J. & Newton, W.E., eds.), Nijhoff/Junk, Dordrecht (The Netherlands), 153. Studies of the electronic states of oxidized P clusters by EPR and MCD spectroscopy.
27. Marritt, S., Faridooon, K.Y., Pierik, A.J., Gormal, C., Howes, B.D., Buck, M., Lowe, D.J., Thomson, A.J. & Smith, B.E. (1993) In: *New Horizons in Nitrogen Fixation* (Palacios, R., Mora, J. & Newton, W.E., eds.), Nijhoff/Junk, Dordrecht (The Netherlands), 144. Spectroscopic studies on variants of the *Klebsiella pneumoniae* nitrogenase MoFe protein with directed mutation of putative P cluster ligands.
28. Hagen, W.R., Pierik, A.J., Van Dongen, W.M.A.M., Duyvis, M.G., Verhagen, M.F.J.M. & Haaker, H. (1993) In: *New Horizons in Nitrogen Fixation* (Palacios, R., Mora, J. & Newton, W.E., eds.), Nijhoff/Junk, Dordrecht (The Netherlands), 137. The redox and magnetic properties of the prosthetic groups in the MoFe-protein of *Azotobacter vinelandii* nitrogenase.
29. Holliger, C., Pierik, A.J., Reijerse, E.J. & Hagen, W.R. (1993) J. Am. Chem. Soc. **115**, 5651-5656. A Spectroelectrochemical Study of Factor F_{430} Nickel(II/I) from Methanogenic Bacteria in Aqueous solution.
30. Hagen, W.R., Verhagen, M.F.J.M., Pierik, A.J., Wolbert, R.B.G., Malleé, L.F. & Voorhorst, W.G.B. (1993) J. Inorg. Biochem. **51**, 28. Axial coordination and reduction potentials of the 16 hemes in high-molecular-weight cytochrome c from *Desulfovibrio vulgaris*.
31. Smith, B.E., Buck, M., Faridooon, K.Y., Gormal, C.A., Howes, B.D., Lowe, D.J., Marritt, S., Pierik, A.J., Richards, R.L. & Thomson, A.J. (1993) J. Inorg. Biochem. **51**, 348 (&357). The metallo-sulphur centres of the nitrogenase MoFe protein (Kp1) from wild-type and mutant strains of *Klebsiella pneumoniae*.
32. Arendsen, A.F., Verhagen, M.F.J.M., Wolbert, R.B.G., Pierik, A.J., Stams, A.J.M., Jetten, M.S.M. & Hagen, W.R. (1993) J. Inorg. Biochem. **52**, 469. The dissimilatory sulfite reductase from *Desulfosarcina variabilis* is a desulforubidin and it contains uncoupled metallated sirohemes and S=9/2 iron-sulfur clusters.

